



Università degli Studi di Roma TRE

XXIII Doctoral school in Physics

**Growth of cosmological perturbations in  
Dark Energy universes**

Cinzia Di Porto

*Advisors:*

Prof. Luca Amendola, Prof. Enzo Branchini

*Director of the Doctoral School:*

Prof. Guido Altarelli



# Contents

<b>Introduction</b>	<b>1</b>
<b>1 Expansion history of the universe</b>	<b>3</b>
1.1 Friedmann equations . . . . .	4
1.2 Perfect fluid models . . . . .	7
1.3 Hubble's law . . . . .	11
1.4 Cosmic distances . . . . .	12
1.4.1 Comoving distance . . . . .	12
1.4.2 Luminosity distance . . . . .	13
1.4.3 Angular diameter distance . . . . .	14
<b>2 What we know from observations</b>	<b>17</b>
2.1 Supernovae . . . . .	17
2.2 The age of the universe . . . . .	18
2.3 Cosmic microwave background . . . . .	20
2.4 Matter density . . . . .	23
<b>3 The cosmological constant</b>	<b>29</b>
3.1 History of the cosmological constant . . . . .	29
3.2 Fine-tuning problem . . . . .	32
3.3 The coincidence problem . . . . .	33
<b>4 Scalar fields and generalizations of General Relativity</b>	<b>37</b>
4.1 Introduction to Field theory . . . . .	37
4.2 Scalar fields in cosmology . . . . .	42
<b>5 Linear perturbation theory</b>	<b>45</b>
5.1 Cosmological horizons . . . . .	46
5.2 Perturbing General Relativity . . . . .	46
5.3 The Newtonian gauge . . . . .	47
5.4 Single fluid model . . . . .	50
5.5 Scales larger than the horizon . . . . .	54
5.6 Scales smaller than the Hubble radius . . . . .	54
5.7 Two-fluid solutions . . . . .	56

<b>6</b>	<b>Correlation function and power spectrum</b>	<b>61</b>
6.1	The Correlation function . . . . .	61
6.2	Measuring the correlation function in real catalogs . . . . .	63
6.3	The power spectrum . . . . .	64
6.4	Normalization of the power spectrum . . . . .	68
6.5	Velocity field . . . . .	69
6.6	Redshift distortion . . . . .	70
<b>7</b>	<b>Statistical methods in cosmology</b>	<b>75</b>
7.1	Introduction to Bayesian statistics . . . . .	75
7.2	Fisher matrix method . . . . .	78
7.3	The Fisher matrix for the power spectrum . . . . .	84
<b>8</b>	<b>Dark energy as a modified form of matter</b>	<b>87</b>
8.1	Quintessence model . . . . .	88
8.2	Coupled Quintessence . . . . .	90
8.3	Background evolution in a coupled Quintessence model . . . . .	91
8.4	Linear perturbations in coupled Quintessence models . . . . .	94
8.5	A generalized fit for the growth rate . . . . .	95
8.6	Comparing the fit to the numerical results. . . . .	97
8.7	Comparing the fit to the observations . . . . .	97
8.8	Comments . . . . .	101
<b>9</b>	<b>Modified gravity theories: <math>f(R)</math> models</b>	<b>105</b>
9.1	The Growth Rate in $f(R)$ . . . . .	105
9.2	A Parametrization of the Growth Rate in $f(R)$ . . . . .	108
9.3	Results . . . . .	111
9.3.1	Improving the fit for small $k$ . . . . .	112
9.4	Future developments . . . . .	112
<b>10</b>	<b>Forecasting constraints from future data</b>	<b>119</b>
10.1	Introduction . . . . .	119
10.2	Models . . . . .	121
10.2.1	Equation of state . . . . .	121
10.2.2	Growth Rate . . . . .	122
10.2.3	Galaxy Biasing . . . . .	123
10.2.4	Reference Cosmological Models . . . . .	123
10.3	Fisher Matrix Analysis . . . . .	124
10.4	Modeling the Redshift Survey . . . . .	128
10.5	Results . . . . .	131
10.5.1	$s$ -parametrization . . . . .	131
10.5.2	Other parametrizations. . . . .	135
10.6	Conclusions . . . . .	138

<b>Conclusions and future developments</b>	<b>147</b>
<b>Bibliography</b>	<b>158</b>



# Introduction

One of the most surprising discoveries of the modern cosmology is that our Universe is not only expanding, but that its expansion is *accelerating*. This is the opposite of what expected for a universe described by a standard Friedmann cosmology, according to which the expansion should decelerate because of the attractive gravitational force exerted by the matter. Indeed the deceleration is easily deduced by solving the Einstein field equations in a metric describing a homogeneous and isotropic space-time, as seems to be our Universe on large scales, and obtaining the so called Friedmann equations.

The data coming from the analysis of very different cosmological observables such as the cosmic microwave background, the luminosity curves of supernovae, the galaxy clusters and many others suggest that the Universe where we live is spatially flat, with a low matter density and dominated by a kind of energy, labeled “dark”, to underline both its feature to not absorb or emitting light and its mysterious nature. This energy is thought to be the responsible of the observed cosmic acceleration. But what is the dark energy?

Its principal features are those of a perfect fluid, homogeneously distributed and with a negative pressure. This could sound strange and Einstein himself was sceptical when he realized that, in order to construct solutions of his field equations, able to describe a steady universe, he needed to take into account the hypothesis of a component with negative pressure. At that time Einstein indeed believed that the Universe did not have a dynamic nature but that it was static and, since a fluid with this peculiarity did not seem to have physical sense, he introduced in its field equations a constant term, such to exerts a force opposed to the expansion. This term was labeled *cosmological constant* and indicated with the Greek letter  $\Lambda$ . When Hubble discovered, through the observation of the recession velocities of distant galaxies, that the universe was actually expanding, Einstein withdrew the hypothesis of the cosmological constant which did not have any reason to exist anymore. According to the legend, Einstein defined  $\Lambda$  “the biggest blunder” of his life, but despite his regret many think that he was right even when he thought to be wrong!

In fact, in the last two decades, the cosmological constant began to gain a growing interest in particle physics, because it can be interpreted as the vacuum energy. Every quantum field has a zero-point energy contributing to the vacuum energy density, which acts just as a cosmological constant. This can then find an origin in theories of fundamental physics and seems therefore the best candidate to the role of dark energy. Shifting it from the original position in the field equations, where was placed by Einstein to act as

a brake to the expansion, to the opposite member, it acts as a source term, able to drive an accelerated expansion even in the absence of matter. But here comes the first problem: to agree with the cosmological observations, its value should be small enough to not perturb the planetary motions, well described by Newtonian gravity. If on the contrary it originates from vacuum energy, the value we expect (according to qualitative but hardly avoidable arguments from quantum mechanics) is definitely much larger: the difference is more than 120 orders of magnitude! This is only one of the problems associated to the cosmological constant which led many authors to find different explanations to the dark energy issue. An incomplete list includes Quintessence models, invoking a dynamic scalar field; modified gravity justified by string theory or, more generally, changes in the action of General Relativity; braneworld universes; “Chaplygin gas” trying to unify dark matter and dark energy considering a fluid whose equation of state interpolates between them; a system of topological defects forcing the universe to an accelerated expansion; void models; phantom fields....and many others!

In this Thesis we will focus our attention mainly on models of coupled Quintessence and to a class of modified gravity theories, the so called  $f(R)$  models, but we will also analyse, marginally, other models. One of the main problems with the various different models of dark energy is that even models with very different physical origins can be degenerate with respect to the observables related only to the expansion history of the universe. Fortunately, the homogeneous observables of the universe on large scales are not the only observable quantities. The growth of primordial perturbations giving rise to the formation of structures in the universe provides a second, important observable, which studied together with the expansion evolution can help to remove the degeneracy and distinguish among the models.

The aim of this Thesis is then to study the growth of cosmological perturbations in different dark energy scenarios, both trying to find differences among them and comparing the results to observational data. One of the problems along this line of research is to express the relevant theoretical quantities (expansion rate and growth function) in a form suitable for a direct comparison with real data. A successful parametrization, i.e. a form that is general enough to describe a large class of models and yet simple enough to be readily integrated into the data analysis pipelines, is an important step in this direction. To this end we will propose several fitting formulas able to describe with a good accuracy the behaviour of the growth rates in different models. These fits will be also used in the comparison of the models to the observations. We will use present data, coming from different distances and several observables, to put constraints on the model parameters but we will also forecast how next generation data will be able to tighten these constraints, helping to distinguish among the models.

# Chapter 1

## Expansion history of the universe

The cornerstone of modern cosmology is known as the *Cosmological Principle* and it is an idea which is both powerful and simple. Although the name ‘principle’ sounds grand, some guiding principles are generally introduced into physics when one has to face with a dearth of observational or experimental data. Such principles are often based on ideas of symmetry, which reduce the number of degrees of freedom one has to consider and assist during the first tentative steps towards a theoretical understanding.

The Cosmological Principle is the assertion that, on sufficiently large scales (beyond those traced by the large-scale structure of the distribution of galaxies), the Universe is both homogeneous and isotropic. Homogeneity is the property of being identical everywhere in space, while isotropy is the property of looking the same in every direction. The Universe is clearly not exactly homogeneous, so cosmologists define homogeneity in an average sense: the Universe is taken to be identical in different places when one averages over sufficiently large pieces. There is quite good observational evidence that the Universe does have these properties, although this evidence is not completely watertight. One piece of evidence is the observed near-isotropy of the cosmic microwave background radiation. Isotropy, however, does not necessarily imply homogeneity without the additional assumption that the place which we, as observers, occupy in the Universe is in no way special<sup>1</sup>: the so-called *Copernican Principle*. Observed isotropy, together with the Copernican Principle, therefore implies the Cosmological Principle.

The strongest force of nature on large scales is gravity, so the most important part of a physical description of the Universe is a theory of gravity. The best candidate we have for this is Einstein’s General Theory of Relativity. However, Einstein’s theory of gravity was found to be too difficult to solve for an arbitrary distribution of matter while it is greatly simplified with the assumption of the Cosmological Principle.

The past cosmic expansion history is then recovered by solving the Einstein equations in the background of the homogeneous and isotropic universe. In this Chapter we provide basic tools to understand the expansion history of the universe.

---

<sup>1</sup>It is funny, then, that for the most part of the history of civilization it was believed that we occupy a very special location, usually the centre, in the scheme of things.

## 1.1 Friedmann equations

The equations of motion describing the dynamics of our universe can be derived solving the Einstein field equations:

$$G_{\mu\nu} = R_{\mu\nu} - \frac{1}{2}g_{\mu\nu}R = 8\pi GT_{\mu\nu} \quad (1.1)$$

where  $G_{\mu\nu}$  is the Einstein tensor,  $R_{\mu\nu}$  and  $R$  are the Ricci tensor and his contraction (the scalar curvature) respectively, both related to the space-time curvature and  $T_{\mu\nu}$  is the energy-momentum tensor which describes the content of matter and energy. The equations (1.1) are in general complicated non linear equations, but can have simple analytical solutions in presence of generic symmetries. Since our universe appears to be homogeneous and isotropic on large scales (that means, it follows the ‘‘Cosmological Principle’’, verified by observations [1, 2, 3]), it is possible to solve eqs (1.1) in the Friedmann-Lemaître-Robertson-Walker (FLRW) metric, which describes such a space-time:

$$ds^2 = g_{\mu\nu}dx^\mu dx^\nu = -dt^2 + a^2(t)d\sigma^2 \quad (1.2)$$

where  $g_{\mu\nu}$  is the metric tensor,  $a(t)$  is the scale factor, telling us how much the universe has expanded from the big bang to time the  $t$  (we put  $c = 1$ , like we will always do in the text, unless when the discussion needs it) and  $d\sigma^2$  is the time-independent metric of the 3-dimensional space with a constant curvature  $K$  :

$$d\sigma^2 = \gamma_{ij}dx^i dx^j = \frac{dr^2}{1 - Kr^2} + r^2(d\theta^2 + \sin^2 d\phi^2) . \quad (1.3)$$

Here  $K = -1, 0, +1$  corresponds to close, flat and open geometries, respectively.  $\gamma_{ij}$  is the 3-dimensional space metric tensor, whose diagonal elements, in polar coordinates  $(x_1, x_2, x_3) = (r, \theta, \phi)$  are  $\gamma_{11} = (1 - Kr^2)^{-1}$ ,  $\gamma_{22} = r^2$ ,  $\gamma_{33} = r^2 \sin^2 \theta$ . In eq. (1.2)  $\mu$  and  $\nu$  run on the time (0) and space (1,2,3) coordinates, whereas in eq. (1.3), the Latin indices  $i$  and  $j$  run only from 1 to 3. We follow Einstein’s convention that the terms with same upper and lower indices are summed over. In addition to the cosmic time  $t$ , we also introduce the conformal time  $\tau$  defined by

$$\tau \equiv \int \frac{1}{a} dt . \quad (1.4)$$

The metric in the conformal time is then given by

$$ds^2 = a^2(\tau)[-d\tau^2 + \frac{dr^2}{1 - Kr^2} + r^2(d\theta^2 + \sin^2 d\phi^2)] . \quad (1.5)$$

Once the metric is defined, we can obtain the Christoffel symbols through:

$$\Gamma_{\mu\nu}^\lambda = \frac{1}{2}g^{\lambda\eta}(g_{\mu\eta,\nu} + g_{\eta\nu,\mu} - g_{\mu\nu,\eta}) , \quad (1.6)$$

where  $g_{\alpha\nu,\lambda} \equiv \partial g_{\alpha\nu}/\partial x^\lambda$ ; note that  $g_{\mu\nu}$  satisfies the relation  $g^{\mu\alpha}g_{\alpha\nu} = \delta_\nu^\mu$  where  $\delta_\nu^\mu$  is Kronecker’s delta ( $\delta_\nu^\mu = 1$  for  $\mu = \nu$  and  $\delta_\nu^\mu = 0$  for  $\mu \neq \nu$ ). For the FLRW metric (1.2) the non-vanishing components of Christoffel symbols are

$$\Gamma_{ij}^0 = a^2 H \gamma_{ij}, \quad \Gamma_{0\nu}^\mu = \Gamma_{\nu 0}^\mu = H \delta_\nu^\mu, \quad (1.7)$$

$$\Gamma_{11}^1 = \frac{Kr}{1 - Kr^2}, \quad \Gamma_{22}^1 = -r(1 - Kr^2), \quad \Gamma_{33}^1 = -r(1 - Kr^2) \sin^2 \theta, \quad (1.8)$$

$$\Gamma_{33}^2 = -\sin \theta \cos \theta, \quad \Gamma_{12}^2 = \Gamma_{21}^2 = \Gamma_{13}^3 = \Gamma_{31}^3 = \frac{1}{r}, \quad \Gamma_{23}^3 = \Gamma_{32}^3 = \cot \theta, \quad (1.9)$$

where

$$H = \frac{1}{a} \frac{da}{dt} \quad (1.10)$$

called the Hubble parameter, describes the expansion rate of the universe, whereas we define the conformal Hubble function as

$$\mathcal{H} = \frac{1}{a} \frac{da}{d\tau} = aH(\tau). \quad (1.11)$$

The Christoffel symbols given in eqs (1.8) and (1.9) correspond to those for the three-dimensional metric (1.3) with the curvature  $K$ .

The Ricci tensor is defined by

$$R_{\mu\nu} = \Gamma_{\mu\nu,\sigma}^\sigma - \Gamma_{\mu\sigma,\nu}^\sigma + \Gamma_{\sigma\rho}^\rho \Gamma_{\mu\nu}^\sigma - \Gamma_{\sigma\mu}^\rho \Gamma_{\rho\nu}^\sigma, \quad (1.12)$$

while its contraction gives the Ricci scalar (scalar curvature)

$$R = g^{\mu\nu} R_{\mu\nu}. \quad (1.13)$$

The Ricci tensor and the scalar curvature are then

$$R_{00} = -3 \left( H^2 + \frac{dH}{dt} \right), \quad R_{0i} = R_{i0} = 0, \quad R_{ij} = a^2 \left( 3H^2 + \frac{dH}{dt} + \frac{2K}{a^2} \gamma_{ij} \right), \quad (1.14)$$

$$R = 6 \left( 2H^2 + \frac{dH}{dt} + \frac{K}{a^2} \right). \quad (1.15)$$

Using the relation  $G_\nu^\mu = g^{\mu\alpha} G_{\alpha\nu}$ , the Einstein tensor  $G_{\mu\nu} \equiv R_{\mu\nu} - \frac{1}{2} g_{\mu\nu} R$  is

$$G_0^0 = -3 \left( H^2 + \frac{K}{a^2} \right), \quad G_i^0 = G_0^i = 0, \quad G_j^i = - \left( 3H^2 + 2 \frac{dH}{dt} + \frac{K}{a^2} \right) \delta_j^i. \quad (1.16)$$

In the FLRW spacetime the energy-momentum tensor of the background matter is restricted to take the perfect fluid form

$$T_\nu^\mu = (p + \rho) u^\mu u_\nu + p \delta_\nu^\mu, \quad (1.17)$$

where  $u^\mu = (-1, 0, 0, 0)$  is the four-velocity of the fluid in comoving coordinates, and  $\rho$  and  $p$  are functions of  $t$ . The (00) and ( $ij$ ) components of  $T_\nu^\mu$  are  $T_0^0 = -\rho$  and  $T_j^i = p \delta_j^i$ . Then  $\rho$  and  $p$  have the meaning of an energy density and a pressure, respectively. Since

we are using the unit  $c = 1$ , the density  $\rho$  is not particularly distinguished from the energy density  $\rho c^2$ . From the (00) and (ii) components of the Einstein equations (1.1) we obtain

$$H^2 = \frac{8\pi G}{3}\rho - \frac{K}{a^2} \quad (1.18)$$

$$3H^2 + 2\frac{dH}{dt} = -8\pi Gp - \frac{K}{a^2}. \quad (1.19)$$

Eliminating the  $K/a^2$  term gives

$$\frac{1}{a} \frac{d^2 a}{dt^2} = -\frac{4\pi G}{3}(\rho + 3p). \quad (1.20)$$

Eqs (1.18) and (1.20) are called Friedmann equations. Using the conformal time (1.4) and the conformal hubble function (1.11), they can be written as

$$\mathcal{H}^2 = \frac{8\pi G a^2}{3}\rho - \frac{K}{a^2} \quad (1.21)$$

$$\dot{\mathcal{H}} = -\frac{4\pi a^2}{3}(\rho + 3p) \quad (1.22)$$

where the dot represents a derivative with respect to the conformal time  $\tau$ .

Multiplying eq. (1.18) by  $a^2$ , differentiating and using eq. (1.20) we find

$$\frac{d\rho}{dt} + 3H(\rho + p) = 0. \quad (1.23)$$

The Einstein tensor satisfies the Bianchi identities

$$G_{\nu;\mu}^{\mu} \equiv G_{\nu,\mu}^{\mu} + \Gamma_{\alpha\mu}^{\mu} G_{\nu}^{\alpha} - \Gamma_{\nu\mu}^{\alpha} G_{\alpha}^{\mu} = 0 \quad (1.24)$$

where the comma “,” stands for the usual derivative  $G_{\nu,\mu}^{\mu} = \partial G_{\nu}^{\mu}/\partial x^{\mu}$  and the symbol “; $\mu$ ” denotes the covariant derivative. From the Einstein equations (1.1) it follows that

$$T_{\nu;\mu}^{\mu} = 0 \quad (1.25)$$

which gives the same equation as (1.23) in the FLRW background. Hence eq. (1.23) is called the *conservation* or *continuity equation*. From eq. (1.18) we can compute the Gauss curvature,  $C_G$ , of the universe:

$$C_G \equiv \frac{K}{a^2} = \left(\frac{1}{a} \frac{da}{dt}\right)^2 \left(\frac{\rho}{\rho_{\text{cr}}} - 1\right), \quad (1.26)$$

where  $\rho_{\text{cr}}$ , defined as

$$\rho_{\text{cr}} \equiv \frac{3H^2}{8\pi G} \quad (1.27)$$

is called critical density. The universe is closed ( $C_G > 0$ ), flat ( $C_G = 0$ ) or open ( $C_G < 0$ ) according to the value of the density parameter

$$\Omega(t) \equiv \frac{\rho(t)}{\rho_{\text{cr}}(t)} \quad (1.28)$$

being greater, equal or less than 1, respectively (actually this is correct in the absence of a cosmological constant, as we will see). It is possible to define a density parameter for every component in the universe. For relativistic particles, non relativistic matter, dark energy and curvature we have, respectively

$$\Omega_r = \frac{8\pi G\rho_r(t)}{3H^2}, \quad \Omega_m = \frac{8\pi G\rho_m(t)}{3H^2}, \quad \Omega_{\text{DE}} = \frac{8\pi G\rho_{\text{DE}}(t)}{3H^2}, \quad \Omega_K = -\frac{K}{(aH)^2}. \quad (1.29)$$

We often refer to present values of the density parameters, where all the time dependent functions are computed at  $t = 0$ . In this case we write

$$\Omega_{r,0} = \frac{8\pi G\rho_{r,0}}{3H_0^2}, \quad \Omega_{m,0} = \frac{8\pi G\rho_{m,0}}{3H_0^2}, \quad \Omega_{\text{DE},0} = \frac{8\pi G\rho_{\text{DE},0}}{3H_0^2}, \quad \Omega_{K,0} = -\frac{K}{(a_0H_0)^2}. \quad (1.30)$$

We will use the subscript  $\gamma$  to identify electromagnetic radiation, rather than all the relativistic particles,  $c$  and  $b$  to distinguish between (cold) dark matter and baryons and  $\Lambda$  for the cosmological constant. Then, we can write eq. (1.18) as

$$\Omega_r + \Omega_m + \Omega_{\text{DE}} + \Omega_K = 1, \quad (1.31)$$

valid for every  $t$ . Observations constrain the present values of the density parameters to be:

$$\Omega_m \simeq 0.25, \quad \Omega_{\text{DE}} \simeq 0.75, \quad \Omega_r \simeq 10^{-4}, \quad \Omega_K \simeq 0, \quad (1.32)$$

like we will better see in the following. In particular, our universe seems to have a flat geometry, which means  $\Omega_K = K = 0$ .

## 1.2 Perfect fluid models

In order to understand the dynamics of the background in a specific cosmological model, we need to solve the Friedmann equations, which we rewrite here

$$H^2 = \frac{8\pi G}{3}\rho - \frac{K}{a^2} \quad (1.33)$$

$$\frac{1}{a} \frac{d^2 a}{dt^2} = -\frac{4\pi G}{3}(\rho + 3p) \quad (1.34)$$

together with the continuity equation

$$\frac{d\rho}{dt} + 3H(\rho + p) = 0. \quad (1.35)$$

The eqs (1.33), (1.34), (1.35) allow one to calculate the time evolution of  $a(t)$  as well as  $\rho(t)$  and  $p(t)$  if we know the equation of state, i.e. the relation between  $\rho$  and  $p$ . In many cases of physical interest, the appropriate equation of state can be cast, either exactly or approximately, in the form

$$p = w\rho c^2 \quad (1.36)$$

where we restore  $c$  for completeness, even if for practical purposes we will use the relation  $p = w\rho$ . For ordinary fluids the parameter  $w$  lies in the so-called Zel'dovich interval

$$0 \leq w \leq 1. \quad (1.37)$$

The case with  $w = 0$  represents *dust* (pressureless material). This is also a good approximation to the behaviour of any form of non-relativistic fluid or gas. Of course, a gas of particles at some temperature  $T$  does exert pressure but the typical thermal energy of a particle (of mass  $m_p$ ) is approximately  $k_B T$  ( $k_B$  is the Boltzmann constant), whereas its rest mass energy is  $m_p c^2$ , usually very much larger. The relativistic effect of pressure is usually therefore negligible. In more detail, an ideal gas of non-relativistic particles of mass  $m_p$ , temperature  $T$ , density  $\rho_m$  and adiabatic index  $\gamma_{ad}$  exerts a pressure

$$p = nk_B T = \frac{k_B T}{m_p c^2} \rho_m c^2 = \frac{k_B T}{m_p c^2} \frac{\rho c^2}{1 + \frac{k_B T}{(\gamma_{ad}-1)m_p c^2}} = w(T) \rho c^2 \quad (1.38)$$

where  $\rho c^2$  is the energy density; a non-relativistic gas has  $w(T) \ll 1$  (since  $m_p c^2 \gg k_B T$ ) and, according to Equation (1.38), will therefore be well approximated by a fluid of dust. At the other extreme, a fluid of non-degenerate, ultrarelativistic particles in thermal equilibrium has an equation of state of the type

$$p = \frac{1}{3} \rho c^2. \quad (1.39)$$

For instance, this is the case for a gas of photons. A fluid with an equation of state of the type (1.39) is usually called a radiative fluid, though it may comprise relativistic particles of any form. It is interesting to note that the parameter  $w$  is also related to the adiabatic sound speed of the fluid

$$c_s = \left( \frac{\partial p}{\partial \rho} \right)_S^{1/2} \quad (1.40)$$

where  $S$  denotes the entropy. In a dust fluid  $c_s = 0$  and a radiative fluid has  $c_s = c/\sqrt{3}$ . Note that the case  $w > 1$  is impossible, because it would imply that  $c_s > c$ . If  $w < 0$ , then it is no longer related to the sound speed, which would have to be imaginary. These two cases form the limits in (1.37). There are, however, physically important situations in which matter behaves like a fluid with  $w < 0$ , as we shall see later. For the moment let's restrict to the case where  $w$  is constant in time. We shall also assume that normal matter, described by an equation of state of the form (1.38), can be taken to have  $w(T) \simeq 0$ . From equations (1.36) with  $c = 1$  and (1.35) we can easily obtain the relation

$$\rho a^{3(1+w)} = \text{const.} = \rho_0 a_0^{3(1+w)} \quad (1.41)$$

In this equation and hereafter we use the suffix '0' to denote a reference time, usually the present. In particular we have, for a dust universe ( $w = 0$ ) or a matter universe described by (1.38),

$$\rho a^3 \equiv \rho_m a^3 = \rho_{m,0} a_0^3 \quad (1.42)$$

(which simply represents the conservation of mass) and for a radiative universe ( $w = 1/3$ )

$$\rho a^4 \equiv \rho_r a^4 = \rho_{r,0} a_0^3 \quad (1.43)$$

If one replaces the expansion parameter  $a$  with the redshift  $z = a^{-1} - 1$  (which will be better defined in the next section), one finds, for dust and non-relativistic matter,

$$\rho_m = \rho_{m,0} (1 + z)^3 \quad (1.44)$$

and, for radiation and relativistic matter,

$$\rho_r = \rho_{r,0} (1 + z)^4 . \quad (1.45)$$

Then the matter density scales, quite obviously, as the inverse of the volume ( $\rho_m \sim a^{-3}$ ). On the other hand, for relativistic particles there is an extra factor  $a$  due to the fact that also their wavelength is “stretched” by the expansion of the universe. Since the energy of the particles is inversely proportional to their wavelength, the total energy must decrease as the fourth power of the scale factor.

All the fluids whose equation of state parameter satisfies

$$w \geq -\frac{1}{3} \quad (1.46)$$

give, through eq. (1.20)

$$\frac{1}{a} \frac{d^2 a}{dt^2} \leq 0 , \quad (1.47)$$

thus a decelerating (or steady in case of equality) universe. Since we observe an accelerated expansion we need to obtain

$$\frac{1}{a} \frac{d^2 a}{dt^2} > 0 \quad (1.48)$$

which means we have to take into account a fluid with

$$w < -\frac{1}{3} . \quad (1.49)$$

So, if we assume the density  $\rho$  to be positive, we are invoking a fluid with negative pressure.

Let’s consider the peculiar case of  $w = -1$ ; then, from eq. (1.41), we simply have

$$\rho(z) = \rho_0 , \quad (1.50)$$

a fluid whose density always remains constant: this is the case of the “cosmological constant” which we will better study in Chapter 3.

Up to now we have only considered constant  $w$ , but we can also compute the evolution of a generic dark energy component with  $w = w(z)$ . In this case we have from eq. 1.35

$$\rho_{\text{DE}}(z) = \rho_{\text{DE},0} \exp \left\{ \int_0^z \frac{3(1 + w_{\text{DE}}(\bar{z}))}{1 + \bar{z}} d\bar{z} \right\} . \quad (1.51)$$

Using the definitions given in (1.29) and (1.30), we can also write down the evolutions of the density parameters:

$$\Omega_m(z) = \frac{8\pi G\rho_m(z)}{3H^2(z)} = \frac{8\pi G\rho_{m,0}(z)}{3H^2(z)}(1+z)^3 = \Omega_{m,0}(1+z)^3 \frac{H_0^2}{H^2} \quad (1.52)$$

and

$$\Omega_r(z) = \Omega_{r,0}(1+z)^4 \frac{H_0^2}{H^2}, \quad (1.53)$$

$$\Omega_{\text{DE}}(z) = \Omega_{\text{DE},0} \exp \left\{ \int_0^z \frac{3(1+w_{\text{DE}}(\bar{z}))}{1+\bar{z}} d\bar{z} \right\} \frac{H_0^2}{H^2}. \quad (1.54)$$

Now let's consider a universe whose components are all the fluids studied above (matter, radiation, dark energy) plus a curvature term. The Friedmann equation (1.18) can then be written as ( $a = (1+z)^{-1}$ )

$$H^2 = \frac{8\pi G}{3}(\rho_m + \rho_r + \rho_{\text{DE}}) - K(1+z)^2 \quad (1.55)$$

or, using the evolutions of density parameters

$$H^2(z) = H_0^2 \left[ \Omega_{m,0}(1+z)^3 + \Omega_{r,0}(1+z)^4 + \Omega_{\text{DE},0} \exp \left\{ \int_0^z \frac{3(1+w_{\text{DE}}(\bar{z}))}{1+\bar{z}} d\bar{z} \right\} + \Omega_{K,0}(1+z)^2 \right] \quad (1.56)$$

or equivalently

$$H^2(a) = H_0^2 \left[ \Omega_{m,0}a^{-3} + \Omega_{r,0}a^{-4} + \Omega_{\text{DE},0} \exp \left\{ \int_{a_0}^a -\frac{3(1+w_{\text{DE}}(\bar{a}))}{1+\bar{a}} d\bar{a} \right\} + \Omega_{K,0}a^{-2} \right]. \quad (1.57)$$

Let us remind that since  $H = a^{-1}da/dt$ , these equations are differential equations whose solution gives the evolution of the scale factor with time. In the simple cases when one fluid with constant  $w$  and density parameter  $\Omega_w$  dominates over the other components (which means  $\Omega_w \simeq 1$ ), we have

$$\frac{1}{a} \frac{da}{dt} = H_0 a^{-\frac{3}{2}(1+w)}, \quad (1.58)$$

which can be easily integrated to give

$$a \sim t^{\frac{2}{3(1+w)}} \rightarrow H(a) \sim a^{-\frac{3}{2}(1+w)}. \quad (1.59)$$

Then, in the cases of matter ( $w = 0$ ) or radiation ( $w = 1/3$ ) domination we have respectively

$$a \sim t^{\frac{2}{3}} \rightarrow H(a) \sim a^{-\frac{3}{2}}, \quad (1.60)$$

$$a \sim t^{\frac{1}{2}} \rightarrow H(a) \sim a^{-2}. \quad (1.61)$$

## 1.3 Hubble's law

In the 1920s Slipher and Hubble discovered that the observed wavelength  $\lambda_0$  of absorption lines in the spectra of distant galaxies is larger than the wavelength  $\lambda$  in the rest frame. Hubble argued that this could be due to a very simple reason: the universe was not steady but it was expanding. In fact, in an expanding Universe the wavelength is stretched in proportion to the scale factor. In order to quantify this effect, we introduce the redshift

$$z \equiv \frac{\lambda_0}{\lambda} - 1 = \frac{a_0}{a} - 1 \quad (1.62)$$

where the present epoch corresponds to  $z = 0$ . In the following we take the present scale factor  $a_0$  to be unity unless otherwise stated. As we go back to the past,  $z$  gets larger.

Any object in the universe has then a recessional velocity  $v$  due to the expansion. As long as this velocity is much smaller than the speed of light  $c$  we have  $\lambda_0 \simeq (1 + v/c)\lambda$  from the Doppler effect, giving

$$z \simeq \frac{v}{c}. \quad (1.63)$$

If we denote with  $\mathbf{x}$  the comoving distance from an observer (at the origin) to an object, then the physical distance  $\mathbf{r}$  in an expanding universe is given by  $\mathbf{r} = a(t)\mathbf{x}$ . The comoving distance is defined in a way that it always remains constant for objects moving with the Hubble flow. If an object possesses an additional velocity, taking the derivative of the equation  $\mathbf{r} = a(t)\mathbf{x}$ , with respect to  $t$ , we obtain

$$\frac{d\mathbf{r}}{dt} = H\mathbf{r} + a\frac{d\mathbf{x}}{dt}. \quad (1.64)$$

The velocity  $\mathbf{v}_H \equiv H\mathbf{r}$  appears because of the presence of the cosmic expansion while the velocity  $\mathbf{v}_p \equiv a d\mathbf{x}/dt$ , called *peculiar velocity*, describes the movement of an object with respect to the local Hubble flow. The speed of the object along the line of sight from the observer to the object is given by

$$v \equiv \frac{\frac{d\mathbf{r}}{dt} \cdot \mathbf{r}}{r} = Hr + \frac{\mathbf{v}_p \cdot \mathbf{r}}{r} \quad (1.65)$$

where  $r = |\mathbf{r}|$ . In most cases the peculiar velocity of galaxies does not exceed  $10^6$  m/s. Under the condition that the term  $\mathbf{v}_p \cdot \mathbf{r}/r$  is negligible relative to the term  $Hr$ , we obtain

$$v \simeq H_0 r, \quad (1.66)$$

which is the well known Hubble's law. Here we have replaced  $H$  for the present value  $H_0$ , which is justified in small redshift regions ( $z \ll 1$ ). In 1929, Hubble reported the law (1.66) by plotting the recessional velocity  $v$  versus the distance  $r$ . Even if his data were scarce and noisy, Hubble concluded correctly that the universe was expanding.

The Hubble constant  $H_0$  is usually written as

$$H_0 = 100h \text{ km sec}^{-1} \text{ Mpc}^{-1} \quad (1.67)$$

where

$$1 \text{ Mpc} = 3.08568 \times 10^{19} \text{ km} = 3.26156 \times 10^6 \text{ light years} \quad (1.68)$$

and  $h$  describes the uncertainty on the value  $H_0$ . The observations of the Hubble Key Project [4] constrain this value to be

$$h = 0.72 \pm 0.08 . \quad (1.69)$$

Using for the gravitational constant the value  $G = 6.67 \times 10^{-8} \text{ cm}^3 \text{ g}^{-1} \text{ sec}^{-2}$ , together with eqs (1.67), (1.68) we can compute the present value of the critical density in eq. (1.27)

$$\rho_{\text{cr},0} \equiv \frac{3H_0^2}{8\pi G} = 1.88h^2 \times 10^{-29} \text{ g cm}^{-3} . \quad (1.70)$$

We also define the Hubble time

$$t_H \equiv \frac{1}{H_0} = 9.78 \times 10^9 h^{-1} \text{ years} , \quad (1.71)$$

which is a rough measure of the age of the universe. The present Hubble radius is defined by

$$D_H \equiv \frac{c}{H_0} = 2998 h^{-1} \text{ Mpc} \quad (1.72)$$

which corresponds roughly to the largest scale we can observe now.

## 1.4 Cosmic distances

In this section we define the most important cosmic distances. They turn out to be very useful in order to discuss observational constraints on the cosmological models. In fact, a large part of the evidence for dark energy comes from measurements of cosmological distances that are directly related to observations in the FLRW spacetime (1.2). Setting  $r = \sin \chi$  ( $K = +1$ ),  $r = \chi$  ( $K = 0$ ) and  $r = \sinh \chi$  ( $K = -1$ ) in eq. (1.3), the 3-dimensional space line-element can be expressed as

$$d\sigma^2 = d\chi^2 + (f_K(\chi))^2(d\theta^2 + \sin^2 \theta d\phi^2) , \quad (1.73)$$

where

$$f_K(\chi) = \begin{cases} \sin \chi & (K = +1) \\ \chi & (K = 0) \\ \sinh \chi & (K = -1) . \end{cases} \quad (1.74)$$

### 1.4.1 Comoving distance

A ray of light travelling along the  $\chi$  direction satisfies the geodesic equation:  $ds^2 = -c^2 dt^2 + a^2(t) d\chi^2 = 0$ , where we have recovered the speed of light  $c$  for clarity. Let us consider the case in which light emitted at time  $t = t_1$  with  $\chi = \chi_1$  reaches an observer at

time  $t = t_0$  with  $\chi = 0$  (corresponding to  $z = 0$ ). Integrating the equation  $d\chi = -cdt/a(t)$ , the comoving distance reads

$$d_c \equiv \chi_1 = \int_0^{\chi_1} d\chi = - \int_{t_0}^{t_1} \frac{c}{a(t)} dt . \quad (1.75)$$

From Eq. (1.62) it follows that  $dt = -dz/[H(z+1)]$ . Then the comoving distance is given by

$$d_c = \frac{c}{a_0 H_0} \int_0^z \frac{d\bar{z}}{E(\bar{z})} , \quad (1.76)$$

where

$$E(z) \equiv \frac{H(z)}{H_0} . \quad (1.77)$$

The integral in eq. (1.76) can be expanded around  $z = 0$ :

$$\int_0^z \frac{d\bar{z}}{E(\bar{z})} = z - \frac{1}{2} \frac{dE(0)}{dz} z^2 + \frac{1}{6} \left[ 2 \left( \frac{dE(0)}{dz} \right)^2 - \frac{d^2 E(0)}{dz^2} \right] z^3 + \mathcal{O}(z^4) . \quad (1.78)$$

If the redshift  $z$  is much smaller than unity, the comoving distance is approximately given by

$$d_c \simeq \frac{c}{a_0 H_0} z, \quad z \ll 1 .$$

On using the relation (1.63), we find

$$v \simeq (a_0 H_0) d_c .$$

This shows that the recessional velocity  $v$  of the object is proportional to  $d_c$  with the proportionality constant  $a_0 H_0$ . For the physical distance  $r = a_0 d_c$  we find  $r \simeq (c/H_0) z \simeq v/H_0$ , which means that Hubble's law (1.66) is satisfied. Hubble's law written as in eq. (1.66) is valid therefore only in the low-redshift region  $z \ll 1$ . For  $z \gtrsim 1$  the higher-order terms in eq. (1.78) become important so that Hubble's law is subject to be modified.

### 1.4.2 Luminosity distance

The luminosity distance  $d_L$  is used in the observations of the Supernovae Ia, in order to link the supernova luminosity with the expansion rate of the Universe. It is defined by

$$d_L^2 \equiv \frac{L_s}{4\pi \mathcal{F}} . \quad (1.79)$$

where  $L_s$  is the absolute luminosity of a source and  $\mathcal{F}$  is an observed flux. Note that the observed luminosity  $L_0$  (detected at  $\chi = 0$  and  $z = 0$ ) is different from the absolute luminosity  $L_s$  of the source (emitted at the comoving distance  $\chi$  with the redshift  $z$ ). The flux  $\mathcal{F}$  is defined by  $\mathcal{F} = L_0/S$ , where  $S = 4\pi(a_0 f_K(\chi))^2$  is the area of a sphere at  $z = 0$ . Then the luminosity distance (1.79) yields

$$d_L^2 = (a_0 f_K(\chi))^2 \frac{L_s}{L_0} . \quad (1.80)$$

We need now to derive the ratio  $L_s/L_0$ . If we write the energy of light emitted at the time-interval  $\Delta t_1$  to be  $\Delta E_1$ , the absolute luminosity is defined by  $L_s = \Delta E_1/\Delta t_1$ . Similarly the observed luminosity is given by  $L_0 = \Delta E_0/\Delta t_0$ , where  $\Delta E_0$  is the energy of light detected at the time-interval  $\Delta t_0$ . Since the energy of a photon is inversely proportional to its wavelength  $\lambda$  we have that  $\Delta E_1/\Delta E_0 = \lambda_0/\lambda_1 = 1 + z$ , where we have used Eq. (1.62). Moreover, the constancy of  $c = \lambda/\Delta t$  implies  $\lambda_1/\Delta t_1 = \lambda_0/\Delta t_0$ , where  $\lambda_1$  and  $\lambda_0$  are the wavelength of light at the points of emission and detection respectively. This leads to the relation  $\Delta t_0/\Delta t_1 = \lambda_0/\lambda_1 = 1 + z$ . Hence we find

$$\frac{L_s}{L_0} = \frac{\Delta E_1}{\Delta E_0} \frac{\Delta t_0}{\Delta t_1} = (1 + z)^2. \quad (1.81)$$

From Eqs. (1.80) and (1.81) the luminosity distance reduces to

$$d_L = a_0 f_K(\chi)(1 + z). \quad (1.82)$$

It is clear that the luminosity distance is directly related to the expansion rate of the universe. In a flat universe ( $\Omega_K = 0$ ), with euclidean geometry, the luminosity distance is given by

$$d_L = \frac{c}{H_0}(1 + z) \int_0^z \frac{d\bar{z}}{E(\bar{z})}. \quad (1.83)$$

We can also explicit the dependence on the cosmological parameters using eq. (1.56)

$$d_L = \frac{c}{H_0}(1 + z) \int_0^z \frac{d\bar{z}}{\left[ \Omega_{m,0}(1 + \bar{z})^3 + \Omega_{r,0}(1 + \bar{z}) + \Omega_{DE,0} \exp \left\{ \int_0^z \frac{3(1+w_{DE}(\bar{z}))}{1+\bar{z}} d\bar{z} \right\} \right]}. \quad (1.84)$$

### 1.4.3 Angular diameter distance

The angular diameter distance  $d_A$  is defined by

$$d_A \equiv \frac{\Delta x}{\Delta \theta}, \quad (1.85)$$

where  $\Delta \theta$  is the angle that subtends an object of actual size  $\Delta x$  orthogonal to the line of sight. This distance is often used for the observations of CMB anisotropies. Since the source lies on the surface of a sphere with radius  $\chi$  with the observer at the centre, the size  $\Delta x$  at time  $t_1$  in the FLRW spacetime (1.2) with (1.73) is given by

$$\Delta x = a(t_1) f_K(\chi) \Delta \theta. \quad (1.86)$$

Hence the diameter distance is

$$d_A = a(t_1) f_K(\chi) = \frac{a_0 f_K(\chi)}{1 + z} \quad (1.87)$$

where we have used  $z = a_0/a(t_1) - 1$ . Comparing eq. (1.87) with Eq. (1.80), we notice the following relation

$$d_A = \frac{d_L}{(1 + z)^2}. \quad (1.88)$$

In the limit  $z \ll 1$  all the distances discussed above reduce to the Euclidean distance in the Minkowski spacetime.

## Suggested Readings



# Chapter 2

## What we know from observations

The combined analysis of data coming from different cosmic observables suggests that the universe where we live is spatially flat, with a low matter density and has an accelerated expansion. Unless otherwise specified, when we refer to matter we usually mean the sum of the baryonic matter and the cold dark matter (CDM) component, being the first only a small fraction of the total. In this chapter we take a look to the principal cosmological observables giving these bits of information about our universe.

### 2.1 Supernovae

Supernovae (SN) are extremely luminous stellar explosions causing a burst of radiation. They can be classified according to their absorption spectral lines at the luminosity peak. The ones lacking of prominent hydrogen lines are known as Type I supernovae, while those having lines associated to hydrogen and heavier elements in their spectra are Type II supernovae. The mechanism that creates a Type II supernova is the catastrophic collapse of the iron core of a massive star, which has completed the nuclear production of heavier and heavier elements, up to the iron. This collapse generates a shock wave and the ensuing ejection of the star's envelope. Type I supernovae can be further classified as Type Ia, if the spectrum contains an absorption line of singly ionized silicon, Type Ib if it contains a line of helium, whereas Type Ic lacks the lines of both silicon and helium. It is believed that Type Ib and Ic are created by similar mechanisms to those of Type II while the explosion of Type Ia occurs when the mass of a white dwarf in a binary system exceeds the Chandrasekhar limit ( $\sim 1.4$  solar masses) by absorbing gas from the companion star. The most important feature of SN Ia, which makes them so important for cosmology, is that their absolute luminosities are almost constant at the peak of brightness, so the distance to a SN Ia can be determined by measuring its observed (apparent) luminosity. Thus the SN Ia is a kind of “standard candle” by which luminosity distance can be measured observationally. In reality things are more complicated than this simple view. The intrinsic spread in absolute magnitudes is actually too large to produce stringent cosmological constraints. However, at the end of the 1990s, a high-quality sample of “local” (i.e.  $z \ll 1$ ) supernovae allowed the absolute magnitude to be correlated with the width of the light curve [5]: brighter supernovae have a broader light

curve. By measuring at the same time the apparent magnitude and the light curve it is possible therefore to predict the absolute magnitude. Although in the following we refer to a universal SN Ia absolute magnitude, we always mean the magnitude corrected for the light curve width. Then, since the (corrected) peak absolute magnitude  $M$  is the same for any SN Ia under the assumption of standard candles we can determine the luminosity distance of a supernova by measuring its apparent magnitude,  $m$ , and using the relation

$$m = M + 25 + 5 \log_{10} d_L(z) , \quad (2.1)$$

where the distance is expressed in Megaparsec. The redshift  $z$  of the corresponding SN Ia can be found by measuring the wavelengths of the spectral lines in the supernova light or in the spectrum of its host galaxy. The observations of many SN Ia provide the dependence of the luminosity distance  $d_L$  in terms of  $z$  and thus the  $m - z$  relation. Comparing observational data with the theoretical distance (1.84), it is possible to reconstruct the expansion history of the Universe for the redshift  $z \lesssim \mathcal{O}(1)$  and put constraints on the cosmological parameters. Qualitatively: from eq. (1.84) we see that if in the universe it is present a negative pressure component ( $w_{\text{DE}} < 0$ ),  $d_L(z)$  gets larger. In other words, the effect of a fluid accelerating the expansion rate of the universe should place the SN more distant than in a non-accelerated universe so they should appear dimmer (i.e. with larger  $m$ ). And this is actually what Riess *et al.* [High-redshift Supernova Search Team (HSST)] [6] and Perlmutter *et al.* [Supernova Cosmology Project (SCP)] [7] independently reported in 1998 through the statistical analysis of nearby and distant SN Ia. Since observational data are prone to statistical and systematic errors, a few data are not enough to conclude that the present Universe is accelerating. Using 42 high-redshift SN Ia at redshifts between 0.18 and 0.83 together with 18 low-redshift SN Ia data from the Calan/Tololo Supernova Survey, Perlmutter *et al.* showed that the cosmological constant is present with 99% probability (see Fig. 2.1). After 1998 more SN Ia data have been collected by a number of high-redshift surveys, including SuperNova Legacy Survey (SNLS), Hubble Space Telescope (HST), and ‘Equation of State: SupErNovae trace Cosmic Expansion’ (ESSENCE) survey. The data from HST survey have been classified as the ‘Gold’ data sets. While the SN Ia data alone are not yet sufficient to place tight bounds on  $w_{\text{DE}}$ , Fig. 2.2 clearly shows the presence of dark energy responsible for the late-time cosmic acceleration ( $w_{\text{DE}} < -1/3$ ). Furthermore, combining them with data coming from other observables such as the CMB or the baryonic acoustic oscillations (BAO) it is possible to put tighter constraint on  $w_{\text{DE}}$  (assumed constant) as shown in Fig. 2.3.

## 2.2 The age of the universe

Another interesting piece of evidence for the existence of a dark energy emerges when we compare the age of the universe ( $t_0$ ) to the age of the oldest stellar populations ( $t_s$ ). For consistency we of course require  $t_0 > t_s$ , but it is difficult to satisfy this condition for a flat cosmological model with a normal form of matter as we will see below. Remarkably, the presence of dark energy can solve this age problem.

First we briefly mention the ages of the oldest stellar objects that have been constrained by a number of groups. For example, Jimenez *et al.* [13] determined the age of Globular clusters in the Milky Way to be  $13.5 \pm 2$  Gyr by using a distance-independent method whereas Carretta *et al.* [14] obtained the value  $12.9 \pm 2.9$  Gyr. Using the white dwarfs cooling sequence method, Richer *et al.* [15] and Hansen *et al.* [16] constrained the age of the globular cluster M4 to be  $12.7 \pm 0.7$  Gyr. Then the age of the universe needs to satisfy the lower bound:  $t_0 > 11 - 12$  Gyr. As we have seen in eq. (1.71), the inverse of the Hubble constant  $H_0$  is a rough measure of the age  $t_0$  of the Universe. Here we shall compute  $t_0$  more precisely and compare it with the age of the oldest stars.

Taking into account radiation, non-relativistic matter, and dark energy as components of the Universe, eq. (1.56) gives the Hubble parameter  $H(z)$  normalized by  $H_0$

$$E(z) = [\Omega_{m,0}(1+z)^3 + \Omega_{r,0}(1+z) + \Omega_{\text{DE},0}(1+z)^{3(1+w_{\text{DE}})} + \Omega_{K,0}(1+z)^2]^{1/2} \quad (2.2)$$

where, for simplicity we assumed that the equation of state of dark energy is a constant, in which case we have  $\rho_{\text{DE}} = \rho_{\text{DE}}(0)(1+z)^{3(1+w_{\text{DE}})}$  from eq. (1.51). From the definition of the Hubble function (1.10), the age of the universe can be expressed as

$$t_0 = \int_0^{t_0} dt = \int_0^{a_0} \frac{da}{a \cdot H(a)} = H_0^{-1} \int_0^\infty \frac{dz}{E(z)(1+z)}, \quad (2.3)$$

where in the last equality we used  $a = (1+z)^{-1}$ . It is a good approximation to neglect the contribution from radiation when we evaluate the integral in eq. (2.3), since at present time  $\Omega_{r,0} \simeq 10^{-4} - 10^{-5}$  and the radiation dominated period is much shorter than the total age of the universe. In other words, the contribution coming from the region  $z \gtrsim 1000$  hardly affects the total integral. In order to simplify the computation, let us consider the case of the cosmological constant ( $w_{\text{DE}} = -1$ ). Then the age of the Universe is given by

$$t_0 = H_0^{-1} \int_1^\infty \frac{dx}{x[\Omega_{m,0}x^3 + \Omega_{\text{DE},0} + \Omega_{K,0}x^2]^{1/2}} \quad (2.4)$$

where  $x = 1+z$  and  $\Omega_{m,0} + \Omega_{\text{DE},0} + \Omega_{K,0} = 1$ . For the flat Universe ( $\Omega_{K,0} = 0$ ), eq. (2.4) is integrated to give

$$t_0 = \frac{H_0^{-1}}{3\sqrt{1-\Omega_{m,0}}} \ln \left( \frac{1 + \sqrt{1-\Omega_{m,0}}}{1 - \sqrt{1-\Omega_{m,0}}} \right), \quad (2.5)$$

where we have used the relation  $\Omega_{m,0} + \Omega_{\text{DE},0} = 1$ . In the limit  $\Omega_{\text{DE},0} \rightarrow 0$  we have

$$t_0 = \frac{2}{3} H_0^{-1}. \quad (2.6)$$

From eq. (1.71) we have

$$H_0^{-1} = 9.78 h^{-1} \text{ Gyr}; \quad (2.7)$$

on using this value together with  $h = 0.72 \pm 0.08$ , the age of the Universe in the absence of the cosmological constant is in the range  $8.2 \text{ Gyr} < t_0 < 10.2 \text{ Gyr}$ , which does not satisfy

the stellar age bound  $t_0 > 11 - 12$  Gyr. Hence, a flat universe without a cosmological constant suffers from a serious age problem.

In an open universe model ( $\Omega_{m,0} < 1$  and  $\Omega_{K,0} > 0$ ), it is also possible to make the cosmic age larger than  $(2/3)H_0^{-1}$  even in the absence of dark energy. Setting  $\Omega_{DE,0} = 0$  in eq. (2.4), we have

$$t_0 = \frac{H_0^{-1}}{1 - \Omega_{m,0}} \left[ 1 + \frac{\Omega_{m,0}}{2\sqrt{1 - \Omega_{m,0}}} \ln \left( \frac{1 - \sqrt{1 - \Omega_{m,0}}}{1 + \sqrt{1 - \Omega_{m,0}}} \right) \right], \quad (2.8)$$

where  $\Omega_{m,0} + \Omega_{k,0} = 1$ . In the limit  $\Omega_{m,0} \rightarrow 1$  we recover the value (2.6) in the flat Universe. Meanwhile, in the limit  $\Omega_{m,0} \rightarrow 0$ , we have a larger value:  $t_0 = H_0^{-1}$ . However, the observations of the CMB constrain the curvature to be very close to flat (see next section), i.e.  $|\Omega_{K,0}| = |\Omega_{m,0} - 1| \ll 1$ . Then, since  $\Omega_{m,0} \sim 1$ , it is not possible to satisfy the condition  $t_0 > 11$  Gyr for  $h = 0.72 \pm 0.08$  in the open Universe without dark energy.

The problem can easily be solved in a flat universe with a cosmological constant ( $\Omega_\Lambda \neq 0$ ), or dark energy with an equation of state  $w_{DE}$  close to  $-1$ . In this case eq. (2.4) gives

$$\begin{aligned} t_0 &= H_0^{-1} \int_0^\infty \frac{dz}{(1+z)\sqrt{\Omega_{m,0}(1+z)^3 + \Omega_{\Lambda,0}}} = \\ &= \frac{2}{3\sqrt{\Omega_{\Lambda,0}}} \ln \left( \frac{1 + \sqrt{\Omega_{\Lambda,0}}}{\sqrt{\Omega_{m,0}}} \right), \end{aligned} \quad (2.9)$$

where  $\Omega_{m,0} + \Omega_{\Lambda,0} = 1$ . Eq. (2.9) shows that  $t_0$  gets larger for decreasing  $\Omega_{m,0}$ . In the limit  $\Omega_{m,0} \rightarrow 0$  we have  $t_0 \rightarrow \infty$ . In order to satisfy the condition  $t_0 > 11$  Gyr we require that  $0 < \Omega_{m,0} < 0.55$ . The WMAP 7-year constraint on the cosmic age (assuming the  $\Lambda$ CDM model) is given by  $t_0 = 13.75 \pm 0.13$  [17].

Thus the presence of dark energy elegantly solves the age-crisis problem.

## 2.3 Cosmic microwave background

The curvature of the universe (as well as other important cosmological parameters) can be measured by the cosmological observable at the highest redshift: the Cosmic Microwave Background Radiation (CMB).

In order to understand its origin let's begin by considering a suitably early time, say when the Universe was one millionth of its present size. We can consider the primordial universe as a fluid of photons, electrons and protons in thermal equilibrium. At that time the temperature would have been about 3,000,000 K. Such a temperature was high enough that the typical energy of a photon in the thermal distribution was considerably more than the ionization energy of hydrogen atoms (13.6 eV), so atoms would not have been able to exist at that epoch; any electron trying to bind to a proton would immediately be blasted away again by collision with a photon of light. The Universe at that time was therefore a sea of free nuclei and electrons, and since photons interact strongly with free electrons (via Thomson scattering), the mean free path of any photon was short.

As the Universe expanded and cooled, the photons of light lost energy and became less and less able to ionize any atoms that form. Eventually all the electrons found their way into the ground state of hydrogen atoms and the photons were no longer able to interact at all. Over a short interval of time, the Universe suddenly switched from being opaque to being completely transparent. The photons were then able to travel unimpeded for the entire remainder of the Universe's evolution. This process is known as *decoupling*.

At the decoupling time the temperature was about  $T \simeq 3000$  K. Since the CMB was originated in an epoch when matter and radiation were almost in equilibrium we expect it to have a black-body spectrum, which is in fact what has been largely verified by observations. The distribution of matter at that time is then impressed on the CMB. The total energy density  $\rho_r$  of radiation at temperature  $T$  can then be found by integrating the energy density over the black-body distribution, obtaining

$$\rho_r = \sigma T^4, \quad (2.10)$$

where  $\sigma$  is the Stefan–Boltzmann constant. We know from eq. (1.43) that  $\rho_r \sim a^{-4}$  then

$$T \sim a^{-1}, \quad (2.11)$$

which mathematically expresses the fact that the universe cools while expands. Today the CMB presents a temperature of 2.73 K. Comparing this value to the decoupling temperature and using eq. (2.11) we conclude that decoupling happened when the Universe was about one-thousandth of its present size, with  $a_{\text{dec}} \simeq 1/1090$  assuming we have normalized  $a(t_0) = 1$ . The corresponding redshift is  $z \simeq 1090$ .

As a first approximation the CMB can be considered homogeneous and isotropic and we can assume that it comes from a spherical shell around us, called last scattering surface, whose radius is the maximum distance that photons have travelled since when they decoupled from matter. But, if at  $z \simeq 1090$  there were primordial perturbations in the homogeneity of matter density, generated by quantum effects during inflation (as stated by the theories of structure formation), their effect on the microwave background takes the form of anisotropies in the radiation temperature and polarization. These anisotropies are divided into two sorts: primary anisotropies, due to the inhomogeneity in matter density on the last scattering surface (Sachs-Wolfe effect, adiabatic effects...), and secondary anisotropies, due to effects such as interactions with hot gas or gravitational potentials, between the last scattering surface and the observer (integrated Sachs-Wolfe effect, Sunyaiev-Zel'dovich effect) and are on much smaller physical scales with respect to the primary anisotropies. Let us consider the origin of the primary anisotropies. In the primordial universe the effect of the competition between gravity and radiation pressure in the fluid leads to the formation of perturbations in the matter and radiation densities, in the form of acoustic oscillations on scales smaller than the combined Jeans length of matter and radiation, otherwise they would collapse into structures (see Chapter 5 for more details). This length then gives the maximum scale on which these perturbations can be detected and corresponds to an angular scale of about  $1^\circ$  (roughly speaking, a spatial inhomogeneity in the CMB temperature of wavelength  $\lambda$  appears as an angular anisotropy of scale  $\theta \approx \lambda/d_A(z)$ , where  $d_A(z)$  is the comoving angular diameter distance

from the observer to redshift  $z$ ). At the decoupling these oscillations were “frozen” in the CMB and today are detected as temperature fluctuations.

As the cosmological principle is not exact at all scales, it had long been expected that anisotropies must exist in the microwave background radiation at some level. In practice, they proved extremely hard to detect, and it was not until 1992 that they were measured by the DMR (Differential Microwave Radiometer) experiment on the COBE satellite. The temperature fluctuations turned out to be

$$\frac{\Delta T}{T} \sim 10^{-5} . \quad (2.12)$$

Since these anisotropies  $\Delta T(\theta, \varphi)$  are present on a spherical surface, they can be expanded in a base of spherical harmonics

$$\Delta T(\theta, \varphi) = \sum_{\ell, m} a_{\ell m} Y_{\ell m}(\theta, \varphi) , \quad (2.13)$$

i.e. in multipoles. A multipole  $\ell$  corresponds to fluctuations of angular scale approximately equal to  $\theta = \pi/\ell$ . For instance,  $\ell = 1$ , the dipole, gives the temperature fluctuation averaged over hemispheres and  $\ell = 2$ , the quadrupole term, corresponds to features that extends over  $90^\circ$ . The acoustic peak at  $\sim 1^\circ$  will then appear at a multipole of  $\ell \sim 180$ . A better estimation of the angular scale of the first acoustic peak gives actually  $\ell \sim 220$ .

The coefficients  $a_{\ell m}$  tell us the size of the irregularities on different scales. As with the galaxy distribution, to compare with theory we are interested only in the statistical properties of these coefficients, quantified by the *radiation angular power spectrum*, now known universally by the notation  $C_\ell$  and defined by

$$C_\ell = \langle |a_{\ell m}|^2 \rangle . \quad (2.14)$$

If we plot the power spectrum as a function of the multipoles  $\ell$ , then we expect a peak for  $\ell \sim 220$ . This peak corresponds to the *acoustic horizon* scale, that is the maximum distance that a wave of pressure can cover from the beginning of the universe to the decoupling. However, the acoustic horizon is subtended by an angular scale of  $1^\circ$  only in flat universe, while the angle is larger (smaller) in an open (closed) universe. Then the angular scale of the first peak, or equivalently its multipole  $\ell$ , is related to the geometry of the universe. In a rough estimation we can use the formula

$$\ell \approx \frac{220}{\sqrt{1 - \Omega_k}} , \quad (2.15)$$

frequently used in the literature (but which should be corrected for  $\Lambda$ -dominated universes [18]). The first accurate measurement of the acoustic peak in the  $C_\ell$  was that of BOOMERANG ([19]). Those data so as the following from several experiments (WMAP, COBE, ...) constrain the geometry to be nearly spatially flat (in fact, from Fig. 2.4, we see that the first peak is around  $\ell = 220$ ).

## 2.4 Matter density

The consensus for a low-matter-density universe ( $\Omega_{m,0} < 1$ ) has been building slowly in the last two decades. The universe's matter density is currently the best-studied of the cosmological parameters, and its determination is supported by a number of independent measurements. We won't go into details on how the matter density parameter is determined both because there are a lot of different methods to do that and because the mathematical tools to understand these methods will be developed in Chapters 5 and 6. Just to cite a few of them, the value of  $\Omega_{m,0}$  can be determined through the study of the galaxy clusters abundance and its evolution, the mass power spectrum and the baryonic acoustic oscillations. But the most important thing to say is that although each observation has its strengths, weaknesses and assumptions, they all indicate that  $\Omega_{m,0} < 1$  and, in particular it is remarkable that a single value of  $\Omega_{m,0}$ ,  $\Omega_{m,0} \sim 0.25$  is consistent with so many, diverse observations. Now let us put together all the pieces of information coming from the observables we have seen so far. Since the CMB power spectrum is consistent with a flat universe ( $\Omega_{\text{tot}} = 1$ ), the fact that  $\Omega_{m,0} \sim 0.25$  forces us to assume the existence of another fluid whose density parameter is  $\sim 0.75$  and which should then be responsible for the observed acceleration of the expansion. Furthermore Fig. 2.3 suggests that the equation of state of such a fluid is  $w \sim 1$ . All these data found agreement in the so called *concordance model*, the  $\Lambda$ CDM already mentioned, as one can see in Fig. 2.5.

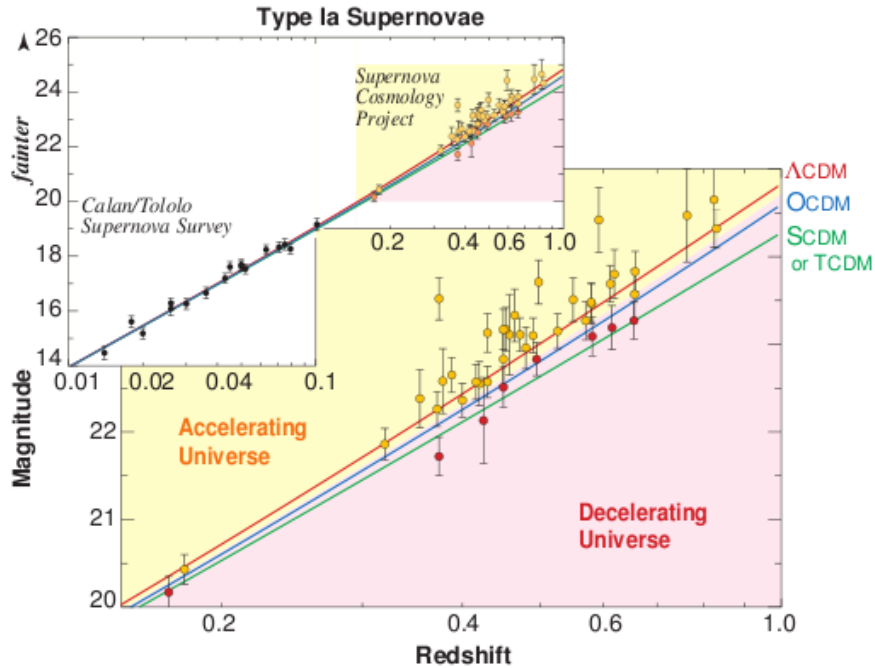


Figure 2.1: [8] The relation of observed brightness (in logarithmic units of magnitude) vs. redshift for Type Ia supernovae observed at low redshift by the Calan-Tololo Supernova Survey and at high redshift by the Supernova Cosmology Project is presented (with  $1\sigma$  error bars) and compared with model expectations. (Brighter is down and dimmer is up.) Several models are considered: an open model (OCDM), with  $\Omega_{m,0} = 1/3$ ,  $\Omega_{\Lambda,0} = 0$ ,  $\Omega_{k,0} = 2/3$ , a standard model (SCDM), with  $\Omega_{m,0} = 1$ ,  $\Omega_{\Lambda,0} = 0$ ,  $\Omega_{k,0} = 0$  and the  $\Lambda$ CDM model with  $\Omega_{m,0} = 1/3$ ,  $\Omega_{\Lambda,0} = 2/3$ ,  $\Omega_{k,0} = 0$ . The strong gravitational pull exerted by  $\Omega_{m,0} = 1$  models (such as Tcdm or Scdm), decelerates the expansion rate of the universe and produces an apparent brightening of high red shift SNIa, whereas the effect of a cosmological constant accelerating the expansion rate (as in  $\Lambda$ CDM) is seen as a relative dimming of the distant SNIa caused by their larger distances. The lower-right plot shows a close-up view of the expected deviations between the three models as a function of red shift. The background colour (and shading of the data points) indicates the region for which the universe's expansion would accelerate (yellow) or decelerate (red) for  $\Omega_{m,0} \sim 0.2$ . Similar results are found by the HZS team [6], as discussed in the text. The results provide evidence for an accelerating expansion rate.

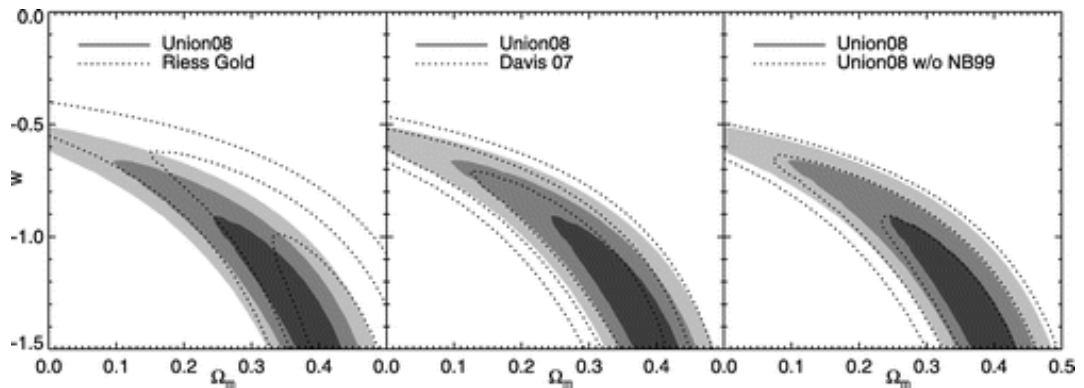


Figure 2.2: [9] Probability regions at at 68.3%, 95.4%, and 99.7% on  $\Omega_{m,0}$  and  $w$ . The results from the Union set are shown as filled contours. The empty contours in the left column represent the Gold sample (Riess et al. 2004, 2007 [10, 11]), and the middle column the constraints from Davis et al. 2007 [12]. The right column shows the impact of the SCP Nearby 1999 data.

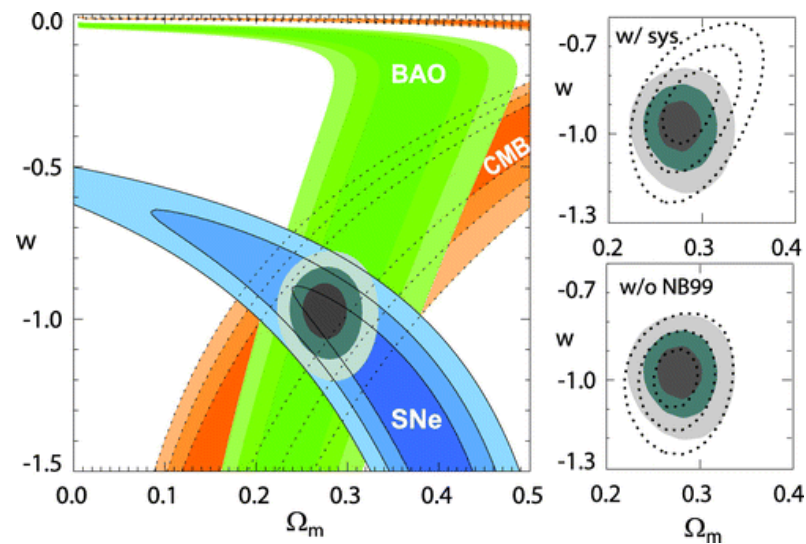


Figure 2.3: [9] Contours at 68.3%, 95.4%, and 99.7% probability level on  $w$  and  $\Omega_{m,0}$ , for a flat universe. The plot shows the individual constraints from CMB, BAO, and the Union SN set, as well as the combined constraints.

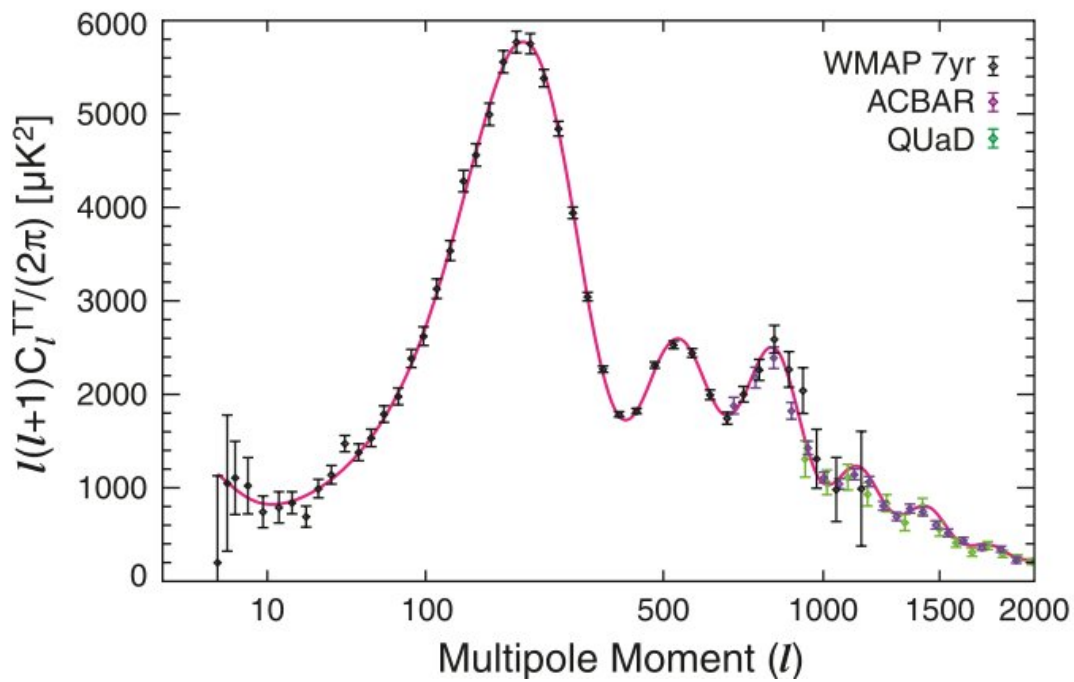


Figure 2.4: The WMAP 7-year temperature power spectrum (Larson et al. 2010 [20]), along with the temperature power spectra from the ACBAR (Reichardt et al. 2009 [21]) and QUaD (Brown et al. 2009 [22]) experiments. The solid line shows the best-fitting 6-parameter flat  $\Lambda$ CDM model to the WMAP data alone.

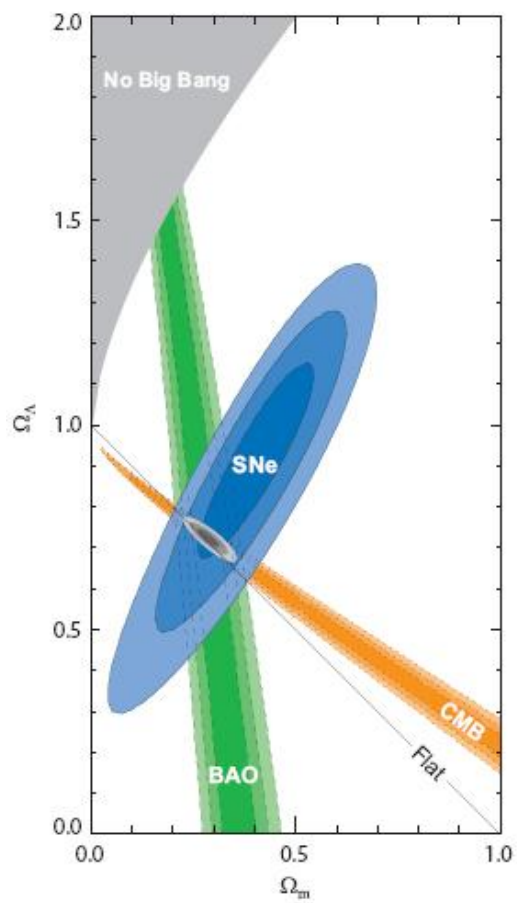


Figure 2.5: [9] Contours at 68.3%, 95.4%, and 99.7% probability level on  $\Omega_{m,0}$  and  $\Omega_{\Lambda,0}$  obtained from CMB, BAO, and the Union SN set, as well as their combination (assuming  $w = -1$ ).



# Chapter 3

## The cosmological constant

As we have seen in the previous chapter, the  $\Lambda$ CDM model has been systematically proved consistent with a large number of observations. The cosmological constant, so called because its energy density is constant in time and space, therefore appears as the simplest candidate for dark energy. However, despite its simplicity, a series of theoretical objections against this interpretation of the acceleration have arisen during the years. In this chapter we give a brief review on the history of the cosmological constant and the problems to it associated.

### 3.1 History of the cosmological constant

Einstein constructed General Relativity in 1915–1916 [23] and then he tried to apply his theory to the Universe in 1917 [24]. At that time Einstein believed that the Universe was static but it is obvious from eq. (1.20) that the scale factor  $a$  can dynamically change in time unless one sets  $H = 0$  and  $a^{-1}d^2a/dt^2 = 0$  in eqs (1.18), (1.20) which gives

$$\rho = -3p = \frac{3K}{8\pi G a^2}. \quad (3.1)$$

Eq. (3.1) shows that either  $\rho$  or  $p$  needs to be negative, but since Einstein considered that the above solution was not physical he introduced the cosmological constant to the original field equations to realize a static Universe. The field equations with this new term read

$$R_{\mu\nu} - \frac{1}{2}g_{\mu\nu}R + \Lambda g_{\mu\nu} = 8\pi G T_{\mu\nu} \quad (3.2)$$

and they can be derived from the action

$$S = \frac{1}{16\pi G} \int d^4x \sqrt{-g} (R - 2\Lambda) + S_m \quad (3.3)$$

This generalization is made possible because the Einstein tensor  $G_{\nu}^{\mu}$  and the energy momentum tensor  $T_{\nu}^{\mu}$  satisfy the Bianchi identities  $G_{\nu;\mu}^{\mu} = 0$  and the energy conservation  $T_{\nu;\mu}^{\mu} = 0$ . Since the metric  $g^{\mu\nu}$  is constant with respect to covariant derivatives ( $g^{\mu\nu}_{;\nu} = 0$ ),

there is a freedom to add a term  $\Lambda g_{\mu\nu}$  in the Einstein equations. Solving eqs (3.2) in the FLRW metric (1.2) gives

$$H^2 = \frac{8\pi G}{3}\rho - \frac{K}{a^2} + \frac{\Lambda}{3} \quad (3.4)$$

$$\frac{1}{a} \frac{d^2 a}{dt^2} = -\frac{4\pi G}{3}(\rho + 3p) + \frac{\Lambda}{3}. \quad (3.5)$$

This clearly demonstrates that the cosmological constant contributes negatively to the pressure term and hence works as a repulsive force against gravity at the background level. In the Universe dominated by a pressureless matter ( $p = 0$ ), we find that the static Universe ( $da/dt = d^2a/dt^2 = 0$ ) corresponds to

$$\rho = \frac{\Lambda}{4\pi G}, \quad \frac{K}{a^2} = \Lambda.$$

This equation shows that the density  $\rho$  in the Universe is determined by  $\Lambda$ . Since  $\rho > 0$  we require that  $\Lambda$  is positive. In order to understand the energy scale of  $\Lambda$  let us derive the Poisson equation from eq. (3.2). By taking the trace of eq. (3.2), we find that  $-R = -4\Lambda + 8\pi GT$  which, inserted again in eq. (3.2) gives

$$R_{\mu\nu} - \Lambda g_{\mu\nu} = 8\pi G \left( T_{\mu\nu} - \frac{1}{2} T g_{\mu\nu} \right). \quad (3.6)$$

Let us consider Newtonian gravity with metric  $g_{\mu\nu} = \eta_{\mu\nu} + h_{\mu\nu}$ , where  $h_{\mu\nu}$  is the perturbation around the Minkowski metric  $\eta_{\mu\nu}$ . If we neglect the time-variation and rotational effect of the metric,  $R_{00}$  can be written by a gravitational potential  $\Phi$  as  $R_{00} \simeq -(1/2)\Delta h_{00} = \Delta\Phi$ . Note that in a weak gravitational field we have  $g_{00} = -1 - 2\Phi$ . In the relativistic limit with  $|p| \ll \rho$ , we have  $T_{00} \simeq -T \simeq \rho$ . Then the 00 component of eq. (3.6) gives

$$\Delta\Phi = 4\pi G\rho - \Lambda. \quad (3.7)$$

In order to reproduce the Poisson equation in Newtonian gravity, we require that  $\Lambda = 0$  or  $\Lambda$  is sufficiently small relative to the  $4\pi G\rho$  term in eq. (3.7). Since  $\Lambda$  has dimensions of  $[\text{Length}]^{-2}$ , the scale corresponding to the cosmological constant needs to be much larger than the scale of stellar objects on which Newtonian gravity works well. In other words, the cosmological constant becomes important on very large scales.

The requirement of a cosmological constant to achieve a static universe can be understood by having a look at the Newton's equation of motion (3.5). Since gravity pulls particle towards the centre of the matter distribution with density  $\rho$ , we need a repulsive force to realize a situation in which  $a$  is a constant. This corresponds to adding a cosmological constant term  $\Lambda/3$  on the right hand side of (3.5).

In 1929 Hubble found the first direct quantitative evidence for the expansion of the Universe by combining his measurements of galaxy distances with Slipher's measurements of the redshifts associated with the galaxies [25]. In an expanding universe the cosmological constant did not have any reason to exist anymore. In the book "The Meaning of Relativity" written by Einstein in 1945 [26], he stated that "if Hubble's expansion had been

discovered at the time of the creation of the general theory of relativity, the cosmological member (the cosmological constant) would never have been introduced.” In 1970 Gamov [27] recalls that “when I was discussing cosmological problems with Einstein, he remarked that the introduction of the cosmological term was the biggest blunder he ever made in his life.” Since then, however,  $\Lambda$  has not died but has been the subject of much interest and serious study on both conceptual and observational grounds. Moreover, in spite of Einstein’s regret, the cosmological constant returned at the end of the century to attract more and more interest because it can account for the late-time cosmic acceleration.

In order to understand why, let’s define the modified energy density and pressure

$$\tilde{\rho} = \rho + \frac{\Lambda}{8\pi G}, \quad \tilde{p} = p - \frac{\Lambda}{8\pi G}, \quad (3.8)$$

which, inserted in eqs (3.4), (3.5) give equations of motion with the same form of eqs (1.18), (1.20):

$$H^2 = \frac{8\pi G}{3}\tilde{\rho} - \frac{K}{a^2} \quad (3.9)$$

$$\frac{1}{a} \frac{d^2 a}{dt^2} = -\frac{4\pi G}{3}(\tilde{\rho} + 3\tilde{p}). \quad (3.10)$$

In an empty universe ( $p = \rho = 0$ ), the definitions (3.8) can be regarded as the density and pressure of the cosmological constant that can be then considered as an additional perfect fluid contributing to the matter energy budget, instead that as a simple geometrical term. Conceptually this corresponds to shift the term  $\Lambda g_{\mu\nu}$  from the left to the right-hand side of eq. (3.2). Then the equation of state of the cosmological constant reads

$$\tilde{p} = -\tilde{\rho} = -\frac{\Lambda}{8\pi G} \quad (3.11)$$

and

$$w = \frac{\tilde{p}}{\tilde{\rho}} = -1, \quad (3.12)$$

as we already mentioned. Since eqs (3.11), (3.12) are obtained in the absence of any “ordinary” fluid, the cosmological constant is often also associated to the vacuum energy of an empty space. This is an important point on which we will return in the next section.

An empty and flat ( $K = 0$ ) universe is described by the *de Sitter model*. Substituting eq. (3.11) in (3.9) we find

$$H^2 = \frac{1}{a} \frac{da}{dt} = \frac{\Lambda}{3}$$

which has a solution of the form

$$a = A \exp \left[ \left( \frac{\Lambda}{3} \right)^{1/2} t \right].$$

Then  $\Lambda$  is able to drive an (exponential) accelerated expansion in an empty universe. This is true even in the case where matter is present but the energy content of the universe

is dominated by the cosmological constant. Of course, in this case the rate of expansion would be smaller than in an empty universe. Since this seems to be the dynamics of our universe at present time, the  $\Lambda$ CDM model turns out to be one of the best explanation to the acceleration problem and the cosmological constant seems the best candidate to the role of dark energy. However, as we will see in the next sections, this explanation suffers of both theoretical and philosophical problems.

### 3.2 Fine-tuning problem

If the cosmological constant originates from a vacuum energy density, then this suffers from a severe fine-tuning problem. In order to realize the cosmic acceleration today, we require that the cosmological constant is of the order of the square of the present Hubble parameter  $H_0$  (see eq. (3.4))

$$\Lambda \approx H_0^2 = (2.13 h \times 10^{-42} \text{GeV})^2 \quad (3.13)$$

If we interpret this as an energy density, it is equivalent to

$$\rho_\Lambda \approx \frac{\Lambda m_{\text{pl}}^2}{8\pi} \approx 10^{-47} \text{GeV}^4 \approx 10^{-123} m_{\text{pl}}^4 \quad (3.14)$$

where we have used  $h = 0.7$  and  $m_{\text{pl}} \approx 10^{19}$  GeV is the Planck mass.

Suppose that the energy density (3.14) comes from the vacuum energy  $\langle \rho \rangle$  of an empty space. The zero-point energy of some field of mass  $m$  with momentum  $k$  and frequency  $\omega$  is given by  $E = \omega/2 = \sqrt{k^2 + m^2}/2$  (in the units of  $\hbar = c = 1$ ). Then the vacuum energy density evaluated by the sum of zero-point energies of such quantum fields is given by

$$\rho_{\text{vac}} = \frac{1}{2} \int_0^\infty \frac{d^3k}{(2\pi)^3} \sqrt{k^2 + m^2} = \frac{1}{4\pi^2} \int_0^\infty dk k^2 \sqrt{k^2 + m^2} \quad (3.15)$$

This exhibits an ultraviolet divergence:  $\rho_{\text{vac}} \propto k^4$ . However we expect that quantum field theory is valid up to some cut-off scale  $k_{\text{max}}$  in which case the integral (3.15) is finite:

$$\rho_{\text{vac}} \approx \frac{k_{\text{max}}^4}{16\pi} . \quad (3.16)$$

For the extreme case of general relativity, we expect it to be valid to just below the Planck mass scale. Hence if we pick up  $k_{\text{max}} = m_{\text{pl}}$  we find that the vacuum energy density in this case is estimated as

$$\rho_{\text{vac}} \approx 10^{74} \text{GeV}^4 \quad (3.17)$$

which is about 121 orders of magnitude larger than the observed value given by eq. (3.14). Even if we take as energy scale that of QCD for  $k_{\text{max}}$ , we obtain  $\rho_{\text{vac}} \approx 10^{-3} \text{GeV}^4$  which is still much larger than  $\rho_\Lambda$ . We note that this contribution is related to the ordering ambiguity of fields and disappears when normal ordering is adopted. Since this procedure of throwing away the vacuum energy is ad hoc, one may try to cancel it by introducing counter terms. However this requires a fine-tuning to adjust  $\rho_\Lambda$  to the present energy

density of the universe. Whether or not the zero point energy in field theory is realistic is still a debatable question.

Well before the observational discovery of dark energy in 1998 the above problem was an open issue. At that time most people believed that the cosmological constant was exactly zero and there had been many attempts to explain why. Since the vanishing of a constant usually implies the existence of some symmetry, a nice resolution of the zero point energy is provided by supersymmetry. In supersymmetric theories, in fact, every bosonic degree of freedom has its Fermi counterpart that contributes to the zero-point energy with an opposite sign thereby canceling the vacuum energy. Indeed, for a field with spin  $j > 0$ , the expression (3.15) for the vacuum energy generalizes to

$$\rho_{\text{vac}} = \frac{(-1)^{2j}}{4\pi^2} (2j + 1) \int_0^\infty dk k^2 \sqrt{k^2 + m^2} \quad (3.18)$$

If supersymmetry is unbroken, there exists an equal number of bosonic and fermionic degrees of freedom for a given value of the mass  $m$  such that the net contribution to the vacuum energy vanishes. It is in this sense that supersymmetric theories do not admit a non-zero cosmological constant. However it is known that supersymmetry is broken at sufficient high energies (and that we do not live in a supersymmetric vacuum state) and the vacuum energy is generally non-zero in the world of broken supersymmetry. For a viable supersymmetric scenario, for instance if it is to be relevant to the so called “hierarchy problem” of gravitational interaction and weak interaction, the supersymmetry breaking scale should be around  $M_{\text{SUSY}} \sim 10^3$  GeV. With supersymmetry breaking around  $10^3$  GeV, we are still far away from the observed value of  $\Lambda$  by many orders of magnitude. At present we do not know how the Planck scale or SUSY breaking scales are really related to the observed vacuum scale.

The above cosmological constant problem has led many authors to try a different approach to the dark energy issue. Instead of assuming we have a small cosmological constant, we ignore it, presume it is zero due to some as yet unknown mechanism, and investigate the possibility that the dark energy is caused by the dynamics of a light scalar field. It does not solve the cosmological constant problem, but it does open up another avenue of attack as we will see in the following.

### 3.3 The coincidence problem

Another issue which is usually addressed as a crucial problem of the cosmological constant as dark energy is that its value is not only very different from all possible fundamental energy scales and requires therefore fine tuning, but also that this particular value is almost identical to the present matter energy density, for no obvious reason. The so-called *coincidence problem* is the following: since matter density scales with the third power of the inverse scale factor while  $\rho_\Lambda$  is always constant, an expanding universe should be first dominated by matter and later dominated by the cosmological constant. The densities of these two fluids should be of the same order of magnitude only in a brief intermediate phase, but observations indicates that we are precisely in this intermediate

phase, since they give  $\Omega_\Lambda \approx 0.75$  and  $\Omega_m \approx 0.25$ . In particular, the redshift at which the matter density  $\rho_{m,0}(1+z)^3$  coincides with the cosmological density  $\rho_{\Lambda,0}$  is given by

$$z_{\text{coinc}} = \left( \frac{\Omega_{\Lambda,0}}{1 - \Omega_{\Lambda,0}} \right)^{1/3} - 1, \quad (3.19)$$

which, for  $\Omega_{\Lambda,0} = 0.7$ , amounts to  $z_{\text{coinc}} \approx 0.3$ , a very recent time.

If we plot the ratio  $\Omega_m/\Omega_\Lambda$  as a function of the logarithm of the scale factor  $\ln a$  (top panel of Fig. 3.1), this appears to be smaller than one order of magnitude only in a brief and recent epoch. Anyway, as argued in [28], the choice of a time scale to plot these quantities is not unique and can lead to different interpretations. In fact, if we plot the above ratio as a function of  $a$  (bottom panel of Fig. 3.1), instead that  $\ln a$ , which turns out to be more reasonable, we see that  $10^{-1} < \Omega_m/\Omega_\Lambda < 10$  for the major part of the history of the universe so far. However this doesn't really solve the problem which could be recast in an "initial conditions" issue: since the cosmological constant energy density and the matter density decrease at different rates as the Universe expands, it appears that their ratio must be set to a specific, infinitesimal value ( $10^{-120}$ , as found in [29]) in the very early Universe in order for the two densities to nearly coincide today, some 13 billion years later. If in the primordial universe this ratio had been slightly different, this could have shifted the coincidence epoch to a very much larger or smaller time than the present one. Were the initial conditions such that now  $\rho_\Lambda/\rho_m$  was just 10 or 100 times smaller we wouldn't have seen any accelerated expansion. Had they been a few orders of magnitude larger than unity the acceleration would have started far in the past and probably we wouldn't have called it a coincidence at all.

Nevertheless we could also wonder if similar situations can still be considered compatible with life. In this sense the coincidence problem is not an issue of fine-tuning of the density parameters at present or early times, but rather an issue of anthropic nature: why do we happen to live in an age of the universe which is not many orders of magnitude smaller or larger than  $t_{\text{coinc}} = t(z_{\text{coinc}})$ ? Anthropic arguments can easily be criticized because they are usually invoked as a way out of doing the hard work of understanding the real reasons behind why we observe the universe the way we do. Furthermore, a sense of disappointment would inevitably accompany the realization that there were limits to our ability to unambiguously and directly explain the observed universe from first principles. It is nevertheless possible that some features of our world have at best an anthropic explanation, and the value of the cosmological constant is perhaps the most likely candidate. We refer to [28, 30, 31] for similar (and even reasonable) explanations.

In fact the coincidence problem is not specific to the cosmological constant but to almost all acceptable dark energy models. To satisfy the constraints due to the observations they need to behave similarly to the cosmological constant and then their  $z_{\text{coinc}}$  turn out to be very close to zero. Cosmologists have proposed, with no real success, several ways out of this problem. If we reject the idea that this coincidence is after all just a coincidence or that all observational evidence in favour of acceleration is systematic wrong the coincidence problem is far from solved (unless invoking some anthropic cause as already mentioned).

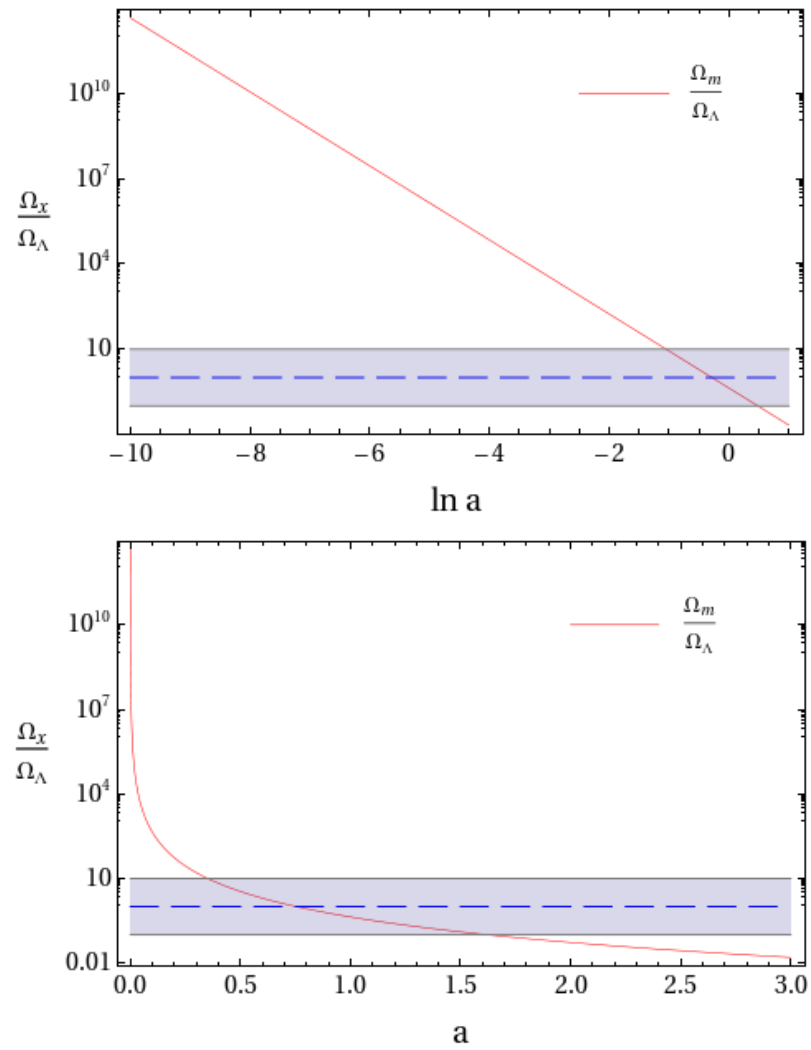


Figure 3.1: Evolution of the ratio between the density parameters of matter and cosmological constant as a function of  $\ln a$  (upper panel) or of  $a$  (lower panel).



# Chapter 4

## Scalar fields and generalizations of General Relativity

In this Chapter we review a few concepts of classical and quantum field theory. In particular we aim to introduce scalar fields which are used in many dark energy models that generalize Einstein's theory of gravitation.

### 4.1 Introduction to Field theory

In spite of the impressive success of Quantum Mechanics in describing atomic physics, it was immediately clear after its formulation that its relativistic extension was not free of difficulties.

The non-relativistic equation for the energy of a free particle is

$$\frac{p^2}{2m} = E \quad (4.1)$$

where  $p$ ,  $m$  and  $E$  are its momentum, mass and energy respectively. In order to quantize this equation we make use of the correspondence principle which relates momentum and energy to the operators  $\nabla$ ,  $\partial/\partial t$ :

$$E \rightarrow i\frac{\partial}{\partial t} \quad (4.2)$$

$$\mathbf{p} \rightarrow -i\nabla. \quad (4.3)$$

Then we get the non-relativistic Schrödinger equation for a free particle

$$-\frac{\hbar^2}{2m}\nabla^2\psi = i\hbar\frac{\partial\psi}{\partial t} \quad (4.4)$$

where  $\psi$  is the wavefunction associated to the particle. The Schrödinger equation suffers from not being relativistically covariant, meaning it does not take into account Einstein's special relativity. In relativistic mechanics, the energy of a free particle is

$$E = \sqrt{p^2c^2 + m^2c^4} \quad (4.5)$$

which, upon using the substitution (4.2), (4.3) becomes

$$\sqrt{-\hbar^2 c^2 \nabla^2 + m^2 c^4} \psi = i\hbar \frac{\partial \psi}{\partial t}. \quad (4.6)$$

This, however, is a cumbersome expression to work with because the differential operator cannot be evaluated while under the square root sign. Klein and Gordon instead began with the square of the eq. (4.5), i.e.

$$E^2 = p^2 c^2 + m^2 c^4, \quad (4.7)$$

which, when quantized, gives

$$(-\hbar^2 c^2 \nabla^2 + m^2 c^4) \psi = \left( i\hbar \frac{\partial}{\partial t} \right)^2 \psi \quad (4.8)$$

or

$$\frac{1}{c^2} \left( \frac{\partial}{\partial t} \right)^2 \psi - \nabla^2 \psi \equiv \square \psi = -\frac{m^2 c^2}{\hbar^2} \psi \quad (4.9)$$

where

$$\square = \frac{1}{c^2} \left( \frac{\partial}{\partial t} \right)^2 - \nabla^2 = \partial_\mu \partial^\mu \quad (4.10)$$

is the D'Alembertian operator. Eq. (4.9) is known as the Klein-Gordon equation. Plane-wave solutions are readily found by inspection,

$$\psi = \frac{1}{\sqrt{V}} \exp\left(\frac{i}{\hbar} \mathbf{p} \cdot \mathbf{x}\right) \exp\left(-\frac{i}{\hbar} Et\right) \quad (4.11)$$

where  $E = \pm \sqrt{p^2 c^2 + m^2 c^4}$ . Note that there is a negative energy solution as well as a positive energy solution for each value of  $\mathbf{p}$ . Naïvely one could just discard the negative energy solution, but in order to have a complete basis of solutions, plane waves with both  $E > 0$  and  $E < 0$  have to be included. And here comes the problem.

Recall the probability density and current in Schrödinger equation. If we multiply the Schrödinger equation by  $\psi^*$  on the left and multiply the conjugate of the Schrödinger equation by  $\psi$ , and then take the difference, we obtain

$$-\frac{\hbar^2}{2m} (\psi^* \nabla^2 \psi - \psi \nabla^2 \psi^*) = i\hbar (\psi^* \dot{\psi} + \dot{\psi} \psi^*) \quad (4.12)$$

which can be written in the form

$$-\frac{\hbar^2}{2m} \nabla (\psi^* \nabla \psi - \psi \nabla \psi^*) = i\hbar \frac{\partial}{\partial t} (\psi^* \psi). \quad (4.13)$$

Using the definitions of the probability density and current,  $\rho_s = \psi^* \psi$  and  $\mathbf{j}_s = \frac{\hbar}{2mi} (\psi^* \nabla \psi - \psi \nabla \psi^*)$ , we then obtain the continuity equation

$$\frac{\partial \rho_s}{\partial t} + \nabla \cdot \mathbf{j}_s = 0. \quad (4.14)$$

Now we can carry out the same procedure for the free-particle Klein-Gordon equation:

$$\psi^* \square \psi = -\frac{m^2 c^2}{\hbar} \psi^* \psi \quad (4.15)$$

$$\psi \square \psi^* = -\frac{m^2 c^2}{\hbar} \psi \psi^* . \quad (4.16)$$

Taking the difference we obtain

$$\psi^* \square \psi - \psi \square \psi^* = \partial_\mu (\psi^* \partial^\mu \psi - \psi \partial^\mu \psi^*) = 0 . \quad (4.17)$$

This suggests that we can define a probability 4-current,

$$j^\mu = \alpha (\psi \partial^\mu \psi^* - \psi^* \partial^\mu \psi) \quad (4.18)$$

(where  $\alpha$  is a constant) which is conserved:  $\partial_\mu j^\mu = 0$ . Its time and space components can be written as  $j^\mu = (j^0, \mathbf{j})$ . In order to make  $\mathbf{j}$  agree with  $j_s$ ,  $\alpha$  is chosen to be  $\alpha = -\frac{\hbar}{2mi}$ . Thus

$$\rho = \frac{j^0}{c} = \frac{i\hbar}{2mc^2} \left( \psi^* \frac{\partial \psi}{\partial t} - \psi \frac{\partial \psi^*}{\partial t} \right) . \quad (4.19)$$

$\rho$  does reduce to  $\rho_s = \psi^* \psi$  in the non-relativistic limit. However,  $\rho$  is not positive-definite and hence cannot describe a probability density for a single particle. The Klein-Gordon equation has to be reinterpreted.

First of all let us note that, being this equation relativistic invariant, it will admit as a solution a scalar function.

In order to correctly interpret the solutions to Klein-Gordon equation, it is useful to make an analogy with electromagnetism.

In classical mechanics, electromagnetism is studied through the action of the electric ( $\mathbf{E}$ ) and magnetic ( $\mathbf{B}$ ) fields generated by charged particles. Such fields satisfy, in vacuum, the well known Maxwell equations:

$$\nabla \cdot \mathbf{E} = 0 \quad (4.20)$$

$$\nabla \wedge \mathbf{B} = \frac{1}{c} \frac{\partial \mathbf{E}}{\partial t} \quad (4.21)$$

$$\nabla \cdot \mathbf{B} = 0 \quad (4.22)$$

$$\nabla \wedge \mathbf{E} = -\frac{1}{c} \frac{\partial \mathbf{B}}{\partial t} \quad (4.23)$$

From the second pair of Maxwell's equation follows the existence of scalar and vector potentials  $\varphi(\mathbf{x}, t)$  and  $\mathbf{A}(\mathbf{x}, t)$  defined by

$$\mathbf{B} = \nabla \wedge \mathbf{A} , \quad \mathbf{E} = -\nabla \varphi - \frac{1}{c} \frac{\partial \mathbf{A}}{\partial t} . \quad (4.24)$$

$\varphi$  and  $\mathbf{A}$  can be thought of as the components of the four potential  $A^\mu = (\varphi, \mathbf{A})$ . Eqs (4.24) do not determine the potentials uniquely, since for any arbitrary function  $f(\mathbf{x}, t)$  the transformation

$$\varphi \rightarrow \varphi' + \frac{1}{c} \frac{\partial f}{\partial t} , \quad \mathbf{A} \rightarrow \mathbf{A}' = \mathbf{A} - \nabla f \quad (4.25)$$

leaves the fields  $\mathbf{E}$  and  $\mathbf{B}$  unaltered. The transformation (4.25) is known as a *gauge transformation* of the second kind.

Defining the antisymmetric field tensor

$$F^{\mu\nu} = \begin{pmatrix} 0 & E_x & E_y & E_z \\ -E_x & 0 & B_z & -B_y \\ -E_y & -B_z & 0 & B_x \\ -E_z & B_y & -B_x & 0 \end{pmatrix} \quad (4.26)$$

it can be easily seen that Maxwell's equations are equivalent to

$$\partial_\nu F^{\mu\nu} = 0, \quad (4.27)$$

$$\partial_\alpha F_{\mu\nu} + \partial_\mu F_{\nu\alpha} + \partial_\nu F_{\alpha\mu} = 0. \quad (4.28)$$

Moreover, replacing the fields with their expression in terms of the potential, the electromagnetic field tensor defined in eq. (4.26) can be cast in the form

$$F^{\mu\nu} = \partial^\nu A^\mu - \partial^\mu A^\nu. \quad (4.29)$$

Combining eqs (4.27) and (4.29) leads to

$$\partial_\nu F^{\mu\nu} = \partial_\nu \partial^\nu A^\mu - \partial_\nu \partial^\mu A^\nu = 0 \quad (4.30)$$

i.e. to the equation

$$\square A^\mu - \partial^\mu (\partial_\nu A^\nu) = 0 \quad (4.31)$$

which is of course also equivalent to Maxwell's non homogeneous equations (4.20), (4.21).

We have already noted that the choice of the four potential is not unique. In fact, like eqs (4.24), eq. (4.31) has the important property of being invariant under the gauge transformations (4.25) which can also be written in the form

$$A^\mu(x) \rightarrow A'^\mu(x) = A^\mu(x) + \partial^\mu f(x). \quad (4.32)$$

Then we have the freedom to choose a particular gauge. For instance, the function  $f$  can be chosen such that the potentials  $\varphi'$  and  $\mathbf{A}'$  satisfy the condition

$$\nabla \cdot \mathbf{A}' + \frac{1}{c} \frac{\partial \varphi'}{\partial t} = 0 \quad \rightarrow \quad \partial_\nu A'^\nu = 0 \quad (4.33)$$

known as the *Lorenz gauge*<sup>1</sup> (or condition).

With this condition eq. (4.31) becomes then

$$\square A^\mu(x) = 0. \quad (4.34)$$

We remark that this is a relativistic covariant equation, whose solution is a vector field,  $A^\mu$ . The Klein-Gordon eq. (4.9) is instead the relativistic scalar invariant, equivalent to

---

<sup>1</sup>It is not a typo! The condition (4.33) is not due to same physicist author of the Lorentz transformations (the Dutch Hendrik A. Lorentz) but to the Danish Ludvig V. Lorenz.

eq. (4.31) with  $m \neq 0$ , and then we can think to its solution in terms of a scalar field, which we label  $\phi$ . In order to obtain the eq. (4.9), the field has to be described by a lagrangian in the form

$$L = \int \mathcal{L}(\phi(x, t), \partial_\mu \phi(x, t)) d^3x = \int \left[ \frac{1}{2} \partial_\mu \phi \partial^\mu \phi - \frac{1}{2} m^2 \phi \right] d^3x \quad (4.35)$$

which corresponds to the action

$$S = \int L dt = \int \left[ \frac{1}{2} \partial_\mu \phi \partial^\mu \phi - \frac{1}{2} m^2 \phi \right] d^4x \quad (4.36)$$

Eq. (4.9) is obtained through minimum action principle

$$0 = \delta S = \int \left[ \frac{\partial \mathcal{L}}{\partial \phi} \delta \phi + \frac{\partial \mathcal{L}}{\partial (\partial_\mu \phi)} \delta (\partial_\mu \phi) \right] d^4x \quad (4.37)$$

where the derivatives are performed with respect to the generalized coordinates given (in this case of a system with infinite degrees of freedom) by the field and its derivatives (while for a discrete system we can use for instance positions  $\mathbf{q}_i$  and velocities  $\dot{\mathbf{q}}_i$  of the particles or, in the case of general relativity, the components of the metric tensor).

The substitutions (4.2), (4.3) are often referred to as *first quantization*. In the *second quantization* the fields themselves become operators whose effect is to create and annihilate particles. For instance, the field  $A^\mu$  can be split into positive and energy negative parts

$$A^\mu(x) = A^{\mu+}(x) + A^{\mu-}(x) \quad (4.38)$$

and expanded in Fourier series

$$A^{\mu+}(x) = \sum_{r\mathbf{k}} \left( \frac{1}{2V\omega_k} \right)^{1/2} \varepsilon_r^\mu(\mathbf{k}) a_r(\mathbf{k}) e^{-ikx} \quad (4.39)$$

$$A^{\mu-}(x) = \sum_{r\mathbf{k}} \left( \frac{1}{2V\omega_k} \right)^{1/2} \varepsilon_r^\mu(\mathbf{k}) a_r^\dagger(\mathbf{k}) e^{ikx} \quad (4.40)$$

where  $\varepsilon_r^\mu(\mathbf{k})$  is the polarization vector and  $a_r(\mathbf{k}), a_r^\dagger(\mathbf{k})$  are the usual annihilation and creation operators. Thus  $A^{\mu+}(x)$  and  $A^{\mu-}(x)$  can be seen as annihilation and creation operators of photons, the mediator particles of the electromagnetic field.

In the same way we can quantize the Klein-Gordon scalar field  $\phi$ , which will be associated to a scalar (i.e. with spin 0) particle.

We can wonder if scalar fields really exist. Even if elementary scalar particles have yet to be found, it is supposed that they do exist. For example the Standard Model of particles hypothesizes the existence of a scalar particle, the well known Higgs boson, associated to the Higgs scalar field. Moreover, the description through scalar fields is very useful in many physical situations. For instance, the spinless pion (which is however a composite and not a fundamental particle) is correctly described by the Klein-Gordon equation through a ‘‘pseudoscalar’’ field, which means it is not invariant under parity transformations which invert the spatial directions, distinguishing it from a true scalar, which is parity-invariant.

## 4.2 Scalar fields in cosmology

Starting from the Hilbert-Einstein action

$$S = \frac{1}{16\pi G} \int d^4x \sqrt{-g} R + S_m \quad (4.41)$$

giving rise to the Einstein field equations, it is possible to consider some generalizations to this standard form of Einstein's theory. The simplest of them is the cosmological constant, studied in Chapter 3.

Another class of models generalizing General Relativity is given by scalar-field theories of gravitation. The name comes from the fact that, beside the metric tensor and the Ricci scalar, in this theories it is also present a fundamental scalar field  $\phi$ . The action takes the form

$$S_G = \int d^4x \sqrt{-g} [f_1(\phi)R + f_2(\phi)(\partial_\mu\phi)(\partial^\mu\phi) + f_3(\phi)] \quad (4.42)$$

where the functions  $f_i(\phi)$  ( $i = 1, 2, 3$ ) define the particular theory of the class. The best known is the Brans-Dicke theory (1961).

Let us note that a scalar field, instead of a vectorial one, is naturally chosen in order to preserve the isotropy of the universe and then the cosmological principle.

The motivation to scalar-tensor theories lies in the hypothesis, formulated by Dirac in 1937, that the gravitational constant  $G$  is just a spatial constant but could vary with time. Dirac had realized that there exist some strange numerical "coincidences", i.e. relations connecting cosmological constants to fundamental quantities of the particle theory. For instance we have

$$\left(\frac{\hbar^2 H_0}{Gc}\right)^{1/3} \approx m_\pi \quad (4.43)$$

where  $m_\pi$  is the pion mass. Similar relations suggest the existence of a deep though unexplainable link between microphysics and cosmology (if they are not purely accidental). Moreover, since in the most of cosmological models the Hubble constant varies with time, whereas all the other quantities of the microscopic world are absolute constants, Dirac proposed that also  $G$  has to vary with time (or alternatively one can consider a variation of the electron charge, coming from similar relations, but we will not deal with this case). Scalar-tensor theories are build up exactly to get a varying  $G$ . In fact, in standard General Relativity, the coefficient of  $R$  in the action is proportional to the inverse of the Newton constant. In scalar-tensor theories this coefficient is replaced by the function  $f_1(\phi)$ , where  $\phi$  is a scalar field varying with respect to time and space.

Apart from its purpose to make the Newton constant variable, which is the physical meaning of  $\phi$ ? It is linked to the so-called Mach's principle. The Austrian philosopher (the first to bring into question Newton absolute space-time) argued that the inertia of a body is determined by its acceleration with respect to the mass distribution of the entire universe. Therefore, the particle masses are not fundamental constants but represent the interaction between the particles themselves and some cosmic field. But, since the scale of particle masses can be measured only through the gravitational acceleration  $Gm/r^2$ ,  $G$  has to be connected in some way to the average value of the cosmic field, coupled to the

mass density of the universe. The scalar field  $\phi$  in the scalar-tensor theories then takes the role of the cosmic field that satisfies Mach's principle and it turns out to be naturally associated to  $G$ .

In Brans-Dicke theories we have

$$f_1(\phi) = \phi \quad f_2(\phi) = -\frac{\omega}{\phi} \quad f_3(\phi) = 0 \quad (4.44)$$

where  $\omega$  is called *Dicke coupling constant*. The field  $\phi$  is determined by the energy-momentum tensor of matter (comprising every fluid but not gravitation and  $\phi$ ) through

$$\square\phi = \frac{8\pi}{3 + 2\omega}T \quad (4.45)$$

The Einstein field equations take the form

$$G_{\mu\nu} = R_{\mu\nu} - \frac{1}{2}g_{\mu\nu}R = \frac{8\pi}{\phi} [T_{\mu\nu} + T_{\mu\nu}^{(\phi)}] \quad (4.46)$$

where  $T_{\mu\nu}^{(\phi)}$  is the field energy-momentum tensor. At this point one can make the assumption that the Einstein equivalence principle (based on the equality of inertial mass and gravitational mass) is still valid. This implies that only  $g_{\mu\nu}$  determines the motion of massive particles and photons, i.e.  $\phi$  is not directly coupled to matter. It only has an indirect effect expressed through the contribution of  $T_{\mu\nu}^{(\phi)}$  to the field equations (and then to the determination of the space-time structure).

As a consequence, the only exchange of energy between matter and gravitation is made through the usual covariant conservation of  $T_{\mu\nu}$

$$T_{\nu;\mu}^{\nu} = 0. \quad (4.47)$$

The field energy-momentum tensor is then determined by the covariant conservation of  $G_{\mu\nu}$

$$G_{\nu}^{\mu}\phi_{;\mu} = 8\pi T_{\nu;\mu}^{\mu(\phi)}. \quad (4.48)$$

The above equation allows to determine  $T_{\mu\nu}^{(\phi)}$ . We get

$$T_{\mu\nu}^{(\phi)} = \frac{1}{8\pi} \left[ \frac{\omega}{\phi} \left( \phi_{;\mu}\phi_{;\nu} - \frac{1}{2}g_{\mu\nu}\phi_{;\rho}\phi^{;\rho} \right) + \phi_{;\mu;\nu} - g_{\mu\nu}\square^2\phi \right]. \quad (4.49)$$

The present experimental tests of General Relativity show that the possible variation of  $G$  with time and space has to be very small and not enough to balance the variation of  $H$ , as supposed by Dirac.

However, the interest in scalar-tensor theories is also due to the possible evidence of a time variation of the fine structure constant  $\alpha$  (coming from observations of the absorption from the interstellar gas of the radiation emitted by quasar). In fact, the relation (4.43) can be written in the form

$$\frac{\hbar^2\alpha^2 H_0}{Gc} = m_e^2 m_p. \quad (4.50)$$

The possible variation of  $\alpha$  with time would then be interpreted as a variation of the speed of light  $c$  and this effect could sum up to the one of  $G$  in a way to balance the variation of  $H$ , in agreement with Dirac's hypothesis.



# Chapter 5

## Linear perturbation theory

Dark energy is defined as a fluid distributed almost homogeneously and capable of driving accelerated expansion. As such, it can be observed mainly through large scale effects such as those relating to the cosmic expansion history. Indeed, the most solid evidence in favour of dark energy comes from the acceleration of the universe as seen in the Hubble diagram of the SN Ia and on the angular size of the acoustic horizon on the CMB, as we saw in Chapter 2. However, all these observables depend ultimately on dark energy only through functions relating to the expansion history, such as  $H(z)$ , the Hubble function. For instance, the luminosity distance in flat space is defined through eq. (1.84), with  $w_{\text{DE}}(z)$  being the equation of state of dark energy. It is clear that at any given redshift there will be different  $w_{\text{DE}}(z)$ 's that give indistinguishable  $d_L(z)$ 's and that the degree of degeneracy increases with redshift (see [32] for a detailed discussion on the observability of  $w_{\text{DE}}(z)$  at high  $z$ ). Similar integrals enter the definitions of angular diameter distance and age and will therefore be subject to the same ambiguity.

Fortunately, the homogeneous observables of the universe on large scales are not the only observable quantities. The content of matter and energy has in fact evolved from a hot, dense and homogeneous state of the primordial universe to a relative cold, diffuse one which, in the case of matter, is clustered in structures. As shown by the anisotropies of the CMB, small fluctuations of the metric have grown up to form “small scale” objects such as stars and galaxies. The fact that these fluctuations are small in amplitude allow us to solve the non linear differential equations, governing the space-time and its matter content, using a first order expansion: that is, as a first approximation we can consider only the linear part of the perturbations.

While the cooling and the global decreasing of matter density are purely due to the expansion of the background (the zero-th order term in the series expansion), the formation of structures is due to the perturbed part (the first order term). Then the growth of perturbations provides a second observable, which studied together with the expansion evolution can help to remove the degeneracy and distinguish among the models. That is the reason why in this chapter we review the basics of cosmological perturbation theory.

## 5.1 Cosmological horizons

The particle horizon  $L_H(t)$  is defined as the physical distance that a ray of light can travel between the times  $t = 0$  and  $t$ . Imposing  $ds = 0$  in a flat FLRW metric

$$ds^2 = dt^2 - a^2[dr - r^2(d\theta^2 + \sin^2\theta d\phi^2)] \quad (5.1)$$

and considering a ray of light that moves along a radial direction ( $d\Omega^2 = 0$ , being  $\Omega$  the solid angle) we have

$$L_H = a(t) \int_0^t \frac{dt'}{a(t')} = a(t) \int_0^a \frac{da'}{Ha'^2}. \quad (5.2)$$

If  $t$  equals the present time,  $t = t_0$ , then  $L_H$  gives the dimension of the *observable universe*. The *observed universe* is instead the distance to the last scattering surface, when the radiation decoupled from matter and the universe became transparent to radiation. Therefore it is the largest distance that a photon reaching us can have travelled. Hence, although a luminous signal can cover a distance  $L_H$ , the scale of the kinematic processes we are interested in, is given by  $D_H = H^{-1}$ . This distance marks the *effective horizon* or Hubble radius; its present value is given by eq. (1.72). We will say that a perturbation of comoving scale  $\lambda$  is inside the horizon (*sub-horizon*) at the time  $t$  if  $a(t)\lambda < H^{-1}(t)$  and outside the horizon if  $a(t)\lambda > H^{-1}(t)$ ; where  $a(t)\lambda = H^{-1}(t)$  the perturbation is said to be in *horizon-crossing*. On using the wavenumber  $k = 2\pi/\lambda$  we have the equivalent definitions  $k > aH$  (sub-horizon),  $k < aH$  (super-horizon) and  $k = aH$  (horizon-crossing), where we neglected terms of the order of unity.

## 5.2 Perturbing General Relativity

In order to perturb the equations of General Relativity one must first of all perturb the metric, writing at first order

$$g_{\mu\nu} = g_{\mu\nu}^{(0)} + \Delta g_{\mu\nu} \quad (5.3)$$

where the perturbation  $\Delta g_{\mu\nu}$  have to be small with respect to the 0-th order metric tensor. We consider cosmological perturbations about the flat FLRW metric given by

$$ds^2 = g_{\mu\nu}^{(0)} dx^\mu dx^\nu = a^2(-d\tau^2 + \delta_{ij} dx^i dx^j). \quad (5.4)$$

We will also use the conformal Hubble function

$$\mathcal{H} \equiv \frac{1}{a} \frac{da}{d\tau} = \frac{\dot{a}}{a}, \quad (5.5)$$

where the dot represents the derivative with respect to the conformal time. As known, in General Relativity the field equations are invariant under a general coordinate change. This means that the difference between a background metric and a perturbed one is not unique: since the interval  $ds = g_{\mu\nu} dx^\mu dx^\nu$  needs to be invariant, changing the coordinates  $dx^\mu$  leads to changes in the metric tensor as well. In order to fix the unperturbed (or

background) metric we select a class of infinitesimal transformations that leaves  $g_{\mu\nu}^{(0)}$  as it is, while the perturbed metric  $\Delta g_{\mu\nu}$  is subject to change. In other words we are considering *gauge transformations*. In the unperturbed Universe, the comoving coordinates are defined in such a way that the fluid elements expanding with the Universe remain at fixed (comoving) coordinates. When perturbations are added, we can either use the same coordinates, or build up a new set of coordinates that free-fall with the fluid elements in the perturbed gravitational field. That is, in practice, we can choose to place the observers on the points in the unperturbed frame or to the perturbed particles. In the former case, called the *Newtonian* or *longitudinal gauge*, the observers will detect a velocity field of particles falling into the clumps of matter and will measure a gravitational potential, in the Newtonian limit. This choice is in fact the most intuitive one and reduces easily to the Newtonian case. However, when the wavelengths of perturbations are larger than the horizon, to place the observers on an invisible background doesn't look as a logic choice. In the second case, called the *comoving proper-time gauge* (or *synchronous gauge*), the observers are placed instead on the free-falling particles, so they do not see any velocity field (unless there are other non-gravitational forces, like pressure gradients) and, being always free falling, do not measure a gravitational potential. This gauge, therefore, does not have a proper Newtonian limit but it is useful for perturbation larger than the horizon mainly because all the observers measure the same time (in every synchronous gauge  $g_{00} = 1$ , then it is possible to synchronize clocks all over the space-time). Since we are mainly interested in the sub-horizon perturbations we choose to write the equation in the Newtonian gauge.

### 5.3 The Newtonian gauge

The most general perturbed metric can be written schematically as in eq. (5.3) where

$$\Delta g_{\mu\nu} = a^2 \begin{pmatrix} -2\Psi & w_i \\ w_i & 2\Phi\delta_{ij} + h_{ij} \end{pmatrix} \quad (5.6)$$

where  $\Psi$  and  $\Phi$  are spatial scalars,  $w_i$  is a 3-vector, and  $h_{ij}$  is a traceless 3-tensor. All the perturbation quantities ( $\Psi, \Phi, w_i$ , etc) depend on space and time. In order that the condition  $g_{\alpha\gamma}g^{\gamma\beta} = \delta_\alpha^\beta$  be still valid (neglecting second order term in the perturbation) the contravariant expression of the metric tensor is given by

$$g^{\mu\nu} = g_{(0)}^{\mu\nu} - \Delta g^{\mu\nu}, \quad (5.7)$$

where

$$\Delta g^{\mu\nu} = -\Delta g_{\alpha\beta} g_{(0)}^{\alpha\mu} g_{(0)}^{\beta\nu}. \quad (5.8)$$

A decomposition analogous to  $g_{\mu\nu}$  can be done for any rank-two tensor as e.g., the energy-momentum tensor. Now, in order to simplify the perturbed metric we make the following steps. Using Helmholtz's theorem we decompose the vector  $w_i$  into a longitudinal and a transverse component

$$w_i = w_i^\perp + w_i^\parallel, \quad (5.9)$$

where by construction

$$\nabla \cdot w_i^\perp = \nabla \times w_i^\parallel = 0. \quad (5.10)$$

The longitudinal component,  $w_i^\parallel$ , being curl-free, can then be written as the gradient of a scalar quantity  $w_s$ :  $w_i^\parallel = \nabla w_s$ . A similar argument holds for the traceless spatial part  $h_{ij}$ . Its longitudinal component can be written as

$$h_{ij}^\parallel = \left( \partial_i \partial_j - \frac{1}{3} \delta_{ij} \nabla^2 \right) B \equiv D_{ij} B, \quad (5.11)$$

where the traceless operator  $D_{ij}$  is defined implicitly and  $B$  is a scalar function. When we derive the Einstein equations for the  $(0i)$  components, we will have therefore longitudinal and transverse terms, both in  $G_{0i}$  and in  $T_{0i}$ . Taking the curl of the equations, we are left with only the transverse equations. On the other hand, taking the divergence, we are left with the longitudinal ones. Therefore, the two components completely *decouple* from each other and evolve independently, and therefore can be treated separately. The density perturbation  $\delta$  is a scalar quantity; since the longitudinal terms can be derived from a scalar quantity, they only couple to the density perturbations. Therefore, we need to take into account only the part of  $w_i$  and  $h_{ij}$  derived from scalars. This can be done by introducing two new scalar functions,  $E$  and  $B$ , that produce the vector  $E_{,i}$  and the tensor  $D_{ij}B$ . Then the perturbed metric is given by

$$\Delta g_{\mu\nu} = a^2 \begin{pmatrix} -2\Psi & E_{,i} \\ E_{,i} & 2\Phi\delta_{ij} + D_{ij}B \end{pmatrix}. \quad (5.12)$$

Now we can impose to the metric up to four conditions corresponding to the choice of the gauge. We choose them to be  $w_i = 0$  (from which  $E = 0$ ) and  $B = 0$ . This finally leaves the perturbed metric in the Newtonian gauge:<sup>1</sup>

$$ds^2 = a^2(\tau) \left[ -(1 + 2\Psi)d\tau^2 + (1 + 2\Phi)\delta_{ij}dx^i dx^j \right]. \quad (5.13)$$

The Einstein tensor  $G_\nu^\mu$  and the energy-momentum tensor  $T_\nu^\mu$  can be split into background and perturbed parts:  $G_\nu^\mu = G_\nu^{\mu(0)} + \Delta G_\nu^\mu$  and  $T_\nu^\mu = T_\nu^{\mu(0)} + \Delta T_\nu^\mu$ . The background cosmological evolution is obtained by solving the zero-th order Einstein equations,  $G_\nu^{\mu(0)} = 8\pi G T_\nu^{\mu(0)}$  whereas the first-order Einstein equations are given by

$$\Delta G_\nu^\mu = 8\pi G \Delta T_\nu^\mu, \quad (5.14)$$

where

$$\Delta G_\nu^\mu = \Delta R_\nu^\mu - \frac{1}{2} \Delta(g_\nu^\mu R) = \Delta R_\nu^\mu - \frac{1}{2} (\Delta g_\nu^\mu R + g_\nu^{\mu(0)} \Delta R). \quad (5.15)$$

The expression of the perturbed Ricci tensor and scalar curvature are obtained from eqs. (1.12) and (1.13) and read

$$\Delta R_{\mu\nu} = \Delta \Gamma_{\mu\nu,\alpha}^\alpha - \Delta \Gamma_{\mu\alpha,\nu}^\alpha + \Delta \Gamma_{\mu\nu}^\alpha \Gamma_{\alpha\beta}^\beta + \Gamma_{\mu\nu}^\alpha \Delta \Gamma_{\alpha\beta}^\beta - \Delta \Gamma_{\mu\beta}^\alpha \Gamma_{\alpha\nu}^\beta - \Gamma_{\mu\beta}^\alpha \Delta \Gamma_{\alpha\nu}^\beta, \quad (5.16)$$

$$\Delta R = \Delta g^{\mu\alpha} R_{\alpha\mu} + g^{\mu\alpha} \Delta R_{\alpha\mu}. \quad (5.17)$$

<sup>1</sup>For the signs of the potentials we follow the choice of [33] and [34].

The only non vanishing unperturbed Christoffel symbols in the metric (5.4) are

$$\Gamma_{0\nu}^\lambda = \mathcal{H}\delta_\nu^\lambda, \quad \Gamma_{\mu\nu}^0 = \mathcal{H}\delta_{\mu\nu}. \quad (5.18)$$

while we can compute the perturbed Christoffel symbols by perturbing eq. (1.6):

$$\Delta\Gamma_{\mu\nu}^\lambda = \frac{1}{2}\Delta g^{\lambda\eta}(g_{\mu\eta,\nu} + g_{\eta\nu,\mu} - g_{\mu\nu,\eta}) + \frac{1}{2}g^{\lambda\eta}(\Delta g_{\mu\eta,\nu} + \Delta g_{\eta\nu,\mu} - \Delta g_{\mu\nu,\eta}). \quad (5.19)$$

The non-vanishing components of perturbed Christoffel symbols are then

$$\Delta\Gamma_{ij}^0 = \delta_{ij} [2\mathcal{H}(\Phi - \Psi) + \dot{\Phi}], \quad (5.20)$$

$$\Delta\Gamma_{00}^0 = \dot{\Psi}, \quad (5.21)$$

$$\Delta\Gamma_{0i}^0 = \Delta\Gamma_{00}^i = \Psi_{,i}, \quad (5.22)$$

$$\Delta\Gamma_{j0}^i = \delta_j^i \dot{\Phi}. \quad (5.23)$$

Thus, from eq. (5.15) we obtain

$$\Delta G_0^0 = \frac{2}{a^2} [3\mathcal{H}(\mathcal{H}\Psi - \dot{\Phi}) + \nabla^2\Phi] \quad (5.24)$$

$$\Delta G_i^0 = \frac{2}{a^2} (\dot{\Phi} - \mathcal{H}\Psi)_{,i} \quad (5.25)$$

$$\begin{aligned} \Delta G_j^i &= \frac{2}{a^2} [(\mathcal{H}^2 + 2\dot{\mathcal{H}})\Psi + \mathcal{H}\dot{\Psi} - \ddot{\Phi} - 2\mathcal{H}\dot{\Phi}] \delta_j^i + \\ &+ \frac{1}{a^2} [\nabla^2(\Psi + \Phi)\delta_j^i - \nabla_i\nabla_j(\Psi + \Phi)]. \end{aligned} \quad (5.26)$$

The last information we need in order to solve the linear perturbation equations of eq. (5.14) is the form of the perturbed energy-momentum tensor  $\delta T_\nu^\mu$ . This is determined once the matter source is specified: we will do it in the next sections for several cases. For the moment we just recall that the energy-momentum tensor satisfies the continuity equation  $T_{\nu;\mu}^\mu = 0$ . The first-order part of this equation,

$$\Delta T_{\nu;\mu}^\mu = 0, \quad (5.27)$$

also gives a number of useful equations, as we will see later. In order to evaluate the perturbed energy-momentum tensor, we also need to perturb the four-velocity  $u^\mu \equiv \frac{dx^\mu}{ds}$ . Neglecting the perturbations higher than the first order, we obtain

$$u^\mu = \left[ \frac{1}{a}(1 - \Psi), \frac{v^i}{a} \right], \quad (5.28)$$

$$u_\mu = g_{\mu\nu}u^\nu = [-a(1 + \Psi), av_i], \quad (5.29)$$

$$u_\mu u^\mu = -1, \quad (5.30)$$

where  $v^i = \frac{dx^i}{d\tau} = a\frac{dx^i}{dt}$  is the matter peculiar velocity with respect to the general expansion.

## 5.4 Single fluid model

In order to compute the first order perturbations in the energy-momentum tensor we need to specify which are the components of the universe in the model we are interested to. Let us first consider a single-fluid model with an energy-momentum tensor  $T_{\mu\nu}$ . The most general energy momentum tensor for a fluid can be written as

$$T_{\mu\nu} = (\rho + p)u_\mu u_\nu + pg_{\mu\nu} + [q_\mu u_\nu + q_\nu u_\mu + \pi_{\mu\nu}] \quad (5.31)$$

where  $\rho$ ,  $p$ ,  $u_\mu$  stand for the usual energy density, pressure and four-velocity vector, while we also introduce the heat flux vector  $q_\mu$  and the viscous shear tensor  $\pi_{\mu\nu}$ . The terms inside square brackets in eq. (5.31) are important only for fluids whose internal energy is a sizable fraction of the total energy density. We have  $q_\mu = 0$  and  $\pi_{\mu\nu} = 0$  for perfect fluids. In the following we limit ourselves to perfect fluids. We also assume that the perturbed fluid remains a perfect fluid. This implies that  $\Sigma_j^i \equiv \delta T_j^i = 0$  ( $i \neq j$ ), a condition that will be used below.

The notation for the perturbed quantities is

$$\delta \equiv \frac{\Delta\rho}{\rho}, \quad \theta \equiv \nabla_i v^i \quad (5.32)$$

where

$$\frac{\Delta\rho}{\rho} \equiv \frac{\rho(x) - \bar{\rho}}{\bar{\rho}} \quad (5.33)$$

is the density contrast ( $\rho(x)$  is the density field at a point  $x$  and  $\bar{\rho}$  is the spatial average) and  $\theta$  is the velocity divergence. In general there are several pairs  $\delta_i$ ,  $\theta_i$ , one for each perfect fluid composing the Universe. All of the perturbed quantities are functions of space  $x$  and time  $t$ .  $\delta(x)$  is in reality a random field which by definition has a zero mean value  $\langle \delta \rangle = 0$ . When we say that  $\delta$  grows or decays we mean that in the linear regime the value of  $\delta(x)$  at any point  $x$  can be written as  $\delta(x, t) = D(t)\delta(x, 0)$ , where  $D(t)$  is the growth (or decay) function. In the linear regime the spatial part is always factored out and its properties are assigned by initial conditions. We will always assume Gaussian initial conditions as predicted in standard inflationary models. From eq. (5.31) the perturbed energy-momentum tensor for a perfect fluid with the equation of state  $w = p/\rho$  can be written as

$$\Delta T_\nu^\mu = \rho [\delta(1 + c_s^2)u_\nu u^\mu + (1 + w)(\delta u_\nu u^\mu + u_\nu \delta u^\mu + c_s^2 \delta \delta_\nu^\mu)] \quad (5.34)$$

where  $\delta_\nu^\mu$  is the usual Kronecker's delta (and not the density contrast  $\delta$ !) and we have introduced the sound velocity,  $c_s^2 \equiv \Delta p / \Delta \rho$ . If  $p$ , even when perturbed, depends on  $\rho$  alone (which is the case called *barotropic fluid*) then

$$c_s^2 \equiv \frac{\Delta p}{\Delta \rho} = \frac{dp}{d\rho} = \frac{\dot{p}}{\dot{\rho}}. \quad (5.35)$$

The last passage is valid only in the FLRW metric where at background level everything depends on time alone ( $c_s$  is calculated at zero-th order since it will always appear as a factor of first-order variables). Since  $c_s$ , just as  $w$ , depends at first-order only on

background quantities, in this case the perturbation equations do not introduce any new free function. In general, however, the pressure  $p$  can depend on internal degrees of freedom of the fluid, say, entropy  $s$ . Then one has

$$c_s^2 = \frac{\delta p(\rho, s)}{\delta \rho} = \frac{\partial p}{\partial \rho} + \frac{\partial p}{\partial s} \frac{\partial s}{\partial \rho} = c_{s(a)}^2 + c_{s(na)}^2 \quad (5.36)$$

where  $c_{s(a)}^2 \equiv \sqrt{\dot{p}/\dot{\rho}}$  is called the *adiabatic* sound speed and  $c_{s(na)}^2$  is the non-adiabatic sound speed. The non-adiabatic sound speed in general will depend on microphysical properties of the fluid and appears as a new free function only at the level of perturbations. The gravitational equations at first-order are then completely specified only if we give for each fluid the equation of state  $w(a)$  and the total sound speed  $c_s(a)$  or, equivalently, if we assign to the fluid a function  $p(\rho, s)$  which determines both. The components of the energy-momentum tensor are

$$\Delta T_0^0 = -\Delta \rho \quad (5.37)$$

$$\Delta T_i^0 = -\Delta T_0^i = (1+w)\rho v^i \quad (5.38)$$

$$\Delta T_1^1 = \Delta T_2^2 = \Delta T_3^3 = c_s^2 \Delta \rho. \quad (5.39)$$

Then the perturbed Einstein equations (5.14) lead to

$$3\mathcal{H}(\mathcal{H}\Psi - \dot{\Phi}) + \nabla^2 \Phi = -4\pi G a^2 \rho \delta \quad (5.40)$$

$$\nabla^2(\dot{\Phi} - \mathcal{H}\Psi) = 4\pi G a^2 (1+w)\rho \theta \quad (5.41)$$

$$\Psi = -\Phi \quad (5.42)$$

$$\ddot{\Phi} + 2\mathcal{H}\dot{\Phi} - \mathcal{H}\dot{\Psi} - (\mathcal{H}^2 + 2\dot{\mathcal{H}})\Psi = -4\pi G a^2 c_s^2 \rho \delta \quad (5.43)$$

Note that eqs. (5.40)–(5.43) come from the (00), (0i), (ij), and (ii) components. Equation (5.42) follows from the property  $\Delta T_j^i = 0$ . One can also derive some useful equations by using the continuity equation (5.27). Recalling that the operation of covariant divergence of a tensor is

$$T_{\nu;\mu}^\mu = T_{\nu,\mu}^\mu - \Gamma_{\nu\beta}^\alpha T_\alpha^\beta + \Gamma_{\beta\alpha}^\alpha T_\nu^\beta \quad (5.44)$$

the  $\nu = 0$  component of eq. (5.27), i.e.  $\Delta T_{0;\mu}^\mu = 0$ , reads

$$\Delta T_{0,\mu}^\mu - \Delta \Gamma_{0\beta}^\alpha T_\alpha^\beta - \Gamma_{0\beta}^\alpha \Delta T_\alpha^\beta + \Delta \Gamma_{\beta\alpha}^\alpha T_0^\beta + \Gamma_{\beta\alpha}^\alpha \Delta T_0^\beta = 0 \quad (5.45)$$

which reduces to

$$\dot{\Delta} \rho + 3\mathcal{H}(\Delta \rho + \Delta p) = -(\rho + p)(\theta + 3\dot{\Phi}) \quad (5.46)$$

where we have employed eqs. (5.20)–(5.23). Using the unperturbed conservation equation  $\dot{\rho} + 3\mathcal{H}(\rho + p) = 0$  together with the relations  $w = p/\rho$  and  $c_s^2 = \Delta p/\Delta \rho$ , we find that eq. (5.46) can be expressed as

$$\dot{\delta} + 3\mathcal{H}(c_s^2 - w)\delta = -(1+w)(\theta + 3\dot{\Phi}), \quad (5.47)$$

which is called the (perturbed) *continuity equation*. For non-relativistic matter with  $w = 0$  and  $c_s^2 = 0$ , this equation reduces to

$$\dot{\delta} = -\theta - 3\dot{\Phi} \quad (\text{for non relativistic matter}). \quad (5.48)$$

According to this equation, the density at position  $x$  increases if there is a velocity divergence in the same place, that is, if there is more matter coming in than going out. The term  $\dot{\Phi}$ , absent in Newtonian dynamics, is negligible at small scales and, of course, for a slowly varying gravitational potential. The equation  $\Delta T_{i;\mu}^\mu = 0$  leads to (writing it in terms of  $v^i$  and taking the divergence  $\nabla_i$ )

$$\dot{\theta} + \left[ \mathcal{H}(1 - 3w) + \frac{\dot{w}}{1 + w} \right] \theta = -\nabla^2 \left( \frac{c_s^2}{1 + w} \delta + \Psi \right). \quad (5.49)$$

For non-relativistic matter, this reduces to

$$\dot{\theta} + \mathcal{H}\theta = -\nabla^2 \Psi - \nabla^2 (c_s^2 \delta) \quad (\text{for non relativistic matter}) \quad (5.50)$$

where now we have included the  $\nabla^2(c_s^2 \delta)$  term. This is called the *Euler equation* in the Newtonian context. It says that the (peculiar) acceleration depends on the sum of the potential and pressure gradients.

In order to describe the distribution of matter in the Universe at a given time and its subsequent evolution one might try to divide it into volumes which initially evolve independently of each other. Fairly soon, however, this independence would no longer hold as the gravitational forces between one cell and its neighbours become strong. It is therefore not a good idea to think of a generic perturbation as a sum of spatial components. It is a much better idea to think of the perturbation as a superposition of plane waves which have the advantage that they evolve independently while the fluctuations are still linear. This effectively means that one represents the distribution as independent components not in real space, but in Fourier transform space, or reciprocal space, in terms of the wavevectors of each component  $\mathbf{k}$ .

That is the reason why we go now to the Fourier space. This means that all perturbation quantities will be Fourier expanded:

$$\Phi = \int e^{i\mathbf{k}\cdot\mathbf{r}} \Phi_k d^3k, \quad \Psi = \int e^{i\mathbf{k}\cdot\mathbf{r}} \Psi_k d^3k \quad (5.51)$$

$$\delta = \int e^{i\mathbf{k}\cdot\mathbf{r}} \delta_k d^3k, \quad \theta = \int e^{i\mathbf{k}\cdot\mathbf{r}} \theta_k d^3k. \quad (5.52)$$

The subscript  $k$  represents a Fourier mode for each wavenumber  $k$  and is a comoving quantity that remains fixed. In the following we drop the subscript  $k$  as long as no confusion arises by doing so. Then in Fourier space we assume that the perturbation variables ( $\delta$ ,  $\theta$ ,  $\Phi$ ,  $\Psi$ , etc.) are the sum of plane waves  $e^{i\mathbf{k}\cdot\mathbf{r}} \delta_k$ . Since the equations are linear, each plane wave obeys the same equations with a different comoving wavenumber  $k$ . Throughout the linear evolution, the physical scale  $\lambda_p$  of the perturbation expands with the cosmic expansion as  $\lambda = (2\pi a)/k$ . Of course, if the perturbation enters a non-linear regime, then this treatment breaks down and the perturbation decouples from the

Hubble expansion and starts collapsing. When we calculate the perturbation equations it is usually very convenient to introduce from the beginning all perturbation variables as Fourier modes, e.g.,  $\delta(x, y, z, t) = \delta_k(t)e^{i\mathbf{k}\cdot\mathbf{r}}$ . Since we are always interested in the direction-averaged equations (i.e. the equations that depend only on the modulus  $k$ ), we could simply put  $\mathbf{k}\cdot\mathbf{r} = k(x + y + z)/\sqrt{3}$ . In practice, each perturbation quantity  $\phi$  and its derivatives can be substituted as follows

$$\phi(x, \tau) \rightarrow e^{i\mathbf{k}\cdot\mathbf{r}}\phi(\tau) \quad (5.53)$$

$$\nabla\phi(x, \tau) \rightarrow ie^{i\mathbf{k}\cdot\mathbf{r}}\mathbf{k}\phi(\tau) \quad (5.54)$$

$$\nabla^2\phi(x, \tau) \equiv \nabla_i\nabla^i\phi(x, \tau) \rightarrow -e^{i\mathbf{k}\cdot\mathbf{r}}k^2\phi(\tau) \quad (5.55)$$

When there are two repeated spatial indices we sum over them without the help of the metric coefficients  $g_{ij}$  (more exactly, we use the induced 3-dimensional spatial metric which for spatially flat spaces is just the Euclidean metric). Furthermore, the Fourier modes  $e^{i\mathbf{k}\cdot\mathbf{r}}$  can be simply dropped out, since the equations are linear and therefore decoupled between different modes.

From eqs. (5.40)–(5.43), (5.47), and (5.49) we obtain the following equations for each Fourier mode:

$$k^2\Phi + 3\mathcal{H}(\dot{\Phi} - \mathcal{H}\Psi) = 4\pi Ga^2\rho\delta \quad (5.56)$$

$$k^2(\dot{\Phi} - \mathcal{H}\Psi) = -4\pi Ga^2(1+w)\rho\theta \quad (5.57)$$

$$\Psi = -\Phi \quad (5.58)$$

$$\ddot{\Phi} + 2\mathcal{H}\dot{\Phi} - \mathcal{H}\dot{\Psi} - (\mathcal{H}^2 + 2\dot{\mathcal{H}})\Psi = -4\pi Ga^2c_s^2\rho\delta \quad (5.59)$$

$$\dot{\delta} + 3\mathcal{H}(c_s^2 - w)\delta = -(1+w)(\theta + 3\dot{\Phi}) \quad (5.60)$$

$$\dot{\theta} + \left[ \mathcal{H}(1 - 3w) + \frac{\dot{w}}{1+w} \right] \theta = k^2 \left( \frac{c_s^2}{1+w}\delta + \Psi \right), \quad (5.61)$$

where now

$$\theta = i\mathbf{k}\cdot\mathbf{v} \quad (5.62)$$

The six equations above are not independent but they are all useful. For instance, we can combine eqs. (5.56) and (5.57) to get the relativistic Poisson equation

$$k^2\Phi = 4\pi Ga^2\rho [\delta + 3\mathcal{H}(w+1)\theta/k^2] = 4\pi Ga^2\rho\delta^*, \quad (5.63)$$

where  $\delta^*$  is the total matter variable:

$$\delta^* \equiv \delta + 3\mathcal{H}(w+1)\theta/k^2 \quad (5.64)$$

while combining eqs. (5.56), (5.58), and (5.59), we can get an equation for  $\Phi$  alone:

$$\ddot{\Phi} + 3\mathcal{H}(1+c_s^2)\dot{\Phi} + (c_s^2k^2 + 3\mathcal{H}^2c_s^2 + \mathcal{H}^2 + 2\dot{\mathcal{H}})\Phi = 0. \quad (5.65)$$

We also give the useful relation

$$\dot{\mathcal{H}} = -\frac{1}{2}(1+3w)\mathcal{H}^2. \quad (5.66)$$

## 5.5 Scales larger than the horizon

Now that we have derived the perturbation equations, we can begin wondering how to solve them. As a first example we work out the simplest case, the large-scale limit  $k \ll \mathcal{H} = aH$ . This corresponds to the scale on which the physical wavelength  $\lambda_p = (2\pi a)/k$  of perturbations is much larger than the Hubble radius  $H^{-1}$ , i.e. super-horizon scales (although notice that the horizon corresponds approximately to  $1/H$  only for some particular case). If the pressure depends only on the energy density and the equation of state  $w$  is a constant then we have  $c_s^2 = w$ , which is valid both for matter and radiation. In this case eq. (5.65), using eq. (5.57), reduces to

$$\ddot{\Phi} + 3\mathcal{H}(1 + c_s^2)\dot{\Phi} = 0 \quad (5.67)$$

Then  $\dot{\Phi} = 0$  is a solution. Equation (5.56) becomes

$$3\mathcal{H}^2\Phi = 4\pi G a^2 \rho \delta, \quad (5.68)$$

where we have neglected the term  $k^2\Phi$ . Using the Friedmann equation,  $3\mathcal{H}^2 = 8\pi G \rho a^2$  it follows that

$$\delta = 2\Phi \quad (5.69)$$

Hence  $\Phi = \text{constant}$  at large scales implies that  $\delta = \text{constant}$ . One easily finds that the result (5.69) is consistent with the other Einstein equations. Equation (5.67) is second-order, so we must have two solutions. It appears immediately that  $\Phi = \text{constant}$  is a growing mode or a dominating solution (at least for  $c_s^2 > -1$ ). Thus we have shown that the gravitational potential remains constant for scales outside the Hubble radius whenever  $c_s^2 = w$  for the total fluid. During the transition from radiation to matter eras this condition is violated and the gravitational potential changes.

## 5.6 Scales smaller than the Hubble radius

Now we work out the opposite case,  $k \gg \mathcal{H}$ , i.e. scales deep inside the Hubble radius (sub-horizon scales). In a general fluid, its pressure opposes gravity acting against the growth of the fluctuations and stopping the collapse. On the contrary, in a pressureless fluid the fluctuations can grow indefinitely because there is no counteracting force. We then begin to derive the equations for a fluid which is pressureless ( $w = 0$ ) in the absence of perturbations, but has a small sound speed:

$$c_s^2 = \frac{\delta p}{\delta \rho} \ll 1 \quad (5.70)$$

In the limit  $k \gg \mathcal{H}$  eq. (5.57) tells us that  $\dot{\Phi} - \mathcal{H}\Psi \simeq 0$ , so that eq. (5.56) corresponds to the Fourier transformed Poisson equation

$$k^2\Phi = 4\pi G a^2 \rho \delta = \frac{3}{2}\mathcal{H}^2\delta \quad (5.71)$$

Taking the derivative of eq. (5.71) and substituting it into eq. (5.60), we obtain

$$\dot{\delta} = -\theta - \frac{9\mathcal{H}^2}{2k^2}\delta \left( 2\frac{\dot{\mathcal{H}}}{\mathcal{H}} + \frac{\dot{\delta}}{\delta} \right) \simeq -\theta. \quad (5.72)$$

Hence this equation reduces to the energy conservation equation in the Newtonian limit. Then the perturbation equations in the sub-horizon limit become

$$\dot{\delta} = -\theta \quad (5.73)$$

$$\dot{\theta} = -\mathcal{H}\theta + c_s^2 k^2 \delta - k^2 \Phi \quad (5.74)$$

plus eq. (5.71). Differentiating eq. (5.72) with respect to  $\tau$  and using eq. (5.74), it follows that

$$\ddot{\delta} + \mathcal{H}\dot{\delta} + \left( c_s^2 k^2 - \frac{3}{2}\mathcal{H}^2 \right) \delta = 0. \quad (5.75)$$

In the Minkowski limit,  $\mathcal{H} \rightarrow 0$ , this equation reduces to the classical fluid wave equation  $\ddot{\delta} + c_s^2 k^2 \delta = 0$ , where  $c_s$  is indeed the sound velocity. Equation (5.75) shows at once that the perturbation does not grow if

$$c_s^2 k^2 - \frac{3}{2}\mathcal{H}^2 > 0, \quad (5.76)$$

i.e. if the physical wavelength  $\lambda_p = (2\pi a)/k$  is smaller than the Jeans length,

$$\lambda_J = c_s \sqrt{\frac{\pi}{G\rho}}. \quad (5.77)$$

For scales smaller than  $\lambda_J$  the perturbations undergo damped oscillations. For the CDM particles the velocity dispersion is always negligible, at least in the regime of validity of our linear treatment. For the photons we have  $c_s = c/\sqrt{3}$ , so that

$$\lambda_J \approx H^{-1}. \quad (5.78)$$

Hence the growth of perturbations is prevented on all scales smaller than the Hubble radius. For the baryons, the sound velocity is comparable to the photon velocity before the decoupling epoch, so that baryon perturbations are damped out (more precisely they drop rapidly to a comoving scale of less than 1 Mpc just after decoupling). Then the baryons are free to fall inside the dark matter potential wells, and their perturbation spectrum catches the dark matter one (like we will see in the next section).

When  $c_s k \ll \mathcal{H}$ , the perturbations grow freely because gravity overcomes the pressure: this is the very important regime of *gravitational instability*. The subhorizon equation for a single pressureless fluid becomes

$$\ddot{\delta} + \mathcal{H}\dot{\delta} - \frac{3}{2}\mathcal{H}^2\delta = 0 \quad (5.79)$$

or, using the time  $t$ ,

$$\frac{d^2\delta}{dt^2} + 2H\frac{d\delta}{dt} - \frac{3}{2}H^2\delta = \frac{d^2\delta}{dt^2} + 2H\frac{d\delta}{dt} - 4\pi G\rho_m\delta = 0, \quad (5.80)$$

where we also used the Friedmann eq. (1.19) (with  $K = 0$ ). The interpretation of this equation is quite simple: perturbations grow according to a source term representing the amount of matter able to cluster ( $\rho_m$ ) but their growth is opposed by a friction term due to the expansion of the universe.

It is often useful to employ the number of e-foldings  $\alpha = \ln a$  in the place of the conformal time. Then eq. (5.79) can be written as

$$\delta'' + \left( \frac{\mathcal{H}'}{\mathcal{H}} + 1 \right) \delta' - \frac{3}{2} \delta = 0, \quad (5.81)$$

where we have used a prime for the derivatives with respect to  $\alpha$ . We can rewrite eq. (5.66) as

$$\frac{\mathcal{H}'}{\mathcal{H}} = -\frac{1}{2} - \frac{3}{2}w. \quad (5.82)$$

For a pressureless fluid ( $w = 0$ ), eq. (5.81) then reduces to

$$\delta'' + \frac{1}{2} \delta' - \frac{3}{2} \delta = 0, \quad (5.83)$$

which is a simple constant coefficients differential equation, whose solutions are linear combinations of

$$\delta = Ae^{m\alpha} = Aa^m. \quad (5.84)$$

The direct substitution of (5.84) in eq. (5.83) gives the solutions  $m_{\pm} = 1, -3/2$ . Then the evolutions of modes during the matter era is given by

$$\delta_+ = Aa, \quad \delta_- = Aa^{-3/2} \quad (5.85)$$

labeled *growing* and *decaying* modes respectively. In terms of the cosmic time  $t$ , the growing solution evolves as  $\delta_+ \propto t^{2/3}$ . The pre-factor is of course fixed by the initial conditions, ultimately established during inflation. The decaying solutions (or in general the slower one) become soon negligible with respect to the growing ones and we will systematically neglect them in the following. Inserting  $\delta_+$  into the Poisson equation (5.71), we see that  $\Phi \propto a^2 H^2 \delta_+ \propto a^2 a^{-3} a^1 \propto \text{constant}$  (recalling that  $H \sim a^{-3/2}$  in the matter dominated era). Hence the gravitational potential remains constant during the pure matter-dominated epoch.

## 5.7 Two-fluid solutions

Now we generalize the single-fluid case to the more realistic case in which both matter ( $w_m = c_s^2 = 0$ ) and radiation ( $w_r = c_s^2 = 1/3$ ) are present. We introduce the matter perturbation variables  $\delta_m, \theta_m$  and the radiation perturbation variables  $\delta_r, \theta_r$  (here radiation means all the components which are massless or relativistic). Since we are considering dark matter as a dominant matter component, there is no explicit interaction term between matter and radiation. The baryonic fraction is also effectively decoupled

after  $z \approx 1000$ , while before this epoch it can be considered as a part of a relativistic photon–baryon plasma. In Fourier space we then have a system of gravitationally coupled equations for the perturbations on sub-horizon scales:

$$\dot{\delta}_m = -(\theta_m + 3\dot{\Phi}) , \quad (5.86)$$

$$\dot{\theta}_m = -\mathcal{H}\theta_m - k^2\Phi , \quad (5.87)$$

$$\dot{\delta}_r = -\frac{4}{3}(\theta_r + 3\dot{\Phi}) , \quad (5.88)$$

$$\dot{\theta}_r = k^2 \left( \frac{3}{4}c_s^2\delta_r - \Phi \right) , \quad (5.89)$$

$$k^2(\dot{\Phi} + \mathcal{H}\Phi) = -4\pi G a^2(1 + w_{\text{eff}})\rho_t\theta_t , \quad (5.90)$$

$$k^2\Phi + 3\mathcal{H}(\dot{\Phi} + \mathcal{H}\Phi) = 4\pi G a^2\rho_t\delta_t . \quad (5.91)$$

The subscript  $t$  represents the total perturbation variables, i.e.

$$\rho_t = \rho_m + \rho_r , \quad (5.92)$$

$$w_{\text{eff}} = \Omega_r w_r + \Omega_m w_m = \frac{\rho_r/3}{\rho_m + \rho_r} , \quad (5.93)$$

$$\theta_t = \frac{(1 + w_m)\Omega_m\theta_m + (1 + w_r)\Omega_r\theta_r}{1 + w_{\text{eff}}} , \quad (5.94)$$

$$\delta_t = \Omega_m\delta_m + \Omega_r\delta_r , \quad (5.95)$$

Here the total effective equation of state  $w_{\text{eff}} = p_t/\rho_t$  is given by

$$w_{\text{eff}} = -1 - \frac{2}{3} \frac{\dot{H}}{H^2} , \quad (5.96)$$

which follows from eqs. (1.18), (1.19) and  $K = 0$ . We remind that  $\Omega_m$  and  $\Omega_r$  are functions of time and must be distinguished from their present values  $\Omega_{m,0}$  and  $\Omega_{r,0}$ . In the sub-horizon limit, eq. (5.91) gives

$$k^2\Phi \simeq 4\pi G a^2(\rho_m\delta_m + \rho_r\delta_r) = \frac{3}{2}\mathcal{H}^2(\Omega_m\delta_m + \Omega_r\delta_r) . \quad (5.97)$$

Following the derivation similar to eq. (5.75), we obtain the following equations for sub-horizon perturbations

$$\ddot{\delta}_m + \mathcal{H}\dot{\delta}_m - \frac{3}{2}\mathcal{H}^2(\Omega_m\delta_m + \Omega_r\delta_r) = 0 , \quad (5.98)$$

$$\ddot{\delta}_r + \frac{k^2}{3}\delta_r = 0 . \quad (5.99)$$

During the radiation-dominated epoch we have  $\Omega_m \simeq 0$  and  $\Omega_r \simeq 1$ . Moreover the second equation shows that the radiation density contrast oscillates rapidly around zero (since we are considering sub-horizon modes,  $k \gg \mathcal{H}$ ). The same is true for the coupled

baryon–photon plasma. Therefore, we can average over the radiation oscillations and put  $\langle \delta_r \rangle \simeq 0$  in the first equation. It then follows that  $\Omega_m \delta_m + \Omega_r \delta_r \simeq 0$  and

$$\ddot{\delta}_m + \mathcal{H} \dot{\delta}_m \simeq 0 . \quad (5.100)$$

The solution of this equation is given by  $\delta_m = C_1 + C_2 \int a^{-1} d\tau$ . During the radiation era the integral  $\int a^{-1} d\tau$  gives only a logarithmic correction, so the matter perturbations evolve only mildly. During the matter era we have  $|\Omega_m \delta_m| \gg |\Omega_r \delta_r|$  in eq. (5.98), so that the evolution of matter perturbations is described by  $\delta_m \propto a$  as we have explained in the previous section. If we consider cold dark matter (perturbation  $\delta_c$ ) and baryonic matter (perturbation  $\delta_b$ ) instead of matter and radiation, eq. (5.98) can be generalized as

$$\ddot{\delta}_c + \mathcal{H} \dot{\delta}_c - \frac{3}{2} \mathcal{H}^2 (\Omega_c \delta_c + \Omega_b \delta_b) = 0 , \quad (5.101)$$

$$\ddot{\delta}_b + \mathcal{H} \dot{\delta}_b - \frac{3}{2} \mathcal{H}^2 (\Omega_c \delta_c + \Omega_b \delta_b) = 0 , \quad (5.102)$$

Since baryons correspond to a small fraction of the total matter fluid, we can assume  $|\Omega_c \delta_c| \gg |\Omega_b \delta_b|$ . This shows that eq. (5.101) decouples from  $\delta_b$  and reduces to the standard equation for matter perturbations. At the same time the baryon equation is “forced” by the term  $\Omega_c \delta_c$ . For such coupled differential equations the asymptotic solution of  $\delta_b$  will approach the forcing term  $\delta_c$ . In other words, the perturbations in baryons will catch up with those in dark matter. This expresses mathematically (in the linear regime) the common expression according to which the baryons fall into the dark matter potential wells.

Analogously, if we consider the sum of pressureless matter and the cosmological constant  $\Lambda$  instead of matter and radiation, we get the term  $\Omega_\Lambda \delta_\Lambda$  in addition to  $\Omega_m \delta_m$ . However  $\rho_\Lambda$  is constant by definition and then  $\delta_\Lambda = 0$ , so that we have a slight modification of eq. (5.79):

$$\ddot{\delta}_m + \mathcal{H} \dot{\delta}_m - \frac{3}{2} \mathcal{H}^2 \Omega_m \delta_m = 0 . \quad (5.103)$$

This equation can be rewritten in terms of the derivative with respect to  $\alpha$ :

$$\delta_m'' + \left( \frac{\mathcal{H}'}{\mathcal{H}} + 1 \right) \delta_m' - \frac{3}{2} \Omega_m \delta_m = 0 . \quad (5.104)$$

If we assume that  $\Omega_m = \text{constant}$ , then the solution is given by  $\delta_m \sim a^{m_\pm}$  with

$$m_\pm = \frac{1}{4} \left( -1 \pm \sqrt{1 + 24\Omega_m} \right) . \quad (5.105)$$

This case occurs when the fraction  $1 - \Omega_m$  is into some form of energy density which has  $w \approx 0$  but contrary to ordinary CDM it does not cluster on sub-horizon scales. The major example of this is massive neutrinos after they become non-relativistic. Supposing for a moment we could apply it also for CDM, this would show that the cosmological constant slows down the perturbation growth. In the limit  $\Omega_m \rightarrow 0$  we have  $m \rightarrow 0$  from eq. (5.105), which is qualitatively correct. However, the density parameter

$$\Omega_m = \frac{\rho_m}{\rho_m + \rho_\Lambda} = \frac{\rho_{m,0} a^{-3}}{\rho_{m,0} a^{-3} + \rho_\Lambda} = \frac{\Omega_{m,0} a^{-3}}{\Omega_{m,0} a^{-3} + \Omega_\Lambda} \quad (5.106)$$

is obviously not a constant. A much better approximation, obtained by an empirical fit, is given by defining the growth rate  $s$  of matter perturbations [35]:

$$s \equiv \frac{d \ln \delta_m}{d \ln a} = \Omega_m^\gamma, \quad (5.107)$$

that is

$$\delta_m(a) = \delta_m(a_i) \exp \left( \int_{a_i}^a \Omega_m(\bar{a})^\gamma \frac{d\bar{a}}{\bar{a}} \right), \quad (5.108)$$

where the growth index  $\gamma$  is  $\approx 0.55$  for the  $\Lambda$ CDM model. With this behaviour we realize that the term  $\mathcal{H}^2 \delta_m$  in the Poisson equation is no longer constant and therefore the gravitational potential on sub-horizon scales is not constant. For the  $\Lambda$ CDM model the gravitational potential is almost constant during the matter era, but it begins to decrease after the universe enters the dark-energy-dominated epoch.



# Chapter 6

## Correlation function and power spectrum

In the previous chapter we have studied the linear evolution of a perturbation described as a plane wave with corresponding wave vector  $\mathbf{k}$ . This representation is useful because a generic perturbation can be represented as a superposition of such plane waves (by the Fourier representation theorem) which, while they are evolving linearly, evolve independently of each other. In general we expect fluctuations to exist on a variety of mass or length scales and the final structure forming will depend on the growth of perturbations on different scales relative to each other. In this chapter we shall therefore look at perturbations in terms of their spectral composition and explain how the various spectral properties might arise.

### 6.1 The Correlation function

Let us set up some useful tools to describe a random distribution of particles, to be identified with astrophysical sources (galaxies, quasars, etc.). If there are  $N$  points in a volume  $V$ , the easiest descriptor is the average numerical density  $\rho_0 = N/V$ , the first order moment of the distribution. But clearly this is insufficient to discriminate among say  $N$  points clustered near the same spot and  $N$  points evenly distributed across the volume, so we need to find more useful descriptors. Let us focus then on some small volume  $dV$  chosen randomly inside the volume  $V$ . Then  $\rho_0 dV$  is the average number of particles in the infinitesimal volume. If  $dN_{ab} = \langle n_a n_b \rangle$  is the average number of *pairs* in the volumes  $dV_a$  and  $dV_b$  (i.e. the product of the number of particles in one volume times the number in another volume), separated by  $r_{ab}$ , then we can define another important descriptor, the 2-point correlation function  $\xi(r_{ab})$ , as

$$dN_{ab} = \langle n_a n_b \rangle = \rho_0^2 dV_a dV_b [1 + \xi(r_{ab})] \quad (6.1)$$

We have implicitly assumed that  $r_{ab} > 0$  i.e. the two volumes do not coincide. The word “average” can usually mean both an *ensemble* average and a *sample* average. The former is obtained by taking many realizations of the distribution, all of them produced

in the same way (e.g., by an N-body computer code or by throwing particles at random), selecting in each realization the volumes  $dV_a, dV_b$  at the same locations and then averaging the pair number  $n_a n_b$ . For the latter one can take the pairs at different spots within the same realization, separated by the same  $r_{ab}$ . If the spots are so distant that they are uncorrelated, then we can consider them as coming from different realizations and the two averaging methods coincide. The problem with the second approach is that we do not know *a priori* whether the spots really are uncorrelated until we can compare them with an ensemble of realizations. This issue is particularly acute in astrophysics since we are given a single Universe (and then a single realization). The sample correlation function does not in general coincide with the one we would obtain from an ensemble. This problem is of course more important for distributions that are inhomogeneous at very large scales. The estimation of the correlation function on scales smaller than the scale of (approximate) homogeneity will not coincide with the ensemble value. Even in those cases, however, the correlation function is a useful descriptor (although a survey-dependent one) and it makes sense to use it. However here we will always assume that the properties of the sample distribution are a good approximation of the ensemble ones.

If the distribution has been obtained by throwing the  $N$  particles at random (i.e. without any preference with respect to the place), or in other words, if their distribution is Poissonian, then there is no reason for  $dN_{ab}$  to depend on the location. Therefore the average number of pairs is exactly equal to the product of the average number of particles in the two volumes,  $\langle n_a \rangle \langle n_b \rangle = \rho_0^2 dV_a dV_b$ , and the correlation  $\xi$  vanishes. Conversely, if  $\xi$  is non-zero, we say that the particles are correlated. Then the correlation function can also be written as a spatial average of the product of the density contrast  $\delta(r_a) = n_a/(\rho_0 dV_a) - 1$  at two different points:

$$\xi(r_{ab}) = \frac{dN_{ab}}{\rho_0^2 dV_a dV_b} - 1 = \langle \delta(r_a) \delta(r_b) \rangle, \quad (6.2)$$

where we have used  $\langle \delta(r_a) \rangle = \langle \delta(r_b) \rangle = 0$ . If this average is taken to be the sample average, then it means we have to average over all possible positions:

$$\xi(\mathbf{r}) = \frac{1}{V} \int \delta(\mathbf{y}) \delta(\mathbf{y} + \mathbf{r}) dV_y. \quad (6.3)$$

When  $\xi(\mathbf{r})$  depends only on the separation  $\mathbf{r}$  and not on  $r_a$  and  $r_b$  individually, the system is said to be *statistically homogeneous* (i.e. it possesses the same statistical properties everywhere). If moreover the ensemble average coincides with the sample average, then the system is said to be *ergodic*. However the latter term refers historically to time processes, not to spatial ones. The term most often used in astrophysics is that the system is a *fair sample* of the Universe.

In practice it is easier to derive the correlation function as the average density of particles at a distance  $r$  from another particle. This is a *conditional* density, that is the density of particles at a distance  $r$  given that there is a particle at  $r = 0$ . Then the number of pairs is given by the number of particles in both volumes divided by the number of particles  $dN_a = \rho_0 dV_a$  in the volume  $dV_a$  at  $r = 0$ :

$$dN_b = \frac{dN_{ab}}{dN_a} = \frac{\rho_0^2 dV_a dV_b [1 + \xi(r_{ab})]}{dN_a} = \rho_0 dV_b [1 + \xi(r_{ab})]. \quad (6.4)$$

Operationally therefore one evaluates the correlation function as follows:

$$\xi(r) = \frac{dN(r)}{\rho_0 dV} - 1 = \frac{\langle \rho_c \rangle}{\rho_0} - 1, \quad (6.5)$$

i.e. as the average number of particles at distance  $r$  from any given particle (or number of neighbours), divided by the expected number of particles at the same distance in a uniform distribution, minus 1 (sometimes this is called *conditional density contrast*). This definition better clarifies the role of the correlation function as a *measure of the excess probability, compared with that expected for a random distribution, of finding a pair of particles at a separation  $r$* .

In a finite volume, when the average density is estimated from the sample itself, i.e.  $\rho_0 = N/V$  it is clear that the integral of  $dN_c(r)$  must converge to the number of particles in the sample:

$$\int dN(r) = \int \rho(r) dV = N, \quad (6.6)$$

which gives an integral constraint on  $\xi(r)$

$$\int \xi(r) dV = \frac{1}{\rho_0} \int \frac{dN}{dV} dV - V = \frac{N}{\rho_0} - V = 0. \quad (6.7)$$

If the correlation  $\xi(r)$  is positive, there are more particles within a distance  $r$  than in a uniform distribution. In this case the distribution is said to be *positively clustered*. Quite often one is interested only in the dependence on the modulus  $r$ , so the volume at distance  $r$  is chosen as a shell around each particle. One could generalize this definition by introducing the anisotropic correlation function as the number of pairs in volumes separated by the vector  $r$ . This is useful whenever there is some reason to suspect that the distribution is indeed anisotropic, as when there is a significant distortion along the line of sight due to the galaxy peculiar velocity.

## 6.2 Measuring the correlation function in real catalogs

The estimator (6.7) requires the knowledge of the number density  $\rho_c$  inside a shell of thickness  $dr$  at distance  $r$  from every particle. In other words, it requires the estimation of the density in every shell. In practice, a direct estimation of the shell density is difficult because of the complicated boundary and selection procedure that a real survey often has. The simplest way to measure  $\xi$  is to compare the real catalog to an artificial random catalog with exactly the same boundaries and the same selection function (obtained for instance through a Monte Carlo simulation). The choice of the estimator is not unique. For instance we can use the Davis-Peebles estimator [36]

$$\xi = \frac{DD}{DR} - 1 \quad (6.8)$$

or that by Landy & Szalay [37]

$$\xi = \frac{DD - 2DR + RR}{RR} \quad (6.9)$$

which turns out to be more robust. Other choices have obviously been proposed. In the above equations  $DD$  means the number of galaxies at distance  $r$  counted by an observer centered on a real galaxy;  $DR$  are the number of pairs at distance  $r$  where one member ( $D$ ) is a real galaxy and the other one ( $R$ ) is a fictitious object taken from a catalog of objects uniformly distributed in a volume and with selection function identical to those of the real catalog. In other words, instead of calculating the volume of the shell (which is a difficult task in realistic cases), we estimate  $\xi$  by counting the galaxies in the Monte Carlo realization. In this way all possible boundaries and selection function can be easily mimicked in the random catalog, which will affect  $DD$  and  $DR$  in the same way.

### 6.3 The power spectrum

As we have seen in the previous sections, in order to describe the distribution of matter in the Universe it is useful to think of the perturbations as superpositions of plane waves in the Fourier space. One of the most employed statistical estimator for density fields in Fourier space is the power spectrum; it is by far the most common descriptor of clustering in the linear and mildly non-linear regime and plays a central role in cosmology.

In order to avoid confusion let us specify the convention we adopt for the 3-dimensional Fourier transformation

$$f(\mathbf{x}) = \frac{V}{(2\pi)^3} \int f_{\mathbf{k}} e^{i\mathbf{k}\cdot\mathbf{x}} d^3k, \quad (6.10)$$

$$f_{\mathbf{k}} = \frac{1}{V} \int f(x) e^{-i\mathbf{k}\cdot\mathbf{x}} d^3x. \quad (6.11)$$

With these conventions,  $f(\mathbf{x})$  and  $f_{\mathbf{k}}$  have the same dimensions. The Dirac's delta function  $\delta_D(\mathbf{x})$  is defined as

$$\delta_D(\mathbf{x}) = \frac{1}{(2\pi)^3} \int e^{i\mathbf{k}\cdot\mathbf{x}} d^3k. \quad (6.12)$$

Analogous definition holds for Dirac's function in Fourier space (which is not the Fourier transform of  $\delta_D(\mathbf{x})$ )

$$\delta_D(\mathbf{k}) = \frac{1}{(2\pi)^3} \int e^{i\mathbf{k}\cdot\mathbf{x}} d^3x, \quad (6.13)$$

and their normalization is such that

$$\int \delta_D(\mathbf{k}) d^3k = \int \delta_D(\mathbf{x}) d^3x = 1 \quad (6.14)$$

In order to understand the meaning of the power spectrum and its relation with the correlation function in real space, let us consider a volume  $V$ , for example a cube of side  $L \gg l_s$ , where  $l_s$  is the maximum scale at which there is a significant structure due to the perturbations;  $V$  can be thought of as a 'fair sample' of the Universe if this is the case. It is possible therefore to construct, formally, a 'realization' of the Universe by dividing it into cells of volume  $V$  with periodic boundary conditions at the faces of each cube. This device will be convenient for many applications but should not be taken too literally.

Indeed, one can take the limit  $V \rightarrow \infty$  in most cases, as we shall see later. Let us denote by  $\rho$  the mean density in a volume  $V$  and  $\rho(\mathbf{x})$  to be the density at a point specified by the position vector  $\mathbf{x}$  with respect to some arbitrary origin. As usual we define the fluctuation  $\delta(\mathbf{x}) = [\rho(\mathbf{x}) - \rho]/\rho$ . As we did in the previous chapter we take this to be expressible as a Fourier series:

$$\delta(\mathbf{x}) = \sum_{\mathbf{k}} \delta_{\mathbf{k}} e^{i\mathbf{k}\cdot\mathbf{x}} = \sum_{\mathbf{k}} \delta_{\mathbf{k}}^* e^{-i\mathbf{k}\cdot\mathbf{x}}, \quad (6.15)$$

where the assumption of periodic boundary conditions  $\delta(L, y, z) = \delta(0, y, z)$ , etc., requires that the wavevector  $\mathbf{k}$  has components

$$k_x = n_x \frac{2\pi}{L}, \quad k_y = n_y \frac{2\pi}{L}, \quad k_z = n_z \frac{2\pi}{L}, \quad (6.16)$$

with  $n_x, n_y$ , and  $n_z$  integers. The Fourier coefficients  $\delta_{\mathbf{k}}$  are complex quantities given, as it is straightforward to see, by

$$\delta_{\mathbf{k}} = \frac{1}{V} \int_V \delta(\mathbf{x}) e^{-i\mathbf{k}\cdot\mathbf{x}} d\mathbf{x}; \quad (6.17)$$

because of conservation of mass in  $V$  we have  $\delta_{\mathbf{k}=0} = 0$ ; because of the reality of  $\delta(\mathbf{x})$  we have  $\delta_{\mathbf{k}}^* = \delta_{-\mathbf{k}}$ .

If, instead of the volume  $V$ , we had chosen a different volume  $V'$ , the perturbation within the new volume would again be represented by a series of the form (6.15), but with different coefficients  $\delta_{\mathbf{k}}$ . If one imagines a large number  $N$  of such volumes, i.e. a large number of ‘realizations’ of the Universe, one will find that  $\delta_{\mathbf{k}}$  varies from one to the other in both amplitude and phase. If the phases are random, not only across the ensemble of realizations, but also from node to node within each realization, then the density field has Gaussian statistics.

Since the mean value of a perturbation variable, such as  $\delta(\mathbf{x}) \equiv \delta$ , across the statistical ensemble is identically zero by definition, the simplest non-trivial statistics corresponds to a quadratic function of the variables, i.e. its variance  $\sigma^2$ . In Fourier space, any real quadratic function of a perturbation variable is called a power spectrum. It is straightforward to show that

$$\sigma^2 \equiv \langle \delta^2 \rangle = \sum_{\mathbf{k}} \langle |\delta_{\mathbf{k}}|^2 \rangle = \frac{1}{V} \sum_{\mathbf{k}} \delta_k^2, \quad (6.18)$$

where the average is taken over an ensemble of realizations. The quantity  $\delta_k$  is defined by the relation (6.18) and one can see from eq. (6.18) that  $\langle |\delta_{\mathbf{k}}|^2 \rangle$  is the contribution to the variance due to waves of wavenumber  $\mathbf{k}$ .

The power spectrum is then defined as

$$P(\mathbf{k}) = V |\delta_{\mathbf{k}}|^2 = V \delta_{\mathbf{k}} \delta_{\mathbf{k}}^*. \quad (6.19)$$

Notice that the power spectrum has the dimension of a volume. It follows that

$$P(\mathbf{k}) = \frac{1}{V} \int \delta(\mathbf{x}) \delta(\mathbf{y}) e^{-i\mathbf{k}\cdot(\mathbf{x}-\mathbf{y})} dV_x dV_y. \quad (6.20)$$

Setting  $\mathbf{r} = \mathbf{x} - \mathbf{y}$ , the spectrum (6.20) reduces to

$$P(\mathbf{k}) = \int \xi(\mathbf{r}) e^{-i\mathbf{k}\cdot\mathbf{r}} dV, \quad (6.21)$$

where  $\xi(\mathbf{r})$  is defined in eq. (6.3). Therefore, the power spectrum is the Fourier transform of the correlation function (Wiener–Khinchin theorem). The converse property is

$$\xi(\mathbf{r}) = \frac{1}{(2\pi)^3} \int P(\mathbf{k}) e^{i\mathbf{k}\cdot\mathbf{r}} d^3k. \quad (6.22)$$

Notice that here and in the following the Fourier volume factor is not included, as in most literature.

If we now assume that the density field is statistically homogeneous and isotropic, i.e. that the correlation function depends only on the modulus  $r = |\mathbf{r}|$ , the spectrum has no dependence on the direction of  $\mathbf{k}$  but only on  $k = |\mathbf{k}|$ :

$$P(k) = \int \xi(r) r^2 dr \int_0^\pi e^{-ikr \cos\theta} \sin\theta d\theta \int_0^{2\pi} d\phi = 4\pi \int \xi(r) \frac{\sin(kr)}{kr} r^2 dr. \quad (6.23)$$

The above definitions of the power spectrum refer to infinite samples and to a continuous field. In reality, we always have a finite sample and a discrete realization of the field, i.e. a finite number of particles. Therefore we have to take into account the effects of both finiteness and discreteness.

To investigate the discreteness, we assume as field a collection of  $N$  particles of dimensionless unitary masses at positions  $\mathbf{x}_i$ , in a volume  $V$ . In the following we will make use of the window function  $W(\mathbf{x})$ , a function that expresses the way in which the particles are selected. A typical selection procedure is to take all particles within a given region, and no particles elsewhere. In this case, the function will be a constant inside the survey, and zero outside (top-hat window function). We will always consider such a kind of window function in the following, and normalize it such that

$$\int W(\mathbf{x}) dV = 1. \quad (6.24)$$

With this normalization,  $W(\mathbf{x}) = 1/V$  inside the survey. The density contrast field we have in a specific sample is therefore the field times the window function (times the sample volume  $V$  because of the way we have normalized  $W$ ):

$$\delta_s = \delta(\mathbf{x}) V W(\mathbf{x}). \quad (6.25)$$

Let us now express the field as a sum of Dirac functions  $\rho(\mathbf{x}) = \sum_i \delta_D(\mathbf{x} - \mathbf{x}_i)$  so that

$$\delta_s(\mathbf{x}) = \left( \frac{\rho(\mathbf{x})}{\rho_0} - 1 \right) V W(\mathbf{x}) = \frac{V}{N} \sum_i w_i \delta_D(\mathbf{x} - \mathbf{x}_i) - V W(\mathbf{x}), \quad (6.26)$$

where  $w_i = V W(\mathbf{x}_i)$  and as usual  $\rho_0 = N/V$ . The Fourier transform is

$$\delta_{\mathbf{k}} = \frac{1}{V} \int \left( \frac{V}{N} \sum_i w_i \delta_D(\mathbf{x} - \mathbf{x}_i) - V W(\mathbf{x}) \right) e^{-i\mathbf{k}\cdot\mathbf{x}} dV = \frac{1}{N} \sum_i w_i e^{-i\mathbf{k}\cdot\mathbf{x}_i} - W_{\mathbf{k}}, \quad (6.27)$$

where we have introduced the  $k$ -space window function

$$W_k = \int W(\mathbf{x}) e^{-i\mathbf{k}\cdot\mathbf{x}} dV \quad (6.28)$$

normalized such that  $W_0 = 1$ . The spherical top-hat function corresponds to

$$W(\mathbf{x}) = \begin{cases} 1/V & \text{inside a spherical volume } V \text{ of radius } R \\ 0 & \text{outside.} \end{cases}$$

We then have

$$W_k = \frac{1}{V} \int_V e^{-i\mathbf{k}\cdot\mathbf{x}} dV = \frac{3}{R^3} \int_0^R \frac{r \sin(kr)}{k} dr = \frac{3[\sin(kR) - kR \cos(kR)]}{(kR)^3}, \quad (6.29)$$

where in the second equality we have integrated out the angular part as we did to derive eq. (6.23). Notice that the function declines rapidly as  $k \rightarrow \pi/R$ . Now squaring and averaging  $\delta_{\mathbf{k}}$  in eq. (6.27) by separating the  $i = j$  terms from the others, we have

$$\langle \Delta^2(\mathbf{k}) \rangle \equiv V \langle \delta_{\mathbf{k}} \delta_{\mathbf{k}}^* \rangle = P(\mathbf{k}) + P_n, \quad (6.30)$$

where the “true” spectrum  $P(\mathbf{k})$  and the pure noise spectrum  $P_n$  are given, respectively, by

$$P(\mathbf{k}) = \frac{V}{N^2} \sum_{i \neq j} \langle w_i w_j \rangle e^{-i\mathbf{k}\cdot(\mathbf{x}_i - \mathbf{x}_j)} - V W_k^2 \quad (6.31)$$

$$P_n = \frac{V}{N^2} \sum_i w_i^2 = \frac{V}{N}, \quad (6.32)$$

where the last equality holds if  $w_i$  equals 0 or 1. In order to derive eq. (6.31) we have used the relation

$$W_k = \left\langle \frac{1}{N} \sum_i w_i e^{-i\mathbf{k}\cdot\mathbf{x}_i} \right\rangle \quad (6.33)$$

obtained averaging eq. (6.27) and remembering that  $\langle \delta_{\mathbf{k}} \rangle = 0$ .

The noise spectrum, negligible only for large densities,  $\rho_0 = N/V \rightarrow \infty$ , is the power spectrum of a distribution with no intrinsic correlation, i.e. obtained by throwing the particles at random (the positions  $\mathbf{x}_i$  and  $\mathbf{x}_j$  are uncorrelated). More exactly, it is the power spectrum of a Poissonian distribution. Since the galaxy distributions are often sparse, the noise is not always negligible and has to be subtracted from the estimate if we want to detect the underlying correlation. Therefore the estimator of the “true” power spectrum  $P(\mathbf{k})$  can be taken as

$$\hat{P}(\mathbf{k}) = \Delta^2(\mathbf{k}) - P_n. \quad (6.34)$$

As for the correlation function, the power spectrum does not characterize a distribution completely, unless we know the distribution has some specific property, e.g., Gaussian, or

Poisson, etc. In particular, if we assume the fluctuations to be Gaussian, we can derive the variance of the power spectrum, defined as

$$\sigma_P^2(\mathbf{k}) \equiv \left\langle [\hat{P}(\mathbf{k}) - P(\mathbf{k})]^2 \right\rangle, \quad (6.35)$$

where  $P(\mathbf{k}) = \langle \hat{P}(\mathbf{k}) \rangle = \langle \Delta^2(\mathbf{k}) \rangle - P_n$ . With some manipulations (see [38] for a complete derivation), eq. (6.35) can be written as

$$\sigma_P^2(\mathbf{k}) = V^2 \langle \delta_{\mathbf{k}} \delta_{\mathbf{k}}^* \rangle^2 = (P(\mathbf{k}) + P_n)^2, \quad (6.36)$$

from which we obtain the fractional variance of the power spectrum with top-hat filtering to be

$$\frac{\sigma_P^2(\mathbf{k})}{P^2(\mathbf{k})} = \left( 1 + \frac{1}{nP(\mathbf{k})} \right)^2, \quad (6.37)$$

where  $n = N/V$  is the number density. This tells us that, if the fluctuations are Gaussian, the error of the root mean square (rms) on the power spectrum is of the order of the power spectrum itself (including the shot noise).

In general we consider the shell-averaged spectrum, i.e. the spectrum for all modes whose wavenumber modulus  $k$  lies within the shell  $\Delta k$  of volume  $V_k$ :

$$P(k) = \frac{1}{V_k} \int_{\Delta k} P(\bar{k}) d^3 \bar{k}. \quad (6.38)$$

If the survey has a volume  $V_s = L^3$ , the lowest wavenumber we can safely construct is  $k_{\min} = 2\pi/L$ . Then the number of independent  $k$ -modes in a volume  $V_k$  is

$$N_k = \frac{V_k}{k_{\min}^3} = \frac{V_k V_s}{(2\pi)^3}. \quad (6.39)$$

Therefore the error on the shell-averaged spectrum  $P(k)$  is reduced by the factor  $1/N_k$  and we obtain

$$\frac{\sigma_P^2(k)}{P^2(k)} \simeq \frac{(2\pi)^3}{V_k V_s} \left( 1 + \frac{1}{nP(k)} \right)^2$$

Another way of looking at this equation is to say that the effective  $k$ -volume resolution  $k_{\min}^3$  degrades due to the shot noise to  $k_{\min}^3 (1 + 1/(nP))^2$ , so that there are effectively less independent  $k$ -volumes to average over.

## 6.4 Normalization of the power spectrum

Let us define the following integral (by definition  $\int W_i dV = 1$  for any window function)

$$\sigma^2 = \int W_1 W_2 \xi_{12} dV_1 dV_2. \quad (6.40)$$

Since  $\xi_{12} = (2\pi)^{-3} \int P(\mathbf{k}) e^{-i\mathbf{k}\cdot(\mathbf{r}_1 - \mathbf{r}_2)} d^3 k$  from eq. (6.22) we have

$$\sigma^2 = (2\pi)^{-3} \int P(\mathbf{k}) e^{-i\mathbf{k}\cdot(\mathbf{r}_1 - \mathbf{r}_2)} W_1 W_2 d^3 k d^3 r_1 d^3 r_2. \quad (6.41)$$

For spherical cells of radius  $R$ , integrating over the angles, this reduces to

$$\sigma_R^2 = \frac{1}{2\pi^2} \int P(k) W_R^2(k) , \quad (6.42)$$

where we have used  $W_R^2(k) = \int e^{i\mathbf{k}\cdot\mathbf{r}_1} W_1 d^3r_1 \int e^{-i\mathbf{k}\cdot\mathbf{r}_2} W_2 d^3r_2$ . If the cells have a radius of  $8 h^{-1}$  Mpc, it turns out that  $\sigma_R$  is close to unity. Conventionally the normalization of the power spectrum is given by quoting  $\sigma_8$  which turns out to be the "linearity scale". This allows to normalize the linear power spectrum, easier to model than the non-linear one.

## 6.5 Velocity field

Another way to measure the mass power spectrum (and constrain  $\Omega_{m,0}$  and  $\gamma$ ) is obtained by analyzing the peculiar motion of the galaxies in clusters. In fact, it is easily arguable that strong peculiar velocities are induced by large fluctuations in the mass density field. One of the important features of this approach is that the velocity field depends on the *total* mass distribution, not only on that of the luminous matter. In order to better understand the relation between the velocity field and the matter distribution let us write eq. (5.73), with  $\theta = \nabla_i v^i$ , in Fourier space:

$$\dot{\delta}_k = -ik_i v^i , \quad (6.43)$$

where

$$\dot{\delta}_k = \frac{d\delta_k}{d\tau} = \frac{d\delta_k}{d\ln a} \frac{d\ln a}{d\tau} = \delta_k \frac{d\ln \delta_k}{d\ln a} \mathcal{H} . \quad (6.44)$$

As we have seen in the previous chapter, this equation applies separately to each pressureless component, such as baryons and CDM. However, the baryons will be driven by the dominating density contrast of the CDM, due to gravitational coupling. The common gravitational field strictly implies that the acceleration, not the velocity, is the same for both species. However, if we also assume similar initial conditions, universality of the gravitational interaction and identical equation of state and sound speed, we can assume that the galaxy velocities are not biased with respect to the dark matter velocity field. Therefore the velocity field  $\mathbf{v}$  can be represented by the galaxy velocity field  $\mathbf{v}_g$ : observing the peculiar velocity field  $\mathbf{v}_g$  of galaxies gives information on the total density contrast. Then we take  $\mathbf{v}$  to refer to the velocity field of galaxies and  $\delta_k$  to refer to the total mass.

Let us rewrite eq. (5.50), which comes from the continuity equation, for  $c_s = 0$ :

$$\dot{v}^i = -\mathcal{H}v^i + ik^i \Phi_k . \quad (6.45)$$

Since we are dealing only with scalar perturbations, the velocity can be written as the gradient of a velocity potential  $v$ , i.e.  $v^i = \nabla^i v \rightarrow ik^i v$ . Then it is clear that  $v^i$  is parallel to  $k^i$  and we can look for solutions of eq. (6.45) in the form  $v^i = F(k, a)k^i$ . This gives from eqs (6.43) and (6.44) the relation between the peculiar velocity field  $v^i$  and the density fluctuation  $\delta_k$  in linear perturbation theory (in the Newtonian regime):

$$v^i = i\mathcal{H} s \delta_k \frac{k^i}{k^2} , \quad (6.46)$$

where  $s$  is the growth rate defined in eq. (5.107). Substituting eq. (6.46) into eq. (6.43), one can easily confirm that the relation  $s = \dot{\delta}_k / (\mathcal{H}\delta_k) = d \ln \delta_k / d \ln a$  follows. During the standard matter-dominated era we have already seen that  $\delta_k \propto a$  and hence  $s = 1$  while more in general  $s = \Omega_m(a)^\gamma$ .

If we consider the present epoch  $a = a_0 = 1$ , which yields  $\mathcal{H} = H_0$ , we have

$$\mathbf{v} = iH_0 s \delta_k \frac{\mathbf{k}}{k^2}. \quad (6.47)$$

The peculiar velocity  $\mathbf{v}(\mathbf{r})$ , at position  $\mathbf{r}$  in real-space, is obtained by Fourier anti-transformation of eq. (6.47):

$$\mathbf{v}(\mathbf{r}) = iH_0 s \frac{V}{(2\pi)^3} \int \delta_k \frac{\mathbf{k}}{k^2} e^{i\mathbf{k}\cdot\mathbf{r}} d^3k, \quad (6.48)$$

where we have assumed  $s$  to be  $k$ -independent. This is true in  $\Lambda$ CDM, but not in every model: for instance, in Chapter 9 we will study a class of modified gravity models of dark energy, the so-called  $f(R)$  models, whose growth rate  $s$  does depend on the scale  $k$ .

## 6.6 Redshift distortion

The typical way to measure the cosmological distance of a galaxy consists in measuring its redshift and then convert it into a distance in real space, assuming a cosmological model. However, in addition to the recession velocity due to the expansion of the universe, the redshift of an object includes also its peculiar velocity, so that there is an error in the distances we assign to galaxies, that alters the 1:1 correspondence between redshift and distance. The net effect is that the apparent distribution of galaxies in redshift space is different from the real one. The distortions can be roughly divided into two classes, depending on the nature of the dominant peculiar motion. The first one of these is the ‘‘Fingers-of-God’’ effect i.e. the fact that virialized structures are not spherical in redshift space, but appear elongated along the line of sight, thus pointing to the observer. Since we are not privileged observers, this effect must be unphysical, a sort of optical illusion. In fact, they are caused by the random non-linear motions of the objects within these structures. They can be modeled by assuming that the motions are completely random and that their distribution function resembles a Gaussian or an exponential. We will come back to this point later.

The other important redshift distortion is the Kaiser Effect [39] which quantifies the effect of coherent, large scale motions associated to the linear growth of density fluctuations. Since these peculiar velocities are due to infall motions toward large cosmic structures, the net effect is to enhance the density contrast of these structures along the line of sight. On large scales, where the growth of fluctuations is described by linear theory, the Kaiser effect can be quantified analytically. Let us call  $\mathbf{v}_p$  the peculiar velocity of a source at position  $\mathbf{r}$  and define the line-of-sight component

$$u(r) \equiv \mathbf{v}_p \cdot \frac{\mathbf{r}}{r}, \quad (6.49)$$

where  $r = |\mathbf{r}|$ . Putting together equations (1.63) and (1.65) and considering that also the observer can have a non zero component on the line-of-sight of its peculiar velocity,  $u(0)$ , we can write the coordinate transformation from real space ( $r$ ) to redshift space ( $s$ ) as

$$s = r \left[ 1 + \frac{u(r) - u(0)}{r} \right], \quad (6.50)$$

where we chose units such that  $H = 1$  and assumed  $c = 1$ . In other words, we express velocities in Megaparsec.

If  $dV_s$  and  $dV_r$  are the volume elements in redshift and real space respectively, with number densities  $n(s)$  and  $n(r)$  we have, to conserve the number of galaxies

$$n(r)dV_r = n(s)dV_s. \quad (6.51)$$

The volume element  $dV_s = d^3s$  can be written in terms of the  $r$  coordinate as

$$dV_s = \left( 1 + \frac{\Delta u(r)}{r} \right)^2 |J| (r^2 \sin \theta) dr d\theta d\phi = \left( 1 + \frac{\Delta u(r)}{r} \right)^2 |J| dV_r, \quad (6.52)$$

where  $\Delta u(r) = u(r) - u(0)$ . The jacobian  $|J|$  is given by the derivatives of  $s$  with respect to  $r$

$$|J| = \left| \frac{\partial s}{\partial r} \right| = 1 + \frac{du}{dr}. \quad (6.53)$$

If the average density is  $n_0$ , the density contrast in  $s$ -space can be written as

$$\delta_s = \frac{n(s)dV_s}{n_0 dV_s} - 1 = \frac{n(r)dV_r}{n_0 dV_s} - 1 = \frac{n(r)}{n_0 (1 + \Delta u(r)/r)^2 |J|} - 1, \quad (6.54)$$

where we have used eqs (6.51) and (6.52).

To first order, this gives

$$\begin{aligned} \delta_s &\simeq \frac{n(r)}{n_0} \left[ 1 - 2 \frac{\Delta u(r)}{r} - \frac{du}{dr} \right] - 1 = \\ &= \delta_r - 2 \frac{\Delta u(r)}{r} - \frac{du}{dr}, \end{aligned} \quad (6.55)$$

where in the last equality we have used the fact that to first order we can approximate  $n(r)$  to be  $n_0$ . Then, one can see that the density contrast differs in the two spaces. This difference will be reflected in the different correlation properties of the two density fields and will have to be accounted for in order to recover the true quantities from the observed one. For example, one will have to correct the observed power spectrum to recover the true one. In order to do this correction, we can use the velocity field computed through linear perturbation theory in the previous section, eq. (6.47). But, as we said, in that case we assumed  $\delta$  to refer to the total mass density contrast,  $\delta_m$ . What we observe is instead the galaxy density contrast  $\delta_g$ , which is different from  $\delta_m$ . Were gravity the only driving force, then the mass and galaxy density contrasts would coincide. However, whenever non-gravitational processes, typically associated to galaxy formation and evolution, are

important, the 1:1 correlation between the two fields is likely to be broken up and galaxies cannot be used as signposts of the dark matter distribution. In the cosmological jargon, galaxies are *biased* tracers of the underlying density field. If the biasing is local, then it can be conveniently quantified as

$$b \equiv \frac{\delta_g}{\delta_m}, \quad (6.56)$$

a quantity that depends on both position and time. Thus, for example, eq. (6.47) should be written as

$$\mathbf{v} = iH_0\beta\delta_k \frac{\mathbf{k}}{k^2}. \quad (6.57)$$

which implies that we should substitute  $s$  with  $\beta \equiv s/b$ . If we deal with filtered density fields, which is often the case, then if the filtering scale is significantly larger than the typical scales affected by galaxy formation processes, then one can assume that the biasing is constant, i.e. that  $b$  is a simple parameter, the bias parameter, that does not depend on the position. In this case eq. (6.48) can be written as

$$\mathbf{v} = iH_0\beta \int (\delta_g)_k e^{i\mathbf{k}\cdot\mathbf{r}} \frac{\mathbf{k}}{k^2} d^3k^*, \quad (6.58)$$

where the differential  $d^3k^*$  includes the Fourier factor  $V/(2\pi)^3$ . The assumption of  $b$  being independent on space implies that the relation in eq. (6.56) holds both in real and Fourier space. In particular, for the power spectra we have

$$P_g(k) = b^2 P_m(k). \quad (6.59)$$

Making use of eq. (6.58), the line-of-sight component (6.49) can be written as

$$u(r) = i\beta \int (\delta_g)_k e^{i\mathbf{k}\cdot\mathbf{r}} \frac{\mathbf{k}\cdot\mathbf{r}}{k^2 r} d^3k^*, \quad (6.60)$$

while its derivative is

$$\frac{du}{dr} = -\beta \int (\delta_g)_k e^{i\mathbf{k}\cdot\mathbf{r}} \left( \frac{\mathbf{k}\cdot\mathbf{r}}{kr} \right)^2 d^3k^*, \quad (6.61)$$

where we have used the relation

$$\frac{d}{dr} e^{i\mathbf{k}\cdot\mathbf{r}} = i \frac{\mathbf{k}\cdot\mathbf{r}}{r} e^{i\mathbf{k}\cdot\mathbf{r}}. \quad (6.62)$$

From eq. (6.55), we have finally

$$\delta_s = \delta_r - \frac{du}{dr} = \delta_r + \beta \int \delta_{rk} e^{i\mathbf{k}\cdot\mathbf{r}} \left( \frac{\mathbf{k}\cdot\mathbf{r}}{kr} \right)^2 d^3k^*, \quad (6.63)$$

where the second term in eq. (6.55) has been neglected because it is small for large  $r$  and the subscript  $g$  in  $\delta$  has been substituted with  $r$  to indicate that this quantity is in real space.

Multiplying eq. (6.63) on both sides by  $V^{-1}e^{i\mathbf{k}'\cdot\mathbf{r}}$  and integrating, we can obtain its Fourier transform by use of eq. (6.11)(5.11):

$$\delta_{sk} = \delta_{rk} + \beta \int \delta_{rk'} I(k, k') d^3 k' , \quad (6.64)$$

where

$$I(k, k') = \frac{1}{(2\pi)^3} \int e^{i(\mathbf{k}'-\mathbf{k})\cdot\mathbf{r}} \left( \frac{\mathbf{k}'\cdot\mathbf{r}}{k'r} \right)^2 d^3 r \quad (6.65)$$

and we switched  $k, k'$ .

One can then see that the effect of the redshift distortion is to introduce a coupling between different modes. However this coupling can be broken if we consider surveys of very small angular scale. In fact, if the survey spans a small solid angle, it is possible to assume that the cosine

$$\mu = \frac{\mathbf{k}\cdot\mathbf{r}}{kr} \quad (6.66)$$

is almost constant. Then we have  $I(k, k') = \mu^2 \delta_D(\mathbf{k}' - \mathbf{k})$  and from eq. (6.64):

$$\delta_{sk} = \delta_{rk}(1 + \beta\mu^2) . \quad (6.67)$$

Thus, the power spectrum defined in eq. (6.19)(5.19) reads

$$P_s(\mathbf{k}) = V\delta_{rk}^2(1 + \beta\mu^2)^2 = P_r(\mathbf{k})(1 + \beta\mu^2)^2 . \quad (6.68)$$

If we average it over angles, we obtain [39]

$$P_s(k) = P_r(k)(1 + 2\beta\langle\mu^2\rangle + \beta^2\langle\mu^4\rangle) , \quad (6.69)$$

where the average  $\langle f(\mu) \rangle = (4\pi)^{-1} \int_0^\pi f(\mu) \sin\theta d\theta \int_0^{2\pi} d\phi = (1/2) \int_{-1}^1 f(\mu) d\mu$  gives

$$\langle\mu^2\rangle = \frac{1}{2} \int_{-1}^1 \mu^2 d\mu = \frac{1}{3} , \quad \langle\mu^4\rangle = \frac{1}{2} \int_{-1}^1 \mu^4 d\mu = \frac{1}{5} . \quad (6.70)$$

Eq. (6.69) becomes

$$P_s(k) = P_r(k) \left( 1 + \frac{2\beta}{3} + \frac{\beta^2}{5} \right) . \quad (6.71)$$

The power spectrum is then boosted in redshift space, because velocities are highly coherent and their vectors typically point toward mass concentrations. As a consequence, galaxy concentrations associated to large, non-virialized structures appear to be enhanced in redshift space.

As already mentioned at the beginning of this section, peculiar motions on small scales also contribute to the redshift distortion. These motions, which are highly incoherent, cause large virialized structure to appear radially elongated: the so called Fingers-of-God effect. This particular distortion removes power from small scales and induces anisotropies in the galaxy clustering and affect both the power spectrum and the correlation function of the galaxies. This effect can be corrected with a statistical approach that is best

understood in configuration (real) space. The two point correlation function is estimated by pair counting. Fingers of God displace close pairs along the line of sight according to the relative velocity of the object. A statistical correction for this effect can be obtained by convolving the observed correlation function with the pairwise velocity distribution function,  $f(\sigma_{12})$ . In Fourier space, the convolution corresponds to multiply the power spectrum by a factor which is substantially the Fourier transformation of  $f(\sigma_{12})$ :

$$P(k, \mu, \text{nl}) = F(k, \mu^2)P(k, \mu, \text{lin}), \quad (6.72)$$

where “nl” and “lin” stand for non-linear and linear respectively. In order to match behavior on large scale, it is required that  $\lim_{k \rightarrow 0} F(k, \mu^2) = 1$ . In general, fingers-of-God are difficult to model well, and their amplitude is strongly dependent on the mean halo mass and satellite fraction of the population under consideration ([40][41]). Unfortunately, there is no precise theoretical prediction for the pairwise velocity distribution function. So far, most works have assumed either a Gaussian or an exponential model (e.g. [42][43]) for the pairwise velocity dispersion in real space. For an exponential model for the pairwise velocity dispersion in real space, we expect a Lorentz damping factor for the power spectrum, while the Gaussian dispersion translates to a Gaussian damping of the power spectrum:

$$F_{\text{exponential}}(k, \mu^2) = [1 + (k\sigma\mu)^2]^{-1} \quad (6.73)$$

$$F_{\text{gaussian}}(k, \mu^2) = \exp[-(k\sigma\mu)^2] \quad (6.74)$$

where  $\sigma$  is the rms velocity dispersion. It is worth pointing out that random errors in the measured redshift also produce some smearing on small scales that can also be modeled with a Gaussian distribution. Then, in order to consider the instrumental error on the redshift measurements (and hence on the distance) we can rescale the power spectrum, multiplying it by a factor

$$e^{-(k\mu\sigma_z)^2}$$

where  $\sigma_z = \delta z/H(z)$  is the absolute error in distance and  $\delta z$  the absolute error in redshift. Assuming then a gaussian distribution for the pairwise velocity distribution we can consider their effect included in the redshift error factor.

# Chapter 7

## Statistical methods in cosmology

In the previous chapter we have defined important statistical tools such as the correlation function and the power spectrum, able to characterize in a statistical way the distribution of matter in the Universe. Here we review some statistical methods largely employed in cosmology to extract information from the data and which will be used in the following chapters. They are based on Bayesian statistics, which we briefly introduce.

### 7.1 Introduction to Bayesian statistics

Usually, in experimental physics, so as in science in general, the values of quantities of physical interest are “hidden” in what we actually observe, i.e. the experimental data. For example, the measure of luminosity distances of SN Ia is needed in order to estimate the values of the cosmological parameters such as  $\Omega_{m,0}$ ,  $w$ ,  $\gamma$  and so on.

The Bayesian statistics provides a coherent frame that allows us to “extract” what we really want to know from the observations. In the following, we will give a very brief description of the theory underlying the Bayesian statistic and its fundamental tool, the *Bayes’ theorem*.

We start by considering two events  $A$  and  $B$ , being them dependent on each other or not. We can wonder how the happening of one of them influences the realization of the other one. According to the theory of *conditional probability*, this is expressed by the formula

$$P(A|B)P_0(B) = P(B|A)P_0(A) \quad (7.1)$$

where with  $P(A|B)$  ( $P(B|A)$ ) we indicate the probability of having  $A$  ( $B$ ) once  $B$  ( $A$ ) has happened while  $P_0(B)$  ( $P_0(A)$ ) is the *a priori* probability of having  $B$  ( $A$ ). This is the fundamental theorem of probability, called *Bayes’ theorem*.

If we now think to experimental data we actually observe as the “effects” ( $D$ ) and to the “true” values of the cosmological parameters of a theory as the “causes” ( $T$ ), the Bayes’ theorem tells us how much is changed our belief of a theory, once we have observed a given effect.

This is mathematically expressed by rearranging eq. (7.1) which gives

$$P(T|D) = \frac{P(D|T)P_0(T)}{P_0(D)}, \quad (7.2)$$

where  $P_0(T)$  is often called the *prior probability*, i.e. the likelihood of the theory *before* having observed the data, and  $P(T|D)$  is consequently called the *posterior probability*, evaluated in the light of the new data.

Two things has to be strongly stressed.

The first one is that although the Bayes' theorem is always valid, its application, in most cases, is allowed only within the context of the *Bayesian interpretation of probability* [44]. In fact, according to frequentism, which defines the probability as the frequency of occurrence of an event, one is allowed to talk of probability only in the presence of repeatable events. To draw an example, from a frequentist standpoint, while it does make sense to evaluate the probability of observing a certain number of events of a given reaction (the “effect”) at the LHC, once the Higgs boson mass is known to be equal to a certain value (the “cause”), it does not make sense at all to evaluate the probability of having the Higgs boson mass in a given interval, once we have observed a certain number of events. This because the value of the Higgs boson mass, although unknown, is not the result of a try of a repeatable event. On the other hand, the bayesian interpretation, and of course the common sense, define the probability for what it really is, i.e. a measure of our belief about the happening of an event. This is why in the following we will stick with the Bayesian interpretation.

The second one is that any probability is always supposed to be conditional on a certain state of information. This amounts to say that the uncertainty we have about any event depends on what we already know or what we do not know about the event itself. Any probability should indeed be expressed as  $P(X|I)$ , indicating that the evaluation of the probability of the event  $X$  depends on the present state of information  $I$ . This will be omitted in the following.

In eqs (7.1-7.2) we have dealt with finite probabilities. The Bayes' theorem can be extended also when we have to deal with continue distribution. In this case, the probabilities appearing in the equations have to be replaced by their respective probability distribution function (PDF).

We can now see how the Bayes' theorem can be used in practice. Let us suppose we know that a random variable  $x$  has a probability distribution function (PDF)  $f(x; \theta)$  that depends on an unknown parameter  $\theta$ . Such a probability is the conditional probability of having the data  $x$ , given the theoretical parameter  $\theta$ . If we repeat the measure and we obtain  $x_1, x_2, x_3, \dots$ , then the law of joint probability tells us that the probability of obtaining  $x_1$  in the interval  $dx_1$  around  $x_1$ ,  $x_2$  in the interval  $dx_2$  around  $x_2$  and so forth is

$$f(x_i; \theta) d^n x_i = \prod_i f_i(x_i; \theta) dx_i = f_1(x_1; \theta) f_2(x_2; \theta) f_3(x_3; \theta) \dots dx_1 dx_2 dx_3 \dots, \quad (7.3)$$

if the measures are independent on each other. Clearly, for every  $\theta$  this multivariate PDF will assume a different value. If we now look again at the Bayes' theorem, we see that the posterior probability is essentially just the data likelihood, eq. (7.3) times the prior

probability, since the denominator of eq. (7.2) acts just as a normalization factor. It is now time to plug our previous knowledge about the parameter in the evaluation of the prior PDF  $p_0(\theta)$ . There is no a “standard” recipe to do this; instead, one has to use all the information he can get (for example results of previous experiments, physical constraints on the values of the parameters, and so on). So we obtain:

$$L(\theta; x_i) \propto f(x_i; \theta)p_0(\theta) , \quad (7.4)$$

where we have indicate the posterior PDF with  $L(\theta; x_i)$ .

Let us now assume that we do not have any previous-to-the-experiment knowledge about  $\theta$ , and we have not reason to think, in principle, that any value of the parameter is more likely than another. In this case,  $p_0(\theta)$  can be expressed by a constant and merged into the normalization constant. So, the posterior PDF basically coincides with the data likelihood  $f(x_i; \theta)$ . The frequentist well-known “maximum likelihood principle”, amounts to state that the “best”(?) estimation of a parameter is the value  $\hat{\theta}$  which maximizes the data likelihood:

$$\left. \frac{\partial f(x_i; \theta)}{\partial \theta} \right|_{\theta=\hat{\theta}} = 0 . \quad (7.5)$$

As we can see from the above equation,  $\hat{\theta}$  is the most likely single value of the parameter *if we assume a uniform prior*. In many problems, this is not the case, since a certain level of information is often available and ignore it can lead to absurd conclusions. Furthermore, even the maximum may not be very representative of the entire PDF, so calling it the “best” estimation is at least questionable. Once we have carried out the posterior  $L(\theta; x_i)$ , drawing the region in which the true value of the parameter is found with a chosen level of probability is pretty straightforward. First of all, we have to correctly normalize the posterior:

$$L(\theta; x_i) = \frac{f(x_i; \theta)p_0(\theta)}{\int_{-\infty}^{+\infty} f(x_i; \theta')p_0(\theta')d\theta'} . \quad (7.6)$$

Numerically, the limits of integration in the denominator can be replaced by the region in which the prior PDF is significantly different from zero. We now evaluate the maximum of the posterior distribution  $\hat{\theta}$  as we did for the data likelihood, eq. (7.5) and calculate  $L_{max} = L(\hat{\theta}; x_i)$ <sup>1</sup>. Then we draw a number  $\alpha < L_{max}$  and find the two values of the parameter  $\theta_{min}(\alpha)$  and  $\theta_{max}(\alpha)$  solutions of the equation:

$$L(\theta; x_i) = \alpha , \quad (7.7)$$

and define the function  $P(\alpha)$  as:

$$P(\alpha) = \int_{\theta_{min}(\alpha)}^{\theta_{max}(\alpha)} L(\theta; x_i)d\theta , \quad (7.8)$$

---

<sup>1</sup>It has to be stressed that, in general, the posterior PDF could not have just one maximum, but may exhibit more complicated features. In most cases, however, it will show one maximum; the procedure described in the text refers to this kind of posteriors.

varying  $\alpha$ . Imposing, for example,  $P(\alpha) = 68\%(95\%)$ , we found that the interval  $\theta_{min}(\alpha) < \theta < \theta_{max}(\alpha)$  has the 68% (95%) of probability to contain the “true” value of the parameter, given the data we have observed and what we knew about the parameter before the experiment.

This procedure can be readily generalized when we have posteriors  $L(\theta_1, \theta_2, \theta_3, \dots; x_i)$  depending on more than one parameter. If we are interested only in a subset of the parameters, let us say  $\{\theta_1, \theta_2\}$ , we can marginalize the posterior integrating over the remaining parameters

$$L_{12}(\theta_1, \theta_2; x_i) = \int d\theta_3 d\theta_4 \dots L(\theta_1, \theta_2, \theta_3, \dots; x_i) . \quad (7.9)$$

So solving the equation

$$L_{12}(\theta_1, \theta_2; x_i) = \alpha , \quad (7.10)$$

will define the contour of the region of integration for  $P(\alpha)$ .

Lastly, we have to mention that, even if the method of finding the most likely single value for a parameter is correctly carried out by maximizing the posterior PDF, it is usual to refer to this method as the “maximum likelihood method” even if, as explained above, the likelihood alone (i.e. without a prior) does not contain all the information we already have about a theory. Only for sake of comparison to other works, we will also employ this terminology which however we do not recommend.

## 7.2 Fisher matrix method

Even though it is a very powerful tool, the maximum likelihood method can require very long computational time when we are dealing with a large number of parameters.

The Fisher matrix method is a way to solve this problem. The idea is to approximate the full likelihood with a multivariate Gaussian distribution

$$L \approx N \exp \left[ -\frac{1}{2} (\theta_i - \hat{\theta}_i) F_{ij} (\theta_j - \hat{\theta}_j) \right] \quad (7.11)$$

where  $\hat{\theta}_i$  are the maximum likelihood estimators and are functions of the data.  $F_{ij}$ , the Fisher (or information) matrix, is the inverse of the correlation matrix.

This is a crucial point that deserves attention. In many physical situations it is assumed that the data follow a Gaussian distribution, but rarely this is true also for the parameters. Here we are assuming that the likelihood is a Gaussian function of the parameters, not (or not only) of the data. It can be considered a crude approximation. However it is justified by the fact that every smooth function (in this case  $\ln L$ ) can be approximated as a quadratic function around a local minimum. So we can hope that our approximation is valid at least near the peak of the distribution and we expect it to work better for  $\theta_i$  close to their estimators  $\hat{\theta}_i$ .

Then let us expand the exponent of a generic likelihood near its peak (i.e. near the maximum likelihood (ML) value  $\hat{\theta}_i$  of the parameters) as

$$\ln L(\theta_i) \approx \ln L(\hat{\theta}_i) + \frac{1}{2} \left. \frac{\partial^2 \ln L(\theta_i)}{\partial \theta_i \partial \theta_j} \right|_{\text{ML}} (\theta_i - \hat{\theta}_i)(\theta_j - \hat{\theta}_j) \quad (7.12)$$

(where the first derivatives obviously vanish at the peak). By comparison with eq. (7.11), we find that the normalization  $N = L(\hat{\theta}_i)$  depends only on the data and that the *Fisher matrix* (FM) is defined as

$$F_{ij} \equiv - \left. \frac{\partial^2 \ln L(\theta_i)}{\partial \theta_i \partial \theta_j} \right|_{\text{ML}} . \quad (7.13)$$

Actually the FM is defined as the expected value of the matrix  $-\partial^2 \ln L / \partial \theta_i \partial \theta_j$ , obtained by averaging the matrix over the data distribution:

$$F_{ij} = - \left\langle \frac{\partial^2 \ln L(\boldsymbol{\theta})}{\partial \theta_i \partial \theta_j} \right\rangle = - \int \frac{\partial^2 \ln L(\boldsymbol{\theta})}{\partial \theta_i \partial \theta_j} L(\mathbf{x}; \boldsymbol{\theta}) d\mathbf{x} . \quad (7.14)$$

However, within the approximation (7.12), the two definitions coincide.

Now we may wonder how to find the ML estimator without computing the likelihood, which is exactly what we are trying to avoid! There are some ways to do that, but the most useful application of the Fisher formalism is to the cases in which we do not need to search for the likelihood peak because we already know from the start the ML estimator: when we are *simulating* an experiment.

In this case we are not dealing with real data but only with predictions of the data errors that future experiments can achieve. So we can arbitrarily assume some (fiducial) values for the parameters, i.e. for the ML estimator, and compute how the errors on data will turn into errors on the parameters. Let us see it in details.

Let us suppose that we have collected a number  $m$  of data which can be related to some cosmological parameters  $p_j$ , for instance the luminosity distances of  $m$  SN Ia,  $d_{L,n} \equiv d_L(z_n)$  (see eq. (1.84)) at different redshifts  $z_n$ , where the parameters  $p_j$  could be  $\Omega_{m,0}$ ,  $\Omega_\Lambda$ , etc... These data are random variables following a probability distribution function (PDF) which we assume to know. For example we can assume they are distributed according to a Gaussian with mean  $d_L(z_n)$  and with known variance  $\sigma_n$ . Then we can immediately form the likelihood (neglecting the normalization constant)

$$L_d \approx \exp \left[ -\frac{1}{2} \sum_n \frac{(d_n - d_L(z_n))^2}{\sigma_n^2} \right] = \exp \left( -\frac{1}{2} \boldsymbol{\mu}_i C_{ij}^{-1} \boldsymbol{\mu}_j \right) ., \quad (7.15)$$

where  $d_n \equiv d_{th}(z_n)$  are the values for the luminosity distances predicted by some theory. As explained in the previous section, this likelihood can be thought (assuming a uniform prior) as the PDF of the theory itself, i.e. of the parameters  $d_n$  that we want to infer from the data and that take the role of variables.

In eq. (7.15) we have expressed the argument of the exponential in a slightly more general way introducing the vector  $\boldsymbol{\mu}_i \equiv d_i - d_L(z_i)$  and the correlation matrix  $C_{ij}$ , that in this particular case is rather trivial

$$\mathbf{C} = \text{diag}(\sigma_1^2, \sigma_2^2, \sigma_3^2, \dots) . \quad (7.16)$$

Now, instead of inferring the probability on the theoretical luminosity distances  $d_n$  we are interested to the theoretical parameters  $p_j$  on which they depend:  $d_n = d(z_n; \Omega_{m,0}, \Omega_\Lambda)$ . In fact, every couple of values  $(\Omega_{m,0}, \Omega_\Lambda)$  will give a different prediction on the theoretical value of  $d_n$ . So we wish to produce a likelihood function of  $\Omega_{m,0}, \Omega_\Lambda$ , something in the form of eq. (7.11):

$$L(\Omega_{m,0}, \Omega_\Lambda) = \exp \left[ -\frac{1}{2} (\Omega_i - \hat{\Omega}_i) F_{ij} (\Omega_j - \hat{\Omega}_j) \right] \quad (7.17)$$

where  $F_{ij}$  is the Fisher matrix and the subscripts  $i, j$  run over the subscripts  $m, \Lambda$  (from now on we drop the subscript 0). Since real data  $(d_L(z_n))$  are not present yet, we cannot compute the ML estimators  $\hat{\Omega}_i$ . However, we are simulating the future experiment, so we may take for estimators the values  $d_n^F = d^F(z_n; \Omega_m^F, \Omega_\Lambda^F)$  obtained using some fiducial cosmology  $\Omega_m^F, \Omega_\Lambda^F$ , for instance  $\Omega_m^F = 0.25, \Omega_\Lambda^F = 0.75$ . This means that we will find the confidence regions only around this particular parameter set. If we decide to change fiducial values, we have to redo our calculations and all our results will change in some way.

The Fisher matrix of the likelihood (7.15) is then

$$F_{ij} = - \left. \frac{\partial \ln L_m}{\partial \Omega_i \partial \Omega_j} \right|_F = \sum_n \frac{1}{\sigma_n^2} \left. \frac{\partial^2 d(z_n; \Omega_m, \Omega_\Lambda)}{\partial \Omega_i \partial \Omega_j} \right|_F. \quad (7.18)$$

Notice that  $F_{ij}$  is not diagonal even if the original correlation matrix  $C_{ij}$  was. Since the same  $\Omega_m, \Omega_\Lambda$  appear in all  $d(z_n; \Omega_m, \Omega_\Lambda)$ , we vary the likelihood of obtaining all  $d_n$  by varying  $\Omega_m, \Omega_\Lambda$ . We can now use eq. (7.17) to derive the errors for  $\Omega_m, \Omega_\Lambda$ . In practice, we have developed a formalism to propagate the observational errors  $\sigma_n$  to the cosmological parameters. The errors  $\sigma_n$ , in turn, must be based on the expected performance of the experiment and often their derivation is the most complicated step, involving many fine details of the observations.

Once we fix the ML estimators to the chosen fiducial values, the elements of the Fisher matrix are easily obtained by calculating numerically the second-order partial derivatives and so the computational time is reduced.

Let us now suppose that we decide to switch from a set of parameters  $x_i$  to another one  $y_j(x_i)$ , for instance from  $\Omega_m, \Omega_\Lambda$  to the spatial curvature  $\Omega_k = 1 - \Omega_m - \Omega_\Lambda$  and their ratio  $R_{m\Lambda} = \Omega_m / \Omega_\Lambda$ . If we know the Fisher matrix for  $x_i$ , the approximate likelihood is

$$L = \exp \left( -\frac{1}{2} \tilde{x}_i F_{ij}^{(x)} \tilde{x}_j \right), \quad (7.19)$$

where  $\tilde{x}_i = x_i - x_i^{\text{ML}}$ . Approximating  $y_j$  near  $x_i^{\text{ML}}$  as

$$y_j \approx y_j^{\text{ML}} + \left. \frac{\partial y_j}{\partial x_i} \right|_{\text{ML}} (x_i - x_i^{\text{ML}}), \quad (7.20)$$

where  $y_j^{\text{ML}} \equiv y_j(x_j^{\text{ML}})$ , we can write

$$\tilde{y}_j \equiv y_j - y_j^{\text{ML}} = J_{ji}^{-1} \tilde{x}_i. \quad (7.21)$$

With  $J_{ji} \equiv (\partial x_j / \partial y_i)_{\text{ML}}$  we have indicated the transformation Jacobian evaluated on the ML estimators. Then we have

$$\tilde{x}_i = J_{il} \tilde{y}_l \quad (7.22)$$

and we can find the new Fisher matrix simply by substituting eq. (7.22) into eq. (7.19)

$$F_{lm}^{(y)} = J_{il} F_{ij}^{(x)} J_{jm} , \quad (7.23)$$

which is summed over indices. We can say that the Fisher matrix transforms as a tensor. The Jacobian matrix is not required to be a square matrix. In fact the old parameters  $x_j$  can be projected into a smaller number of new parameters  $y_i$ .

We could wonder why the Jacobian does not enter also in the transformation from the volume element  $dx_1 dx_2 \dots$  to the new element  $dy_1 dy_2 \dots$ , so that  $L(y_j) = |J| L[x_i(y_j)]$ . This would imply an additional logarithmic term  $\ln |J|$  in the transformed probability function, not allowing to go on using the Gaussian approximation. However near the ML values we can approximate  $|J|$  with  $|J_{\text{ML}}|$  and include this constant factor in the overall normalization.

Now let us see what to do if we want to maximize the likelihood with respect to some parameter, which means to fix one of the parameters to its maximum likelihood estimator. With the Fisher matrix this is really trivial, since fixing a parameter to its maximum likelihood estimator means putting the difference  $\theta_i - \hat{\theta}_i = 0$  and therefore to discard all entries in the Fisher matrix related to the  $i$ -th parameter. In practice, this corresponds to remove from the Fisher matrix the rows and columns of the maximized parameters.

And if we want to marginalize over some parameters? Let us consider a general Gaussian PDF with only two parameters  $x_1$  and  $x_2$ :

$$G(x_1, x_2) = N \exp \left[ -\frac{1}{2(1-\rho^2)} \left( \frac{x_1^2}{\sigma_1^2} + \frac{x_2^2}{\sigma_2^2} - 2\frac{\rho x_1 x_2}{\sigma_1 \sigma_2} \right) \right] , \quad (7.24)$$

where  $\rho$  the correlation factor. This PDF can be written as

$$G(X_i) = N \exp \left[ -\frac{1}{2} (X_i C_{ij}^{-1} X_j) \right] , \quad (7.25)$$

where  $X_i \equiv x_i - \mu_i$  and

$$\mathbf{C} = \begin{pmatrix} \sigma_1^2 & \rho \sigma_1 \sigma_2 \\ \rho \sigma_1 \sigma_2 & \sigma_2^2 \end{pmatrix} , \quad (7.26)$$

is the correlation matrix. Let us now marginalize over the parameter  $x_2$ , which corresponds to evaluate the integral  $\int G(x_1, x_2) dx_2$  over the whole real domain. The result is given by

$$G(x_1) = \tilde{N} \exp \left[ -\frac{x_1^2}{2\sigma_1^2} \right] , \quad (7.27)$$

where  $\tilde{N}$  is a new normalization constant. The new correlation matrix is now only one dimensional, simply  $C_{11} = \sigma_1^2$ .

In terms of the Fisher matrix  $\mathbf{F} = \mathbf{C}^{-1}$  we see that the result of the marginalization corresponds to the removal from  $\mathbf{F}^{-1} = \mathbf{C}$  of the rows and columns related to the second parameter. This trick remains true for any number of dimensions: to marginalize over the  $j$ -th parameter, one simply needs to remove from the inverse of the Fisher matrix  $\mathbf{F}^{-1}$  the  $j$ -th row and column; to marginalize at once over several parameters, one removes all the rows and columns related to those parameters. As a consequence, the diagonal of the inverse Fisher matrix contains the fully marginalized  $1\sigma$  errors of the corresponding parameters (i.e. the errors one gets on the  $i$ -th parameter after marginalizing over all the others)

$$\sigma_i^2 = (\mathbf{F}^{-1})_{ii}. \quad (7.28)$$

This latter property is probably the most useful and time-saving feature of the whole Fisher method. Be warned however that the procedure of inverting and striking out rows and columns is in general numerically unstable if the matrix contains small eigenvalues. There are more stable algorithms that perform this operation [45].

Often we want to reduce the Fisher matrix to a  $2 \times 2$  matrix  $\mathbf{F}_2$  for two parameters, say  $\theta_1, \theta_2$ , because then it is easy to plot the resulting two-dimensional confidence regions, defined as the regions of constant likelihood that contain a predetermined fraction of the total likelihood volume. Since the problem has been reduced from the start to Gaussianity, we will necessarily have ellipsoidal confidence regions on the plane  $\theta_1, \theta_2$ . Looking at the form of the two-dimensional Gaussian PDF (7.24), you will realize that the semiaxes of the ellipses are oriented along the eigenvectors of  $\mathbf{F}_2^{-1}$ , that is, they form an angle

$$\tan 2\alpha = \frac{2\rho\sigma_1\sigma_2}{\sigma_1^2 - \sigma_2^2}, \quad (7.29)$$

with the coordinate axes. Moreover, the semiaxes ratio is equal to the square root of the eigenvalues ratio. The length of the semiaxes depends clearly on the level of confidence. If we take the semiaxes length along the  $i$ -th eigenvector equal to  $\sqrt{\lambda_i}$ , where  $\lambda_i$  is the  $i$ -th eigenvalue, we are finding the  $1\sigma$  region, but because we are in two dimensions, this level does not contain 68.3% of the probability but rather less than 40%. Instead, we find by integrating a two-dimensional Gaussian that the onedimensional “ $1\sigma$ ” region corresponding to 68.3% of probability content is found for semiaxes which are roughly 1.51 times the eigenvalues. Regions at 95.4% and 99.7% correspond to semiaxes 2.49 and 3.44 times the eigenvalues, respectively. The area of the 68.3% ellipses is  $\pi ab$ , if  $a$  and  $b$  are the semiaxes length, that is 1.51 times the eigenvalues. The area is therefore equal to  $(1.51)^2\pi(\det \mathbf{F}_2)^{-1/2}$ . Since an experiment is more constraining when the confidence region is smaller, one can define a simple but useful figure of merit (FOM) as [45]

$$\text{FOM} = \frac{1}{\sqrt{\det \mathbf{F}_2}}. \quad (7.30)$$

Notice however that the FOM is often defined to be the area at 95%, or some other similar but not equivalent choice. The FOM is particularly relevant to dark energy parameters such as  $w_0, w_1$ . The FOM naturally depends on how many parameters have been marginalized. Every parameter marginalization increases (or more exactly, does not

reduce) the amount of uncertainty with respect to a maximized likelihood and therefore decreases the available information and the FOM of the final set of parameters.

With all these simple rules the Fisher matrix turns out to be a very simple method. Unfortunately, this is not free of problems. The major problem, in practice, is when the Fisher matrix itself is singular. Being its determinant null, we cannot in fact invert it and then marginalizing it. This obviously happens only when rows or columns are not linearly independent: if  $L(\theta_1, \theta_2)$  depends on the two parameters through a constant combination, e.g.,  $a\theta_1 + b\theta_2$ , then the Fisher matrix will be singular.

Even in this case, not all is wasted and we can still learn something. In fact, if the Fisher matrix is singular, then it means that there is a linear combination of two or more parameters hidden somewhere in the likelihood. Therefore, we can substitute a new parameter  $\hat{\theta}$  in place of that combination, e.g.  $\hat{\theta} = a\theta_1 + b\theta_2$  and remove the singularity by restricting ourselves to  $\hat{\theta}$  instead of the original pair. Actually we should have done this from the start, since if the physics depends only on the combination  $a\theta_1 + b\theta_2$  there is no way we can distinguish between  $\theta_1, \theta_2$ . It is only this combination that matters and we should replace it by  $\hat{\theta}$ . We say in this case that there is a degeneracy between  $\theta_1$  and  $\theta_2$ . Sometimes, however, it is not obvious at all that this was the case and the singularity of the Fisher matrix is a warning for us to look harder.

The only real problem is when there is almost a singularity. If the combination is given by  $a\theta_1 + b\theta_2 + cf(z)\theta_1^2$ , then there should be no singularity because of the non-constant term (we are thinking here of observations at several  $z$ 's). However, if  $a, b$  are of the order of unity while  $c = 10^{-10}$ , then there is a high degree of degeneracy, even if not a total one. In this case the Fisher matrix may behave in a dangerous way, with extremely small eigenvalues and unstable inversions. So we have to pay attention, try to understand the physical cause of this quasi-degeneracy and redefine the parameters, perhaps giving up the possibility of discriminating between  $\theta_1, \theta_2$  and focusing on the combined term  $\hat{\theta} = a\theta_1 + b\theta_2 + cf(z)\theta_1^2$ . Otherwise, we may find additional priors (e.g., other experiments) that give separate information on one of the quasi-degenerate parameters and break the degeneracy.

This introduces another advantage of the Fisher matrix approach: the possibility to add priors in a very simple way. If the prior is the outcome of another experiment and we have the Fisher matrix  $F_{ij}^{(p)}$  of that experiment, then the problem reduces to multiplying a Gaussian likelihood by another Gaussian likelihood, obtaining a new Gaussian likelihood. If the experiments have the same ML estimators or the same fiducial model, as in the case in which we simulate them, the new Fisher matrix is given by

$$F_{ij}^{(\text{tot})} = F_{ij} + F_{ij}^{(p)} . \quad (7.31)$$

Combining the information from two forecasts (with the same fiducial model) means then summing their Fisher matrices. In so doing one has to ensure that the parameters and their order are exactly the same for both matrices: trivial, but a most likely source of practical confusion. If one of the experiments constrains only a subset of the total parameters (for instance, supernovae experiments do not constrain the primordial perturbation slope  $n_s$ ), it means that it contains no information on that subset, and therefore the

corresponding rows and columns are to be put to zero. This means that the two Fisher matrices are rendered of the same rank by filling the one with less parameters with zeros in the correct position. For instance if we only want to add the information that the single  $m$ -th parameter comes with an error  $\sigma_m$  then we add the Fisher matrix (no sum on  $m$ )

$$F_{ij}^{(p)} = \frac{\delta_i^m \delta_j^m}{\sigma_m^2} \quad (7.32)$$

So you see that in this case  $\mathbf{F}^{(p)}$  would be utterly singular but the total  $\mathbf{F}^{(\text{tot})}$  is not (unless of course we are so unlucky that  $\mathbf{F}$  was singular as well for the same parameter).

Let us mention the final point about the Fisher matrix. A statistical theorem known as Cramer–Rao inequality states that the minimal variance of an unbiased estimator cannot be less than  $(\mathbf{F}^{-1})_{ii}$ . In this sense the Fisher matrix gives the minimal error one can hope to achieve.

### 7.3 The Fisher matrix for the power spectrum

Now we have all the tools to derive a very useful result, the Fisher matrix for an experiment that measures the galaxy power spectrum.

Suppose a future experiment will provide us with the Fourier coefficients  $\delta_{\mathbf{k}}$  of a galaxy distribution and their power spectrum calculated for a set of  $m$  wavenumbers  $\mathbf{k}_i$  in some redshift bin  $z, z + \Delta z$ . Our theory predicts the spectrum  $P(k, z; p_i)$  as a function of, say,  $p_i \equiv \Omega_{m,0}, \Omega_{b,0}, h, n_s$  etc. In any real survey with a galaxy density  $n(z)$ , however, the power spectrum will include the Poisson noise part that we estimated in eq. (6.30):

$$\Delta_{\mathbf{k}}^2 \equiv \langle \delta_{\mathbf{k}} \delta_{\mathbf{k}}^* \rangle = \langle \delta_{\mathbf{k}} \delta_{-\mathbf{k}} \rangle = P(\mathbf{k}, z) + \frac{1}{n}, \quad (7.33)$$

Since the average galaxy density is estimated from the survey itself we have by construction  $\langle \delta(x) \rangle = 0$  and therefore  $\langle \delta_{\mathbf{k}_i} \rangle = 0$  for any  $\mathbf{k}_i$ . The coefficients  $\delta_{\mathbf{k}_i}$  are complex variables in which the real and imaginary parts obey the same Gaussian statistics. So now we calculate the Fisher matrix for only, say, the real parts of  $\delta_{\mathbf{k}_i}$  and the Fisher matrix for the whole  $\delta_{\mathbf{k}_i}$  is simply the sum of two identical Fisher matrices, i.e. twice the result for the real parts. However when we count the total number of independent modes we have to remember that only half of them are statistically independent since  $\delta_{\mathbf{k}}^* = \delta_{-\mathbf{k}}$  so in fact we should finally divide by two the final result. That is, we can forget both factors. If we assume the galaxy distribution to be well approximated by a Gaussian we can write the likelihood:

$$L = \frac{1}{(2\pi)^{m/2} \prod_i \Delta_i} \exp \left[ -\frac{1}{2} \sum_i^m \frac{\delta_i^2}{\Delta_i^2} \right], \quad (7.34)$$

(where to simplify notation we write  $\Delta_i = \Delta_{\mathbf{k}_i}$ ,  $\delta_i = \text{Re} \delta_{\mathbf{k}_i}$ ) assuming that the measures at every  $\mathbf{k}_i$  are statistically independent. When we simulate a future experiment,  $P(k, z)$

is taken to be the theoretical spectrum of our fiducial model described by the parameters  $p_j^F$ . Then we have

$$\mathcal{L} = \ln L = \frac{m}{2} \ln(2\pi) + \sum_i \ln \Delta_i + \sum_i \frac{\delta_i^2}{2\Delta_i^2}. \quad (7.35)$$

We further simplify the notation by suppressing the index  $i$  running over the  $k$  bins from  $\Delta_i$ ,  $\delta_i$  and denote the differentiation with respect to the  $j$ -th parameter as  $\Delta_{,j}$ . Now from eq. (7.13) the Fisher matrix for a particular  $z$  bin is

$$\begin{aligned} F_{lm} &= \left\langle \frac{\partial^2 \mathcal{L}}{\partial p_l \partial p_m} \right\rangle = \sum \left[ \frac{\Delta_{,lm}}{\Delta} - \frac{\Delta_{,l} \Delta_{,m}}{\Delta^2} - \langle \delta^2 \rangle \left( \frac{\Delta_{,lm}}{\Delta} - 3 \frac{\Delta_{,l} \Delta_{,m}}{\Delta^4} \right) \right] = \\ &= \frac{1}{2} \sum_i \frac{\partial \ln P_i}{\partial p_l} \frac{\partial \ln P_i}{\partial p_m} \left( \frac{n P_i}{1 + n P_i} \right)^2, \end{aligned} \quad (7.36)$$

(where we used  $\langle \delta^2 \rangle = \Delta^2$  from eq. (7.33)) calculated on the fiducial model. For a more compact expression we can now approximate the sum with an integral over  $k$ . To do this we need to count how many modes lie in the bin defined by the modulus interval  $k$ ,  $k + dk$  and cosine interval  $d\mu$ , i.e. in the Fourier volume  $2\pi k^2 dk d\mu$ . The number of modes we can really use is limited by two factors: the size of the volume and the shot noise. Modes larger than the survey volume cannot be measured. Short modes sampled by only a few galaxies cannot be reliably measured either. To take into account these limitations we discretize the Fourier space into cells of volume  $V_{\text{cell}} = (2\pi)^3 / V_{\text{survey}}$ , so that we have  $2\pi k^2 dk d\mu / V_{\text{cell}} = (2\pi)^{-2} V_{\text{survey}} k^2 dk d\mu$  modes in the survey volume. The integral form of the Fisher matrix is therefore given by [46, 47]

$$F_{lm} = \frac{1}{8\pi^2} \int_{-1}^{+1} d\mu \int_{k_{\min}}^{k_{\max}} k^2 dk \frac{\partial \ln P(k, \mu)}{\partial p_l} \frac{\partial \ln P(k, \mu)}{\partial p_m} \left[ \frac{n P(k, \mu)}{1 + n P(k, \mu)} \right]^2 V_{\text{survey}}. \quad (7.37)$$

The factor

$$V_{\text{eff}} = \left[ \frac{n P(k, \mu)}{1 + n P(k, \mu)} \right]^2 V_{\text{survey}} \quad (7.38)$$

can be seen as an effective survey volume. When  $nP \gg 1$  the sampling is good enough to derive all the cosmological information that can be extracted from the survey and there is no need of more sources. For  $nP \ll 1$  the effective volume is severely reduced. If we subdivide the data into several  $z$  independent bins, we can simply sum the Fisher matrices for every bin.



## Chapter 8

# Dark energy as a modified form of matter

We have learnt in the previous chapters that although the cosmological constant seems to be the best candidate for the role of dark energy, it suffers serious theoretical problems. That's the reason which led many authors to find alternative explanations for the cosmic acceleration.

An alternative approach can be to assume that the underlying  $\Lambda$  problem is solved in a way that its value completely vanishes and then trying to find another mechanism to explain the cosmic acceleration. There are basically two ways to do that which consist in modifying either the r.h.s or the l.h.s. of the Einstein equations. The first corresponds then to modify the matter content of the universe, assuming that the energy-momentum tensor  $T_{\mu\nu}$  on the r.h.s. of the Einstein equations contains an exotic matter source with a negative pressure. On the other side, the second approach corresponds to modify the gravity, which means to change the Einstein tensor.

However, it is important to underline that this distinction is not very sharp and that there is no way, within General Relativity, i.e. by using only gravitational interactions, to distinguish modified matter from modified gravity. This division has then the only practical purpose of classifying the different dark energy models.

However, regardless their belonging to the first or the second class, one of the constraints that every dark energy model needs to satisfy is the one on the present value of the equation of state of the dark energy,  $w$ . The observations constrain the present value of  $w$  to be very close to that of a cosmological constant,  $w = -1$ , but they say relatively little about its time evolution allowing us to broaden our horizons and consider dark energy as a fluid whose equation of state changes with time. The key idea of many "modified matter" models is to consider, rather than an effective cosmological constant, a fluid with the same  $\Lambda$  behaviour at present, but whose density (and then its  $w$ ) is free to vary slowly with time in order to be small during the radiation/matter eras and dominating at present. This is usually done by assuming that such a fluid behaves like a dynamical scalar field. This approach is justified by several reasons: first of all, scalar fields are natural ingredients in particle physics and their existence is hypothesized by many fundamental theories (string theory, Brans-Dicke theory, etc...), so that it is natu-

ral to look at their cosmological consequences. Furthermore, a scalar field which slow rolls on a potential can mimic the behavior of a cosmological constant at present and, unlike  $\Lambda$ , it can satisfy tighter constraints thanks to its dynamic nature. Moreover, the additional source of fluctuations, produced by the scalar field can give new observable effects on the CMB and on the growth of structure, so it could be possible to distinguish it from the standard  $\Lambda$ CDM model.

For all these reasons, so far a large number of scalar-field dark energy models have been proposed, including phantoms, K-essence, tachyon, ghost condensates and dilatonic dark energy amongst many.

In this chapter we focus our attention on those models of “modified matter”, where the role of dark energy is played by a scalar field minimally coupled to gravity, a field which was named Quintessence [48].

## 8.1 Quintessence model

Quintessence is described by an ordinary scalar field  $\phi$  minimally coupled to gravity, but with particular potentials that lead to late time inflation. The action for Quintessence is given by

$$S_\phi = \int d^4x \sqrt{-g} \left[ -\frac{1}{2}(\nabla\phi)^2 - V(\phi) \right], \quad (8.1)$$

where  $(\nabla\phi)^2 = g^{\mu\nu}\partial_\mu\phi\partial_\nu\phi$  and  $V(\phi)$  is the potential of the field. Varying the action with respect to  $\phi$  gives the Klein-Gordon equation

$$\square\phi + V_{,\phi} = 0, \quad (8.2)$$

where  $V_{,\phi} \equiv dV/d\phi$  and the symbol  $\square$  stands for the D’Alambertian which is given by

$$\square\phi \equiv \phi_{;i}^i = (-g)^{-1/2}\partial_\mu(-g)^{1/2}g^{\mu\nu}\partial_\nu\phi. \quad (8.3)$$

In the flat FRLW metric (1.2) we then have

$$\frac{d^2\phi}{dt^2} + 3H\frac{d\phi}{dt} + V_{,\phi} = 0, \quad (8.4)$$

while in the conformal time metric (1.5)

$$\ddot{\phi} + 2\mathcal{H}\dot{\phi} + a^2V_{,\phi} = 0. \quad (8.5)$$

Both equations (8.4) and (8.5) represent the Klein-Gordon equation for the field  $\phi$  in the expanding universe.

The energy-momentum tensor of the field is derived by varying the action (8.1) with respect to the generalized coordinates, which are given in this case by the components of the metric tensor  $g^{\mu\nu}$  and its derivatives:

$$T_{\mu\nu}^{(\phi)} = -\frac{1}{\sqrt{-g}}\frac{\delta S_\phi}{\delta g^{\mu\nu}}. \quad (8.6)$$

Taking note that  $\delta\sqrt{-g} = -(1/2)\sqrt{-g}g_{\mu\nu}\delta g^{\mu\nu}$ , we find

$$T_{\mu\nu}^{(\phi)} = \partial_\mu\phi\partial_\nu\phi - g_{\mu\nu}\left[\frac{1}{2}g^{\alpha\beta}\partial_\alpha\phi\partial_\beta\phi + V(\phi)\right]. \quad (8.7)$$

In the FRLW metric, from the components (0,0) and (i,i) of eq. (8.7) we obtain the energy density and pressure of the scalar field

$$\rho(t) = -T_0^{0(\phi)} = \frac{1}{2}\left(\frac{d\phi}{dt}\right)^2 + V(\phi) \quad (8.8)$$

$$p(t) = T_i^{i(\phi)} = \frac{1}{2}\left(\frac{d\phi}{dt}\right)^2 - V(\phi). \quad (8.9)$$

The equation of state of the field is then

$$w_\phi(t) = \frac{p_\phi}{\rho_\phi} = \frac{\frac{1}{2}\left(\frac{d\phi}{dt}\right)^2 - V(\phi)}{\frac{1}{2}\left(\frac{d\phi}{dt}\right)^2 + V(\phi)} \neq \text{constant} \quad (8.10)$$

and changes with time.

Inserting eqs (8.8) and (8.9) in eqs (1.18) and (1.20) and considering a matter component besides the scalar field, we obtain new Friedmann equations

$$H^2 = \frac{8\pi G}{3}\left[\frac{1}{2}\left(\frac{d\phi}{dt}\right)^2 + V(\phi) + \rho_m\right], \quad (8.11)$$

$$\frac{1}{a}\frac{d^2a}{dt^2} = -\frac{8\pi G}{3}\left[\left(\frac{d\phi}{dt}\right)^2 + \rho_m + p_m\right]. \quad (8.12)$$

The continuity equation for  $\phi$

$$\frac{d\rho_\phi}{dt} + 3H(\rho_\phi + p_\phi) = 0 \quad (8.13)$$

can be derived by combining these Friedmann equations. In order to realize the late-time cosmic acceleration, we require the condition  $w_\phi < -1/3$  which translates into the condition  $(d\phi/dt)^2 < V(\phi)$ : the kinetic energy of the field must be smaller than its potential energy. Hence the scalar potential needs to be shallow enough for the field to evolve slowly along the potential, a situation similar to that of inflationary cosmology. In the context of inflation the slow-roll parameters

$$\epsilon_s \equiv \frac{m_{\text{pl}}^2}{16\pi}\left(\frac{V_{,\phi}}{V}\right)^2, \quad \eta_s \equiv \frac{m_{\text{pl}}^2}{8\pi}\frac{V_{,\phi\phi}}{V} \quad (8.14)$$

are often used to check the existence of an inflationary solution for the model (8.1) [49]. Inflation occurs if the slow-roll conditions  $\epsilon_s \ll 1$  and  $|\eta_s| \ll 1$  are satisfied. In the context of dark energy these conditions are not completely reliable since there exists dark matter as well as dark energy. However they still provide a good way to check the existence of a solution with an accelerated expansion.

We note that the equation of state for the field  $\phi$  ranges in the region  $-1 \leq w_\phi \leq 1$ . The slow-roll limit gives the condition  $(d\phi/dt)^2 \ll V(\phi)$  which corresponds to  $w_\phi \simeq -1$ : the field then mimics the effect of a cosmological constant.

## 8.2 Coupled Quintessence

As we have already mentioned, the energy density of the dark energy and that of matter have the same order of magnitude in the present Universe. This suggests that there may be some relation between them, that is they could be “coupled” by some interaction.

We will consider here the particular case of a coupling between a quintessence field  $\phi$  and dark matter with an interaction of the form  $C\rho_m\dot{\phi}$ .

An interesting aspect of such a coupled dark energy scenario is that the system can approach scaling solutions with an associated accelerated expansion. With a suitable choice of the coupling and of the potential of the field is in fact possible to build models where both the densities of the dark components scale in the same way, from a certain time on. Henceforth, their proportion will be frozen for ever. These models can therefore solve the coincidence problem in an elegant way, rendering the present condition an attractor solution. Unfortunately they usually introduce several other problems, as for instance the lack of a matter dominated era, necessary to explain the formation of cosmic structures. At the moment there is not yet a viable model of dark energy solving the coincidence problem.

However several different ways to realize this coupling between dark energy and dark matter have been explored so far.

A scalar field is expected to couple explicitly (beyond the gravitational coupling) to ordinary matter, with a strength comparable to gravity, as shown by Carroll [50], unless some special symmetry prevents or suppresses the coupling. Such a strong coupling would render the scalar field interaction as strong as gravity, and would therefore have been already detected. However, a residual coupling still below detection cannot be excluded; moreover, if the coupling to baryons is different from the coupling to dark matter, as proposed by Damour *et al.* [51], then even a strong coupling is indeed possible. Exactly the same arguments hold if one supposes the quintessence field to be coupled to gravity, rather than to matter, as investigated by Uzan [52], Chiba [53], Chen and Kamionkowski [54] and Perrotta *et al.* [55]. Indeed, the two models, although physically different, are related mathematically by a conformal transformation as we will see in the following.

In minimal coupling theories the Lagrangian is the sum of the Einstein-Hilbert gravity Lagrangian and of the scalar field sector. The non-minimal coupling (NMC) adds a new term which, in its simplest form, may be written as

$$f(\phi)R. \quad (8.15)$$

Then, let us consider the Lagrangian of a NMC scalar field plus a perfect fluid matter component

$$L_{tot} = L(\phi, R) + 2\kappa^2 L_\phi + 2\kappa^2 L_m, \quad (8.16)$$

$$L(\phi, R) = -f(\phi)R, \quad (8.17)$$

$$L_\phi = \frac{1}{2}\phi_{,\mu}\phi^{,\mu} - V(\phi). \quad (8.18)$$

where  $\kappa^2 = 8\pi G$ . Applying the minimum action principle, we obtain the new Einstein

equations

$$G_{\mu\nu} = \frac{1}{L,R} \left[ \frac{1}{2} g_{\mu\nu} (L - L_{,R} R) - g_{\mu\nu} \square L_{,R} + (L_{,R})_{;\mu\nu} + \kappa^2 T_{\mu\nu}^{(\phi)} + \kappa^2 T_{\mu\nu}^{(m)} \right], \quad (8.19)$$

where  $L_{,R} \equiv dL/dR$  and the energy momentum tensors  $T_{\mu\nu}^{(\phi)}$  and  $T_{\mu\nu}^{(m)}$  are given in eqs (8.7) and (1.17) respectively. It can be shown that under the conformal transformation

$$\tilde{g}_{\mu\nu} = e^{2\omega} g_{\mu\nu} \quad (8.20)$$

with

$$2\omega = \log f \quad (8.21)$$

the equations in the rescaled metric (sometimes called Einstein frame, while the old metric is the Jordan frame) can be reduced to the canonical form of eqs (1.1)

$$\tilde{G}_{\mu\nu} = \kappa^2 \left[ \tilde{T}_{\mu\nu}^{(\phi)} + \tilde{T}_{\mu\nu}^{(m)} \right], \quad (8.22)$$

where  $\tilde{G}_{\mu\nu}$ ,  $\tilde{T}_{\mu\nu}^{(\phi)}$  and  $\tilde{T}_{\mu\nu}^{(m)}$  are the redefinition of the Einstein tensor and of the energy momentum tensors in the new metric

$$\tilde{T}_{\mu\nu}^{(m)} \equiv e^{-2\omega} T_{\mu\nu}^{(m)}. \quad (8.23)$$

The parameter  $\omega$  can be written in terms of a coupling constant therefore, after performing the conformal rescaling of the metric, the NMC system is written as a scalar field in pure General Relativity and an extra coupling to the ordinary matter.

## 8.3 Background evolution in a coupled Quintessence model

Let us consider a general system with a scalar field, matter (CDM plus baryons) and radiation. General covariance requires the conservation of the sum of their energy momentum tensors, so that it is possible to consider a coupling such that, for instance,

$$T_{\nu;\mu(c)}^{\mu} = -C_c(\phi) T_{(c)} \phi_{;\mu} \quad (8.24)$$

$$T_{\nu;\mu(b)}^{\mu} = -C_b(\phi) T_{(b)} \phi_{;\mu} \quad (8.25)$$

$$T_{\nu;\mu(\phi)}^{\mu} = [C_b(\phi) T_{(b)} + C_c(\phi) T_{(c)}] \phi_{;\mu} \quad (8.26)$$

$$T_{\nu;\mu(\gamma)}^{\mu} = 0. \quad (8.27)$$

Here radiation remains uncoupled because it is conformally invariant. Such a model can arise introducing in the Lagrangian a field with a gravity-coupling term of the form  $f(\phi)R = \frac{1}{2}\xi\phi^2 R$ . It can be shown that, in the limit of a small positive coupling, one obtains  $C = \kappa\sqrt{\xi}$ . In particular we are considering a species-dependent scalar coupling.

In a flat conformal FLRW metric these equations become

$$\begin{aligned}
\ddot{\phi} + 2\mathcal{H}\dot{\phi} + a^2 V_{,\phi} &= \kappa a^2 (\beta_c \rho_c + \beta_b \rho_b), \\
\dot{\rho}_c + 3\mathcal{H}\rho_c &= -\kappa \beta_c \rho_c \dot{\phi}, \\
\dot{\rho}_b + 3\mathcal{H}\rho_b &= -\kappa \beta_b \rho_b \dot{\phi}, \\
\dot{\rho}_\gamma + 4\mathcal{H}\rho_\gamma &= 0, \\
3\mathcal{H}^2 &= \kappa^2 a^2 (\rho_b + \rho_c + \rho_\phi + \rho_\gamma),
\end{aligned} \tag{8.28}$$

where  $\beta_c = C_c/\kappa$ ,  $\beta_b = C_b/\kappa$  (note that we use a coupling  $\beta$  which is  $\sqrt{2/3}$  the  $\beta$  used in ref. [56]). The matter conservation equation can be integrated to give

$$\rho_{c,b} = \rho(0)_{c,b} a^{-3} \exp \left\{ - \int \beta_{c,b}(\phi) d\phi \right\}. \tag{8.29}$$

This shows one of the basic properties of dark energy interactions: although pressureless, matter density does not scale with the inverse of volume. In other words, matter appears to be nonconserved to observers unaware of dark energy. The potential  $V(\phi)$  can be written in all generality as

$$V(\phi) = A e^{-\kappa \mu f(\phi) \phi}, \tag{8.30}$$

where  $\mu$  is a dimensionless constant. The exponential case studied in [57] and [56] corresponds therefore to  $f = 1$ , a constant potential to  $\mu = 0$  and the power law  $V(\phi) \sim \phi^{-n}$  to  $f(\phi) = n \log \phi / (\kappa \mu \phi)$ . We also give some useful definitions:

$$\frac{dV}{d\phi} = -\kappa \mu f_1 V \tag{8.31}$$

$$f_1 = \frac{df}{d\phi} \phi + f. \tag{8.32}$$

The system (8.28), is best studied in the variables [56, 58]

$$x = \kappa \frac{\phi'}{\sqrt{6}}, \quad y = \frac{\kappa}{H} \sqrt{\frac{V}{3}}, \quad v = \frac{\kappa}{H} \sqrt{\frac{\rho_b}{3}}, \quad z = \frac{\kappa}{H} \sqrt{\frac{\rho_\gamma}{3}}, \tag{8.33}$$

where the prime stands for a derivative with respect to  $\alpha = \ln a$ . Then we obtain

$$\begin{aligned}
x' &= \left( \frac{z'}{z} - 1 \right) x - \sqrt{\frac{2}{3}} \mu f_1 y^2 + \sqrt{\frac{2}{3}} \beta_c (1 - x^2 - y^2 - v^2 - z^2) + \sqrt{\frac{2}{3}} \beta_b v^2, \\
y' &= \sqrt{\frac{2}{3}} \mu f_1 x y + y \left( 2 + \frac{z'}{z} \right), \\
z' &= -\frac{z}{2} (1 - 3x^2 + 3y^2 - z^2), \\
v' &= -\frac{v}{2} (3\sqrt{\frac{2}{3}} \beta_b x - 3x^2 + 3y^2 - z^2), \\
\frac{H'}{H} &= -\frac{1}{2} (3 + 3x^2 - 3y^2 + z^2).
\end{aligned} \tag{8.34}$$

We notice that  $x^2$ ,  $y^2$ ,  $z^2$  and  $v^2$  give the fraction of total energy density carried by the field kinetic energy, the field potential energy, the baryons and the radiation, respectively:

$$\Omega_\phi = x^2 + y^2, \quad (8.35)$$

$$\Omega_\gamma = z^2, \quad (8.36)$$

$$\Omega_b = v^2. \quad (8.37)$$

Clearly, the dark matter energy density fraction is the complement to unity of  $x^2 + y^2 + v^2 + z^2$ :

$$\Omega_c = 1 - x^2 - y^2 - v^2 - z^2 \quad (8.38)$$

In terms of the new variables we can also write an expression for the parameter of the equation of state of the scalar field:

$$w_\phi = \frac{x^2 - y^2}{x^2 + y^2}, \quad (8.39)$$

while the equation of state of the total cosmic fluid is given by

$$p_{tot} = w_{eff} \rho_{tot}, \quad (8.40)$$

where

$$w_{eff} = x^2 - y^2 - z^2/3 = \Omega_\gamma(w_\gamma - 1) + \Omega_\phi(w_\phi - 1) \quad (8.41)$$

and  $w_\gamma = 1/3$  is the equation of state for the radiation.

To close the system (8.34) one also needs the relation  $f_1(y, H)$  which depends on the form of the potential. If we assume a power law potential and give arbitrary values to the coupling constants  $\beta$ , we can solve the system obtaining the behaviours of the density parameters, plotted in Fig. 8.1.

The baryonic and the radiation components are subdominant at present so we will neglect them. In particular, in order to simplify the analysis and to satisfy local gravity constraints we put from now on  $\beta_b = 0$  and  $\beta_c = \beta = const$ . Since  $\beta_b = 0$  implies that the standard matter is conserved (while the dark matter is not), the theoretical predictions of this model can be directly compared with observations. Quantities calculated in different frames should instead be converted back before comparison.

As it has been shown in refs. [56], for  $\beta < \sqrt{3/2}$  the standard matter era that precedes the final acceleration is replaced in this coupled model by an epoch in which the energy density fractions  $\Omega_m = \Omega_c + \Omega_b$ ,  $\Omega_\phi$  of matter and field are constant and equal to

$$\Omega_\phi = \frac{2}{3}\beta^2, \quad (8.42)$$

and  $\Omega_m = 1 - \Omega_\phi$ . During this epoch one has  $\phi' = 2\beta$  (the prime stands for  $d/d \log a$ ) and the scale factor grows as  $a \sim t^{\frac{2}{3(1+w_e)}}$  with  $w_e = 2\beta^2/3$  (these values are approximated since are obtained neglecting both baryons and radiation). This new matter era has been denoted as  $\phi$ MDE. This occurs when the potential is negligible with respect to the field kinetic energy. Since the potential is dominating the final accelerated epoch, it is clear

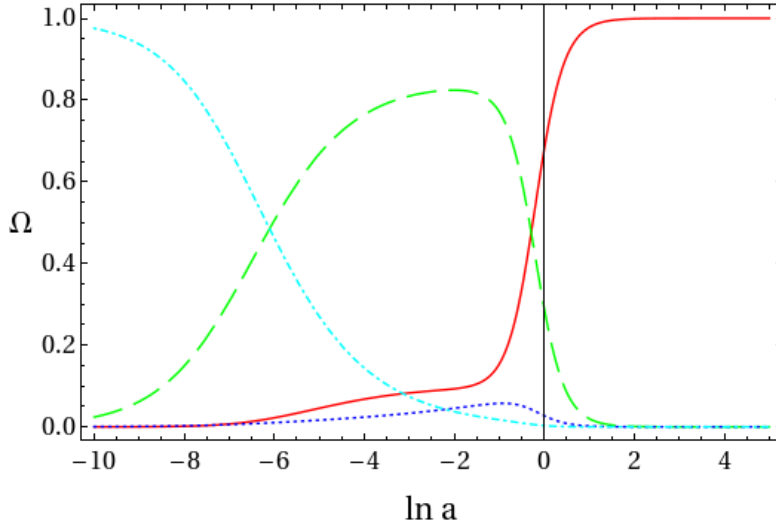


Figure 8.1: Behaviour of the density parameters  $\Omega_c$  (green, longdashed line),  $\Omega_\phi$  (red, solid line),  $\Omega_b$  (blue, dotted line) and  $\Omega_\gamma$  (cyan, dot-dashed line) as a function of  $\ln a$  for a power law potential  $V(\phi) = \phi^{-1}$  and  $\beta_b = \beta_c = 0.5$ . Notice that for the coupled quintessence models there is the transient regime  $\phi$ MDE in which both the matter and the scalar field energy density are nonvanishing. Baryons and radiation are subdominant at the present epoch.

that the  $\phi$ MDE generically will take place before acceleration and, of course, after the radiation era. This in fact is what has been observed in several numerical and analytical investigations, for instance in the case of exponentials and inverse power-law potentials  $V(\phi) = A\phi^{-n}$  [59]. As we will see, this stage is responsible for most of the differences with respect to ordinary quintessence, especially for what concerns the growth of cosmic structures.

## 8.4 Linear perturbations in coupled Quintessence models

We now show that during  $\phi$ MDE the growth of fluctuations is faster than in a standard matter era. In ref. [60] it has been shown that the perturbation equation in the sub-horizon regime is

$$\delta_c'' + \left(1 + \frac{\mathcal{H}'}{\mathcal{H}} - \beta_c \phi'\right) \delta_c' - \frac{3}{2}(\gamma_{cc}\delta_c\Omega_c + \gamma_{bc}\delta_b\Omega_b) = 0, \quad (8.43)$$

where again the prime stands for derivation with respect to  $\alpha \equiv \log a$  and where  $\gamma_{ij} = 1 + 2\beta_i\beta_j$  and  $\mathcal{H}$  is the conformal Hubble function  $\mathcal{H} \equiv aH$ . This equation is to be compared to eq. (5.101) derived in Section 5.7. Now we assume the baryon component to be negligible, then the fluctuation equation can be solved analytically during the  $\phi$ MDE:

$$\delta \sim a^{1+2\beta^2}, \quad (8.44)$$

from which it appears that the growth rate, defined in eq. (5.107), is  $s = 1 + 2\beta^2 > 0$ .

Let us briefly digress to evaluate the perturbation growth in the Jordan frame, where we assume an universal coupling,  $\beta = \beta_c = \beta_b$ , and where the total matter is conserved. In this case, the  $\phi$ MDE corresponds to the standard solution of the Brans-Dicke original theory (which is derived in absence of a potential)

$$a_J \sim t^{\frac{2+2\omega}{4+3\omega}}, \quad (8.45)$$

upon the substitution

$$\beta^2 = \frac{1}{2(3+2\omega)}, \quad (8.46)$$

where  $\omega$  is the Brans-Dicke coupling parameter. Therefore, the  $\phi$ MDE is quite a generic feature of scalar-tensor models and it also shows up in some  $f(R)$  models [61], that we will study in Chapter 9. The growth rate in Jordan frame is

$$\delta_J \sim a^{\frac{2+\omega}{1+\omega}} \sim a^{\frac{1+2\beta^2}{1-2\beta^2}}, \quad (8.47)$$

which again gives a rate larger than unity. When the  $\phi$ MDE ends and acceleration takes over, the rate  $s$  declines steadily to zero as in standard cases. Therefore, as anticipated,  $s$  goes from a value larger than unity to a value smaller than unity both in the interacting model and in the Jordan frame of scalar-tensor theories.

In the rest of the chapter, we focus on the interacting model defined by eq. (8.28).

## 8.5 A generalized fit for the growth rate

We now proceed to find a convenient fit to the full evolution of  $\delta(a)$  for the coupled models introduced in the previous section. In the standard scenario  $\delta$  obeys the equation

$$\delta''(\alpha) + \left(1 + \frac{\mathcal{H}'}{\mathcal{H}}\right)\delta'(\alpha) - \frac{3}{2}\Omega_m\delta(\alpha) = 0, \quad (8.48)$$

where

$$\frac{\mathcal{H}'}{\mathcal{H}} = -\frac{1}{2}(1 + 3w_\phi(\alpha)\Omega_\phi(\alpha)) = -\frac{1}{2}\left(1 + \frac{\Omega'_m}{\Omega_m}\right) \quad (8.49)$$

The solution can then be approximated as

$$\delta(\alpha) = e^{\int_0^\alpha d\alpha' \Omega_m(\alpha')^\gamma}. \quad (8.50)$$

In our interacting model, eq. (8.48) becomes

$$\delta'' + \left(1 + \frac{\mathcal{H}'}{\mathcal{H}} - \beta\phi'\right)\delta' - \frac{3}{2}\Omega_m(1 + 2\beta^2)\delta = 0, \quad (8.51)$$

so the solution will depend parametrically on the value of the coupling constant  $\beta$ . By solving this differential equation numerically for different values of  $\beta$  we find as expected that the growth rate  $s = \delta'/\delta$  is larger than unity in the past: the standard parametrization

(8.50) is therefore unable to describe a similar behaviour. To solve this problem, one simple possibility would be to generalize (8.50) as

$$\delta(\alpha) = e^{\int_0^\alpha d\alpha' \Omega_m(\alpha')^{\gamma(1+c\beta^2)}}, \quad (8.52)$$

with  $c$  a parameter to be determined by a least square fit. The choice of a  $\beta^2$  behavior is suggested by the fact that the  $\phi$ MDE depends only on  $\beta^2$ . This parametrization introduces a single new parameter,  $\eta = c\beta^2$ , in addition to those already in use to describe the growth factor, i.e.  $\Omega_m(0)$ ,  $\gamma$  and  $w$  (of course  $w$  itself could also be described by more parameters). This new parameter appears well justified: for instance, if future data will show that  $\eta$  is significantly different from zero then the standard growth of perturbations would be ruled out. However, this new fit is not very practical because it contains the function  $\Omega_m(\alpha)$  that should be obtained by numerically integrating the background equations and therefore depends on the field potential. To overcome this difficulty, we propose to use instead the *standard expression* for  $\Omega_m$  :

$$\Omega_m^{(s)}(a) = \frac{\Omega_{m,0}}{\Omega_{m,0} + (1 - \Omega_{m,0})a^{-3\hat{w}}}, \quad (8.53)$$

where  $\hat{w}(a) = (\log a)^{-1} \int_{a_0}^a w(a') da'/a'$  and the subscript 0 denotes the present time. Note that the present values of  $\Omega_m^{(s)}$  and  $\Omega_m$  coincide. For the coupled dark energy model we are considering here, we approximate  $w(z) \approx w_\phi(z=0)$ ; although one could easily expand  $w(z)$  to higher orders, our approximation is sufficient to show that our generalized fit works well. Therefore we define the rate

$$s_{fit} = \Omega_m^{(s)}(\alpha)^{\gamma(1+c\beta^2)} \quad (8.54)$$

where  $c$  will be determined below by fitting to numerical results. In this way, the growth rate can be parametrized by  $\Omega_{m,0}$ ,  $\gamma$ , and the combination  $\eta \equiv c\beta^2$ , plus the parameters that enter  $w(z)$ . With the new parameterization, even in the limit  $\Omega_m \rightarrow 1$ , one has  $s \neq 1$ . In the next section we show that this generalized fit is indeed a good approximation. Since we know that during the  $\phi$ MDE (i.e. at high  $z$ , for which  $\Omega_m^{(s)} \approx 1$ ) one has  $s = 1 + 2\beta^2$  we can anticipate that the result will be close to  $c \approx 2$ .

Concluding this section we note that eq. (8.54) should be seen for what it is, i.e. a phenomenological fit. The relation of  $\Omega_{m,0}$ ,  $w(z)$ ,  $\gamma$  and  $\eta$  to the underlying theory will of course depend on the theory itself. For instance, the identification of  $\Omega_{m,0}$  with the presently clustered mass in galaxies and clusters of galaxies is actually a model-dependent assumption; if gravity is not standard this assumption is likely to be incorrect. The value of  $\Omega_m(a)$  we adopt in our fit (8.54) must be inferred from observations of the background (as e.g. supernovae Ia) performed with a standard Hubble function  $H(z)$ . That is, we assume here that the Friedmann equation (which accounts only for the background data) can be written as the sum of two components, one that dilutes as  $\Omega_{m,0}a^{-3}$  and the other as  $(1 - \Omega_{m,0})a^{-3(1+\hat{w})}$ ; if the gravitational equations are not standard, one has to define  $\Omega_m(a)$  such that the above parametrization is still valid. The advantage of using (8.53-8.54) is that both background and linear growth are fitted by the same expression for  $w(a)$ ; that

is, once one adopts a prescription for  $w(a)$  one can fit all the data by simply adding the two parameters  $\gamma$  and  $\eta$  (plus possibly further parameters to account for the anisotropic stress, see eg. [62]). In this way we will be able to use in Sect. 8.7 the constraints from supernovae Ia directly on  $\Omega_{m,0}, w$ . Of course, in principle one could proceed in different ways: for instance, one could parametrize  $\Omega_m(a)$  so that values larger than unity in the past were allowed so as to force  $s > 1$ . Trivially, in fact, our parametrization above could be written equivalently defining a new density  $\hat{\Omega}_m \equiv \Omega_m^{(s)}(1 + \eta)^{1/\gamma}$ ; however, this density parameter would not be the same quantity that appears in the Friedmann equation.

## 8.6 Comparing the fit to the numerical results.

We solved numerically the background equations of the system (8.28) neglecting the fraction of baryons and radiation and choosing an exponential form for the potential,  $V(\phi) = A \exp(\mu\phi)$ . The constant  $A$  is determined by the present time condition on  $\Omega_{m,0}$ . Then we solved numerically the perturbation equation (8.51), thus obtaining a solution (that we denote  $\delta_{exact}$ ) which depends on the value of the coupling constant  $\beta$ . For  $\beta$  ranging between 0 and 0.5 and  $\mu$  within 0.1 and 1 (both varied in steps of 0.1), we found that the values of the parameters  $\gamma, c$  appearing in (8.54), which give the least square fit to  $\delta_{exact}$  are  $\gamma = 0.56$  and  $c = 2.1$ . Our best fit is therefore

$$\delta_{fit}(\alpha, \beta) \equiv e^{\int_0^\alpha d\alpha' \Omega_m^{(s)}(\alpha')^{0.56(1+2.1\beta^2)}}, \quad (8.55)$$

where we remark again that we use the standard expression for  $\Omega_m(a)$ .

This new function is indeed a good approximation to the exact solution  $\delta_{exact}$  as one can see in Fig. 8.2 where the curves of the growth factor  $g \equiv \delta/a$  for two different  $\beta$  and the corresponding  $g_{fit}$  are plotted. In Fig. 8.3 we present the level of accuracy of the fitting formula. We find fits to better than  $\approx 1\%$  for different values of  $\beta$ . Moreover, we find that the best fit values of the parameters do not depend on the actual value of the present matter density  $\Omega_{m,0}$ . We experimented also with an inverse power-law potential and found that also in this case eq. (8.55) is a good fit (see curve for  $\beta = 0.1$  in Fig. 8.2). Without the  $\eta$ -correction the relative error  $(\delta_{fit} - \delta_{exact})/\delta_{exact}$  becomes larger than 15% already for  $\beta = 0.2$ .

## 8.7 Comparing the fit to the observations

In the previous section we have seen that the expression

$$\Omega_m^{(s)}(\alpha)^\gamma (1 + \eta), \quad (8.56)$$

where  $\Omega_m^{(s)}(\alpha)$  is given by eq. (8.53) gives a good fit to the evolution of  $\delta'/\delta$  during both the decelerated and accelerated regimes for coupled dark energy models if  $\gamma \approx 0.56$  and  $\eta = 2.1\beta^2$ . Here we take some preliminary steps towards comparing the fit (8.56) to the observations. An indication for a positive  $\eta$  could signal an attractive force additional to standard gravity as in a scalar-tensor model; on the other hand one can speculate that a

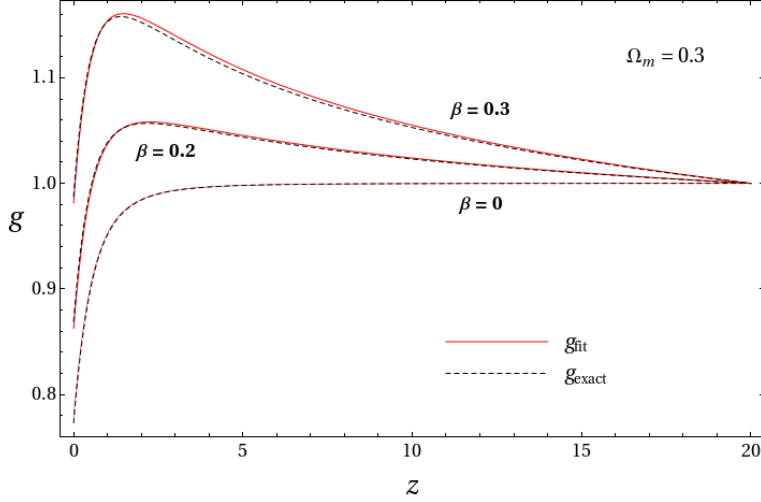


Figure 8.2: We compare the functions  $g_{fit} \equiv \delta_{fit}/a$  (red solid curves), given by the fitting formula (8.52) with the best fit (parameters  $\gamma=0.56$ ,  $c = 2.1$ ) for two different values of  $\beta$ , to the exact solutions  $g_{exact} \equiv \delta_{exact}/a$  (black dashed curves) of the differential equation (8.48) for the growth rate. The curve for  $\beta = 0$  also gives the standard best fit (i.e. for  $c = 0$ ). All curves are normalized at unity at  $z = 20$  and refer to an exponential potential with  $\mu = 1$ .

negative  $\eta$  could be related to a different physics, for instance a slowed growth induced by a hot matter component.

We consider the following data: *a*) Lyman- $\alpha$  power spectra at an average redshift  $z = 2.125$ ,  $z = 2.72$  [63],  $z = 3$  [64]; *b*) the normalization  $\sigma_8$  inferred from Lyman- $\alpha$  at  $z$  ranging between 2 and 3.8 [65]; *c*) galaxy power spectra at low  $z$  from SDSS [66] and 2dF [1]. From the three Lyman- $\alpha$  and the SDSS spectra we estimate the ratios

$$r(k_i; z_1, z_2) = \frac{P(k_i, z_1)}{P(k_i, z_2)}, \quad (8.57)$$

for the values of  $k_i$  for which there are tabulated value of the spectra (or for interpolated values and errors when the tabulated wavenumbers differ). For the  $\sigma_8$  data we estimate the ratios between successive values of  $z$ ,

$$r(z_1, z_2) = \frac{\sigma_8^2(z_1)}{\sigma_8^2(z_2)}. \quad (8.58)$$

Note that ref. [65] reports the values of  $\sigma_8$  extrapolated at the present epoch using the growth  $\delta$  of a  $\Lambda$ CDM model with  $\Omega_{m,0} = 0.27$ ,  $\Omega_{\Lambda,0} = 0.73$  ( $\sigma_8(z) = \sigma_8(0) \cdot \delta(z)$ ). So we use that same model to extrapolate them back to the observation redshifts. Then we see that  $r(z_1, z_2) = \delta^2(z_1)/\delta^2(z_2)$

For the Lyman spectrum at  $z = 3$  and for 2dF ( $z = 0.15$ ), the authors of [64, 1] give directly their estimation of the growth rate,  $s^{obs} = 0.49 \pm 0.10$  for 2dF and  $s^{obs} = 1.46 \pm 0.29$  for the Lyman- $\alpha$  data. Then we compare the observations to our fit by using the likelihood function

$$L = N \exp \sum_i \left( -\frac{(r_i^{obs} - r_i^{theory})^2}{2\sigma_i^2} \right) \exp \sum_j \left( -\frac{(s_j^{obs} - s_j^{theory})^2}{2\sigma_j^2} \right), \quad (8.59)$$

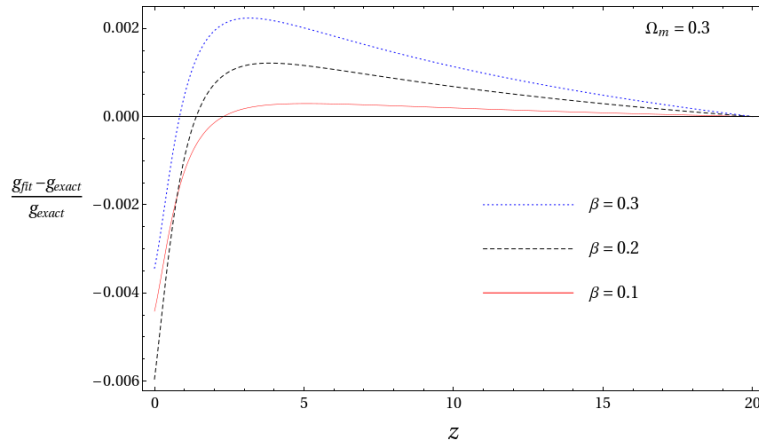


Figure 8.3: Level of accuracy of the best fit to the exact solution for the growth rate. For  $\beta$  ranging between 0 and 0.3 the fits are better than 0.6%. Without the correction the relative errors would be larger than 15% already for  $\beta = 0.2$ .

where the errors  $\sigma_i$  are obtained from the quoted errors on  $P(k)$  and  $\sigma_8$  by standard error propagation.

As we will see the data available at the present are not sufficient to set stringent limits to the growth function. Moreover, there are several sources of possible systematic effects that we cannot account for. For instance, the matter spectra derived from Lyman- $\alpha$  clouds are obtained through calibration (i.e. bias correction) with  $N$ -body simulations; these simulations have been generated only for a limited set of cosmological models and the results might depend on the assumptions (see e.g. [67]). It is difficult to quantify the impact of this limitation upon our results; the fact that we consider *ratios* of spectra from similar sources (eg Lyman- $\alpha$  clouds) might however alleviate the problem since one can expect that the calibration errors are only weakly dependent on redshift. For this reason we consider separately the ratios of the high- $z$  Lyman- $\alpha$  spectra to the low- $z$  SDSS galaxy spectra; our final results do not take these into account.

The current observational situation is summarized in Fig. (8.4) (and the associated Table 8.1), in which we plot the data we used in this work with  $1\sigma$  errors, along with the  $\Lambda$ CDM growth rate and with our best fit (see below). This figure gives a clear idea of the potential for improvement in the observational estimation of the growth rate.

We assume that the function  $s$  depends on four parameters,  $(\Omega_{m,0}, w_0, \gamma, \eta)$ . We assume also a flat prior  $\Omega_{m,0} \in (0.05, 0.4)$  and  $w_0 \in (-1, -0.6)$  which generously accounts for the supernovae constraints (neglecting the phantom region). Our main result is contained in Fig. (8.6), which displays the likelihood contour plots at 68%, 95% and 99.7% of probability in the plane  $(\gamma, \eta)$ , marginalizing over  $\Omega_{m,0}, w_0$ . Remarkably, the best fit values practically coincide with the  $\Lambda$ CDM prediction,  $(\eta, \gamma) = (0, 0.6)$ . However the likelihood extends considerably on both negative and positive  $\eta$  and even negative values of  $\gamma$  are not excluded beyond 99.7% probability. In Figs. (8.7-8.8) we plot the marginalized 1D likelihoods for  $\gamma$  and  $\eta$ . The results are tabulated in Table 8.2. The best fit values and

$z$	$s$
ref. [63]	
2.125-2.72	$0.74 \pm 0.24$
ref. [65]	
2.2 - 3	$0.99 \pm 1.16$
2.4 - 3.2	$1.13 \pm 1.07$
2.6 - 3.4	$1.66 \pm 1.35$
2.8 - 3.6	$1.43 \pm 1.34$
3 - 3.8	$1.30 \pm 1.50$
ref. [64]	
3	$1.46 \pm 0.29$
ref. [1]	
0.15	$0.49 \pm 0.10$

Table 8.1: Summary of observational data. We report in the  $z$  and  $s$  columns either the corresponding ranges or the central value and  $1\sigma$  errors. For the  $\sigma_8$  data or ref. [65] we chose to report the errorboxes on  $s$  obtained using the ratios at the given redshifts.

	68%	95%	99.7%
$\eta$	$0.00^{+0.28}_{-0.18}$	$+0.58$ $-0.38$	$+1.1$ $-0.58$
$\gamma$	$0.60^{+0.41}_{-0.30}$	$+0.97$ $-0.49$	$+1.6$ $-0.74$
$\gamma_{standard}$	$0.60^{+0.34}_{-0.26}$	$+0.77$ $-0.40$	$+1.4$ $-0.50$

Table 8.2: Best fit and errors (marginalized over all other parameters).

$1\sigma$  errors are

$$\gamma = 0.60^{+0.41}_{-0.30}, \quad \eta = 0.00^{+0.28}_{-0.18}. \quad (8.60)$$

As we anticipated, the current data impose only very weak constraints on  $\gamma, \eta$ . For completeness, we also quote in Table 8.2 the best fit and errors on  $\gamma_{standard}$ , i.e. assuming a standard model in which  $\eta = 0$ . Even in this case the likelihood distribution for  $\gamma$  remains very broad, although now negative values are rejected at more than 99.7% probability. Including the ratio of Lyman- $\alpha$  to SDSS power spectra has a minor effect on  $\gamma$  and moves the best fit of  $\eta$  to  $-0.2$ .

Assuming  $\eta < 0.58$  with 95% probability we can derive an upper limit to the coupling  $\beta$  introduced in Sect. 2,

$$\beta < 0.52 \quad (8.61)$$

(with 95% probability). This limit is very weak when compared to the CMB limits [59] but it is nevertheless interesting since it is independent and derived uniquely from the growth rate at small redshifts.

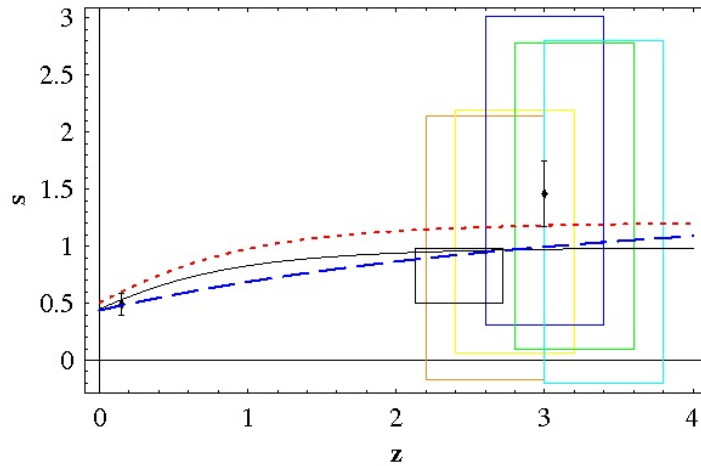


Figure 8.4: Summary of experimental data for the growth rate  $s$ , as detailed in Table I. The big coloured errorboxes represent the ratios  $\sigma(z_1)/\sigma(z_2)$  for various  $z$  intervals given in ref. [65] (three additional very large errorboxes have been excluded from the plot but not from the analysis); the smaller black box represents the average spectral ratio for the Lyman- $\alpha$  data of ref. [63]. The two points with errorbars are from ref. [1] and ref. [64]. The black solid line is the  $\Lambda$ CDM model, the red dotted curve is the coupled dark energy model with  $\Omega = 0.2$  and  $\beta = 0.4$  (i.e.  $\eta = 0.34$ ) and the dashed blue curve is the overall best fit  $(\Omega_{m,0}, w_0, \gamma, \eta) = (0.05, -0.6, 0.4, 0.45)$ .

## 8.8 Comments

The search for useful parametrizations of the dark dynamics is important since as it has been shown several times every parametrization introduces some arbitrariness in the way data are analysed [68]. In particular, with the advent of models of dark energy based on modification of Einstein's gravity, we have become aware of many possible trends, both at the background and at the perturbation level, that are not easily accounted for with earlier parametrizations. With this work we introduced a generalized form of parametrization of the growth rate that allows for a rate  $s \neq 1$ , i.e. faster or slower than the standard matter-dominated growth. We showed that this parametrization is suitable to model the fluctuation growth in coupled dark energy models and in scalar-tensor models.

We have analysed the current data in search of observational constraints on  $\gamma, \eta$ . Considering data from Lyman- $\alpha$  and galaxy power spectra at various redshifts we have obtained (rather weak) constraints on both parameters. The best fit turns out to be very close to the  $\Lambda$ CDM predictions. Many future experiments based on weak lensing or baryon oscillations will be able to estimate the growth rate and other fluctuation parameters with much higher precision, as we will show in the next chapter. We expect therefore that the constraints derived in this work will soon be superseded by much more precise ones and that new estimates of the growth factor will help clarify the nature of dark energy.

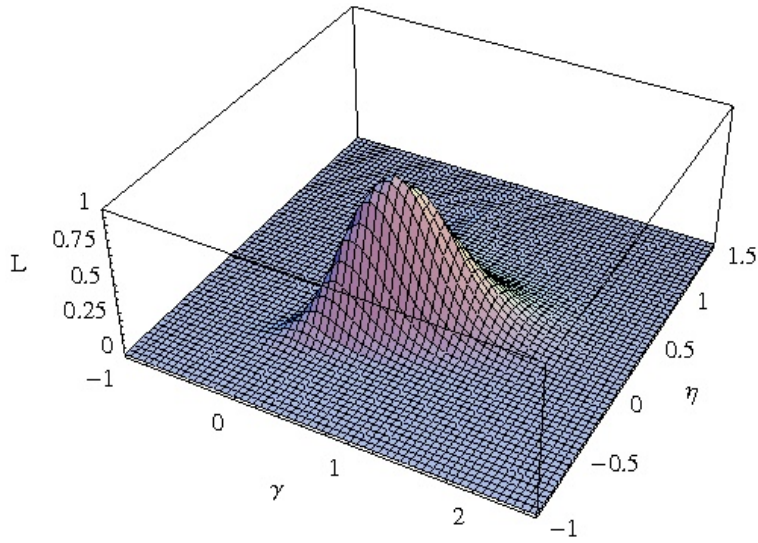


Figure 8.5: Tridimensional likelihood function marginalized on  $\Omega_{m,0}$  and  $w_0$ . The peak corresponds to  $(\gamma, \eta) = (0.6, 0)$ .

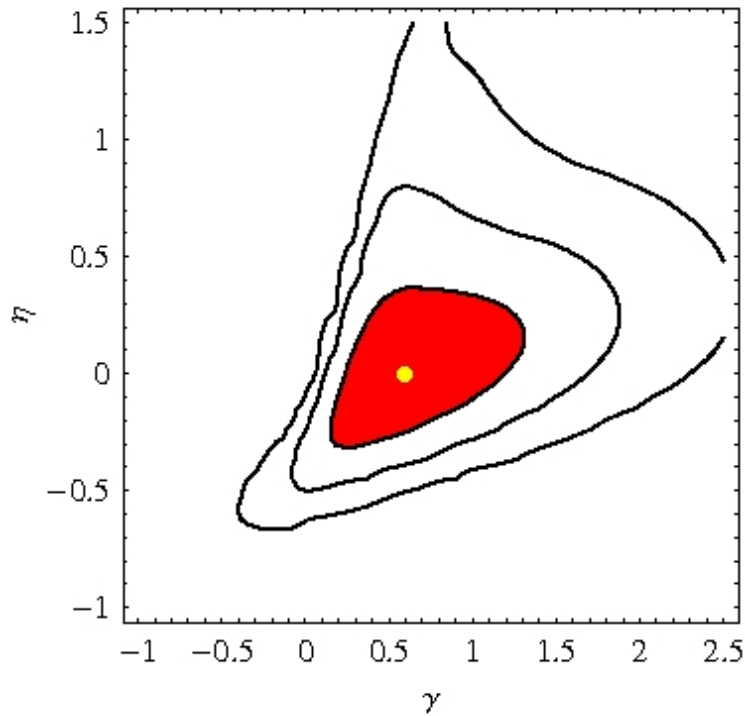


Figure 8.6: Contour plot of the likelihood marginalized over  $\Omega_{m,0}$  and  $w_0$ . The contours, from inside to outside, are at the 68% (red zone), 95%, 99.7% of probability. The dot marks the peak  $(\gamma, \eta) = (0.6, 0)$ .

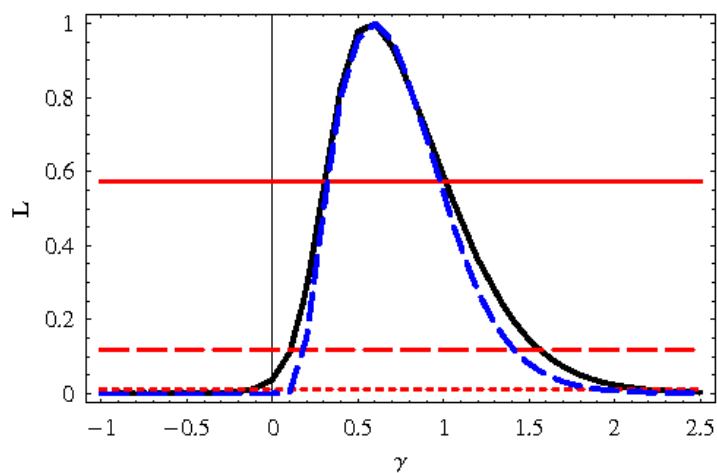


Figure 8.7: Marginalized likelihood for  $\gamma$  (solid line) and for  $\gamma_{standard}$ , i.e. fixing  $\eta = 0$  (dashed line). The three horizontal lines intersect the curve marking the intervals at 68, 95, 99.7% of probability, from top to bottom.

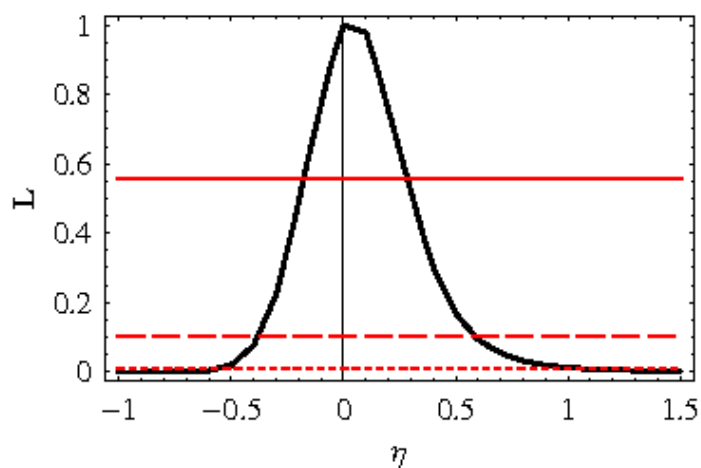


Figure 8.8: Marginalized likelihood for  $\eta$ . The three horizontal lines intersect the curve marking the intervals at 68, 95, 99.7% of probability, from top to bottom.



# Chapter 9

## Modified gravity theories: $f(R)$ models

In this chapter we will study the cosmological perturbations in a class of modified gravity theories, the so called  $f(R)$ .

As seen in sec. 4.2, scalar-tensor models represent one of the simplest classes of modification of gravity and as such are among the most studied models of dark energy since they provide a benchmark against which to compare standard gravity. A sub-class of scalar-tensor models takes the form of  $f(R)$  models, where the gravitational equations are derived by varying a Lagrangian written as a general function of Ricci's scalar (here we focus our analysis on the metric formalism). These simple models capture a wide range of interesting phenomena that are absent in Einstein's gravity: the equations are fourth order and new cosmological solutions can be found, including accelerated expansion, phantom behaviors etc. It is then interesting to study also their predictions on the growth of cosmological perturbations. Several papers tried to extend the  $\gamma$ -parametrization to dark energy models with non-Einsteinian gravity but this has been successfully done only either in a limited range of redshifts or scales and/or by pre-selecting a limited number of models.

The aim of this chapter is to extend the  $\gamma$ -parametrization to a large class of  $f(R)$  models, paying particular attention to finding a parametrization which is based, at least partially, on analytical expectations and which is as general as possible. For  $f(R)$  models it turns out that the growth rate  $s$ , contrary to  $\Lambda$ CDM and other standard dark energy models, is scale-dependent. We propose a form of  $s$  that fits a considerable range in redshift, in scales and that applies to many models. Moreover, our parametrization does not encounter the aforementioned difficulty of the standard  $\gamma$ -parametrization for  $s$  to cross unity. This is crucial as  $f(R)$  models, which are a particular case of scalar-tensor gravity, indeed have  $s > 1$  at intermediate redshifts.

### 9.1 The Growth Rate in $f(R)$

The  $f(R)$  modified gravity models are described by the following action in the Jordan Frame

$$S = \int d^4x \sqrt{-g} \left[ \frac{1}{2\kappa^2} f(R) + \mathcal{L}_{\text{rad}} + \mathcal{L}_{\text{m}} \right], \quad (9.1)$$

where  $\kappa^2 = 8\pi G$  while  $G$  is a bare gravitational constant (i.e. the standard Newtonian constant of “not modified” General Relativity),  $f(R)$  is some arbitrary function of the Ricci scalar  $R$ , and  $\mathcal{L}_m$  and  $\mathcal{L}_{\text{rad}}$  are the Lagrangian densities of dust-like matter and radiation respectively.

Here we concentrate on spatially flat Friedman-Robertson-Walker (FRW) universes with a time-dependent scale factor  $a(t)$  and a metric

$$ds^2 = -dt^2 + a^2(t) d\mathbf{x}^2. \quad (9.2)$$

The Einstein equations in this metric can be written as (hereafter a dot stands for a derivative with respect to  $t$ )

$$3FH^2 = \kappa^2(\rho_m + \rho_{\text{rad}}) + (FR - f)/2 - 3H\dot{F}, \quad (9.3)$$

$$-2F\dot{H} = \kappa^2[\rho_m + (4/3)\rho_{\text{rad}}] + \ddot{F} - H\dot{F}. \quad (9.4)$$

where  $F(R) \equiv df/dR$ , where the subscripts  $m$  and  $\text{rad}$  stand for matter and radiation, respectively and the Ricci scalar  $R$  is expressed by the Hubble parameter  $H$  as

$$R = 6(2H^2 + \dot{H}). \quad (9.5)$$

Following [69] we introduce the dimensionless variables:

$$\begin{aligned} x_1 &\equiv -\frac{\dot{F}}{HF}, & x_2 &\equiv -\frac{f}{6FH^2}, \\ x_3 &\equiv \frac{R}{6H^2}, & x_4 &\equiv \frac{\kappa^2\rho_{\text{rad}}}{3FH^2}, \end{aligned} \quad (9.6)$$

together with the following quantities

$$\begin{aligned} \Omega_m &\equiv \frac{\kappa^2\rho_m}{3FH^2} = 1 - x_1 - x_2 - x_3 - x_4, \\ \Omega_{\text{DE}} &\equiv x_1 + x_2 + x_3, \\ \Omega_{\text{rad}} &\equiv x_4. \end{aligned} \quad (9.7)$$

We will always ensure  $F_0 = 1$  so that the present value  $\Omega_{m,0}$  coincides with the standard definition. It is straightforward to derive the following differential equations [69]:

$$x'_1 = -1 - x_3 - 3x_2 + x_1^2 - x_1x_3 + x_4, \quad (9.8)$$

$$x'_2 = \frac{x_1x_3}{m} - x_2(2x_3 - 4 - x_1), \quad (9.9)$$

$$x'_3 = -\frac{x_1x_3}{m} - 2x_3(x_3 - 2), \quad (9.10)$$

$$x'_4 = -2x_3x_4 + x_1x_4, \quad (9.11)$$

where the prime denotes differentiation with respect to  $\alpha = \ln a$  and

$$m \equiv \frac{d \ln F}{d \ln R} = \frac{Rf_{,RR}}{f_{,R}}, \quad (9.12)$$

$$r \equiv -\frac{d \ln f}{d \ln R} = -\frac{Rf_{,R}}{f} = \frac{x_3}{x_2}. \quad (9.13)$$

From Eq. (9.13) one can express  $R$  as a function of  $x_3/x_2$ . Since  $m$  is a function of  $R$ , it follows that  $m$  is a function of  $r$ , i.e.  $m = m(r)$ . The  $\Lambda$ CDM model,  $f(R) = R - 2\Lambda$ , corresponds to  $m = 0$ . Hence the quantity  $m$  characterizes the deviation from the  $\Lambda$ CDM model. The effective equation of state of the system is

$$w_{\text{eff}} = -\frac{1}{3}(2x_3 - 1), \quad (9.14)$$

The dark energy equation of state,  $w \equiv p_{\text{DE}}/\rho_{\text{DE}}$ , is directly related to the one used in the standard analysis of SN Ia observations and it is given by

$$w = -\frac{2B\dot{H} + 3BH^2 + \kappa^2\rho_r/3}{3BH^2 - \kappa^2(\rho_m + \rho_r)} \simeq \frac{w_{\text{eff}}}{1 - F\Omega_m}, \quad (9.15)$$

where  $B$  is some constant and the last approximate equality in is valid in the regime where the radiation energy density  $\rho_r$  is negligible relative to the matter density.

We will make use of the relation

$$\frac{\mathcal{H}'}{\mathcal{H}} = 1 + \frac{H'}{H} = -\frac{1}{2} - \frac{3}{2}w_{\text{eff}}. \quad (9.16)$$

The perturbation equations can be written in the comoving gauge (where the velocity perturbation of non-relativistic matter vanishes) as

$$\begin{aligned} \ddot{\delta}_m + \left(2H + \frac{\dot{F}}{2F}\right) \dot{\delta}_m - \frac{\rho_m}{2F} \delta_m \\ = \frac{1}{2F} \left[ \left(-6H^2 + \frac{k^2}{a^2}\right) \delta F + 3H\delta\dot{F} + 3\delta\ddot{F} \right], \end{aligned} \quad (9.17)$$

$$\begin{aligned} \delta\ddot{F} + 3H\delta\dot{F} + \left(\frac{k^2}{a^2} + \frac{f_{,R}}{3f_{,RR}} - \frac{R}{3}\right) \delta F \\ = \frac{1}{3}\rho_m\delta_m + \dot{F}\dot{\delta}_m, \end{aligned} \quad (9.18)$$

where  $k$  is the comoving wavenumber. Note that these equations can in turn be written using the variables  $x_i$  of (9.6) and primes instead of dots, both of which are convenient for numerical integration. Neglecting the contribution of radiation, one has:

$$\begin{aligned} \delta_m'' + \left(x_3 - \frac{1}{2}x_1\right) \delta_m' - \frac{3}{2}(1 - x_1 - x_2 - x_3)\delta_m \\ = \frac{1}{2} \left[ \left\{ \frac{k^2}{x_5^2} - 6 + 3x_1^2 - 3x_1' - 3x_1(x_3 - 1) \right\} \delta\tilde{F} \right. \\ \left. + 3(-2x_1 + x_3 - 1)\delta\tilde{F}' + 3\delta\tilde{F}'' \right], \end{aligned} \quad (9.19)$$

$$\begin{aligned} \delta\tilde{F}'' + (1 - 2x_1 + x_3)\delta\tilde{F}' \\ + \left[ \frac{k^2}{x_5^2} - 2x_3 + \frac{2x_3}{m} - x_1(x_3 + 1) - x_1' + x_1^2 \right] \delta\tilde{F} \\ = (1 - x_1 - x_2 - x_3)\delta_m - x_1\delta_m', \end{aligned} \quad (9.20)$$

where  $\delta\tilde{F} \equiv \delta F/F$ , and the new variable  $x_5 \equiv aH$  satisfies

$$x'_5 = (x_3 - 1)x_5. \quad (9.21)$$

The above equations (9.17) and (9.18) can be much simplified considering only cosmologically viable  $f(R)$  models. In fact, in these cases the variation of  $F$  is small ( $|F'| \ll F$ ) so that the terms including  $\dot{F}$  can be neglected. If we also neglect the oscillating mode of  $\delta F$  relative to the mode induced by matter perturbations  $\delta_m$ , it follows that for sub-Hubble scales ( $k \gg \mathcal{H}$ ) the matter fluctuation equation becomes

$$\delta''_m + \left(1 + \frac{\mathcal{H}'}{\mathcal{H}}\right) \delta'_m - \frac{3}{2}\Omega_m \delta_m Q(k, a) = 0, \quad (9.22)$$

where

$$\begin{aligned} Q &= 1 + \frac{1}{3} \frac{k^2/M^2}{a^2 + k^2/M^2} \\ &= 1 + \frac{1}{3} \frac{m}{\lambda^2[1 - 3w(1 - \Omega_m)] + m}, \end{aligned} \quad (9.23)$$

where in turn we defined the effective mass  $M \equiv \sqrt{R/3m}$  of the scalar degree-of-freedom and in the last step also  $\lambda \equiv aH/k$ , the scale length in units of the Hubble radius. The last expression is a particular case of the scalar-tensor expression

$$Q = 1 + \frac{2\beta^2 k^2/M^2}{a^2 + k^2/M^2}, \quad (9.24)$$

where  $\beta$  is the scalar-tensor coupling and  $M^2 \equiv F^{-1}d^2V/d\phi^2$ . Although we discuss the sub-Hubble form (9.22) now, the numerical solutions are always obtained integrating the full set. Notice that  $Q \rightarrow 1$  for large scales,

$$k \ll k_{min} \equiv a(R/m)^{1/2}, \quad (9.25)$$

and that  $Q \rightarrow 4/3$  for  $k \gg k_{min}$  (small scales). In order to derive (9.23) we have also used the condition

$$M^2 \gg R \sim H^2 \quad (9.26)$$

which is satisfied for viable  $f(R)$  models in the past cosmic expansion history of the universe.

## 9.2 A Parametrization of the Growth Rate in $f(R)$

We try now to find an approximation for

$$s \equiv \frac{\delta'}{\delta}, \quad (9.27)$$

which obeys the equation

$$3w\Omega_m(1 - \Omega_m) \frac{ds}{d\Omega_m} + \left[ \frac{1}{2} - \frac{3}{2}w(1 - F\Omega_m) \right] s + s^2 - \frac{3}{2}\Omega_m Q = 0. \quad (9.28)$$

Since  $F(z) \approx 1$  in the redshift range of interest we can approximate  $\tilde{\Omega}_m \equiv F\Omega_m$  with  $\Omega_m$  (we verified that this doesn't affect our results). One possible parametrization one could think of is a straightforward generalization of the  $\gamma$ -parametrization given by:

$$s \equiv Q (\Omega_m)^\gamma. \quad (9.29)$$

This would raise the upper bound on  $s$  to  $4/3$ , which encompasses the usual  $s > 1$  behavior of some  $f(R)$  models [70]. If  $\Omega_m \approx 1$  and  $\gamma$  is slowly varying we can write  $ds/d\Omega_m = (\Omega_m)^{\gamma-1}\gamma Q$ , expand and obtain (linearized around  $\Omega_m = 1$ )

$$\gamma = \frac{3(1-w)}{(1+4Q-6w)} - \frac{2(1-2Q)}{(1-\Omega_m)(1+4Q-6w)} \quad (9.30)$$

(notice that  $\gamma = 6/11$  for  $\Lambda$ CDM).

The above proposed parametrization however has the disadvantage of not being a solution to (9.28) for  $\Omega_m = 1$ , around which we expand our approximation. To account for this we propose instead the parametrization given by:

$$s \equiv \frac{1}{4} \left( -1 + \sqrt{1+24Q} \right) (\Omega_m)^\gamma. \quad (9.31)$$

Substituting the above on (9.28) linearized around  $\Omega_m = 1$ , one gets

$$\gamma = \frac{12Q + 3w(1 - \sqrt{1+24Q})}{24Q + (1 - \sqrt{1+24Q})(1+6w)}, \quad (9.32)$$

which does not depend on  $\Omega_m$  itself. The above can be written in a simpler form by defining

$$\tilde{Q} \equiv \frac{1}{4} \left( -1 + \sqrt{1+24Q} \right). \quad (9.33)$$

Note that from the definition above  $Q = 1 \rightarrow \tilde{Q} = 1$  and that  $Q = 4/3 \rightarrow \tilde{Q} \simeq 1.19$ . One then has

$$\text{Fit 1: } s(k, z) = \tilde{Q} (\Omega_m)^\gamma, \quad (9.34)$$

$$\gamma = \frac{1 + 2\tilde{Q} - 3w}{1 + 4\tilde{Q} - 6w}, \quad (9.35)$$

which we shall dub Fit 1. It is clear that such a parametrization should not be relied upon whenever  $w$  is close to  $5/6$ . This indeed happens in most viable models for  $z \gtrsim 3$ , since around this redshift there is a generic phantom crossing [71] which makes  $w$  diverge and then become positive as  $z$  increases. Nevertheless this in practice is not a big issue as the vast majority of currently planned future data will come from the region  $z \lesssim 2$ . In any case, we find numerically that in all models here considered the above parametrization is actually valid even for higher  $z$ . The definition (9.32) also ensures that  $\gamma$  is numerically close to the  $\Lambda$ CDM value of  $6/11 = 0.545$ : for  $-3 < w < 0$  one has  $0.52 < \gamma < 0.6$  for any value of  $Q$ . In fact, since the value of  $Q$  (and also that of  $\tilde{Q}$ ) is always close to 1

(remember  $1 < Q < 4/3$ ), one can also expand this parametrization around  $\tilde{Q} = 1$ . Doing so, one gets

$$\gamma \simeq \frac{17 - 2\tilde{Q} + 3w(-11 + 6w)}{(5 - 6w)^2}. \quad (9.36)$$

In (9.32) we expanded (9.28) to first order in  $\Omega_m$ . If one includes also second order corrections on  $\Omega_m$ , then the fractional difference  $|\Delta s/s|$  (between first and second order expansions) for  $-3 < w < 0$  is smaller than 4% for  $\Omega_m = 0.25$  and smaller than 1% for  $\Omega_m > 0.5$ . Therefore if one is only interested in an accuracy of a few percent on  $s$ , a first order expansion should be enough.

In the following we compare this fit with the results of the numerical integration. However we also introduce another fit, similar to Fit 1, designed to improve upon Fit 1 both in terms of accuracy and in terms of simplicity. Fit 1 infact requires the integration of the background equations in order to obtain the functions  $m(z), \Omega_m(z), w(z)$  that enters  $Q(k, z)$ . This of course is impractical if one wishes to cover many  $f(R)$  models, for instance when looking for forecasts of future experiments. Moreover, since the condition that  $\gamma$  is approximately constant is actually not well fulfilled, as we will see, we introduce an additional parameter,  $A$ , that will serve the purpose of improving the accuracy.

Our Fit 2 is then defined as

$$\text{Fit 2: } s(k, z) \equiv \frac{\delta'}{\delta} = \tilde{Q}^A (\Omega_m)^\gamma, \quad (9.37)$$

$$E(z)^2 \equiv H^2/H_0^2 = [\Omega_{m,0}(1+z)^3 + (1 - \Omega_{m,0})(1+z)^{3(1+w_0)}], \quad (9.38)$$

$$\Omega_m(z) = \Omega_{m,0}(1+z)^3/E(z)^2. \quad (9.39)$$

and we assume a constant equation of state  $w(z) = w_0$ , being  $w_0$  the present value. This, indeed, happens to be a rather good approximation for small redshifts. Fit 2 depends entirely on presently observed quantities,  $w_0, \Omega_{m,0}$  and on the universal (i.e., independent of  $f(R)$ ) parameters  $A, \gamma$ , that we are going to fix in the following. Notice that the function  $m(z)$  itself is analytically fixed by assigning  $w_0, \Omega_{m,0}$ :  $m(R)$  is infact an analytical function of  $R$ , and  $R$  is an analytical function of  $E(z)$ . In this way, once the  $f(R)$  is given, one can easily compute all the relevant quantities ( $m, R...$ ) without integrating the background.

Of course, one can also rephrase our parametrization in terms of a scale and time dependent  $\hat{\gamma}$  function defined implicitly as  $s = \Omega_m^{\hat{\gamma}}$  by writing

$$\hat{\gamma}(k, z) = \gamma + A \frac{\log \tilde{Q}}{\log \Omega_m} \quad (9.40)$$

The growth function  $s$  is already constrained by large-scale structure and redshift distortion experiments and is a primary target for future large scale surveys that aim at measuring it to within a few percent and down to  $z \approx 2$ .

## 9.3 Results

Our goal is finding a simple parametrization for all cosmologically viable  $f(R)$  theories in the range

$$(0.005 \leq k \leq 0.5) h/\text{Mpc}, \quad z < 3. \quad (9.41)$$

Our fit is good also for larger values of  $k$ , however in this region the linear approximation breaks down. On the other hand, for smaller  $k$  it is the sub-Hubble approximation that breaks down.

In order to test our fits, we have studied a number of  $f(R)$  models whose  $m(r)$ 's satisfy basic cosmological requirements and local gravity constraints, as it has been shown in [69]. All these models can be written in the form

$$f(R) = R - \lambda R_c f_1(x) \quad x \equiv R/R_c \quad (9.42)$$

where  $R_c (> 0)$  defines a characteristic value of the Ricci scalar  $R$  and  $\lambda$  is some positive free parameter.

The  $\Lambda$ CDM, for which  $f(R) = R - 2\Lambda$  is recovered putting

- (A)  $f_1(x) = \frac{2\Lambda x}{\lambda R}$ .

In particular we tested the following classes of models

- (B)  $f_1(x) = x^{2n}/(x^{2n+1}) \quad (n > 0)$ ,
- (C)  $f_1(x) = 1 - (1 + x^2)^{-n} \quad (n > 0)$ ,
- (D)  $f_1(x) = 1 - e^{-x}$ ,
- (E)  $f_1(x) = \tanh(x)$ .

For every class, we studied different models obtained varying the values of the parameters  $\lambda, n, \Omega_{m,0}$  and computing  $R_c$  using the approximate relation

$$R_c \approx 6H_0^2(1 - \Omega_{m,0})/\lambda. \quad (9.43)$$

Once these parameters are specified, we can solve the background equations, finding by trial and errors the initial conditions such to reproduce the specified value for  $\Omega_{m,0}$ , and then the perturbation equations. Then we compute the accuracy of our fits in reproducing the exact solution. Results are shown in Fig. 9.2, Fig. 9.3, Fig. 9.4, Fig. 9.5, for four different models, each for every class. Their  $m(r)$  trajectories are plotted in figure Fig. 9.1. We have found that Fit 1 is accurate to more than 14% in the range (9.41). In order to use a universal value for the parameter  $A$  in Fit 2, we compute its best fit value through a minimum least square fit over the range (9.41) and over all the studied models, finding the value  $A = 0.7$ . Fixing the parameter  $A$  this way, we have computed its accuracy in reproducing the exact solution, which we found to be at worst 6%, a big improvement over Fit 1. Fit 2 has the advantage to be much easier to evaluate since it requires only the knowledge of  $\Omega_{m0}, w_0$ . Furthermore, the use of a constant  $w(z) = w(0) \equiv w_0$ , lacking of any singularity, allows us to extend this fit up to higher redshifts. See for instance Fig 9.6 where the fit is extrapolated to very high  $z$ .

### 9.3.1 Improving the fit for small $k$

If we don't use the sub-Hubble approximation ( $k^2/a^2 \gg H^2$ ) to derive eq.(9.23), or in another words we don't neglect the term  $-6H^2\delta F/2F$  in eq. (9.17), we can rewrite  $Q$  as

$$Q = 1 + \frac{1}{3} \frac{k^2/M^2 - 6H^2a^2/M^2}{a^2 + k^2/M^2} \quad (9.44)$$

Since, for scales  $k < 0.005$  we have  $k^2/M^2 \sim H^2/M^2$  around  $z = 0$ , taking into account this term improves the fit for small  $k$  at low redshift (see Fig. 9.7 for a comparison, where for Fit new we mean Fit 1 with  $Q$  given by eq. (9.44)).

## 9.4 Future developments

We have seen how our parametrization Fit 2 can reproduce the growth rate for a large class of  $f(R)$  models with an accuracy being at worse 6%. We think it is already a good result, however, our task is to improve the fit, reducing the accuracy even more. In order to do that, we studied the dependence of the parameter  $A$  on the scale  $k$ , fitting the growth rates keeping  $k$  fixed. The plot in Fig. 9.8 suggests that we could use a  $k$ -dependent parameter instead of a constant one. The behavior of  $A$  with respect to  $k$  is well fitted by the functional form

$$A(k) = 1 - b \cdot k^{-1/c}, \quad (9.45)$$

thus we changed our Fit 2 to the form

$$\text{Fit 3 : } s = \tilde{Q}^{A(k)} \Omega_m, \quad (9.46)$$

where  $A(k)$  is given by eq. (9.45) while  $b$  and  $c$  are two parameters to be fixed through a least square fit to exact solution for the growth rate. For the model (B) with  $\lambda = 1, 55; n = 1; \Omega_{m,0} = 0, 24$  we obtain

$$b = 0.057, \quad c = 2.78. \quad (9.47)$$

Using the above values we plot the exact solution for the growth rate and its behavior reproduced by Fit 3 for several scales. In Fig. 9.9 one can see how the use of the function  $A(k)$ , which takes into account the dependence on the scale  $k$ , can help reducing the accuracy making this fit a very good tool in order to reproduce the growth rate and to compare it to observational data. Therefore, the future developments of this work are testing this fit for the other  $f(R)$  models, trying eventually to find universal values for the parameters  $b, c$ , as we did for the parameter  $A$  in Fit 2.

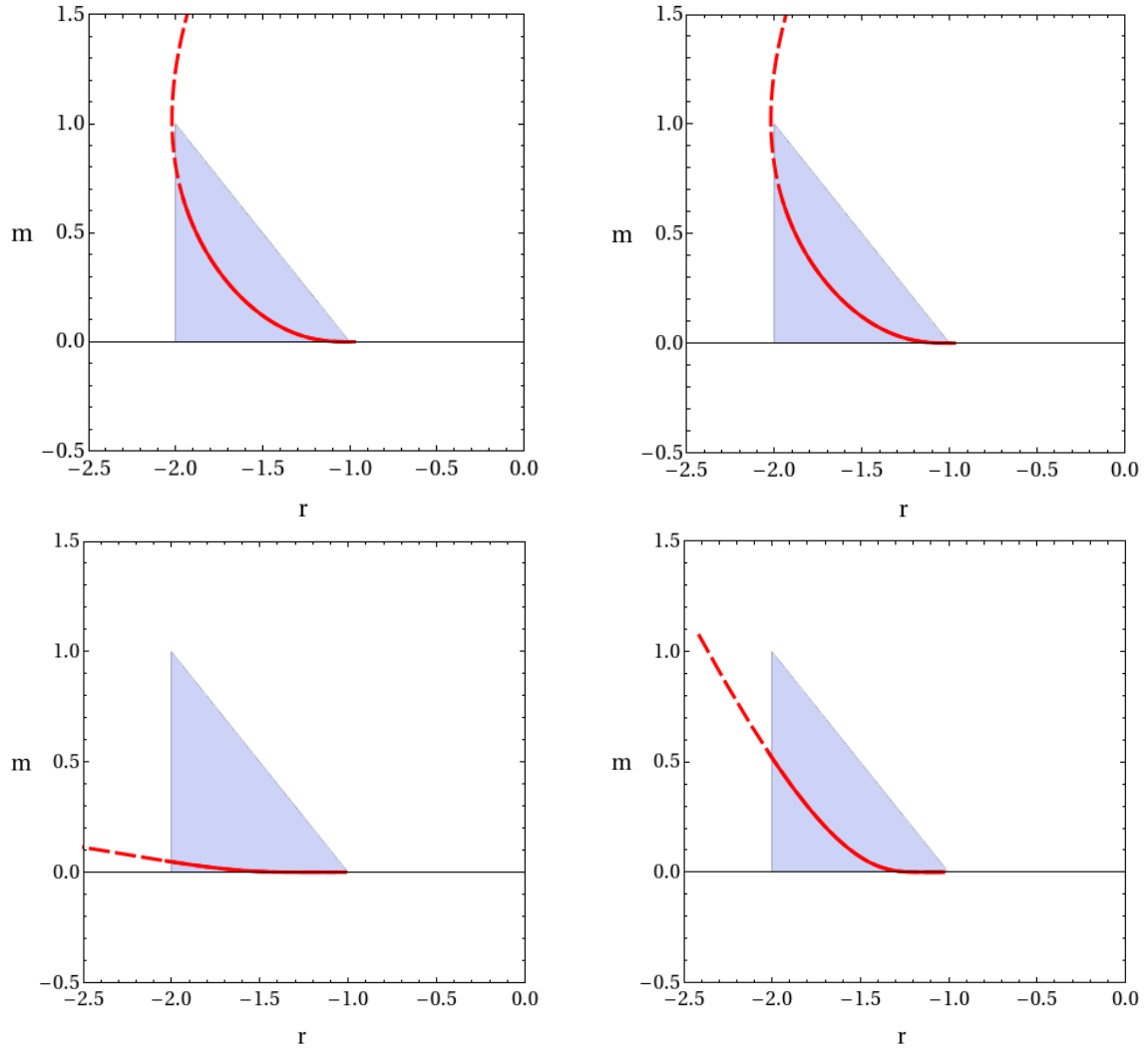


Figure 9.1:  $(r, m)$  plane for four different models. Upper left panel: model (B) with  $\lambda = 1.55$ ,  $n = 1$ ,  $\Omega_{m,0} = 0.24$ ; upper right panel: model (C) with  $\lambda = 1.55$ ,  $n = 1$ ,  $\Omega_{m,0} = 0.28$ ; lower left panel: model (D) with  $\lambda = 3$ ,  $\Omega_{m,0} = 0.20$ ; lower right panel: model (D) with  $\lambda = 1$ ,  $\Omega_{m,0} = 0.24$ . The red solid curve is the trajectory effectively covered by the background integration, while the red dashed curve is its analytic extension. The shaded triangle represents the allowed region for the  $m(r)$  trajectory to connect the matter point, situated at  $(r, m) = (-1, 0)$ , to the De Sitter point, situated along the segment  $0 < m \leq 0$  at  $r = -2$  (see [69] for further details).

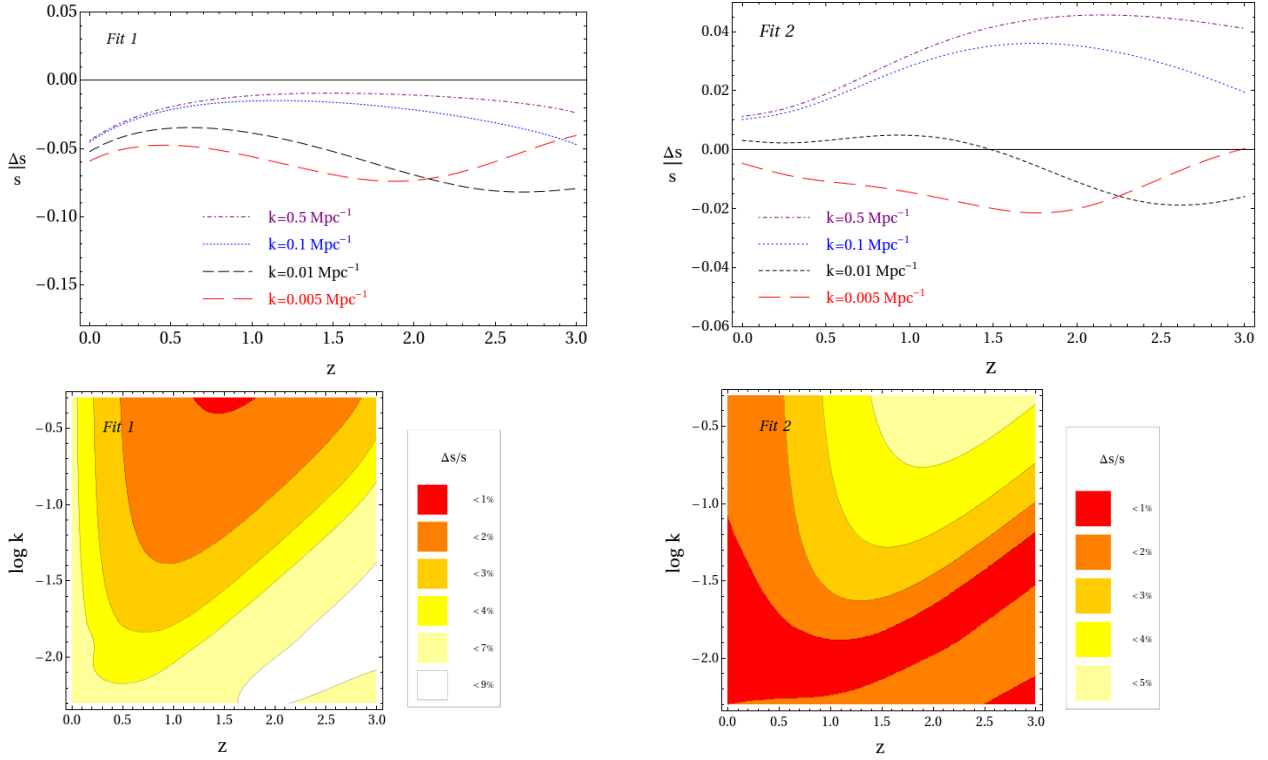


Figure 9.2: In these figures are shown the results relative to the model (B) with  $\lambda = 1.55$ ,  $n = 1$ ,  $\Omega_{m,0} = 0.24$  and  $w_0 = -0.92$ . In the left panels is shown the accuracy of the Fit 1 in reproducing the exact growth rate as a function of  $z$  (top) and as a function of both  $z$  and  $k$  (bottom), while the right panels are the accuracy for Fit 2 with  $A = 0.7$ .

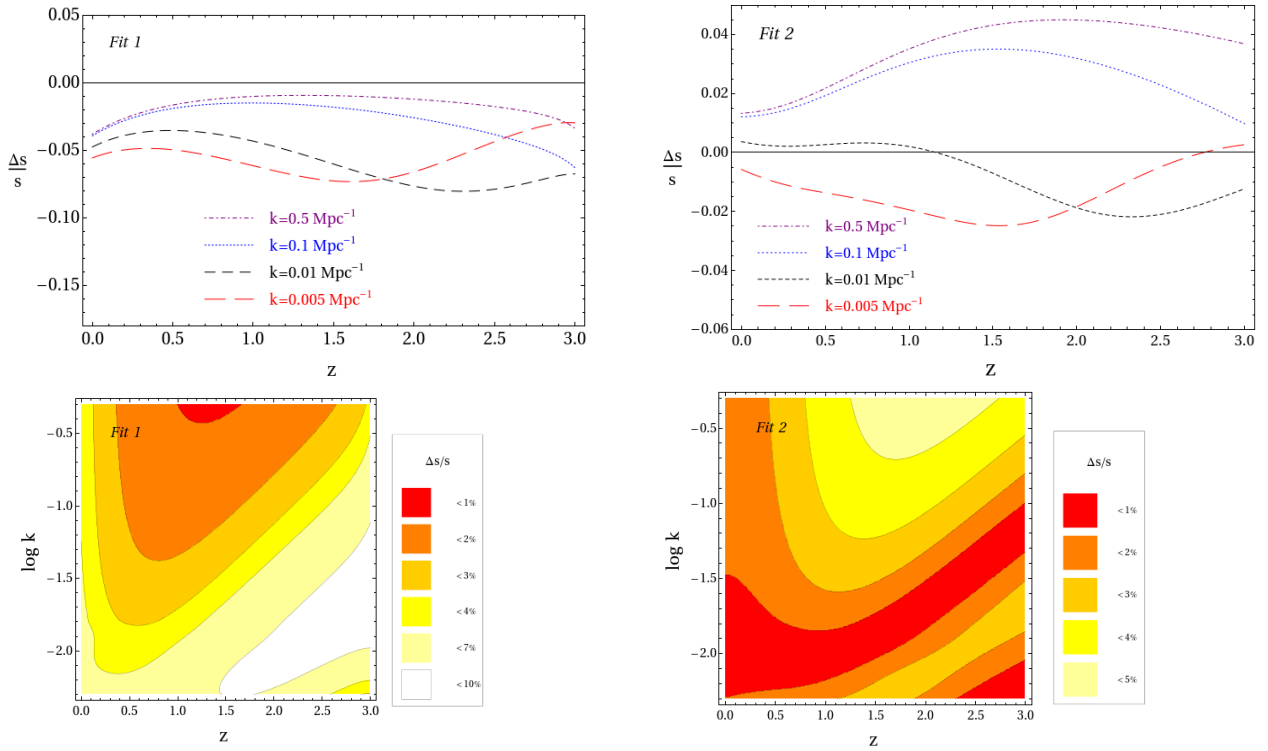


Figure 9.3: Same as Fig. 9.2, for the model (C) with  $\lambda = 1.55$ ,  $n = 1$ ,  $\Omega_{m,0} = 0.28$  and  $w_0 = -0.92$ .

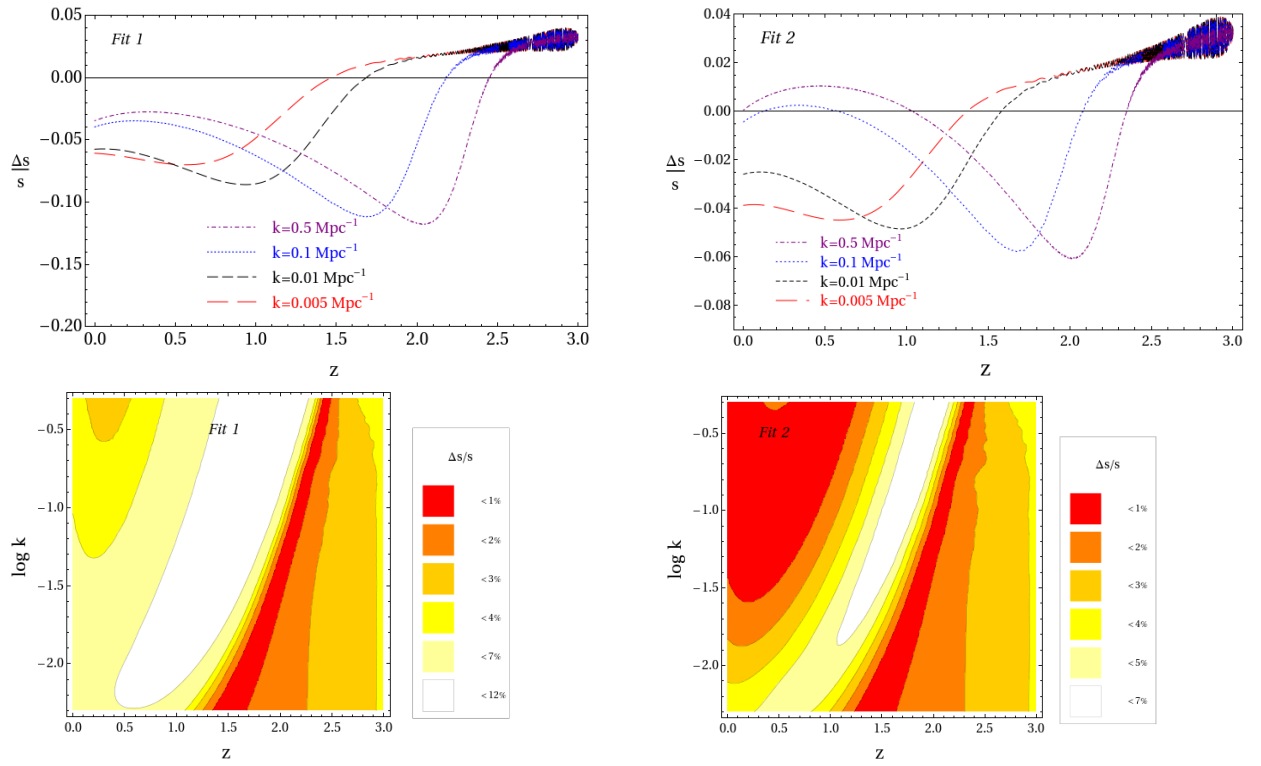


Figure 9.4: Same as Fig. 9.2, for the model (D) with  $\lambda = 3, \Omega_{m,0} = 0.20$  and  $w_0 = -0.99$ .

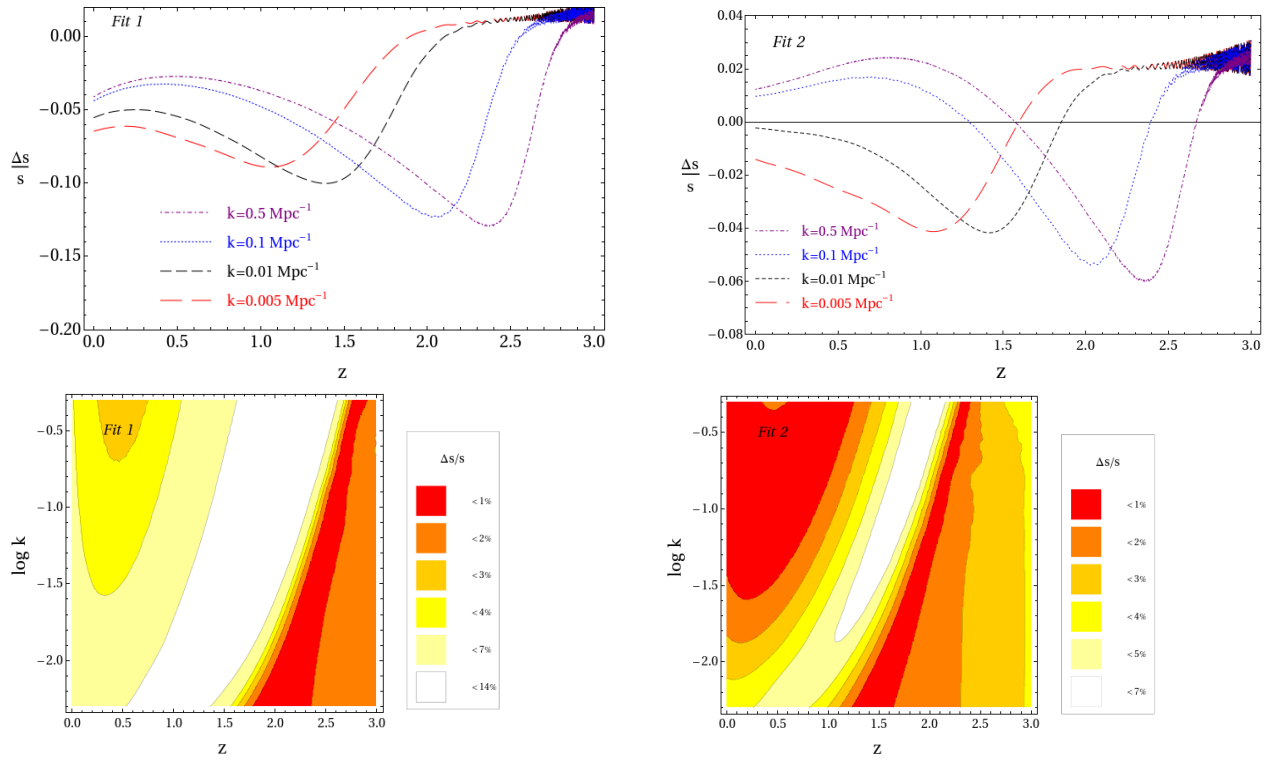


Figure 9.5: Same as Fig. 9.2, for the model (E) with  $\lambda = 1, \Omega_{m,0} = 0.24$  and  $w_0 = -0.95$ .

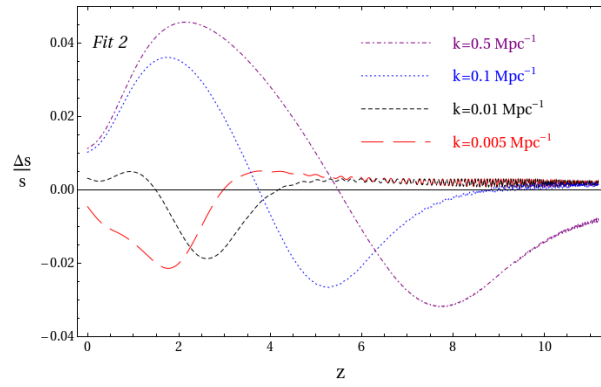


Figure 9.6: Accuracy of Fit 2 up to  $z > 10$  for model (B).

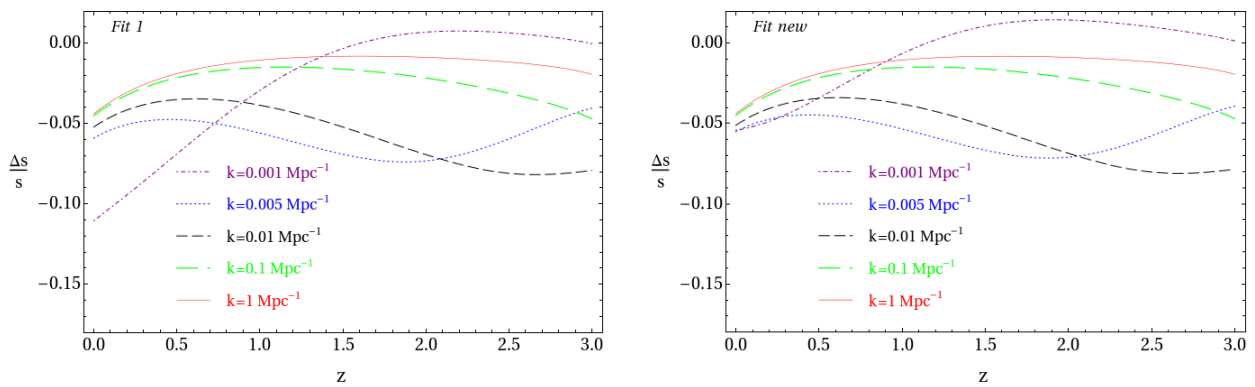


Figure 9.7: Comparison between the accuracy of Fit 1 (left panel) and that of Fit new for  $0.001 \leq k \leq 1$ . The latter can better reproduce the growth for small  $k$ .

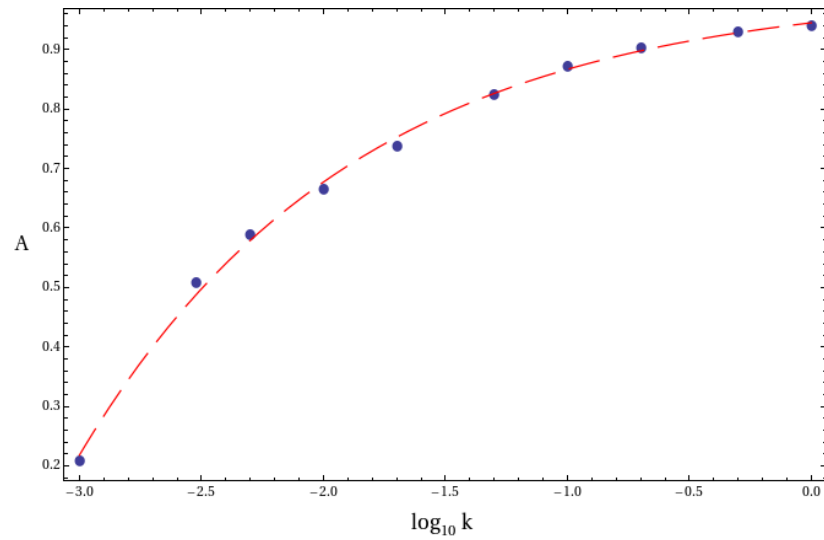


Figure 9.8: Dots represent the values assumed by the parameter  $A$  in Fit 2 when the fit to the exact solution is made keeping  $k$  fixed, for model (B) with  $\lambda = 1.55$ ,  $n = 1$ ,  $\Omega_{m,0} = 0.24$  and  $w_0 = -0.92$ . The red curve is a fit to the behavior of  $A$  with respect to  $k$ .

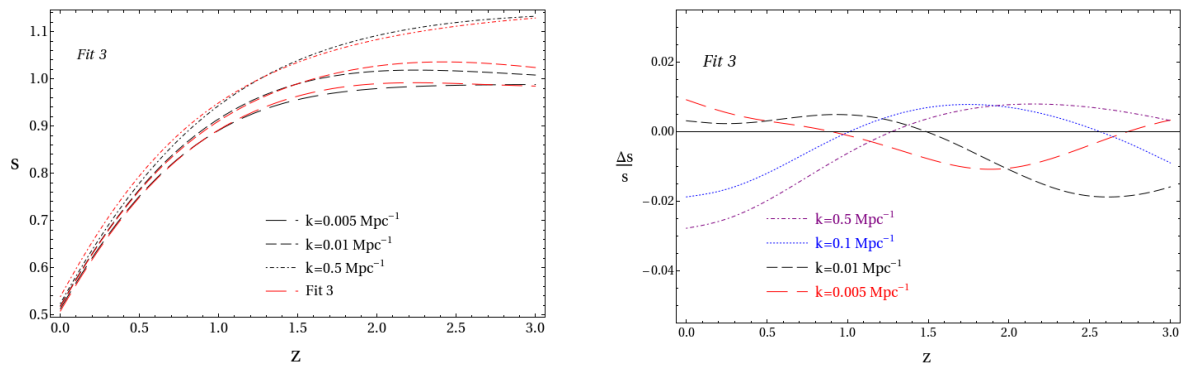


Figure 9.9: Fit 3 for model (B) with  $\lambda = 1.55$ ,  $n = 1$ ,  $\Omega_{m,0} = 0.24$  and  $w_0 = -0.92$ . Left panel: black curves are the exact solution for the growth rates, while red curves are their behaviors reproduced by Fit 3; right panel: accuracy of Fit 3.



# Chapter 10

## Forecasting constraints from future data

Many experiments in the near future will test dark energy through its effects on the linear growth of matter perturbations. In this chapter we discuss the constraints that future large-scale redshift surveys can put on three different parametrizations of the linear growth factor and how these constraints will help ruling out different classes of dark energy and modified gravity models. We will also show that a scale-independent bias can be estimated to a few percent per redshift slice by combining redshift distortions with power spectrum amplitude, without the need of an external estimation.

### 10.1 Introduction

The linear growth rate of matter perturbations is one of the most interesting observable quantities since it allows to explore the dynamical features related to the build-up of cosmic structures beyond the background expansion. For example it can be used to discriminate between cosmological models based on Einstein's gravity and alternative models like  $f(R)$  modifications of gravity (see e.g. [72]) or multi-dimensional scenarios like in the Dvali-Gabadaze-Porrati (DGP) [73] theory (e.g. [74] and references therein). In addition, the growth rate is sensitive to dark energy clustering or to dark energy-dark matter interaction. For instance, as we have seen in Chapter 9, in models with scalar-tensor couplings or in  $f(R)$  theories the growth rate at early epochs can be larger than in  $\Lambda$ CDM models and can acquire a scale dependence [75, 76, 70] (see for instance [34] for a review on dark energy).

Simultaneous information on geometry and growth rate can be obtained by measuring the galaxy power spectrum or the 2-point correlation function and their anisotropies observed in redshift space. As explained in Sec. 6.6, these redshift distortions arise from peculiar velocities that contribute, together with the recession velocities, to the observed redshift. The net effect is to induce a radial anisotropy in galaxy clustering that can be measured from standard two-point statistics like the power spectrum or the correlation function [77]. The amplitude of the anisotropy is determined by the typical amplitude of peculiar velocities which, in linear theory, is set by the growth rate of perturbations (see

eqs (6.47), (6.48)):

$$s \equiv \frac{d \log G}{d \log a}, \quad (10.1)$$

where  $G(z) \equiv \delta(z)/\delta(0)$  is the growth function,  $\delta(z)$  the matter density contrast and the scale factor  $a$  is related to the redshift  $z$  through  $a = (1+z)^{-1}$ . Since however we only observe the clustering of galaxies and not that of the matter, the quantity that is accessible to observations is actually

$$\beta \equiv \frac{s}{b}, \quad (10.2)$$

where the bias  $b$  is defined in eq. (6.56) as the ratio of density fluctuations in galaxies and matter. The bias is in general a function of scale and redshift, but in the following we will consider it as a simple scale-independent function.

Once the power spectrum is computed in  $k$ -space, the analysis proposed in [47] can be exploited to constrain not only geometry but also the growth rate (as pointed out in [78]; see also [79, 74]), provided that the power spectrum is not marginalized over its amplitude. In configuration space, the first analysis of the two-point correlation function explicitly aimed at discriminating models of modified gravity from the standard  $\Lambda$ CDM scenario has been performed by [80]. There are several experimental estimates of the growth factor currently available that derive either from the analysis of the redshift space distortions [81, 82, 83, 84, 80, 85, 86, 87] or have been derived indirectly from the *rms* mass fluctuation  $\sigma_8$  inferred from Ly $\alpha$  absorbers at different redshifts [64]. Although these data have been already compared to model predictions (e.g. [88, 89]), current uncertainties are too large to discriminate among alternative cosmological scenarios.

On-going redshift surveys like VIPERS [90] or BOSS [91] will certainly provide more stringent constraint and will be able to test those models that deviate most from the standard cosmological model. However, only next generation large-scale redshift surveys at  $z \approx 1$  and beyond like EUCLID [92] or BigBOSS [93] will provide an efficient way to discriminate competing dark energy models.

The growth rate  $s$  clearly depends on the cosmological model. As already mentioned, it has been found in several works [94, 95, 96, 97, 98] that a simple yet effective parametrization of  $s$  captures the behavior of a large class of models. Putting

$$s = \Omega_m^\gamma, \quad (10.3)$$

where  $\Omega_m(z)$  is the matter density in units of the critical density as a function of redshift, a value  $\gamma \approx 0.545$  reproduces well the  $\Lambda$ CDM behavior while departures from this value characterize different models. For instance the DGP is well approximated by  $\gamma \approx 0.68$  [99, 100] while viable models of  $f(R)$  are approximated by  $\gamma \approx 0.4$  for small scales and small redshifts [76, 70]. However, as seen in Chapter 8, this simple parametrization is not flexible enough to accommodate all cases. A constant  $\gamma$  cannot for instance reproduce a growth rate larger than  $s = 1$  in the past (as we have in  $f(R)$  and scalar-tensor models) allowing at the same time  $s < 1$  at the present epoch if  $\Omega_m \leq 1$ . Even in standard cases, a better approximation requires a slowly-varying, but not strictly constant,  $\gamma$ .

In addition, the measures of the growth factor obtained from redshift distortions require an estimate of the galaxy bias, which can be obtained either independently, using higher order statistics (e.g. [82, 101]) or inversion techniques [102], or self consistently, by assuming some reasonable form for the bias function *a priori* (for instance, that the bias is independent of scale, as we will assume here).

The goal of this paper is to forecast the constraints that future observations can put on the growth rate. In particular we use representative assumptions for the parameters of the EUCLID survey to provide a baseline for future experiments and we focus on the following issues. *i)* We assess how well one can constrain the bias function from the analysis of the power spectrum itself and evaluate the impact that treating bias as a free parameter has on the estimates of the growth factor. We compare the results with those obtained in the more common hypothesis of fixing the bias factor (and its error) to some independently determined value. *ii)* We estimate how errors depend on the parametrization of the growth factor and on the number and type of degrees of freedom in the analysis. *iii)* We explicitly explore the case of coupling between dark energy and dark matter and assess the ability of measuring the coupling constant.

We do this in the context of the Fisher Matrix analysis, explained in Chapter 7. This is a common approach that has been adopted in several recent works, some of which exploring the case of a EUCLID-like survey as we do. In this work we do not try to optimize the parameter of the EUCLID survey in order to improve the constraints on the relevant parameters, as in [103]. Instead, we adopt a representative sets of parameters that describe the survey and derive the expected errors on the interesting quantities. In addition, unlike [104] and [105], we do not explicitly aim to study the correlation between the parameters that describe the geometry of the system and the growth parameters, although in our approach we also take into account the degeneracy between geometry and growth. Although, as we mentioned, in general  $s$  might depend on scale, we limit this work to an exploration of time-dependent functions only.

## 10.2 Models

The main scope of this work is to quantify the ability of future redshift surveys to constrain the growth rate of density fluctuations. In particular we want to quantify how this ability depends on the parametrization assumed for  $s$  and for the equation of state of the dark energy  $w$  and on the biasing parameter. For this reason we explore different scenarios detailed below.

### 10.2.1 Equation of state

- *w-parametrization.* In order to represent the evolution of the equation of state parameter  $w$ , we use the popular CPL parametrization [106, 107]

$$w(z) = w_0 + w_1 \frac{z}{1+z} . \quad (10.4)$$

As a special case we will also consider the case of a constant  $w$  (i.e. we do not take into account the presence of  $w_1$ ).

### 10.2.2 Growth Rate

As anticipated, in this work we assume that the growth rate,  $s$ , is a function of time but not of scale. Here we explore three different parametrizations of  $s$ :

- *s-parametrization.* This is in fact a non-parametric model in which the growth rate itself is modeled as a step-wise function  $s(z) = s_i$ , specified in different redshift bins. The errors are derived on  $s_i$  in each  $i$ -th redshift bin of the survey.
- *$\gamma$ -parametrization.* As a second parametrization we assume

$$s \equiv \Omega_m(z)^{\gamma(z)}. \quad (10.5)$$

where the  $\gamma(z)$  function is parametrized as

$$\gamma(z) = \gamma_0 + \gamma_1 \frac{z}{1+z}. \quad (10.6)$$

As shown by [108, 109], this parametrization is more accurate than that of eq. (10.3) for both  $\Lambda$ CDM and DGP models. Furthermore, this parametrization is especially effective to distinguish between a  $w$ CDM model (i.e. a dark energy model with a constant equation of state) that has a negative  $\gamma_1$  ( $-0.020 \lesssim \gamma_1 \lesssim -0.016$ , for  $0.20 \leq \Omega_{m,0} \leq 0.35$ ) and a DGP model that instead, has a positive  $\gamma_1$  ( $0.035 < \gamma_1 < 0.042$ ). In addition, as seen in Chapter 9, modified gravity models show a strongly evolving  $\gamma(z)$  [70, 110, 109], in contrast with conventional Dark Energy models. As a special case we also consider  $\gamma = \text{constant}$  (only when  $w$  also is assumed constant), to compare our results with those of previous works.

- *$\eta$ -parametrization.* To explore models in which perturbations grow faster than in the  $\Lambda$ CDM case, like in the case of a coupling between dark energy and dark matter [75], we assume the parameterization given by eq. 8.54 in which  $\gamma$  is constant and the growth rate varies as

$$s \equiv \Omega_m(z)^\gamma (1 + \eta), \quad (10.7)$$

where  $\eta$  quantifies the strength of the coupling. The example of the coupled quintessence model worked out in Chapter 8 illustrates this point. We remind that in this model, the numerical solution for the growth rate can be fitted by the formula (10.7), with  $\eta = c\beta_c^2$ , where  $\beta_c$  is the dark energy-dark matter coupling constant and best fit values  $\gamma = 0.56$  and  $c = 2.1$ . In this simple case, observational constraints over  $\eta$  can be readily transformed into constraints over  $\beta_c$ .

### 10.2.3 Galaxy Biasing

In the analysis of the redshift distortions,  $s(z)$  is degenerate with the bias function  $b(z)$ . In absence of a well-established theory of galaxy formation and evolution, most analyses assume some arbitrary functional form for  $b(z)$ . However, biasing need to be neither deterministic nor linear. Stochasticity in galaxy biasing is supposed to have little impact on two-point statistics, at least on scales significantly larger than those involved with galaxy evolution processes [111]. On the other hand, deviations from linearity (which imply scale dependency) might not be negligible. Current observational constraints based on self consistent biasing estimators [82, 102] show that nonlinear effects are of the order of a few to  $\sim 10\%$ , depending on the scale and the galaxy type [101, 112]. To account for current uncertainties in both modeling and measuring galaxy bias we consider the following choices for the functional form of  $b$ :

- *Redshift dependent bias.* We assume  $b(z) = \sqrt{1+z}$  (already used in [113]) since this function provides a good fit to  $H_\alpha$  line galaxies with luminosity  $L_{H_\alpha} = 10^{42} \text{ erg}^{-1} \text{ s}^{-1} \text{ cm}^{-2}$  modeled by [114] using the semi-analytic *GALFORM* models of [115]. We consider  $H_\alpha$  line objects since they will likely constitute the bulk of galaxies in the next generation slitless spectroscopic surveys like EUCLID. The luminosity corresponds to the limiting flux at  $z = 1.5$ .
- *Constant bias.* For the sake of comparison, we will also consider the case of constant  $b = 1$  corresponding to the rather unphysical case of a redshift-independed population of unbiased mass tracers.

### 10.2.4 Reference Cosmological Models

As it will be better explained in the next section, to perform the Fisher Matrix analysis we need to adopt a fiducial cosmological model. We choose the one recommended by the Dark Energy Task Force (DETF) [45]. In this “pseudo”  $\Lambda$ CDM model the growth rate values are obtained from eq. (10.3) with  $\gamma = 0.545$  and  $\Omega_m(z)$  is given by the standard evolution

$$\Omega_m(z) = \Omega_{m,0}(1+z)^3 \frac{H_0^2}{H(z)^2}, \quad (10.8)$$

where

$$H(z)^2 = H_0^2 \left[ \Omega_{m,0}(1+z)^3 + \Omega_k(1+z)^2 + (1 - \Omega_{m,0} - \Omega_k) e^{3 \int (1+w_0+w_1 \frac{z}{1+z}) \frac{dz}{1+z}} \right]. \quad (10.9)$$

Then  $\Omega_m(z)$  is completely specified by setting  $\Omega_{m,0} = 0.25$ ,  $\Omega_k = 0$ ,  $w_0 = -0.95$ ,  $w_1 = 0$ . We wish to stress that regardless the parametrization adopted, our fiducial cosmology is always chosen as the DETF one. In particular we choose as fiducial values  $\gamma_1 = 0$  and  $\eta = 0$ , when employed.

One of the goals of this work is to assess whether the analysis of the power spectrum in redshift-space can distinguish the fiducial model from alternative cosmologies, characterized by their own set of parameters (apart from  $\Omega_{m,0}$  which is set equal to 0.25 for all of them). The alternative models that we consider in this work are:

- *DGP model.* We consider the flat space case studied in [116]. When we adopt this model then we set  $\gamma_0 = 0.663$ ,  $\gamma_1 = 0.041$  [109] or  $\gamma = 0.68$  [99] and  $w = -0.8$  when  $\gamma$  and  $w$  are assumed constant.
- *$f(R)$  model.* Here we consider the one proposed in [117] (and already studied in Chapter 9), depending on two parameters,  $n$  and  $\lambda$ , which we fix to  $n = 2$  and  $\lambda = 3$ . In this case we assume  $\gamma_0 = 0.43$ ,  $\gamma_1 = -0.2$ , values that apply quite generally in the limit of small scales (provided they are still linear, see [70]) or  $\gamma = 0.4$  and  $w = -0.99$ .
- *coupled dark energy (CDE) model.* This is the coupled model proposed by [56, 57]. In this case we assume  $\gamma_0 = 0.56$ ,  $\eta = 0.056$  (this value comes from putting  $\beta_c = 0.16$  as coupling, which is of the order of the maximal value allowed by CMB constraints) [59]. As already explained, this model cannot be reproduced by a constant  $\gamma$ .

### 10.3 Fisher Matrix Analysis

In order to constrain the parameters, we use the Fisher matrix method [118] (see [119] for a review) explained in Chapter 7, that we apply to the power spectrum analysis in redshift space following [47]. For this purpose we need an analytic model of the power spectrum in redshift space as a function of the parameters that we wish to constrain. The analytic model is obtained in three steps. (i) First of all we compute with CMBFAST [120] the linear power spectrum of the matter in real space at  $z = 0$ ,  $P_{0r}(k)$ , choosing a reference cosmology where the parameters to be given as input (i.e.  $\Omega_{m,0}h^2$ ,  $\Omega_{b,0}h^2$ ,  $h$ ,  $n_s$  also employed in the Fisher matrix analysis, plus the other standard parameters needed by the CMBFAST code) are set to the values given in the III column of Tab. 10.1 while for the normalization of the spectrum we use  $\sigma_8 = 0.8$ .

(ii) Now we need to estimate the observed power spectrum at redshift  $z$  in any other cosmology. In fact the cosmological model influences the spectrum in many ways. It changes the shape of the spectrum at  $z = 0$  and its amplitude at any  $z$  through the growth factor. It also affects the separation between galaxies and therefore the wavenumbers  $k$  in the spectrum. Finally, it also changes the volume in which the spectrum is calculated. Thus, among many others, the features of the power spectrum that depend on cosmology are the position of the overall peak (or turnaround), the overall amplitude and the slope. Then we need to understand how to recover the power spectrum for any cosmology, starting from the computed  $P_{0r}(k)$ , making the dependence on cosmology as explicit as possible.

First of all: two different cosmological models will measure different distances. Nevertheless these two measures can be linked one to the other. In fact, suppose we observe a particular feature extending over an angle  $\theta$ , which subtends a transverse comoving scale  $\lambda_1$  at  $z$ . The angular diameter distance is then  $d_1(z) = \lambda_1/[(1+z)\theta]$  where the subscript 1 refers to a given cosmology, i.e. some values of cosmological parameters ( $\Omega_{m,0}$ ,  $\Omega_\Lambda$ , etc)

and we made use of eqs (1.86), (1.87) with  $\Delta\mathbf{x} \equiv \lambda_1$  and  $a(t_1) = a(t_0) = 1$ . In a different cosmology (for which we use the subscript 2), the angular diameter distance will be  $d_2(z) = \lambda_2/[(1+z)\theta]$ . Then we see that the scale has to change in order to keep the same subtending angle at the same redshift. Therefore the ratio  $d/\lambda$  for each given angle is a constant. The same is true in Fourier space, for the combination  $k_\perp d$  where  $k_\perp \propto \lambda^{-1}$  is the transverse wavenumber corresponding to that transverse scale. Thus, given a reference cosmology  $r$ , the transverse wavenumber for any other cosmology is given by

$$k_\perp = k_{r\perp} \frac{d_r}{d}. \quad (10.10)$$

Now let us see what happens to the comoving scale extending along the line of sight between two redshifts,  $z_1$  and  $z_2$ . This scale is approximately given by (see eq. (1.76))  $\lambda = dz/H(z)$  where  $dz = z_2 - z_1$ . This time we need  $dz$  and therefore the product  $\lambda H(z)$  to remain constant when changing cosmology. It follows that for radial modes we have

$$k_\parallel = k_{r\parallel} \frac{H}{H_r}. \quad (10.11)$$

Since any wave vector  $\mathbf{k}$  can be decomposed into its parallel  $k_\parallel$  and perpendicular  $k_\perp$  components, the above relations apply to any perturbation mode. In this way it is made explicit its dependence on the reference cosmology  $\mathbf{k}_r$  and on the cosmological parameters inside  $d$  and  $H$ . It is then possible to know how the wavenumber changes with cosmology. For instance, if in the reference cosmology the power spectrum is isotropic, it will become anisotropic for any other cosmology since  $k_\parallel$  and  $k_\perp$  change differently: this effect is known as Alcock-Paczynski effect [121]. However we are measuring more than just the anisotropy: all the scale-dependent information contained in the power spectrum will be automatically employed to constrain cosmology.

The relations between the wavenumber modulus  $k$  and the direction cosine  $\mu = \mathbf{k} \cdot \mathbf{r}/k$  (where  $\mathbf{r}$  is the unit vector parallel to the line of sight) in the reference cosmology and in the generic cosmology can be derived from eqs (10.10), (10.11) and read

$$k = (k_\parallel^2 + k_\perp^2)^{1/2} = R k_r, \quad (10.12)$$

$$\mu = \frac{k_\parallel}{(k_\parallel^2 + k_\perp^2)^{1/2}} = \frac{H \mu_r}{H_r R}, \quad (10.13)$$

where

$$R = \frac{\sqrt{H^2 d^2 \mu_r^2 - H_r^2 d_r^2 (\mu_r^2 - 1)}}{H_r d}.$$

We know from its definition (6.19) that the power spectrum is proportional to the volume  $V$  in which the perturbations are measured, so it is necessary to evaluate also how  $V$  depends on cosmology. If the spectrum is measured in a shell of thickness  $dr$ , in a solid angle  $\theta^2 \text{rad}^2$ , the volume is given by

$$V = \theta^2 r^2 dr = d^2(z) \frac{dr(z)}{dz} dz = \frac{d^2}{H} dz, \quad (10.14)$$

where  $dr/dz = 1/H(z)$  and  $d = r(z)\theta$ . It follows that the combination  $VH/d^2$  has to remain constant and then

$$V = V_r \frac{H_r d^2}{H d_r^2}. \quad (10.15)$$

A reference cosmology is needed in order to convert angles and redshifts into distances or wave vectors and obtain a power spectrum from real data. Through the above relations we can now relate the reference power spectrum to a general one for any given cosmology. The power spectrum  $P(k) = V\delta_k^2$  for the true cosmology can in fact be converted into the one for the reference cosmology by multiplying the former by  $V_r/V$  and by converting  $k, \mu$  into  $k_r, \mu_r$ .

Therefore we have at any redshift [122]

$$P_r(k_r, z) = \frac{H(z)d_r^2(z)}{H_r(z)d^2(z)} P(Rk_r, z). \quad (10.16)$$

We computed our initial spectrum at  $z = 0$ , but in order to evolve it through redshift it must be multiplied by the growth factor squared:  $P(k, z) = G(z)^2 P(k, 0)$ . Furthermore, this spectrum represents the amount of the *total* matter, while the data refer only to the observed galaxy power spectrum (unless we are using data such as those coming from weak lensing observations), to which the former can be related by multiplying it by the bias factor  $b^2(k, z)$ . Finally we must connect the observations in redshift space to the theoretical predictions which are performed in real space. As seen in sec. 6.6, this requires a factor  $(1 + \beta\mu^2)^2$  [39], where  $\beta$  is the redshift distortion parameter. Putting everything together we finally obtain

$$P_{\text{obs}}(z; k_r, \mu_r) = P_{0r}(k) \frac{d_r^2(z)H(z)}{d^2(z)H_r(z)} G^2(z) b^2(z) (1 + \beta\mu^2)^2 + P_s(z). \quad (10.17)$$

We also added the term  $P_s(z)$ , a scale-independent offset due to a possible incomplete removal of shot-noise (see eq. (6.34)).

As shown in [78, 79] and recently in [103], the inclusion of growth rate information reduces substantially the errors on the parameters, improving the figure of merits. (*iii*) As a third and final step we account for nonlinear effects. On scales larger than ( $\sim 100 h^{-1}\text{Mpc}$ ) where we focus our analysis, nonlinear effects can be represented as a displacement field in Lagrangian space modeled by an elliptical Gaussian function. Therefore, following [123, 124], to model nonlinear effect we multiply  $P_{0r}(k)$  by the factor

$$\exp \left\{ -k^2 \left[ \frac{(1 - \mu^2)\Sigma_{\perp}^2}{2} + \frac{\mu^2\Sigma_{\parallel}^2}{2} \right] \right\}, \quad (10.18)$$

where  $\Sigma_{\perp}$  and  $\Sigma_{\parallel}$  represent the displacement across and along the line of sight, respectively. They are related to the growth factor  $G$  and to the growth rate  $s$  through  $\Sigma_{\perp} = \Sigma_0 G$  and  $\Sigma_{\parallel} = \Sigma_0 G(1 + s)$ . The value of  $\Sigma_0$  is proportional to  $\sigma_8$ . For our reference cosmology where  $\sigma_8 = 0.8$  [17], we have  $\Sigma_0 = 11 h^{-1}\text{Mpc}$ .

The observed power spectrum in a given redshift bin depends therefore on a number of parameters, denoted collectively as  $p_i$ , such as the Hubble constant at present  $h$ , the

reduced matter and baryon fractions at present,  $\Omega_{m,0}h^2$  and  $\Omega_{b,0}h^2$ , the curvature density parameter  $\Omega_k$ , the spectral tilt  $n_s$  plus the parameters that enter in the parametrizations described in the previous section:  $w_0$ ,  $w_1$  (or simply  $w$ );  $\gamma_0$ ,  $\gamma_1$  (or  $\gamma$ ) and  $\gamma$ ,  $\eta$ . They are listed in Tab. 10.1 and are referred to as ‘‘Cosmological parameters’’. These parameters will be left free to vary while we always fix  $\sigma_8=0.8$  since the overall amplitude is degenerate with growth and bias. The other free parameters depend on the redshift. They are listed in the lower part of Tab. 10.1 and include the expansion history  $H(z)$ , the growth factor  $G(z)$ , the angular diameter distance  $d(z)$ , the shot noise  $P_s(z)$ , the growth rate  $s(z)$ , the redshift distortion parameter  $\beta(z)$  and the galaxy bias  $b(z)$ .

Given the model power spectrum we calculate, numerically or analytically, the derivatives

$$\left( \frac{\partial \ln P_{\text{obs}}}{\partial p_i} \right)_{\text{ref}}, \quad (10.19)$$

evaluated at the parameter values of the reference (or ‘‘fiducial’’) model and we obtain for the  $i$ -th redshift bin all the elements of the Fisher matrix through [46]

$$F_{ij} = \frac{1}{8\pi^2} \int_{-1}^{+1} d\mu \int_{k_{\text{min}}}^{k_{\text{max}}} dk k^2 \left( \frac{\partial \ln P_{\text{obs}}}{\partial p_i} \frac{\partial \ln P_{\text{obs}}}{\partial p_j} \right)_{\text{ref}} V_{\text{eff}}(k, \mu) \exp[-k^2 \Sigma_{\perp}^2 - k^2 \mu^2 (\Sigma_{\parallel}^2 - \Sigma_{\perp}^2)], \quad (10.20)$$

where

$$V_{\text{eff}}(k, \mu) = \left[ \frac{nP(k, \mu)}{nP(k, \mu) + 1} \right]^2 V_{\text{survey}}, \quad (10.21)$$

is the effective volume of the survey sampled at the scale  $k$  along the direction  $\mu$ .  $V_{\text{survey}}$  and  $n$  represent the volume of the survey and the mean number density of galaxies in each redshift bin.

As a fiducial model we assume a ‘‘pseudo’’  $\Lambda$ CDM with  $w_0 = -0.95$ ; the differences with the standard  $w_0 = -1.0$   $\Lambda$ CDM model are rather small. For example, in the case of the  $\gamma$ -*parametrization*, our fiducial model has  $\gamma_0 = 0.545$ ,  $\gamma_1 = 0$  whereas the standard  $\Lambda$ CDM model has  $\gamma_0 = 0.556$ ,  $\gamma_1 = 0.018$  [109]. To summarize, our fiducial model is the same model recommended by the Dark Energy Task Force [45], i.e.:  $\Omega_{m,0}^F = 0.25$ ,  $\Omega_{b,0}^F = 0.0445$ ,  $\Omega_k^F = 0$ ,  $h^F = 0.7$ ,  $n_s^F = 1$ ,  $w_0^F = -0.95$ ,  $w_1^F = 0$ ,  $\gamma^F = 0.545$ ,  $P_s^F = 0$ . In addition, we assume that  $\gamma_1^F = 0$ ,  $\eta^F = 0$ . The fiducial values for the redshift dependent parameters are computed in every bin through the standard Friedmann-Robertson-Walker relations

$$\frac{H^F(z)}{100h^F} = \left[ \Omega_{m,0}^F (1+z)^3 + (1 - \Omega_{m,0}^F) (1+z)^{3(1+w_0^F)} \right]^{1/2}, \quad (10.22)$$

$$d^F(z) = (1+z)^{-1} \int_0^z \frac{dz'}{H^F(z')}, \quad (10.23)$$

$$s^F(z) = \Omega_m^F(z) \gamma^F, \quad (10.24)$$

$$G^F(z) = \exp \left\{ \int_0^z s^F(z) \frac{dz}{1+z} \right\}, \quad (10.25)$$

$$\beta^F(z) = \frac{\Omega_m^F(z) \gamma^F}{b^F(z)}, \quad (10.26)$$

$$b^F(z) = 1 \quad \text{or} \quad b^F(z) = \sqrt{1+z}, \quad (10.27)$$

$$P_s^F(z) = 0, \quad (10.28)$$

where we changed the subscript *ref* with the superscript *F* referring to the fiducial model. Now our analysis splits into two methods, according to the choice of *z*-dependent parameters in which we explicit the power spectrum:

- *Internal bias method.*

We assume some fiducial form for  $b(z)$  ( $z$ -dependent or constant) and express the growth function  $G(z)$  and the redshift distortion parameter  $\beta(z)$  in terms of the growth rate  $s$  (see eqs. (10.29), (10.2)). When we compute the derivatives of the spectrum (eq. (10.19)),  $b(z)$  and  $s(z)$  are considered as independent parameters in each redshift bin. In this way we can compute the errors on  $b$  (and  $s$ ) self consistently by marginalizing over all other parameters.

- *External bias method.*

In this case we also assume the same forms for  $b(z)$  as in the *Internal bias* case but we do not explicit  $G(z)$  and  $\beta(z)$  in terms of  $s$ . The independent parameters are now the product  $G(z) \cdot b(z)$  (if we considered them separately, the Fisher matrix would result singular) and  $\beta(z)$ . In this case we compute the errors over  $\beta(z)$  marginalizing over all other parameters. Since we also marginalize over  $(G * b)^2$ , in this case we cannot estimate the error over  $b$  from the Fisher matrix. Thus, in order to obtain the error over  $s$  (related to  $\beta$  through  $s = \beta \cdot b$ ) with standard error propagation, we need to assume an “external” error for  $b(z)$ . We allow the relative error  $\Delta b/b$  to be either 1% or 10%, two values that bracket the ranges of expected errors contributed by model uncertainties and deviations from linear biasing.

## 10.4 Modeling the Redshift Survey

The main goals of next generation redshift surveys will be to constrain the Dark Energy parameters and to explore models alternative to standard Einstein Gravity. For

Cosmological parameters in $P_{obs}(z; k, \mu)$		Fiducial values
Reduced total matter density	$\Omega_{m,0}h^2$	$0.25 \cdot (0.7)^2$
Reduced baryon density	$\Omega_{b,0}h^2$	$0.0445 \cdot (0.7)^2$
Curvature density	$\Omega_k$	0
Hubble constant at present	$h$	0.7
Primordial fluctuation slope	$n_s$	1
Constant growth index	$\gamma$	0.545
$\gamma$ - <i>parametrization</i> parameters	$\gamma_0, \gamma_1$	0.545, 0
$\eta$ - <i>parametrization</i> parameters	$\gamma, \eta$	0.545, 0
Redshift dependent parameters		
Hubble parameter	$\log H$	eq. (10.22)
Angular diameter distance	$\log D$	eq. (10.23)
Growth rate	$\log s$	eq. (10.24)
Growth factor	$\log G$	eq. (10.25)
Redshift distortion parameter	$\log \beta$	eq. (10.26)
Shot noise	$P_s$	0
Bias	$\log b$	$1, \sqrt{1+z}$

Table 10.1: Parameters.

these purposes they will need to consider very large volumes that encompass  $z \sim 1$ , i.e. the epoch at which dark energy started dominating the energy budget, spanning a range of epochs large enough to provide a sufficient leverage to discriminate among competing models at different redshifts. The additional requirement is to observe some homogeneous class of objects that are common enough to allow a dense sampling of the underlying mass density field.

As anticipated in the introduction, in this paper we consider the spectroscopic survey proposed by the EUCLID collaboration as a reference case [92]. We stress that our aim is not to focus on this particular redshift survey and assess how the constraints on the relevant parameters depends on the survey characteristics in order to optimize future observational strategies. On the contrary, under the hypothesis that next-generation space-based all-sky redshift surveys will be similar to the EUCLID spectroscopic survey, we consider the latter as a reference case and estimate how the expected errors on the bias, growth rate, coupling constant and other relevant quantities will change when one consider slightly different observational setups. For this purpose we take advantage of the huge effort made by the EUCLID team to simulate the characteristic of the target objects and compute the expected selection function and detection efficiency of the survey and adopt the same survey parameters presented in [125].

Here we consider a survey covering a large fraction of the extragalactic sky ( $|b| \geq 20^\circ$ ), corresponding to  $\sim 20000 \text{ deg}^2$  capable to measure a large number of galaxy redshifts out to  $z \sim 2$ . A promising observational strategy is to target  $H_\alpha$  emitters at near-infrared wavelengths (which implies  $z > 0.5$ ) since they guarantee both relatively dense sampling (the space density of this population is expected to increase out to  $z \sim 2$ ) and an efficient

method to measure the redshift of the object. The limiting flux of the survey should be the tradeoff between the requirement of minimizing the shot noise, the contamination by other lines (chiefly among them the  $[\text{OII}]$  line), and that of maximizing the so-called efficiency  $\varepsilon$ , i.e. the fraction of successfully measured redshifts. To minimize shot noise one should obviously strive for a low flux. Indeed, the authors in [125] found that a limiting flux  $f_{\text{H}\alpha} \geq 1 \times 10^{-16} \text{ erg cm}^{-2}\text{s}^{-1}$  would be able to balance shot noise and cosmic variance out to  $z = 1.5$ . However, simulated observations of mock  $\text{H}\alpha$  galaxy spectra have shown that  $\varepsilon$  ranges between 30 % and 60% (depending on the redshift) for a limiting flux  $f_{\text{H}\alpha} \geq 3 \times 10^{-16} \text{ erg cm}^{-2}\text{s}^{-1}$  [92]. Moreover, contamination from  $[\text{OII}]$  line drops from 12% to 1% when the limiting flux increases from  $1 \times 10^{-16}$  to  $5 \times 10^{-16}$  [125]. Taking all this into account we adopt a conservative choice and consider three different surveys characterized by a limiting flux of 3, 4 and  $5 \times 10^{-16} \text{ erg cm}^{-2}\text{s}^{-1}$ .

The number density of  $\text{H}\alpha$  galaxies at a given redshift,  $n(z)$ , can be obtained by integrating the  $\text{H}\alpha$  luminosity function above the minimum luminosity set by the limiting flux  $L_{\text{H}\alpha, \text{min.}} = 4\pi D_L(z)^2 f_{\text{H}\alpha}$  where  $D_L(z)$  is the luminosity distance. We consider the model for  $\text{H}\alpha$  luminosity function obtained using the latest empirical data [125]. To obtain the effective number density one has to account for the success rate in measuring galaxy redshifts from  $\text{H}\alpha$  lines. The effective number density is then obtained by multiplying  $n(z)$  by the already mentioned efficiency,  $\varepsilon$ . In the range of redshifts and fluxes considered in this work the value of  $\varepsilon$  varies in the interval [30%, 50%] (see Fig. A.1.4 of [92]).

In an attempt to bracket current uncertainties in modeling galaxy surveys, we consider the following choices for the survey parameters:

- *Reference case (ref.)*. Limiting flux:  $f_{\text{H}\alpha} \geq 4 \times 10^{-16} \text{ erg cm}^{-2}\text{s}^{-1}$ , which gives the galaxy number densities listed in Col. 2 of Tab. 10.2. The efficiency is set to  $\varepsilon = 0.5$ .
- *Optimistic case (opt.)*. Limiting flux:  $f_{\text{H}\alpha} \geq 3 \times 10^{-16} \text{ erg cm}^{-2}\text{s}^{-1}$ , which gives the galaxy number densities listed in Col. 1 of Tab. 10.2. The efficiency is set to  $\varepsilon = 0.5$ .
- *Pessimistic case (pess.)*. Limiting flux:  $f_{\text{H}\alpha} \geq 5 \times 10^{-16} \text{ erg cm}^{-2}\text{s}^{-1}$ , which gives the galaxy number densities listed in Col. 3 of Tab. 10.2. The efficiency is set to  $\varepsilon = 0.3$ .

The total number of observed galaxies ranges from  $3 \cdot 10^7$  (pess.) to  $9 \cdot 10^7$  (opt.). For all cases we assume that the relative error on the measured redshift is  $\sigma_z = 0.001$ , independent of the limiting flux of the survey. So-called ‘‘catastrophic’’ redshift errors may occur in slitless spectroscopy due to the wrong identification of emission lines or to the association of a true line to a wrong object with overlapping spectrum. The fraction of catastrophic errors estimated through simulated observations of mock catalogs (10-15 %) can be significantly reduced when one compare the spectroscopic redshift to the photometric one [92]. For this reason we ignore the impact of catastrophic errors in our analysis.

$z$	$n_1(z) \times 10^{-3}$	$n_2(z) \times 10^{-3}$	$n_3(z) \times 10^{-3}$
0.5-0.7	4.69	3.56	2.8
0.7-0.9	3.33	2.42	1.84
0.9-1.1	2.57	1.81	1.33
1.1-1.3	2.1	1.44	1.03
1.3-1.5	1.52	0.99	0.68
1.5-1.7	0.92	0.55	0.35
1.7-1.9	0.54	0.29	0.17
1.9-2.1	0.31	0.15	0.08

Table 10.2: Expected galaxy number densities in units of  $(h/\text{Mpc})^3$  for EUCLID survey.

## 10.5 Results

In this section we present the main result of the Fisher matrix analysis that we split into sections to stress the different emphasis given in the two approaches. We note that in all tables below we always quote errors at 68% probability level and draw in the plots the probability regions at 68% and/or 95% (denoted for shortness as 1 and  $2\sigma$  values). Moreover, in all figures, all the parameters that are not shown have been marginalized over or fixed to a fiducial value when so indicated.

### 10.5.1 $s$ -parametrization

This analysis has two main goals: figuring out our ability to estimate the biasing parameter and that of estimating the growth rate with no assumptions on its redshift dependence. The parameters that enter in the Fisher matrix analysis are 45: 5 parameters that describe the background cosmology ( $\Omega_{m,0}h^2, \Omega_{b,0}h^2, h, n, \Omega_k$ ) and 8  $z$ -dependent parameters specified in 8 redshift bins evenly spaced in the range  $z = [0.5, 2.1]$ . They are  $P_s(z), D(z), H(z), s(z), b(z)$  in the *internal bias* case, while we have  $\beta(z)$  and  $G(z) \cdot b(z)$  in the place of  $s(z)$  and  $b(z)$  when we use the *external bias* method.

The subsequent analysis depends on the bias method adopted.

- In case of the *internal bias* method, the fiducial growth function  $G(z)$  in the  $(i+1)$ -th redshift bin is evaluated from a step-wise, constant growth rate  $s(z)$  as

$$G(z) = \exp \left\{ \int_0^z s(z) \frac{dz}{1+z} \right\} = \prod_i \left( \frac{1+z_i}{1+z_{i-1}} \right)^{s_i} \left( \frac{1+z}{1+z_i} \right)^{s_{i+1}}. \quad (10.29)$$

To obtain the errors on  $s_i$  and  $b_i$  we compute the elements of the Fisher matrix and marginalize over all other parameters. In this case one is able to obtain, self-consistently, the error on the bias and on the growth factor at different redshifts, as detailed in Tab. 10.3 and Tab. 10.4 respectively.

Tab. 10.3 illustrates one important result: through the analysis of the redshift-space galaxy power spectrum in a next-generation EUCLID-like survey, it will be possible to measure galaxy biasing in  $\Delta z = 0.2$  redshift bins with less than 3.5% error,

provided that the bias function is independent on scale. Moreover, the precision in measuring the bias has a little dependence on the  $b(z)$  form. This fact can be appreciated in Fig. 10.1 in which we show the expected relative error as a function of redshift for both  $b(z)$  functions and for the survey *Pessimistic case*. Errors are very similar but in the outermost redshift shells. We show the *Pessimistic case* since with a more favorable survey configuration, like the *Reference case*, the errors would be almost identical. Indeed, as we have verified, errors on all parameters of interest computed in this Section are quite insensitive to the form of  $b(z)$ . The largest discrepancy between the  $b(z) = 1$  and  $b(z) = \sqrt{1+z}$  cases is  $\sim 3\%$  and refers to the expected errors on the growth rate at  $z = 2$  in the *Pessimistic case*. Differences are typically much smaller for all other parameters or, for  $s(z)$  at lower redshifts or with a more favorable survey setup. For all these reasons in the following we only refer to the  $b(z) = \sqrt{1+z}$  case.

In Fig. 10.2 we show the errors on the growth rate  $s$  as a function of redshift, overplotted to our fiducial  $\Lambda$ CDM (green solid curve). The three sets of errorbars are plotted in correspondence of the 8 redshift bins and refer (from left to right) to the *Optimistic*, *Reference* and *Pessimistic* cases, respectively. The other curves show the expected growth rate in three alternative cosmological models: flat DGP (red dashed curve),  $f(R)$  (blue dotted curve) and CDE (purple, dot-dashed curve). This plot clearly illustrates the ability of next generation surveys to distinguish between alternative models, even in the less favorable choice of survey parameters.

- In case of the *external bias* method we marginalize over the overall amplitude ( $G \times b$ )<sup>2</sup>. Since, in this case, we cannot find errors self-consistently, we assume that bias has been determined *a priori* with errors per redshift bin of 1% and 10%, two values that should bracket the expected range of uncertainties. We note that the *external bias* method can be considered more conservative, especially in the case of large errors although we see no obvious reason why it should be preferred to the *internal bias* method that seems to provide similar results. Indeed, the errors on  $s$  relative to the 1% bias error listed in Table 10.5 are quite similar to those of the *internal bias* case. As obvious, errors on  $s$  increase significantly when the bias is known with 10% accuracy rather than 1%. However, even in this case, one keeps the ability of distinguishing between most of the competing cosmological models at  $1\sigma$  level, as shown in Fig. 10.3.

The main results of this section can be summarized as follows.

1. The ability of measuring the biasing function is not too sensitive to the characteristic of the survey ( $b(z)$  can be constrained to within 1.5% in the *Optimistic* scenario and up to 3.5% in the *Pessimistic* one) provided that the bias function is independent on scale. Moreover, the precision in measuring the bias has a very little dependence on the  $b(z)$  form.
2. The growth rate  $s$  can be estimated to within 1-3% in each bin for the *Reference case* survey with no need of estimating the bias function  $b(z)$  from some dedicated,

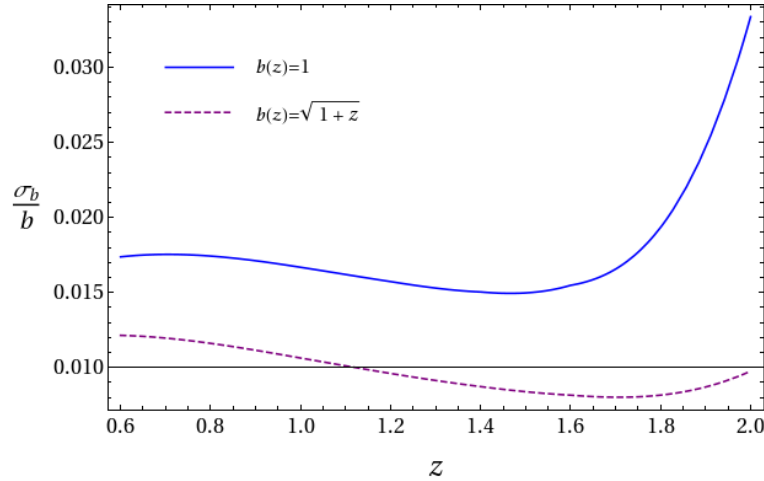


Figure 10.1: Relative errors over the bias parameter as a function of redshift, computed through the Fisher matrix analysis with the “internal bias” method for the *Pessimistic case*. The blue solid line refers to the fiducial bias  $b = 1$ , while the purple dashed line refers to  $b = \sqrt{1+z}$ . The precision in measuring the bias has a little dependence on the  $b(z)$  form: errors are very similar (the discrepancy is less than 1%) but in the outermost redshift shells (where however is less than 3%).

independent analysis using higher order statistics [82] or full-PDF analysis [102].

3. If the the bias were measured to within 1% in each slice, then the error over  $s$  would be very similar (just 1-2% larger) to that obtained by the internal estimate of  $b(z)$ .
4. The estimated errors on  $s$  depends little on the fiducial model of  $b(z)$ .

$b(z) = 1$ (internal)			$z$	$b(z) = \sqrt{1+z}$ (internal)		
$\sigma_b$				$\sigma_b$		
ref.	opt.	pess.		ref.	opt.	pess.
0.014	0.012	0.017	0.6	0.012	0.011	0.015
0.014	0.012	0.017	0.8	0.012	0.011	0.016
0.013	0.012	0.017	1.0	0.012	0.011	0.015
0.012	0.011	0.016	1.2	0.011	0.010	0.014
0.012	0.011	0.015	1.4	0.011	0.010	0.013
0.012	0.010	0.025	1.6	0.010	0.010	0.013
0.012	0.010	0.019	1.8	0.010	0.010	0.014
0.016	0.011	0.033	2.0	0.011	0.010	0.017

Table 10.3:  $1\sigma$  marginalized errors for the bias in each redshift bin obtained with the “internal bias” method.

$b(z) = 1$ (internal)			$z$	$s^F$	$b(z) = \sqrt{1+z}$ (internal)		
$\sigma_s$					$\sigma_s$		
ref.	opt.	pess.			ref.	opt.	pess.
0.011	0.010	0.013	0.6	0.73	0.010	0.010	0.012
0.011	0.010	0.015	0.8	0.78	0.011	0.010	0.013
0.013	0.011	0.016	1.0	0.83	0.012	0.010	0.015
0.013	0.012	0.018	1.2	0.86	0.013	0.011	0.017
0.014	0.012	0.019	1.4	0.89	0.014	0.012	0.019
0.016	0.013	0.023	1.6	0.91	0.016	0.013	0.022
0.019	0.015	0.032	1.8	0.92	0.018	0.015	0.028
0.027	0.018	0.057	2.0	0.93	0.024	0.017	0.044

Table 10.4:  $1\sigma$  marginalized errors for the growth rates in each redshift bin (Fig. 10.2) obtained with the “internal bias” method.

$b(z) = 1$ (external)						$z$	$b(z) = \sqrt{1+z}$ (external)					
$\Delta b/b = 1\%$			$\Delta b/b = 10\%$				$\Delta b/b = 1\%$			$\Delta b/b = 10\%$		
$\sigma_s$			$\sigma_s$			$\sigma_s$			$\sigma_s$			
ref.	opt.	pess.	ref.	opt.	pess.	ref.	opt.	pess.	ref.	opt.	pess.	
0.014	0.013	0.015	0.074	0.074	0.074	0.6	0.015	0.014	0.016	0.074	0.074	0.074
0.012	0.012	0.014	0.079	0.079	0.079	0.8	0.013	0.013	0.015	0.079	0.079	0.079
0.012	0.011	0.014	0.083	0.083	0.083	1.0	0.013	0.012	0.014	0.083	0.083	0.083
0.012	0.012	0.015	0.086	0.086	0.087	1.2	0.013	0.012	0.015	0.086	0.087	0.087
0.014	0.012	0.018	0.089	0.089	0.089	1.4	0.014	0.013	0.027	0.089	0.089	0.089
0.017	0.014	0.025	0.092	0.091	0.094	1.6	0.016	0.014	0.022	0.092	0.091	0.093
0.023	0.017	0.042	0.095	0.093	0.101	1.8	0.019	0.016	0.031	0.094	0.093	0.097
0.036	0.023	0.082	0.099	0.096	0.124	2.0	0.027	0.019	0.052	0.097	0.095	0.107

Table 10.5:  $1\sigma$  marginalized errors for the growth rates in each redshift bin (Fig. 10.3) obtained with the “external bias” method.

### 10.5.2 Other parametrizations.

In this section we assess the ability of estimating  $s(z)$  when it is expressed in one of the parametrized forms described in Section 10.2.2. More specifically, we focus on the ability of determining  $\gamma_0$  and  $\gamma_1$ , in the context of the  $\gamma$ -*parametrization* and  $\gamma, \eta$  in the  $\eta$ -*parametrization*. In both cases the Fisher matrix elements have been estimated by expressing the growth factor as

$$G(z) = \delta_0 \exp \left[ (1 + \eta) \int_0^z \Omega_m(z')^{\gamma(z)} \frac{dz'}{1 + z'} \right], \quad (10.30)$$

where for the  $\gamma$ -*parametrization* we fix  $\eta = 0$ . In this section we adopt the *internal bias* approach and assume that  $b(z) = \sqrt{1 + z}$  since, as we have checked, in the case of  $b(z) = 1$  one obtains very similar results.

- *$\gamma$ -parametrization.* We start by considering the case of constant  $\gamma$  and  $w$  in which we set  $\gamma^F = 0.545$  and  $w^F = -0.95$ . As we will discuss in the next Section, this simple case will allow us to cross-check our results with those in the literature. In Fig. 10.4 we show the marginalized probability regions, at 1 and  $2\sigma$  levels, for  $\gamma$  and  $w$ . The regions with different shades of green illustrates the *Reference case* for the survey whereas the blue long-dashed and the black short-dashed ellipses refer to the *Optimistic* and *Pessimistic* cases, respectively. Errors on  $\gamma$  and  $w$  are listed in Tab. 10.6 together with the corresponding figures of merit [FOM] defined to be the squared inverse of the Fisher matrix determinant (see eq. 7.30) and therefore equal to the inverse of the product of the errors in the pivot point, see [45]. Contours are centered on the fiducial model. The blue triangle and the blue square represent the flat DGP and the  $f(R)$  models' predictions. It is clear that, in the case of constant  $\gamma$  and  $w$ , the measurement of the growth rate in a EUCLID-like survey will allow us to discriminate among these models. These results have been obtained by fixing the curvature to its fiducial value  $\Omega_k = 0$ . If instead, we consider it as a free parameter and marginalize over, the errors on  $\gamma$  and  $w$  increase significantly, as shown in Table 10.7, and yet the precision is high enough to distinguish the different models. For completeness, we also computed the fully marginalized errors over the other Cosmological parameters for the reference survey, given in Tab. 10.8.

As a second step we considered the case in which  $\gamma$  and  $w$  evolve with redshift according to eqs. (10.6) and (10.4) and then we marginalize over the parameters  $\gamma_1$ ,  $w_1$  and  $\Omega_k$ . The marginalized probability contours are shown in Fig. 10.5 in which we have shown the three survey setups in three different panels to avoid overcrowding. Dashed contours refer to the  $z$ -dependent parametrizations while red, continuous contours refer to the case of constant  $\gamma$  and  $w$  obtained after marginalizing over  $\Omega_k$ . Allowing for time dependency expand the confidence ellipses since the Fisher matrix analysis now accounts for the additional uncertainties in the extra-parameters  $\gamma_1$  and  $w_1$ ; marginalized error values are in columns  $\sigma_{\gamma_{\text{marg},1}}$ ,  $\sigma_{w_{\text{marg},1}}$  of Tab. 10.9. We note, however, that errors are still small enough to distinguish the fiducial model from the  $f(R)$  and DGP scenarios.

	case	$\sigma_\gamma$	$\sigma_w$	FOM
$b = \sqrt{1+z}$	ref.	0.02	0.02	2115
	opt.	0.019	0.019	2806
$\Omega_k$ fixed	pess.	0.03	0.03	1296

Table 10.6: Numerical values for  $1\sigma$  constraints on parameters in Fig. 10.4 and figures of merit. Here we have fixed  $\Omega_k$  to its fiducial value.

We have also projected the marginalized ellipses for the parameters  $\gamma_0$  and  $\gamma_1$  and calculated their marginalized errors and figures of merit, which are reported in Tab. 10.10. The corresponding uncertainties contours are shown in Fig. 10.7. Once again we overplot the expected values in the  $f(R)$  and DGP scenarios to stress the fact that one is expected to be able to distinguish among competing models, irrespective on the survey's precise characteristics.

As a further test we have estimated how the errors on  $\gamma_0$  depend on the number of parameters explicitly involved in the Fisher matrix analysis. Fig. 10.8 show the expected  $1\sigma$  errors on  $\gamma$  (Y axis) as a function of the number of parameters that are fixed when computing the element of the Fisher matrix (the different combinations of the parameters are shown on the top of the histogram elements). We see that error estimates can decrease up to  $\sim 50\%$  when parameters are fixed to some fiducial, or independently determined, value.

- *$\eta$ -parametrization.*

We have repeated the same analysis as for the  $\gamma$ -parametrization, i.e. we have modeled the growth factor according to eq. (10.7) and the dark energy equation of state as in eq. (10.4) and marginalized over all parameters, including  $\Omega_k$ . The marginalized errors are shown in columns  $\sigma_{\gamma_{\text{marg},2}}$ ,  $\sigma_{w_{\text{marg},2}}$  of Tab. 10.9 and the significance contours are shown in the three panels of Fig. 10.6 which is analogous to Fig. 10.5. The ellipses are now larger than in the case of the  $\gamma$ -parametrization and show that DGP and  $f(R)$  models could be rejected at  $> 1\sigma$  level only if the redshift survey parameter will be more favorable than in the *Pessimistic case*.

Marginalizing over all other parameters we can compute the uncertainties in the  $\gamma$  and  $\eta$  parameters, as listed in Tab. 10.11. The relative confidence ellipses are shown in the left panel of Fig. 10.9. This plot shows that next generation EUCLID-like surveys will be able to distinguish the reference model with no coupling (central, red dot) to the CDE model proposed by [59] (white square) only at the 1-1.5  $\sigma$  level.

Finally, in order to explore the dependence on the number of parameters and to compare our results to previous works, we also draw the confidence ellipses for  $w_0$ ,  $w_1$  with three different methods: a) fixing  $\gamma_0, \gamma_1$  to their fiducial values and marginalizing over all the other parameters; b) marginalizing over all parameters plus  $\gamma_0, \gamma_1$  but fixing  $\Omega_k$ ; c) marginalizing over all parameters but  $w_0, w_1$ . As one can see in Fig. 10.10 and Tab. 10.12 this progressive increase in the number of marginalized parameters reflects in

bias	case	$\sigma_\gamma$	$\sigma_w$	FOM
$b = \sqrt{1+z}$	ref.	0.03	0.04	1179
	opt.	0.03	0.03	1568
	pess.	0.04	0.05	706

Table 10.7: Numerical values for  $1\sigma$  constraints on parameters  $\gamma$  and  $w$  (no parametrization), relative to the red ellipses in Figs 10.5, 10.6 and figures of merit. Here we have marginalized over  $\Omega_k$ .

	case	$\sigma_h$	$\sigma_{\Omega_m h^2}$	$\sigma_{\Omega_b h^2}$	$\sigma_{\Omega_k}$	$\sigma_{n_s}$
$b = \sqrt{1+z}$	ref.	0.024	0.008	0.002	0.01	0.02

Table 10.8: Numerical values for marginalized  $1\sigma$  constraints on Cosmological parameters using constant  $\gamma$  and  $w$ .

bias	case	$\sigma_{\gamma_{marg,1}}$	$\sigma_{w_{marg,1}}$	FOM	$\sigma_{\gamma_{marg,2}}$	$\sigma_{w_{marg,2}}$	FOM
$b = \sqrt{1+z}$	ref.	0.08	0.11	241.1	0.09	0.11	104.1
	opt.	0.07	0.09	323.5	0.07	0.09	138.2
	pess.	0.11	0.14	142.5	0.11	0.15	61.6

Table 10.9:  $1\sigma$  marginalized errors for parameters  $\gamma$  and  $w$  expressed through  $\gamma$  and  $\eta$  parametrizations. Columns  $\gamma_{0,marg1}, w_{0,marg1}$  refer to marginalization over  $\gamma_1, w_1$  (Fig. 10.5) while columns  $\gamma_{0,marg2}, w_{0,marg2}$  refer to marginalization over  $\eta, w_1$  (Fig. 10.6).

bias	case	$\sigma_{\gamma_0}$	$\sigma_{\gamma_1}$	FOM
$b = \sqrt{1+z}$	ref.	0.08	0.17	178.4
	opt.	0.07	0.15	227.5
	pess.	0.11	0.22	112.4

Table 10.10: Numerical values for  $1\sigma$  constraints on parameters in Fig. 10.7 and figures of merit.

bias	case	$\sigma_\gamma$	$\sigma_\eta$	FOM
$b = \sqrt{1+z}$	ref.	0.08	0.04	464.1
	opt.	0.07	0.03	608.2
	pess.	0.11	0.05	280.3

Table 10.11: Numerical values for  $1\sigma$  constraints on parameters in Fig. 10.9 and figures of merit.

	$\sigma_{w_0}$	$\sigma_{w_1}$	FOM
$\gamma_0, \gamma_1$ fixed	0.04	0.24	166
$\Omega_k$ fixed and marginalization over $\gamma_0, \gamma_1$	0.12	0.36	97.3
marginalization over all other parameters	0.12	0.43	41.3

Table 10.12:  $1\sigma$  marginalized errors for the parameters  $w_0$  and  $w_1$ , obtained with three different methods (reference case, see Fig. 10.10 ).

a widening of the ellipses with a consequent decrease in the figures of merit. These results are in agreement with those of other authors (e.g. [103]).

The results obtained this Section can be summarized as follows.

1. If both  $\gamma$  and  $w$  are assumed to be constant and fixing  $\Omega_k = 0$  then, a redshift survey described by our *Reference case* will be able to constrain these parameters to within 4% and 2%, respectively.
2. Marginalizing over  $\Omega_k$  degrades these constraints to 5.5% and 4% respectively.
3. If  $w$  and  $\gamma$  are considered redshift-dependent and parametrized according to eqs (10.6) and (10.4) then the errors on  $\gamma_0$  and  $w_0$  obtained after marginalizing over  $\gamma_1$  and  $w_1$  increase by a factor  $\sim 4, 5$ , i.e. we expect to measure  $\gamma_0$  and  $w_0$  with a precision of 13-15% and 11-14% respectively, where the interval reflects the uncertainties in the characteristic of the survey. With this precision we will be able to distinguish the fiducial model from the DGP and  $f(R)$  scenarios with more than  $2\sigma$  significance.
4. The ability to discriminate these models with a significance above  $2\sigma$  is confirmed by the confidence contours drawn in the  $\gamma_0$ - $\gamma_1$  plane, obtained after marginalizing over all other parameters.
5. If we allow for a coupling between dark matter and dark energy, and we marginalize over  $\eta$  rather than over  $\gamma_1$ , then the errors on  $\gamma_0$  and  $w_0$  are almost identical to those obtained in the case of the  $\gamma$ -*parametrization*. However, our ability in separating the fiducial model from the CDE model is significantly hampered: the confidence contours plotted in the  $\gamma$ - $\eta$  plane show that discrimination can only be performed with 1-1.5 $\sigma$  significance.

## 10.6 Conclusions

In this chapter we addressed the problem of determining the growth rate of density fluctuations from the estimate of the galaxy power spectrum at different epochs in future redshift survey. As a reference case we have considered the proposed EUCLID spectroscopic survey modeled according to the latest, publicly available survey characteristics [92, 125]. In this work we focused on a few issues that we regard as very relevant and that were not treated in previous, analogous Fisher Matrix analysis mainly aimed at

optimizing the survey setup and the observational strategy. These issues are: *i*) the ability in measuring self-consistently galaxy bias with no external information and the impact of treating the bias as an extra-free parameter on the error budget; *ii*) the impact of choosing a particular parametrization in determining the growth rate and in distinguishing dark energy models with very different physical origins. In particular we focus on the  $\Lambda$ CDM,  $f(R)$  and the DGP, models that are still degenerate with respect to present growth rate data; *iii*) the estimate of how errors on the growth rate depend on the degrees of freedom in the Fisher matrix analysis; *iv*) the ability of estimating a possible coupling between dark matter and dark energy.

The main results of the analysis were already listed in the previous Section, here we recall the most relevant ones.

1. With the “internal bias” method we were able to estimate bias with 1% accuracy in a self consistent way using only galaxy positions in redshift-space. The precision in measuring the bias has a very little dependence on the functional form assumed for  $b(z)$ . Measuring  $b$  with 1% accuracy will be a remarkable result also from an astrophysical point of view, since it will provide a strong, indirect constraint on the models of galaxy evolution.
2. We have demonstrated that measuring the amplitude and the slope of the power spectrum in different  $z$ -bin allows to constrain the growth rate with good accuracy, with no need to assume an external error for  $b(z)$ . In particular, we found that  $s$  can be constrained at  $1\sigma$  to within 3% in each of the 8 redshift bin from  $z = 0.5$  to 2.1. This result is robust to the choice of the biasing function  $b(z)$  and to the choice of the biasing treatment (“external” vs “internal” methods). The accuracy in the measured  $s$  will be good enough to discriminate among the most popular competing models of dark energy and modified gravity.
3. Taking into account the possibility of a coupling between dark matter and dark energy has the effect of loosening the constraints on the relevant parameters, decreasing the statistical significance in distinguishing models (from  $\gtrsim 2\sigma$  to  $\lesssim 1.5\sigma$ ). However, this is a remarkable achievement if compared to current constraints, as it can be seen in Fig. 10.9, where we compare the constraints expected by next generation data to the present ones. Moreover, the reference survey will be able to constrain the parameter  $\eta$  to within 0.04. Reminding that we can write  $\eta = 2.1\beta_c^2$  [75], this means that the coupling parameter  $\beta_c$  between dark energy and dark matter can be constrained to within 0.14, solely employing the growth rate information. This is comparable to existing constraints from the CMB but is complementary since obviously it is obtained at much smaller redshifts. A variable coupling could therefore be detected by comparing the redshift survey results with the CMB ones.

It is worth pointing out that, whenever we have performed statistical tests similar to those already discussed by other authors in the context of a EUCLID-like survey, we did find consistent results. Examples of this are the values of FOM and errors for  $w_0$ ,  $w_1$ , similar to those in [103] and the errors on constant  $\gamma$  [92]. However, let us notice

that all these values strictly depend on the parametrizations adopted and on the numbers of parameters fixed or marginalized over. In particular, we also found that all these constraints can be improved if one uses additional information from e.g. CMB and other observations. We produced a first step in this direction in Fig. (10.8), which shows how the errors on a constant  $\gamma$  decrease when more and more parameters are fixed by external priors.

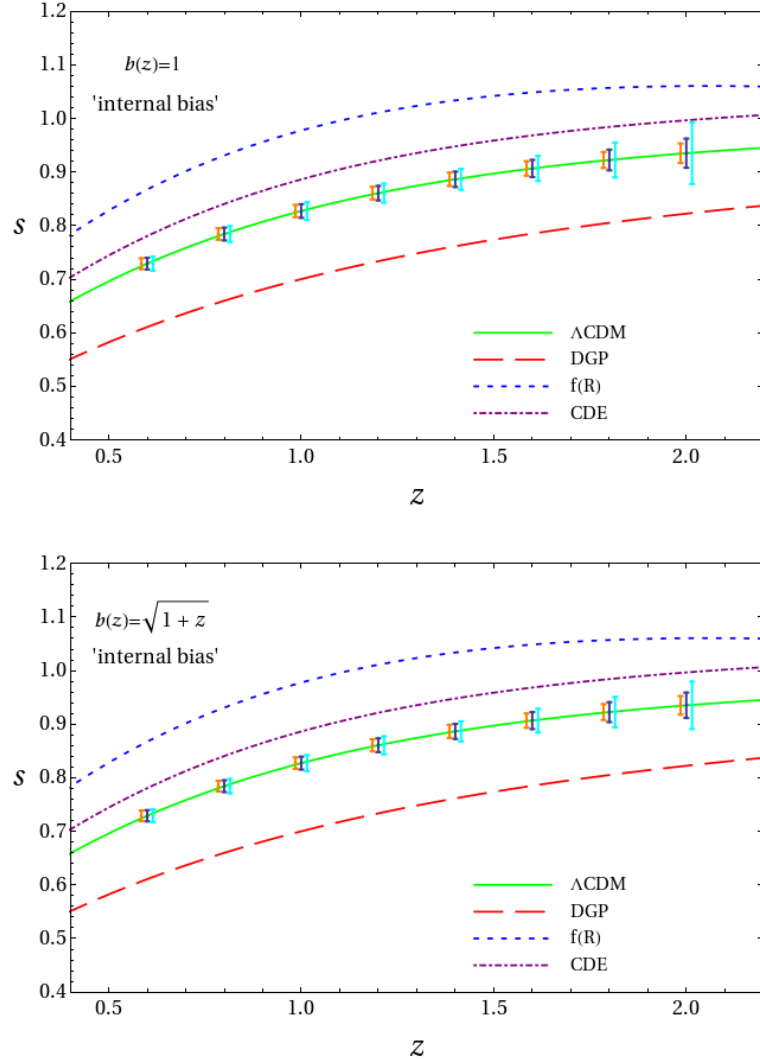


Figure 10.2: Expected constraints on the growth rates in each redshift bin (using the “internal bias” method). The upper panel refers to  $b = 1$ , while the lower panel to  $b = \sqrt{1+z}$ . For each  $z$  the central error bars refer to the *Reference case* while those referring to the *Optimistic* and *Pessimistic* case have been shifted by  $-0.015$  and  $+0.015$  respectively. The growth rates for four different models are also plotted:  $\Lambda$ CDM (green solid curve), flat DGP (red dashed curve),  $f(R)$  model (blue dotted curve) and a model with coupling between dark energy and dark matter (purple, dot-dashed curve). In this case, where the errors for the bias are obtained directly from the Fisher matrix, it will be possible to distinguish these models with next generation data.

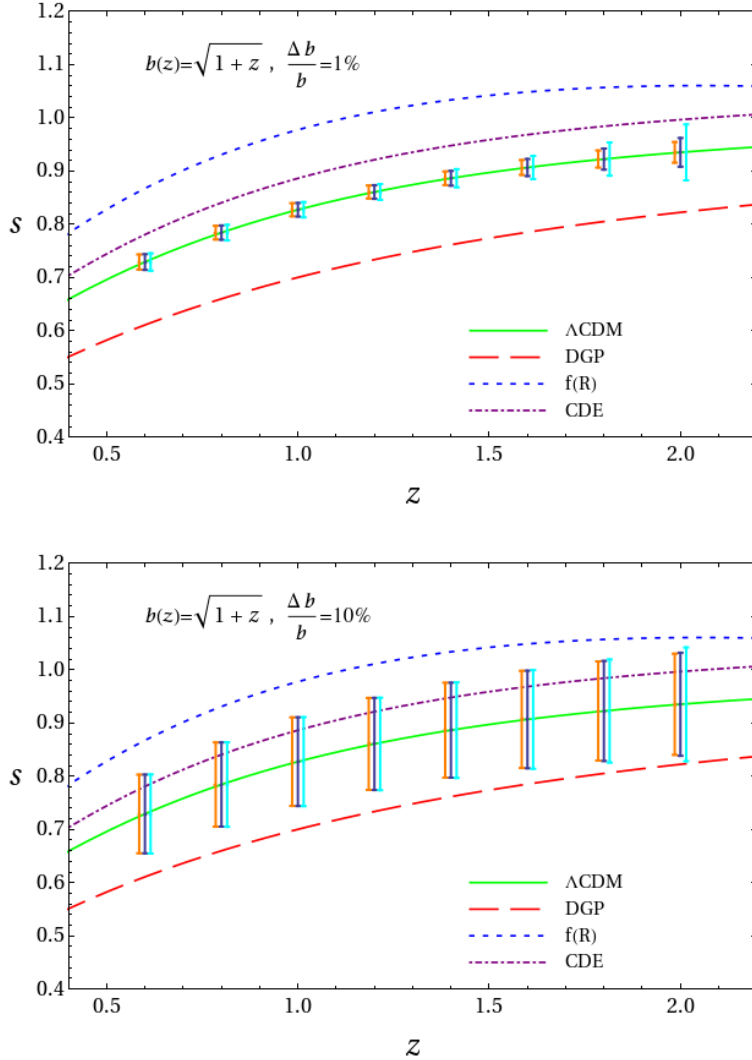


Figure 10.3: Expected constraints on the growth rates in each redshift bin (using the “external bias” method), assuming for the bias a relative error of 1% (upper panel) and 10% (lower panel). For each  $z$  the central error bars refer to the *Reference case* while those referring to the *Optimistic* and *Pessimistic* case have been shifted by  $-0.015$  and  $+0.015$  respectively. The growth rates for four different models are also plotted:  $\Lambda$ CDM (green solid curve), flat DGP (red dashed curve),  $f(R)$  model (blue dotted curve) and a model with coupling between dark energy and dark matter (purple, dot-dashed curve). Even in the case of large errors (10%) for the bias it will be possible to distinguish among three of these models with next generation data.

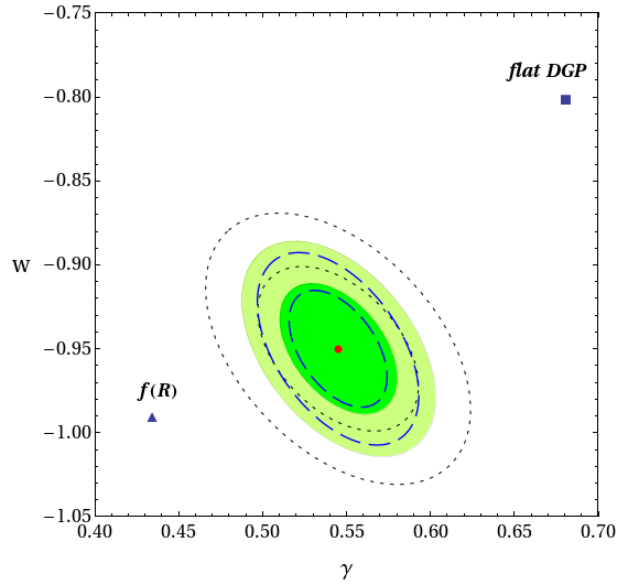


Figure 10.4:  $\gamma$ -parametrization. 1 and  $2\sigma$  marginalized probability regions for constant  $\gamma$  and  $w$ : the green (shaded) regions are relative to the *Reference case*, the blue long-dashed ellipses to the *Optimistic case*, while the black short-dashed ellipses are the probability regions for the *Pessimistic case*. The red dot marks the fiducial model; two alternative models are also indicated for comparison.

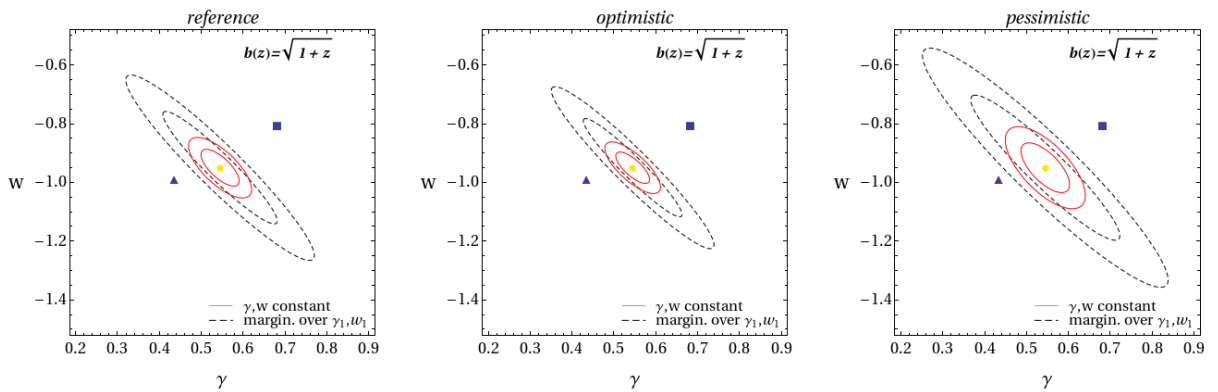


Figure 10.5:  $\gamma$ -parametrization. 1 and  $2\sigma$  marginalized probability regions obtained assuming constant  $\gamma$  and  $w$  (red solid curves) or assuming the parametrizations (10.6) and (10.4) and marginalizing over  $\gamma_1$  and  $w_1$  (black dashed curves); marginalized error values are in columns  $\sigma_{\gamma_{\text{marg},1}}$ ,  $\sigma_{w_{\text{marg},1}}$  of Tab. 10.9. Yellow dots represent the fiducial model, the triangles a  $f(R)$  model and the squares mark the flat DGP.

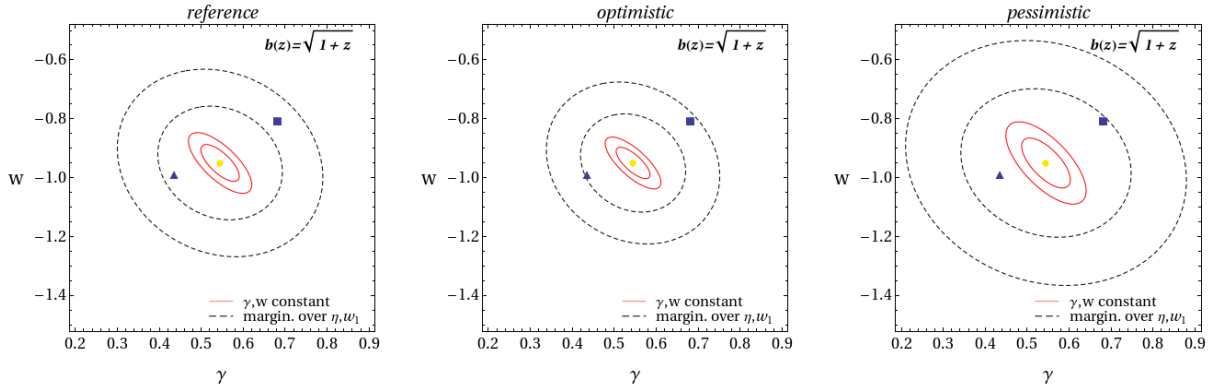


Figure 10.6:  $\eta$ -parametrization.  $1$  and  $2\sigma$  marginalized probability regions obtained assuming constant  $\gamma$  and  $w$  (red solid curves) or assuming the parametrizations (10.7) and (10.4) and marginalizing over  $\eta$  and  $w_1$  (black dashed curves); marginalized error values are in columns  $\sigma_{\gamma_{\text{marg},2}}$ ,  $\sigma_{w_{\text{marg},2}}$  of Tab. 10.10. Yellow dots represent the fiducial model, the triangles stand for a  $f(R)$  model and the squares mark the flat DGP.

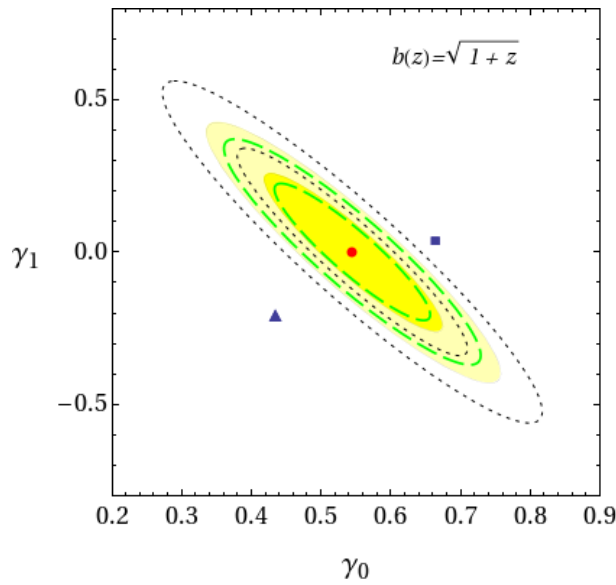


Figure 10.7:  $\gamma$ -parametrization.  $1$  and  $2\sigma$  marginalized probability regions for the parameters  $\gamma_0$  and  $\gamma_1$ , relative to the *Reference case* (shaded yellow regions), to the *Optimistic case* (green long-dashed ellipses), and to the *Pessimistic case* (black dotted ellipses). Red dots represent the fiducial model, blue squares mark the DGP while triangles stand for the  $f(R)$  model. Then, in the case of  $\gamma$ -parametrization, one could distinguish these three models (at 95% probability).

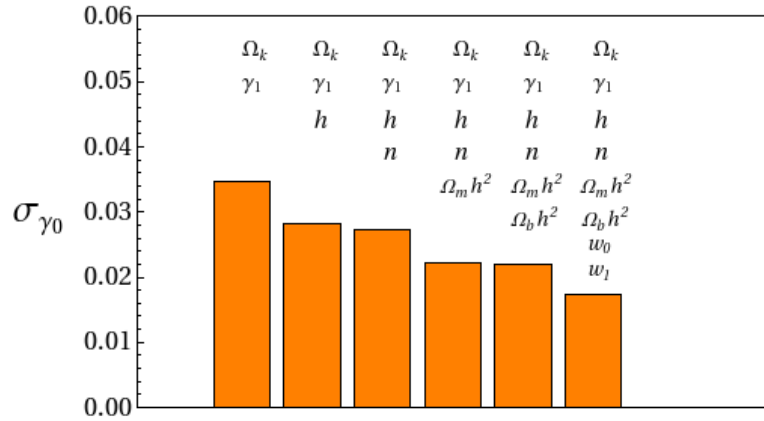


Figure 10.8: The bars represent the errors on the growth index  $\gamma_0$  obtained using the  $\gamma$ -parametrization and fixing an increasing number of cosmological parameters as indicated over each bar and marginalizing over the others. The progressive increase in the number of fixed parameters reflects in a decrease of the error.

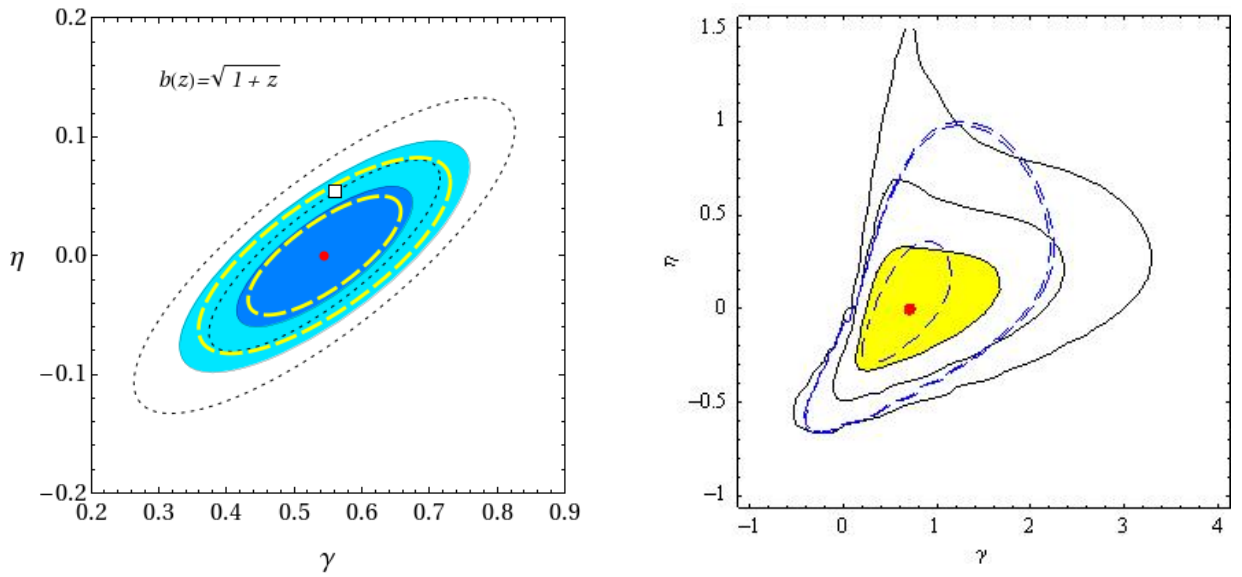


Figure 10.9:  $\eta$ -parametrization. Left panel: 1 and  $2\sigma$  marginalized probability regions for the parameters  $\gamma$  and  $\eta$  in eq. (10.7) relative to the reference case (shaded blue regions), to the optimistic case (yellow long-dashed ellipses) and to the pessimistic case (black short-dashed ellipses). The red dot marks the fiducial model while the square represents the coupling model. Right panel: present constraints on  $\gamma$  and  $\eta$  computed through a full likelihood method (here the red dot marks the likelihood peak) [75]; long-dashed contours are obtained assuming a prior for  $\Omega_{m,0}$ .

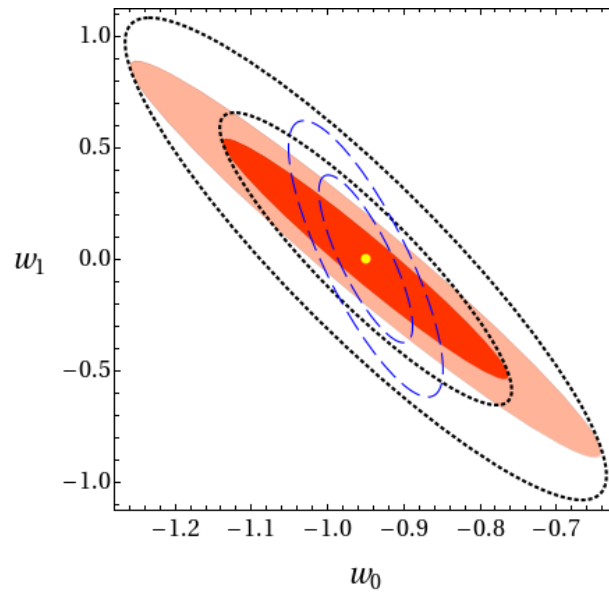


Figure 10.10: Errors on the equation of state. 1 and  $2\sigma$  marginalized probability regions for the parameters  $w_0$  and  $w_1$ , relative to the reference case and constant bias  $b = 1$ . The blue dashed ellipses are obtained fixing  $\gamma_0, \gamma_1$  to their fiducial values and marginalizing over all the other parameters; for the red shaded ellipses instead, we also marginalize over  $\gamma_0, \gamma_1$  but we fix  $\Omega_k = 0$ . Finally, the black dotted ellipses are obtained marginalizing over all parameters but  $w_0$  and  $w_1$ . The progressive increase in the number of parameters reflects in a widening of the ellipses with a consequent decrease in the figures of merit (see Tab. 10.12).

# Conclusions and future developments

In this Thesis we have studied cosmological models which take into account the existence of dark energy, considered the responsible of the accelerated expansion rate of the Universe. In particular we studied both models of modified matter, such as Quintessence, and modified gravity such as  $f(R)$  theories. The main results of this Thesis can be summarized as follows:

- We explored the differences arising between the predictions of coupled Quintessence models on the linear fluctuation growth with respect to standard cases with no coupling, finding that the former give a fluctuation growth rate faster than standard. In order to reproduce this behavior we built up new generalized fits, able to describe the evolution of the growth factor also in models of coupled quintessence. For a comparison between the model and the observations, we carried out the first preliminary analysis which makes use of data coming from different cosmological observables and redshifts.
- We also built up new generalized fits, able to describe with a good accuracy the evolution of the growth factor in different classes of  $f(R)$  models, which can be faster than standard and also acquire a scale-dependence.
- Through the Fisher matrix method we estimated the constraints that future experiments will put on the growth factor, for different dark energy models and we found out that it will be possible to discriminate those models.

Future developments along this line of research are first of all testing our parametrization for a large class of  $f(R)$  models, and consequently use it as a tool to compare those models to data (present and future) in order to constrain the functional form of the  $f(R)$  itself.



# Bibliography

- [1] **The 2DFGRS Collaboration** Collaboration, M. Colless *et al.*, “The 2dF Galaxy Redshift Survey: Spectra and redshifts,” *Mon.Not.Roy.Astron.Soc.* **328** (2001) 1039, [arXiv:astro-ph/0106498](#) [astro-ph].
- [2] **SDSS Collaboration** Collaboration, I. Zehavi *et al.*, “Galaxy clustering in early SDSS redshift data,” *Astrophys.J.* **571** (2002) 172–190, [arXiv:astro-ph/0106476](#) [astro-ph].
- [3] F. Hoyle, P. Outram, T. Shanks, S. Croom, B. N. Loaring, *et al.*, “The 2df qso redshift survey. 4. The qso power spectrum from the 10k catalogue,” *Mon.Not.Roy.Astron.Soc.* **329** (2002) 336, [arXiv:astro-ph/0102163](#) [astro-ph].
- [4] **HST Collaboration** Collaboration, W. Freedman *et al.*, “Final results from the Hubble Space Telescope key project to measure the Hubble constant,” *Astrophys.J.* **553** (2001) 47–72, [arXiv:astro-ph/0012376](#) [astro-ph].
- [5] M. Hamuy, M. Phillips, R. A. Schommer, N. B. Suntzeff, J. Maza, *et al.*, “The Absolute luminosities of the Calan/Tololo type IA supernovae,” *Astron.J.* **112** (1996) 2391, [arXiv:astro-ph/9609059](#) [astro-ph].
- [6] **Supernova Search Team** Collaboration, A. G. Riess *et al.*, “Observational evidence from supernovae for an accelerating universe and a cosmological constant,” *Astron.J.* **116** (1998) 1009–1038, [arXiv:astro-ph/9805201](#) [astro-ph].
- [7] **Supernova Cosmology Project** Collaboration, S. Perlmutter *et al.*, “Measurements of  $\Omega$  and  $\Lambda$  from 42 high redshift supernovae,” *Astrophys.J.* **517** (1999) 565–586, [arXiv:astro-ph/9812133](#) [astro-ph]. The Supernova Cosmology Project.
- [8] N. A. Bahcall, J. P. Ostriker, S. Perlmutter, and P. J. Steinhardt, “The Cosmic triangle: Assessing the state of the universe,” *Science* **284** (1999) 1481–1488, [arXiv:astro-ph/9906463](#) [astro-ph].
- [9] **Supernova Cosmology Project** Collaboration, M. Kowalski *et al.*, “Improved Cosmological Constraints from New, Old and Combined Supernova Datasets,” *Astrophys.J.* **686** (2008) 749–778, [arXiv:0804.4142](#) [astro-ph].

- [10] **Supernova Search Team** Collaboration, A. G. Riess *et al.*, “Type Ia supernova discoveries at  $z < 1$  from the Hubble Space Telescope: Evidence for past deceleration and constraints on dark energy evolution,” *Astrophys.J.* **607** (2004) 665–687, [arXiv:astro-ph/0402512](#) [astro-ph].
- [11] A. G. Riess, L.-G. Strolger, S. Casertano, H. C. Ferguson, B. Mobasher, *et al.*, “New Hubble Space Telescope Discoveries of Type Ia Supernovae at  $z \leq 1$ : Narrowing Constraints on the Early Behavior of Dark Energy,” *Astrophys.J.* **659** (2007) 98–121, [arXiv:astro-ph/0611572](#) [astro-ph].
- [12] T. M. Davis, E. Mortsell, J. Sollerman, A. Becker, S. Blondin, *et al.*, “Scrutinizing Exotic Cosmological Models Using ESSENCE Supernova Data Combined with Other Cosmological Probes,” *Astrophys.J.* **666** (2007) 716–725, [arXiv:astro-ph/0701510](#) [astro-ph].
- [13] R. Jimenez, P. Thejll, U. Jorgensen, J. MacDonald, and B. Pagel, “Ages of globular clusters: a new approach,” [arXiv:astro-ph/9602132](#) [astro-ph].
- [14] E. Carretta, R. G. Gratton, G. Clementini, and F. Fusi Pecci, “Distances, ages and epoch of formation of globular clusters,” *Astrophys.J.* **533** (2000) 215–235, [arXiv:astro-ph/9902086](#) [astro-ph].
- [15] H. B. Richer, J. Brewer, G. G. Fahlman, B. K. Gibson, B. M. Hansen, *et al.*, “The Lower main sequence and mass function of the globular cluster Messier 4,” *Astrophys.J.* **574** (2002) L151–L154, [arXiv:astro-ph/0205086](#) [astro-ph].
- [16] B. M. Hansen, J. Brewer, G. G. Fahlman, B. K. Gibson, R. Ibata, *et al.*, “The white dwarf cooling sequence of the globular cluster messier 4,” *Astrophys.J.* **574** (2002) L155–L158, [arXiv:astro-ph/0205087](#) [astro-ph].
- [17] E. Komatsu, K. Smith, J. Dunkley, C. Bennett, B. Gold, *et al.*, “Seven-Year Wilkinson Microwave Anisotropy Probe (WMAP) Observations: Cosmological Interpretation,” [arXiv:1001.4538](#) [astro-ph.CO].
- [18] A. Melchiorri and L. M. Griffiths, “From anisotropy to Omega,” *New Astron.Rev.* **45** (2001) 321–328, [arXiv:astro-ph/0011147](#) [astro-ph].
- [19] **Boomerang Collaboration** Collaboration, P. de Bernardis *et al.*, “A Flat universe from high resolution maps of the cosmic microwave background radiation,” *Nature* **404** (2000) 955–959, [arXiv:astro-ph/0004404](#) [astro-ph].
- [20] D. Larson, J. Dunkley, G. Hinshaw, E. Komatsu, M. Nolta, *et al.*, “Seven-Year Wilkinson Microwave Anisotropy Probe (WMAP) Observations: Power Spectra and WMAP-Derived Parameters,” [arXiv:1001.4635](#) [astro-ph.CO].
- [21] C. Reichardt, P. Ade, J. Bock, J. Bond, J. Brevik, *et al.*, “High resolution CMB power spectrum from the complete ACBAR data set,” *Astrophys.J.* **694** (2009) 1200–1219, [arXiv:0801.1491](#) [astro-ph].

- [22] **QUaD collaboration** Collaboration, . M. Brown *et al.*, “Improved measurements of the temperature and polarization of the CMB from QUaD,” *Astrophys.J.* **705** (2009) 978–999, [arXiv:0906.1003 \[astro-ph.CO\]](#).
- [23] A. Einstein, “The foundation of the general theory of relativity,” *Annalen Phys.* **49** (1916) 769.
- [24] A. Einstein, “Cosmological considerations in the General Theory of Relativity,” *Sitzungsber. Preuss. Akad. Wiss. Phys.-math. Klasse VI* (1917) 142.
- [25] E. Hubble, “A relation between distance and radial velocity among extra-galactic nebulae,” *Proc. Nat. Acad. Sci.* **15** (1929) 168.
- [26] A. Einstein, *The Meaning of Relativity*. Princeton University, Princeton, 1945.
- [27] G. Gamov, *My World Line*. Viking, New York, 1970.
- [28] E. Bianchi and C. Rovelli, “Why all these prejudices against a constant?,” [arXiv:1002.3966 \[astro-ph.CO\]](#).
- [29] I. Zlatev, L.-M. Wang, and P. J. Steinhardt, “Quintessence, cosmic coincidence, and the cosmological constant,” *Phys.Rev.Lett.* **82** (1999) 896–899, [arXiv:astro-ph/9807002 \[astro-ph\]](#).
- [30] A. Vilenkin, “Predictions from quantum cosmology,” *Phys.Rev.Lett.* **74** (1995) 846–849, [arXiv:gr-qc/9406010 \[gr-qc\]](#).
- [31] G. Efstathiou, “An anthropic argument for a cosmological constant,” *Mon.Not.Roy.Astron.Soc.* **274** (1995) L73–L76.
- [32] J. Kujat, A. M. Linn, R. J. Scherrer, and D. H. Weinberg, “Prospects for determining the equation of state of the dark energy: What can be learned from multiple observables?,” *Astrophys.J.* **572** (2002) 1–14, [arXiv:astro-ph/0112221 \[astro-ph\]](#).
- [33] S. Dodelson, *Modern Cosmology*. Academic Press (Elsevier), New York, 2003.
- [34] L. L. Amendola and T. S., *Dark energy Theory and Observations*. Cambridge University Press, 2010.
- [35] J. Peebles, *The Large-Scale Structure of the Universe*. Princeton University Press, 1980.
- [36] M. Davis and J. Peebles, “A survey of galaxy redshifts: V - The two-point position and velocity correlations,” *Astrophys. J.* **267** (1983) 465D.
- [37] S. D. Landy and A. S. Szalay, “Bias and variance of angular correlation functions,” *Astrophys. J.* **412** (1993) 64L.

- [38] H. A. Feldman, N. Kaiser, and J. A. Peacock, “Power spectrum analysis of three-dimensional redshift surveys,” *Astrophys.J.* **426** (1994) 23–37, [arXiv:astro-ph/9304022](#) [astro-ph].
- [39] N. Kaiser, “Clustering in real space and in redshift space,” *Mon.Not.Roy.Astron.Soc.* **227** (1987) 1–21.
- [40] U. Seljak, “Redshift space bias and  $\beta$  from the halo model,” *Mon.Not.Roy.Astron.Soc.* **325** (2001) 1359.
- [41] M. J. White, “The Redshift space power spectrum in the halo model,” *Mon.Not.Roy.Astron.Soc.* **321** (2001) 1, [arXiv:astro-ph/0005085](#) [astro-ph].
- [42] S. Cole, K. B. Fisher, and D. H. Weinberg, “Constraints on Omega from the IRAS redshift surveys,” *Mon.Not.Roy.Astron.Soc.* **275** (1995) 515, [arXiv:astro-ph/9412062](#) [astro-ph].
- [43] J. Peacock and S. Dodds, “Nonlinear evolution of cosmological power spectra,” *Mon.Not.Roy.Astron.Soc.* **280** (1996) L19, [arXiv:astro-ph/9603031](#) [astro-ph].
- [44] G. D’Agostini, *Bayesian reasoning in data analysis*. World Scientific Publishing, 2003.
- [45] A. Albrecht, G. Bernstein, R. Cahn, W. L. Freedman, J. Hewitt, *et al.*, “Report of the Dark Energy Task Force,” [arXiv:astro-ph/0609591](#) [astro-ph].
- [46] M. Tegmark, “Measuring cosmological parameters with galaxy surveys,” *Phys.Rev.Lett.* **79** (1997) 3806–3809, [arXiv:astro-ph/9706198](#) [astro-ph].
- [47] H.-J. Seo and D. J. Eisenstein, “Probing dark energy with baryonic acoustic oscillations from future large galaxy redshift surveys,” *Astrophys.J.* **598** (2003) 720–740, [arXiv:astro-ph/0307460](#) [astro-ph].
- [48] R. Caldwell, R. Dave, and P. J. Steinhardt, “Cosmological imprint of an energy component with general equation of state,” *Phys.Rev.Lett.* **80** (1998) 1582–1585, [arXiv:astro-ph/9708069](#) [astro-ph].
- [49] B. A. Bassett, S. Tsujikawa, and D. Wands, “Inflation dynamics and reheating,” *Rev.Mod.Phys.* **78** (2006) 537–589, [arXiv:astro-ph/0507632](#) [astro-ph].
- [50] S. M. Carroll, “Quintessence and the rest of the world: Suppressing Long-Range Interactions,” *Phys.Rev.Lett.* **81** (1998) 3067–3070, [arXiv:astro-ph/9806099](#) [astro-ph].
- [51] T. Damour, G. W. Gibbons, and C. Gundlach, “Dark matter, time-varying G, and a dilaton field,” *Phys.Rev.Lett.* **64** (1990) 123–126.

- [52] J.-P. Uzan, “Cosmological scaling solutions of nonminimally coupled scalar fields,” *Phys.Rev.* **D59** (1999) 123510, [arXiv:gr-qc/9903004 \[gr-qc\]](#).
- [53] T. Chiba, “Quintessence, the gravitational constant, and gravity,” *Phys.Rev.* **D60** (1999) 083508, [arXiv:gr-qc/9903094 \[gr-qc\]](#).
- [54] X.-l. Chen and M. Kamionkowski, “Cosmic microwave background temperature and polarization anisotropy in Brans-Dicke cosmology,” *Phys.Rev.* **D60** (1999) 104036, [arXiv:astro-ph/9905368 \[astro-ph\]](#).
- [55] F. Perrotta, C. Baccigalupi, and S. Matarrese, “Extended quintessence,” *Phys.Rev.* **D61** (2000) 023507, [arXiv:astro-ph/9906066 \[astro-ph\]](#).
- [56] L. Amendola, “Coupled quintessence,” *Phys.Rev.* **D62** (2000) 043511, [arXiv:astro-ph/9908023 \[astro-ph\]](#).
- [57] C. Wetterich, “The Cosmon model for an asymptotically vanishing time dependent cosmological ‘constant’,” *Astron.Astrophys.* **301** (1995) 321–328, [arXiv:hep-th/9408025 \[hep-th\]](#).
- [58] E. J. Copeland, A. R. Liddle, and D. Wands, “Exponential potentials and cosmological scaling solutions,” *Phys.Rev.* **D57** (1998) 4686–4690, [arXiv:gr-qc/9711068 \[gr-qc\]](#).
- [59] L. Amendola and C. Quercellini, “Tracking and coupled dark energy as seen by WMAP,” *Phys.Rev.* **D68** (2003) 023514, [arXiv:astro-ph/0303228 \[astro-ph\]](#).
- [60] L. Amendola, “Linear and non-linear perturbations in dark energy models,” *Phys.Rev.* **D69** (2004) 103524, [arXiv:astro-ph/0311175 \[astro-ph\]](#).
- [61] L. Amendola, R. Gannouji, D. Polarski, and S. Tsujikawa, “Conditions for the cosmological viability of  $f(R)$  dark energy models,” *Phys.Rev.* **D75** (2007) 083504, [arXiv:gr-qc/0612180 \[gr-qc\]](#).
- [62] L. Amendola, M. Kunz, and D. Sapone, “Measuring the dark side (with weak lensing),” *JCAP* **0804** (2008) 013, [arXiv:0704.2421 \[astro-ph\]](#).
- [63] M. Viel, M. G. Haehnelt, and V. Springel, “Inferring the dark matter power spectrum from the Lyman- $\alpha$  forest in high-resolution QSO absorption spectra,” *Mon.Not.Roy.Astron.Soc.* **354** (2004) 684, [arXiv:astro-ph/0404600 \[astro-ph\]](#).
- [64] **SDSS Collaboration** Collaboration, P. McDonald *et al.*, “The Linear theory power spectrum from the Lyman- $\alpha$  forest in the Sloan Digital Sky Survey,” *Astrophys.J.* **635** (2005) 761–783, [arXiv:astro-ph/0407377 \[astro-ph\]](#).

- [65] M. Viel and M. G. Haehnelt, “Cosmological and astrophysical parameters from the Sloan Digital Sky Survey flux power spectrum and hydrodynamical simulations of the Lyman- $\alpha$  forest,” *Mon.Not.Roy.Astron.Soc.* **365** (2006) 231–244, [arXiv:astro-ph/0508177](#) [astro-ph].
- [66] **SDSS Collaboration** Collaboration, M. Tegmark *et al.*, “The Three-Dimensional power spectrum of galaxies from the Sloan Digital Sky Survey,” *Astrophys.J.* **606** (2004) 702–740, [arXiv:astro-ph/0310725](#) [astro-ph].
- [67] V. Desjacques and A. Nusser, “Joint modeling of the probability distribution and power spectrum of the Ly- $\alpha$  forest: Comparison with observations at  $z = 3$ ,” *Mon.Not.Roy.Astron.Soc.* **361** (2005) 1257–1272, [arXiv:astro-ph/0410618](#) [astro-ph].
- [68] B. A. Bassett, P. S. Corasaniti, and M. Kunz, “The Essence of quintessence and the cost of compression,” *Astrophys.J.* **617** (2004) L1–L4, [arXiv:astro-ph/0407364](#) [astro-ph].
- [69] L. Amendola, R. Gannouji, D. Polarski, and S. Tsujikawa, “Conditions for the cosmological viability of  $f(R)$  dark energy models,” *Phys.Rev.* **D75** (2007) 083504, [arXiv:gr-qc/0612180](#) [gr-qc].
- [70] R. Gannouji, B. Moraes, and D. Polarski, “The growth of matter perturbations in  $f(R)$  models,” *JCAP* **0902** (2009) 034, [arXiv:0809.3374](#) [astro-ph].
- [71] L. Amendola and S. Tsujikawa, “Phantom crossing, equation-of-state singularities, and local gravity constraints in  $f(R)$  models,” *Phys.Lett.* **B660** (2008) 125–132, [arXiv:0705.0396](#) [astro-ph].
- [72] A. De Felice and S. Tsujikawa, “ $f(R)$  theories,” *Living Rev.Rel.* **13** (2010) 3, [arXiv:1002.4928](#) [gr-qc].
- [73] G. Dvali, G. Gabadadze, and M. Porrati, “4-D gravity on a brane in 5-D Minkowski space,” *Phys.Lett.* **B485** (2000) 208–214, [arXiv:hep-th/0005016](#) [hep-th].
- [74] Y. Wang, “Differentiating dark energy and modified gravity with galaxy redshift surveys,” *JCAP* **0805** (2008) 021, [arXiv:0710.3885](#) [astro-ph].
- [75] C. Di Porto and L. Amendola, “Observational constraints on the linear fluctuation growth rate,” *Phys.Rev.* **D77** (2008) 083508, [arXiv:0707.2686](#) [astro-ph].
- [76] S. Tsujikawa, R. Gannouji, B. Moraes, and D. Polarski, “The dispersion of growth of matter perturbations in  $f(R)$  gravity,” *Phys.Rev.* **D80** (2009) 084044, [arXiv:0908.2669](#) [astro-ph.CO].

- [77] A. Hamilton, “Linear redshift distortions: A Review,” [arXiv:astro-ph/9708102 \[astro-ph\]](#). Published in *The Evolving Universe*. Edited by D. Hamilton, Kluwer Academic, 1998, p. 185-275.
- [78] L. Amendola, C. Quercellini, and E. Giallongo, “Constraints on perfect fluid and scalar field dark energy models from future redshift surveys,” *Mon.Not.Roy.Astron.Soc.* **357** (2005) 429–439, [arXiv:astro-ph/0404599 \[astro-ph\]](#).
- [79] D. Sapone and L. Amendola, “Constraining the growth factor with baryon oscillations,” [arXiv:0709.2792 \[astro-ph\]](#).
- [80] L. Guzzo, M. Pierleoni, B. Meneux, E. Branchini, O. Fevre, *et al.*, “A test of the nature of cosmic acceleration using galaxy redshift distortions,” *Nature* **451** (2008) 541–545, [arXiv:0802.1944 \[astro-ph\]](#).
- [81] E. Hawkins, S. Maddox, S. Cole, D. Madgwick, P. Norberg, *et al.*, “The 2dF Galaxy Redshift Survey: Correlation functions, peculiar velocities and the matter density of the universe,” *Mon.Not.Roy.Astron.Soc.* **346** (2003) 78, [arXiv:astro-ph/0212375 \[astro-ph\]](#).
- [82] L. Verde, A. F. Heavens, W. J. Percival, S. Matarrese, C. M. Baugh, *et al.*, “The 2dF Galaxy Redshift Survey: The Bias of galaxies and the density of the Universe,” *Mon.Not.Roy.Astron.Soc.* **335** (2002) 432, [arXiv:astro-ph/0112161 \[astro-ph\]](#).
- [83] **SDSS Collaboration** Collaboration, M. Tegmark *et al.*, “Cosmological Constraints from the SDSS Luminous Red Galaxies,” *Phys.Rev.* **D74** (2006) 123507, [arXiv:astro-ph/0608632 \[astro-ph\]](#).
- [84] N. P. Ross, J. da Angela, T. Shanks, D. A. Wake, R. D. Cannon, *et al.*, “The 2dF-SDSS LRG and QSO Survey: The 2-Point Correlation Function and Redshift-Space Distortions,” *Mon.Not.Roy.Astron.Soc.* **381** (2007) 573–588, [arXiv:astro-ph/0612400 \[astro-ph\]](#).
- [85] J. da Angela, T. Shanks, S. Croom, P. Weilbacher, R. Brunner, *et al.*, “The 2dF-SDSS LRG and QSO Survey: QSO clustering and the  $L - z$  degeneracy,” *Mon.Not.Roy.Astron.Soc.* **383** (2008) 565–580, [arXiv:astro-ph/0612401 \[astro-ph\]](#).
- [86] J. A. Peacock, S. Cole, P. Norberg, C. M. Baugh, J. Bland-Hawthorn, *et al.*, “A Measurement of the cosmological mass density from clustering in the 2dF Galaxy Redshift Survey,” *Nature* **410** (2001) 169–173, [arXiv:astro-ph/0103143 \[astro-ph\]](#).
- [87] C. Blake, S. Brough, M. Colless, W. Couch, S. Croom, *et al.*, “The WiggleZ Dark Energy Survey: the selection function and  $z = 0.6$  galaxy power spectrum,” *Mon.Not.Roy.Astron.Soc.* **406** (2010) 803–821, [arXiv:1003.5721 \[astro-ph.CO\]](#).

- [88] S. Nesseris and L. Perivolaropoulos, “Testing  $\Lambda$ CDM with the Growth Function  $\delta(a)$ : Current Constraints,” *Phys.Rev.* **D77** (2008) 023504, [arXiv:0710.1092](#) [[astro-ph](#)].
- [89] J. Dossett, M. Ishak, J. Moldenhauer, Y. Gong, and A. Wang, “Constraints on growth index parameters from current and future observations,” *JCAP* **1004** (2010) 022, [arXiv:1004.3086](#) [[astro-ph.CO](#)].
- [90] L. Guzzo and O. Le Fèvre, “Redshift-space distortions in deep redshift surveys as a probe of the invisible Universe,” in *INVISIBLE UNIVERSE: Proceedings of the Conference*, vol. 1241 of *American Institute of Physics Conference Series*, pp. 39–45. June, 2010.
- [91] D. Schlegel, M. White, and D. Eisenstein, “The Baryon Oscillation Spectroscopic Survey: Precision measurements of the absolute cosmic distance scale,” [arXiv:0902.4680](#) [[astro-ph.CO](#)].
- [92] R. Laureijs *et al.*, “Euclid Assessment Study Report for the ESA Cosmic Visions,” [arXiv:0912.0914](#) [[astro-ph.CO](#)].
- [93] D. J. Schlegel, C. Bebek, H. Heetderks, S. Ho, M. Lampton, *et al.*, “BigBOSS: The Ground-Based Stage IV Dark Energy Experiment,” [arXiv:0904.0468](#) [[astro-ph.CO](#)].
- [94] P. J. E. Peebles., “The Peculiar Velocity Field in the Local Supercluster,” *Astrophys.J.* **205** (1976) 318–328.
- [95] O. Lahav *et al.*, “Dynamical effects of the cosmological constant,” *Mon.Not.Roy.Astron.Soc.* **251** (1991) 128–136.
- [96] D. Polarski and R. Gannouji, “On the growth of linear perturbations,” *Phys.Lett.* **B660** (2008) 439–443, [arXiv:0710.1510](#) [[astro-ph](#)].
- [97] E. V. Linder, “Cosmic growth history and expansion history,” *Phys.Rev.* **D72** (2005) 043529, [arXiv:astro-ph/0507263](#) [[astro-ph](#)].
- [98] L.-M. Wang and P. J. Steinhardt, “Cluster abundance constraints on quintessence models,” *Astrophys.J.* **508** (1998) 483–490, [arXiv:astro-ph/9804015](#) [[astro-ph](#)].
- [99] E. V. Linder and R. N. Cahn, “Parameterized Beyond-Einstein Growth,” *Astropart.Phys.* **28** (2007) 481–488, [arXiv:astro-ph/0701317](#) [[astro-ph](#)].
- [100] H. Wei, “Growth Index of DGP Model and Current Growth Rate Data,” *Phys.Lett.* **B664** (2008) 1–6, [arXiv:0802.4122](#) [[astro-ph](#)].
- [101] C. Marinoni, O. Le Fèvre, B. Meneux, A. Iovino, A. Pollo, *et al.*, “The VIMOS VLT Deep Survey: Evolution of the non-linear galaxy bias up to  $z=1.5$ ,” *Astron.Astrophys.* **442** (2005) 801–825, [arXiv:astro-ph/0506561](#) [[astro-ph](#)].

- [102] Y. Sigad, E. Branchini, and A. Dekel, “Measuring the nonlinear biasing function from a galaxy redshift survey,” *Astrophys.J.* **540** (2000) 62–73, [arXiv:astro-ph/0002170](#) [astro-ph].
- [103] Y. Wang, W. Percival, A. Cimatti, P. Mukherjee, L. Guzzo, *et al.*, “Designing a space-based galaxy redshift survey to probe dark energy,” *Mon.Not.Roy.Astron.Soc.* **409** (2010) 737–749, [arXiv:1006.3517](#) [astro-ph.CO].
- [104] F. Simpson and J. A. Peacock, “Difficulties Distinguishing Dark Energy from Modified Gravity via Redshift Distortions,” *Phys.Rev.* **D81** (2010) 043512, [arXiv:0910.3834](#) [astro-ph.CO].
- [105] L. Samushia, W. J. Percival, L. Guzzo, Y. Wang, A. Cimatti, *et al.*, “Effects of cosmological model assumptions on galaxy redshift survey measurements,” *Mon.Not.Roy.Astron.Soc.* (2010) in press, [arXiv:1006.0609](#) [astro-ph.CO].
- [106] M. Chevallier and D. Polarski, “Accelerating universes with scaling dark matter,” *Int.J.Mod.Phys.* **D10** (2001) 213–224, [arXiv:gr-qc/0009008](#) [gr-qc].
- [107] E. V. Linder, “Exploring the expansion history of the universe,” *Phys.Rev.Lett.* **90** (2003) 091301, [arXiv:astro-ph/0208512](#) [astro-ph].
- [108] P. Wu, H. W. Yu, and X. Fu, “A Parametrization for the growth index of linear matter perturbations,” *JCAP* **0906** (2009) 019, [arXiv:0905.3444](#) [gr-qc].
- [109] X.-y. Fu, P.-x. Wu, and H.-w. Yu, “The Growth of linear perturbations in the DGP model,” *Phys.Lett.* **B677** (2009) 12–15, [arXiv:0905.1735](#) [gr-qc].
- [110] H. Motohashi, A. A. Starobinsky, and J. Yokoyama, “Phantom behaviour and growth index anomalous evolution in viable  $f(R)$  gravity models,” [arXiv:1002.0462](#) [astro-ph.CO].
- [111] A. Dekel and O. Lahav, “Stochastic nonlinear galaxy biasing,” *Astrophys.J.* **520** (1999) 24–34, [arXiv:astro-ph/9806193](#) [astro-ph].
- [112] K. Kovac, C. Porciani, S. Lilly, C. Marinoni, L. Guzzo, *et al.*, “The nonlinear biasing of the 10k zCOSMOS galaxies up to  $z \sim 1$ ,” [arXiv:0910.0004](#) [astro-ph.CO].
- [113] A. Rassat, A. Amara, L. Amendola, F. J. Castander, T. Kitching, *et al.*, “Deconstructing Baryon Acoustic Oscillations: A Comparison of Methods,” [arXiv:0810.0003](#) [astro-ph].
- [114] A. Orsi, C. Baugh, C. Lacey, A. Cimatti, Y. Wang, *et al.*, “Probing dark energy with future redshift surveys: A comparison of emission line and broad band selection in the near infrared,” *Mon.Not.Roy.Astron.Soc.* **405** (2010) 1006–1024, [arXiv:0911.0669](#) [astro-ph.CO].

- [115] C. M. Baugh, C. Lacey, C. Frenk, G. Granato, L. Silva, *et al.*, “Can the faint submillimetre galaxies be explained in the  $\Lambda$  cold dark matter model?,” *Mon.Not.Roy.Astron.Soc.* **356** (2005) 1191–1200, [arXiv:astro-ph/0406069](#) [[astro-ph](#)].
- [116] R. Maartens and E. Majerotto, “Observational constraints on self-accelerating cosmology,” *Phys.Rev.* **D74** (2006) 023004, [arXiv:astro-ph/0603353](#) [[astro-ph](#)].
- [117] W. Hu and I. Sawicki, “Models of  $f(R)$  Cosmic Acceleration that Evade Solar-System Tests,” *Phys.Rev.* **D76** (2007) 064004, [arXiv:0705.1158](#) [[astro-ph](#)].
- [118] R. A. Fisher, “The logic of inductive inference,” *J. Roy. Stat. Soc.* **98** (1935) 39–54.
- [119] M. Tegmark, A. Taylor, and A. Heavens, “Karhunen-Loève eigenvalue problems in cosmology: How should we tackle large data sets?,” *Astrophys.J.* **480** (1997) 22, [arXiv:astro-ph/9603021](#) [[astro-ph](#)].
- [120] U. Seljak and M. Zaldarriaga, “A Line of sight integration approach to cosmic microwave background anisotropies,” *Astrophys.J.* **469** (1996) 437–444, [arXiv:astro-ph/9603033](#) [[astro-ph](#)].
- [121] C. Alcock and B. Paczynski, “An evolution free test for non-zero cosmological constant,” *Nature* **281** (1979) 358–359.
- [122] W. Ballinger, J. Peacock, and A. Heavens, “Measuring the cosmological constant with redshift surveys,” *Mon.Not.Roy.Astron.Soc.* **282** (1996) 877–888, [arXiv:astro-ph/9605017](#) [[astro-ph](#)].
- [123] D. J. Eisenstein, H.-j. Seo, and . White, Martin J., “On the Robustness of the Acoustic Scale in the Low-Redshift Clustering of Matter,” *Astrophys.J.* **664** (2007) 660–674, [arXiv:astro-ph/0604361](#) [[astro-ph](#)].
- [124] H.-J. Seo and D. J. Eisenstein, “Improved forecasts for the baryon acoustic oscillations and cosmological distance scale,” *Astrophys.J.* **665** (2007) 14–24, [arXiv:astro-ph/0701079](#) [[astro-ph](#)].
- [125] J. Geach, A. Cimatti, W. Percival, Y. Wang, L. Guzzo, *et al.*, “Empirical  $H\alpha$  emitter count predictions for dark energy surveys,” *Mon.Not.Roy.Astron.Soc.* **402** (2010) 1330–1338, [arXiv:0911.0686](#) [[astro-ph.CO](#)].